

# DISSERTATION

Titel der Dissertation:

**Circumstellar Habitable Zones in Binary Star Systems**

Verfasser:

**MMag.rer.nat. Siegfried Eggl, Bakk.rer.nat**

angestrebter akademischer Grad:

**Doktor der Naturwissenschaften (Dr.rer.nat.)**

Wien, 2013

Studienkennzahl lt. Studienblatt:	A 091 413 Dr.-Studium der Naturwissenschaften Astronomie UniStG
Dissertationsgebiet lt. Studienblatt:	413 Astronomie
Betreuer:	Univ.-Prof. Dr. Rudolf Dvorak



*To my loved ones.*





## Acknowledgments

First and foremost, I would like to acknowledge the fertile intellectual environment provided by the Astro Dynamics Group (ADG) at the IfA, University of Vienna. Especially Dr. Elke Pilat-Lohinger and Prof. Dr. Rudolf Dvorak have been supportive in every way imaginable. During the years I have had the pleasure of being a member of the ADG, I have come to see them as my second family.

I am also grateful for the financial support provided by the University of Vienna in the framework of the "Forschungsstipendium 2012" as well as FWF projects P20216-N16 "Evolution of planetary systems in binary stars" and S11608-N16 "Binary Star Systems and Habitability" - both directed by Dr. Elke Pilat-Lohinger, where the latter is a sub-project of the "Nationales Forschungs Netzwerk: Pathways to Habitability" headed by Prof. Dr. Manuel Güdel.

Furthermore, I would like to express my gratitude towards Dr. Nikolaos Georgakarakos for valuable discussions and mathematical hints.

Last but not least, I thank Dr. Nader Haghighipour and the Institute for Astronomy and NASA Astrobiology Institute at the University of Hawaii-Manoa for their hospitality during July 2012. This collaboration was supported by FWF project P20216-N16.

This research has made use of the Hipparcos catalog as well as the Washington Double Star Catalog maintained at the U.S. Naval Observatory.



## Glossary

<b>2BP</b>	two body problem
<b>3BP</b>	three body problem
<b>AHZ</b>	Average Habitable Zone
<b>AM</b>	astrometry
<b>CHZ</b>	Continuously Habitable Zone
<b>CR3BP</b>	circular restricted three body problem
<b>EBM</b>	energy balance model
<b>EHZ</b>	Extended Habitable Zone
<b>EIH</b>	Einstein-Infeld-Hoffmann
<b>ESA</b>	European Space Agency
<b>ESO</b>	European Southern Observatory
<b>EUV</b>	extreme ultra violet
<b>FLI</b>	Fast Lyapunov Indicator
<b>GCM</b>	General/Global Circulation Model
<b>GHZ</b>	Galactic Habitable Zone
<b>GR</b>	general relativity
<b>HD</b>	Henry Draper
<b>HIP</b>	Hipparchos catalog identifier
<b>HZ</b>	Habitable Zone
<b>IR</b>	infrared
<b>KAM</b>	Kolmogorov-Arnold-Moser
<b>KHZ</b>	Classical/Kasting's Habitable Zone
<b>LCO</b>	Lower Critical Orbit
<b>LEBM</b>	Latitudinal Energy Balance Model
<b>NASA</b>	National Aeronautics and Space Agency
<b>PHZ</b>	Permanently Habitable Zone
<b>P-Type</b>	the planet moves around both stars of a stellar binary
<b>R3BP</b>	restricted three body problem
<b>RBM</b>	radiation balance model
<b>RMS</b>	root mean square
<b>RV</b>	radial velocity
<b>SPH</b>	smoothed-particle hydrodynamics
<b>S-Type</b>	the planet moves around one star of a stellar binary
<b>TD</b>	transit depth
<b>TP</b>	transit photometry
<b>UCO</b>	Upper Critical Orbit
<b>UV</b>	ultra violet
<b>VLBI</b>	Very Long Baseline Interferometer
<b>WDC</b>	The Washington Visual Double Star Catalog
<b>WDS</b>	Washington Double Star catalog
<b>XUV</b>	extreme ultra violet
<b>ZAMS</b>	Zero Age Main Sequence



## Non SI units and constants

<b>au (AU)</b>	astronomical unit	149597870700 m
<b>D</b>	days	86400 SI seconds
		at mean sea level (Earth)
<b>deg (°)</b>	degree	$\pi/180^\circ$ rad
<b>°C</b>	degree Centigrade	+273.15 K
<b>Ga</b>	gigayears	$10^9$ years
<b>k</b>	Gaussian gravitational constant	$0.01720209895 \text{ au}^{3/2} \text{ M}_\odot^{-1/2} \text{ D}^{-1}$
<b>L<sub>⊙</sub></b>	solar luminosity	$\approx 4 \cdot 10^{26} \text{ W}$
<b>M<sub>⊙</sub></b>	solar mass	$\approx 1.989 \cdot 10^{30} \text{ kg}$
<b>R<sub>J</sub></b>	Jupiter radius	$\approx 7 \cdot 10^7 \text{ m}$
<b>S<sub>⊙</sub></b>	solar constant at 1 au	$\approx 1360 \text{ W/m}^2$
<b>pc</b>	parsec	$\approx 3.085678 \cdot 10^{16} \text{ m}$
<b>yr</b>	Gregorian year	$3.1557 \cdot 10^7 \text{ SI seconds}$



# Contents

<b>Acknowledgments</b>	<b>i</b>
<b>Glossary</b>	<b>iii</b>
<b>Non SI units and constants</b>	<b>v</b>
<b>1 Introduction</b>	<b>1</b>
1.1 Binary Stars . . . . .	2
1.2 Habitable Zones . . . . .	5
1.2.1 Coining the Term . . . . .	5
1.2.2 Defining Habitability . . . . .	5
1.2.3 Kasting's Approach . . . . .	6
1.2.4 Habitability after 1993 . . . . .	8
1.2.5 Habitability of Planets in Binary Star Systems . . . . .	11
1.2.6 Galactic Habitability . . . . .	14
1.3 Orbital Dynamics . . . . .	14
1.3.1 Stability . . . . .	16
1.3.2 Perturbation Theory . . . . .	19
1.3.3 Kaula's Approach . . . . .	20
1.3.4 Brouwer's Approach . . . . .	22
1.3.5 Georgakarakos' Approach . . . . .	26
1.A Georgakarakos' Solution for the Inner Eccentricity . . . . .	30
<b>2 An Analytic Method To Determine Habitable Zones For S-Type Planetary Orbits In Binary Star Systems</b>	<b>37</b>
<b>3 Detectability of Earth-like Planets in Circumstellar Habitable Zones of Bi- nary Star Systems with Sun-like Components</b>	<b>49</b>
<b>4 Circumstellar Habitable Zones of Binary Star Systems in the Solar Neigh- borhood</b>	<b>63</b>
<b>5 Discussion</b>	<b>75</b>
5.1 Analytic Insolation Estimates . . . . .	75
5.2 Insolation Averaging . . . . .	80
5.3 Mutual Inclination . . . . .	88
5.4 Retrograde Planetary Motion . . . . .	91
5.5 Initial Planetary Eccentricity . . . . .	92

5.6	General Relativity and R3BP Approximations . . . . .	93
5.7	Planetary Atmospheric Models . . . . .	96
5.A	Updated HZ Borders for Nearby Binary Stars . . . . .	101
<b>6</b>	<b>The Road Ahead</b>	<b>103</b>
<b>7</b>	<b>Summary &amp; Conclusions</b>	<b>109</b>
	<b>References</b>	<b>111</b>
	<b>Errata</b>	<b>117</b>
	<b>Abstract</b>	<b>119</b>
	<b>Curriculum Vitae</b>	<b>123</b>



*"Vidit Alcor at non Lunam plenam."*

Arabian proverb, Latin translation (Wallis, J. 1693).



# Chapter 1

## Introduction

The discovery of extrasolar planets<sup>1</sup> has led to a scientific gold rush during the past two decades (e.g. Campbell et al. 1988, Dumusque et al. 2012, Mayor & Queloz 1995, Wolszczan & Frail 1992). Hundreds of specimen orbiting all sorts of host stars are known to date (Schneider et al. 2011), with thousands of candidates waiting in line to be confirmed (e.g. Batalha et al. 2013, Borucki & Koch 2011). Many scientific disciplines from astronomy over geophysics and chemistry to meteorology are nowadays involved in the attempt to find new exoplanets and explain the properties of the discovered ones. An especially intriguing question in this respect is, of course, whether we will find evidence for life as we know it on other worlds. The field of exobiology has, thus, been established to provide suggestions on how to trace possible extra-terrestrial life-forms. This is, however, a tricky endeavor. Even the prerequisites for life on Earth are hard to pin down (Benner 2010). Accounting for alien environments, e.g. greater surface gravity on an exoplanet heavier than our Earth, differences in insolation and atmosphere or climate variations caused by a changing planetary orbit make this task rather challenging (Lammer et al. 2011). Increased stellar UV flux for instance, may prove adverse to surface inhabitants (Buccino et al. 2006), but might not matter so much for deep-sea life forms or subsurface ocean dwellers. The scientific consensus today seems to require a planet to support liquid water on its surface as well as to show a certain degree of climatic stability in order to be considered capable of hosting life as we know it. Planets that fulfill such criteria are called "habitable". Investigations on where to find such exoplanets have become more and more intricate over the years showing that habitability research is a very active scientific field, see section 1.2. Up until now, most resources have been devoted to looking for terrestrial planets around single stars. Yet, the implicit assumption that a second Earth may be found in an analogon to our Solar System is, perhaps, unnecessarily restrictive. Observational evidence shows that stellar multiplicity, for instance, does not prevent the existence of planets (Roell et al. 2012, Welsh et al. 2012). Since more than half of the F and G type stars in the solar neighborhood are members of stellar multiple systems (Duquennoy & Mayor 1991, Raghavan et al. 2010), such constellations should not be ignored in the search for habitable worlds. The discovery of a telluric planet in the double star system  $\alpha$ -Centauri AB (Dumusque et al. 2012) emphasizes this point<sup>2</sup>.

Given the number of potential targets for observation campaigns, an efficient way of identifying systems that could harbor habitable worlds is needed to guide observational efforts. Of

---

<sup>1</sup>Extrasolar planets (exoplanets) are planets orbiting other stars than our Sun.

<sup>2</sup>The  $\alpha$  Centauri system is generally thought to contain more than two stars. Proxima Centauri, however, is so far away from the AB binary that its actual membership to  $\alpha$  Centauri is debatable (Wertheimer & Laughlin 2006).

## 1. INTRODUCTION

---

course, determining habitable zones for Earth-like planets in binary star systems requires the synthesis of several astrophysical aspects. The influence of the combined radiation of both stars on the planet has to be considered. A planet's insolation is strongly linked to the evolution of its orbit which makes a detailed understanding of the gravitational interactions between the binary star and the planet essential. Naturally, the dynamical stability of the system needs to be confirmed as well.

It is the aim of this work, to develop an analytic framework that will allow a quick assessment of binary star systems regarding their potential for harboring habitable Earth-like planets. Hereby, the focus will be put on circumstellar (S-Type) configurations (Dvorak 1984) in which the planet orbits one star only, as these are thought to be the most abundant in the solar neighborhood (Duquennoy & Mayor 1991, Eggleton 2006). Such a method is presented in chapter 2 and applied to nearby binary star systems in chapters 3 & 4. It will also be shown in chapter 3 that habitable Earth-like planets might, in fact, be easier to spot in binary star systems than around single stars. Chapter 5 contains an extensive discussion on the advantages and restrictions of the proposed analytic method while chapter 6 points out possibilities to apply and improve the established analytic methodologies in future. The chapter at hand provides the necessary background as well as an introduction to the relevant physical and mathematical concepts. A brief summary (chapter 7) concludes this thesis.

### 1.1 Binary Stars

The phenomenological observation that some stars appear to be much closer on the sky than others can be traced back several thousands of years. The explicit mentioning of the Pleiades in the Homer's Iliad and Odyssey (Laoupi 2006), as well as their occurrence in the Christian Bible (Driver 1956) support this notion. One of the most impressive artifacts that can be interpreted to show the uneven distribution of stars in the night sky is doubtlessly the so-called "Sky Disc of Nebra", which has been dated to 1600 BC (Müller 2004, Pernicka & Wunderlich

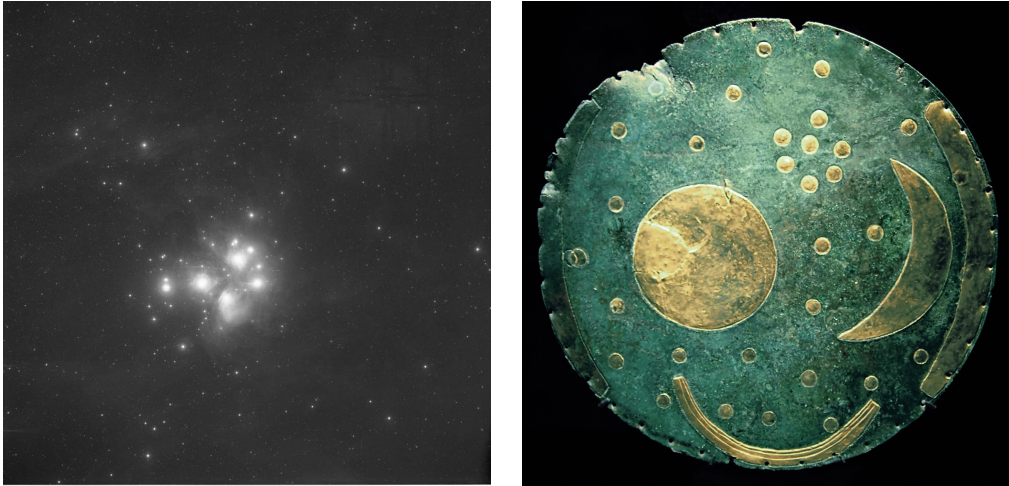


**Figure 1.1:** *Left:* The Pleiades (M 45) in J-band. Image credits: CDS-Aladin, POSSI 1986. *Right:* The Sky Disc of Nebra (Himmelsscheibe von Nebra). Assuming the small golden dots represent stars, the grouping of stars in the upper right quadrant can be interpreted as a multiple star system, perhaps the Pleiades (Müller 2004). Image credits: Rainer Zenz, creative commons license.

2002), see Figure 1.1.

Seemingly close associations encompassing more than one star are generally referred to as *multiple star systems*. The special case of two stars flocking together will be referred to as double star system or simply *double star*. Identifying multiple star systems observationally is not a trivial task, since configurations that look close on the plane of the sky might not be physically close at all. One such example is  $\alpha$ -1/2 Capricorni, see Figure 1.2. While this association seems like a perfectly nice example for a double star, its constituents are separated by roughly 200 pc. Cases which only seem to be close from an Earth based observer’s perspective are called *optical doubles* or *virtual double stars*. It took Sir Frederick William Herschel about 25 years to collect enough data on double stars to support his hypothesis that some of them do not only appear to be close. In fact, he could show that the mutual gravitational attraction between close stars had altered their apparent relative positions on the sky (Herschel 1803). Herschel named double stars which were so close that their gravitational attraction was sufficient to put them on a mutual orbit *binary stars*, or *binaries*. This thesis will focus on binaries, especially those with mutual separations smaller than 50 au will be of interest to us. Among such, a variety of observationally motivated classifications exist, such as *visual double stars*<sup>1</sup> or *spectroscopic binaries*<sup>2</sup>. Furthermore, there are *interferometric double stars*, *astrometric binaries* and *common proper motion pairs*<sup>3</sup> which are all classified after the method used to expose them as members of a binary or a multiple association (Mullaney 2005).

From an astrophysical standpoint, the most relevant distinctions are probably the stars’

<sup>1</sup>Visual double stars can be optically separated with telescopes, but they do not necessarily have to be physically close.

<sup>2</sup>Spectroscopic binaries are stars so close that they cannot be resolved optically. A distinction between the two stellar components is only possible, if e.g. RV variations in their common spectrum can be observed.

<sup>3</sup>Stars that exhibit the same direction of motion with respect to the Earth are called proper motion pairs.



**Figure 1.2:** *Left:* a J-band image of the virtual double star  $\alpha$ -1/2 Capricorni. The two stars seem to form a binary systems, but they are separated by roughly 200 pc. Image credits: CDS-Aladin, SERC 1979. *Right:* The Big Dipper’s multiple system Alcor (left) and Mizar (right) captured in the E-band. They constitute a proper motion pair and both Alcor *and* Mizar are binary stars themselves (Mullaney 2005). Image credits: CDS-Aladin, POSSI 1953. Projected distances on the sky alone are not sufficient to provide evidence as to which systems are actually multiple, and which systems only appear to be multiple.

## 1. INTRODUCTION

---

mass and luminosity ratios, as well as their true mutual distance. The latter determines in which ways the stars will interact with each other. Close stars will experience tidal forces that can change their shape as well as their mutual orbit (Zahn 1989). If the stars are very close and their radii extend beyond the so-called Roche lobes<sup>1</sup> they can exchange material. This in turn can alter not only their spectral and photometric signatures, but it can ultimately lead to a common evolution different from their single-star main sequence counterparts (Eggleton 2006). Such arrangements are referred to as *contact binaries*.

Even if the stars are not close enough to exchange material directly, interactions with stellar winds and tidal deformations can lead to observable changes in their spectra and/or light curves. Only beyond a separation of approximately 10-12 au can a G2V-G2V binary be regarded as consisting of two separate stars, which evolve independently of each other (Eggleton 2006). For circumstellar planetary systems (S-Type), which have been chosen as the main targets of this thesis, the assumption of the two stars having properties close to their single star counterparts is reasonable. This will allow us to apply the globally averaged habitability estimates by Kasting et al. (1993), Underwood et al. (2003) and Kopparapu et al. (2013) later on, which were derived assuming a planet receives insolation from a single ZAMS star<sup>2</sup>. Furthermore, tidal interactions between the stars as well as GR effects can be neglected at such distances, which simplifies the construction of analytical estimates.

Binaries are not only interesting objects to study in their own right, they also offer the only direct access to measuring stellar masses. These can be gained either by combining astrometric, parallaxic and radial velocity measurements<sup>3</sup> of binary stars (Torres et al. 2010), or by observing light curves of eclipsing binaries and merging them with stellar atmosphere models to determine effective temperatures as well as the stars' mutual distance<sup>4</sup> (Eggleton 2006). Conversely, if the stars' properties have been derived via theoretical models, the binary's orbital motion offers the unique chance to test the validity of these models, or separate observed binaries in well modeled and poorly measured/understood sub-groups (see chapter 4).

Another good reason to be interested in binary and multiple star systems is their relative abundance. More than 50% of the Sun-like stars in the solar neighborhood seem to be members of multiple systems (Duquennoy & Mayor 1991, Raghavan et al. 2010)! This result has been confirmed by recent SPH simulations<sup>5</sup> of star-cluster formation from interstellar gas-clouds (Bate 2012). In fact, some studies propose that initially most - if not all - of the stars in the galactic field form in associations of binary and multiple systems (Marks & Kroupa 2011). Single stars would then be a mere byproduct of dynamical relaxation of newly formed multiple systems. Such dynamical relaxation processes are also known to "harden" existing binaries over time, i.e. to shrink their semimajor axes (Bate 2012, Hut 1985), especially if the formation clusters are relatively large. Yet, very tight binary systems do not allow for circumstellar planetary motion (Holman & Wiegert 1999, Pilat-Lohinger & Dvorak 2002, Rabl & Dvorak

---

<sup>1</sup>Roche-lobes are the regions in which a star's material is gravitationally bound to its core.

<sup>2</sup>The restriction to zero age main sequence stars comes from the fact that AGB stars might evolve into a rapid state of atmosphere and mass loss (van Winckel 2003). Such effects are not accounted for in the planetary atmosphere treatment by Kasting et al. (1993), Underwood et al. (2003) and Kopparapu et al. (2013).

<sup>3</sup>See chapter 3 for a quantitative description of these procedures.

<sup>4</sup>If the double star's mutual distance is small, relativistic and tidal corrections have to be applied to the Keplerian motion.

<sup>5</sup>Simulations describing star formation require the modeling of hydrodynamical processes on vastly different length- and density-scales. This makes the use of grid based codes impractical. In order to deal with similarly asymmetric hydrodynamical problems, Gingold & Monaghan (1977) developed a method based on N-body approaches, where hydrodynamical properties are attributed to particles. Modeling observables such as pressure and density require the particles to be smoothed over finite regions of space - hence the name smoothed-particle hydrodynamics (SPH).

1988). Also, binary stars with spectral classes F-M<sup>1</sup> are the most interesting to be investigated with respect to habitability, because their relatively long lifetime supports a sustainable climate on planets within HZs over gigayears (Kasting et al. 1993). Thus follows the question: Are there any systems left containing F-M stars which have semi-major axes large enough to allow for dynamically stable circumstellar planets?

As it turns out, the current distribution of binary periods for F and G dwarfs actually peaks between  $10^4$  and  $10^6$  days (Duquennoy & Mayor 1991, Eggleton 2006, Heintz 1969). This roughly corresponds to semimajor axes between 10 and 150 au which is wide enough for stable circumstellar planetary motion to occur (see section 1.3.1). In chapter 2 we will make use of this result when selecting fictitious systems to test our analytical method.

The fact that binaries with relatively wide separations do exist in our stellar neighborhood may also indicate that this area of our galaxy is fairly calm as far as interstellar dynamical interactions are concerned. This is an important condition for habitability, since the long lifetime of a planet's host star may not be very helpful if the planet is ejected during a stellar scattering event. Stellar encounters are a valid concern for habitable worlds in single as well as multiple star systems. Other conditions for worlds to be habitable are discussed in the following sections.

## 1.2 Habitable Zones

### 1.2.1 Coining the Term

Predating the discovery of the first exoplanet by roughly three decades, Huang (1959) is now credited with introducing the term "habitable zone". Originally a habitable zone was defined as the region around a star where: "... The heat received by the living beings on a planet must be neither too large nor too small. ..." (Huang 1959). It is not hard to imagine that this statement has motivated the colloquial use of "Goldilocks Zone"<sup>2</sup> for regions around a star where a planet such as our Earth is supposed to be able to support life. Although Huang (1959) gave first analytical estimates on the approximate extent of such a circumstellar region, his predictions on how much radiation a planet had to receive in order to stay at "just the right temperature" were necessarily vague. The following decades have seen a great number of studies aimed at proving that - unlike the porridge in the fairytale of Goldilocks - the extent of habitable zones around stars including our Sun is not a mere matter of taste.

### 1.2.2 Defining Habitability

Dole (1964), for instance, claimed habitability for a planet on which more than 10% of the surface had a mean temperature between  $0^\circ\text{C}$  and  $30^\circ\text{C}$ . Also, he postulated that temperature extremes should not exceed  $-10^\circ\text{C}$  or  $40^\circ\text{C}$ , as such conditions seemed appropriate for human habitation.<sup>3</sup> In contrast, Hart (1978, 1979), Kasting (1988), Rasool & de Bergh (1970) and Kasting et al. (1993) relied on the concept of liquid water on a planet's surface as an indicator for habitability. Some advocate other rules and possibilities for a life sustaining environment. Buccino et al. (2006) for instance suggest to take the impact of UV radiation on lifeforms

<sup>1</sup>For a detailed discussion on the current issues with habitable planets around M-stars see chapter 4.

<sup>2</sup>In the fairy tale "The Story of the Three Bears" a little girl called "Goldilocks" wanders into the home of three bears and, since she is hungry, tries from the three bowls of porridge standing on the kitchen table. After finding that the content of one bowl was too hot and another was too cold, she finally came across a porridge that was "just right".

<sup>3</sup>Climate records for Earth indicate that extreme temperatures can easily surmount  $50^\circ\text{C}$  and be as low as  $-89^\circ\text{C}$ . (<http://www.ncdc.noaa.gov/oa/climate/globalextremes.html>, retrieved 12.02.2013)

## 1. INTRODUCTION

---

more seriously. Lammer et al. (2009) allow for life in subsurface oceans below ice mantles and Schulze-Makuch & Irwin (2004) postulate that it is necessary to expand our search-parameters to biochemistries altogether different from ours based on solvents other than water. In the end, the "liquid surface water" criterion has become the standard against which planetary habitability is measured. Yet, the fact that we consider water to be a necessary ingredient for life as we know it (Des Marais et al. 2002) is not the only reason for the predominance of the liquid surface water hypothesis. Vast amounts of surface water such as we encounter on Earth also play an important role in stabilizing a terrestrial planet's climate (Kasting 1988). This is due to the fact that on the one hand water does have a considerable specific heat capacity [ $\simeq 4\text{kJ}/(\text{kg K})$ ] allowing oceans to regulate local as well as global temperatures effectively. On the other hand, water vapor in the atmosphere interacts with visible and near infrared light and can, thus, act as a greenhouse regulator trapping Earth's thermal radiation while reflecting visible Sunlight (Kaltenegger et al. 2007). Using a convective radiation balance model (RBM) which included the most fundamental photochemical and physical processes Kasting (1988) found, that an Earth-like planet's surface temperature was much more sensitive to the amount of water vapor in the atmosphere than to  $\text{CO}_2$ . If the amount of water vapor changes drastically via photochemical reactions, weathering or thermal forcing such as high (effective) insolation, strong climatic changes can be expected.

### 1.2.3 Kasting's Approach

Following this line of thought, Kasting et al. (1993) established boundaries for habitable zones around main sequence stars by investigating the changes in a planet's atmosphere that follow from alterations in the amount and spectral distribution of stellar insolation. To be more precise, Kasting et al. (1993) were looking for insolation thresholds that would lead to climatic runaway states on a terrestrial planet with an initially Earth-like atmosphere. Runaway states are unstable climatic conditions in which small changes in insolation are no longer buffered by the atmosphere. Such processes generally lead to extreme surface temperatures (Spiegel et al. 2008). Known runaway states include, for instance, a total evaporation of surface oceans, which would lead to photo-dissociation of water-molecules in the upper atmosphere and, ultimately, cause a sever loss of hydrogen to space. The opposite runaway process starts with a complete freeze-out of all greenhouse gases in the atmosphere resulting in a high surface albedo due to (water and  $\text{CO}_2$ ) ice. This, in turn, will cause a rapid drop in planetary surface temperatures leading to so-called "snowball states", see Figure 1.3.

Using the spectral type and luminosity of a main sequence star, Kasting et al. (1993) and later Selsis et al. (2007), Underwood et al. (2003) and Kopparapu et al. (2013) were able to derive habitable zone limits for planets on circular orbits around their stellar hosts:

$$d = 1 \text{ au} \left( \frac{L/L_{\odot}}{S_{eff}} \right)^{0.5} \quad (1.1)$$

where  $d$  is the planet's distance to its host star, and  $L$  is the host star's luminosity. The parameter  $S_{eff}$  represents the normalized stellar flux at a distance of 1 au, which allows a planet to maintain a given surface temperature. The interaction between a planet's atmosphere and the incoming stellar radiation is a highly complex process involving radiative transfer, scattering and photo-chemistry. Therefore, a numerical treatment is required in all but the most rudimentary studies. Combining the effects of insolation quantity and quality on a planet's atmosphere in a single parameter, namely  $S_{eff}$ , Kasting et al. (1993) provide numerically determined  $S_{eff}$  values for three given stellar spectral types, and for the inner and outer borders of the respective habitable zones. In other words, Kasting et al. (1993) found threshold insolation values for



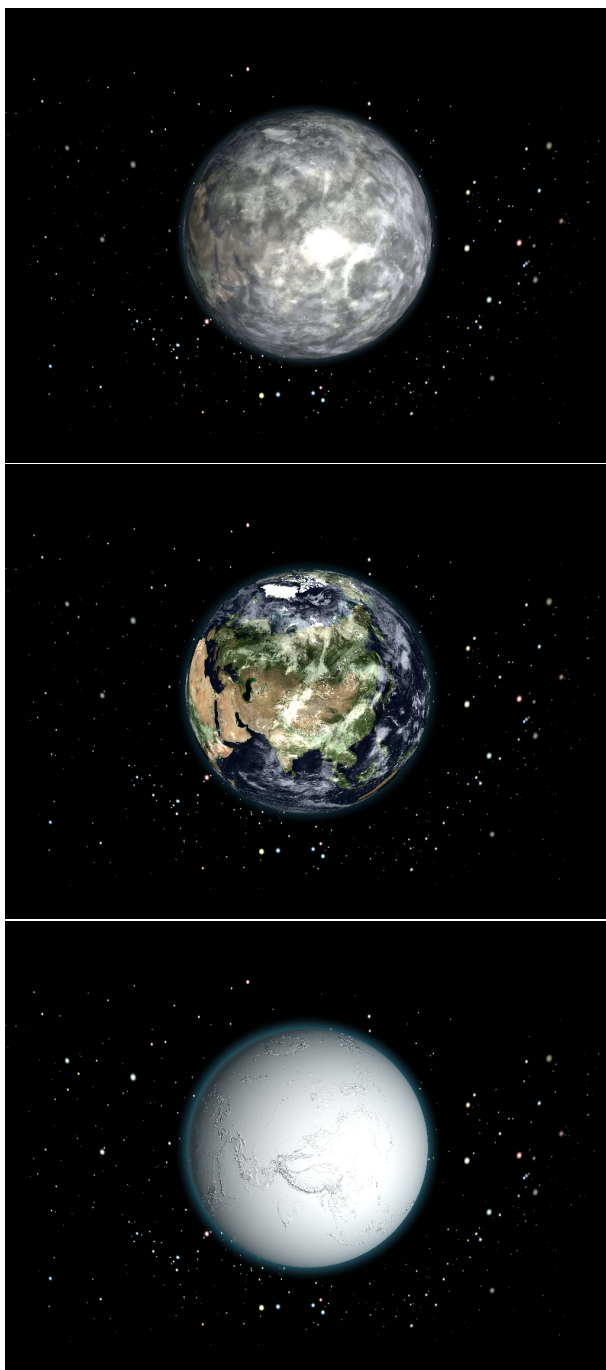


**Figure 1.3:** Concepts of climatic runaway states for an Earth-like planet following Kasting et al. (1993). *Top:* A planet orbits too close to its host star, i.e. beyond the inner border of the habitable zone. A complete evaporation of its oceans followed by a quick rise in surface temperatures might be the consequence. *Mid:* If the planet remains within habitable insolation boundaries, oceans and greenhouse gases such as water vapor and  $\text{CO}_2$  can stabilize its climate. *Bottom:* Too little insolation and all greenhouse gases will freeze out leaving the atmosphere more transparent in the infrared (IR) spectrum. This in turn will cause an even faster decline of surface temperature, since the peak of Earth's thermal radiation lies in the IR. Texture credit NASA Visible Earth (<http://visibleearth.nasa.gov>).

## 1. INTRODUCTION

---

different kinds of stars that would cause an Earth-like atmosphere to be captured into a runaway state. Whereas it is straight forward to see that different amounts of insolation are required to vaporize oceans or cause a complete freeze-out of atmospheric greenhouse gases, the role of stellar spectral classes might not be so obvious. Roughly speaking, one could say that, if both G and M stars had the same luminosity, an M star's effect would be much more pronounced on the Earth's climate. An M star's spectrum is shifted towards the red end of the spectrum compared to a G star. Earth's current thermal radiation curve also rises towards the red end of the visible spectrum and peaks in the infrared (IR). Kirchhoff's radiation law tells us that the spectral bands in which a body radiates its thermal energy most effectively are also the wavelengths where it absorbs radiation most efficiently. Due to the fact that the M star's spectral properties are more similar to the Earth's, an M star could feed the planet more energy than a G star assuming both had a similar energy output. A listing of effective insolation limits for F, G and M stars is given in chapter 2, Table 1.

Applying the climatic collapse conditions of runaway greenhouse (evaporating oceans) and maximum greenhouse (CO<sub>2</sub> freeze-out) to the Solar System will put the habitable zone between 0.84 au and 1.67 au (Kasting et al. 1993). Recent estimates by Kopparapu et al. (2013) corrected these values to 0.97 au for the inner and 1.70 au for the outer border of the Solar System's HZ. If the Earth was in the vicinity of Mars, these results would mean that it could still be habitable assuming a best-case greenhouse scenario. Due to its reduced luminosity, an M-class star would only support habitable worlds within distances between roughly 0.03 au - 0.5 au. Although Kasting's has become the most widespread approach, the values given in Kasting et al. (1993) are by no means strict limits. For one, Kasting et al. (1993) themselves give alternate borders if for example the onset of water loss was chosen over collapse states. Also, the limits presented are snapshots of stars on the zero age main sequence (ZAMS). When host-stars evolve, their luminosities change and so do their habitable zones. As a consequence, stellar spectral types younger than F-class are mostly excluded in the search for habitable worlds, since their lifetimes are deemed to be too short for complex life to evolve. For this purpose, Hart (1979) introduced the concept of the Continuously Habitable Zone (CHZ), i.e. the region around a star where a planet could hold liquid surface water despite the changes in luminosity due to stellar evolution. Hart (1979) gives very strict limits for the CHZ ( $d_{outer} - d_{inner} = 0.046$  au), but CHZs by Kasting et al. (1993) are about 4-20 times broader.

### 1.2.4 Habitability after 1993

In spite of the popularity of Kasting's approach, many points of critique have been raised over the past decades. The following arguments reside among the most prevalent:

- Convective RBMs can only account for globally averaged climates. They can neither model local surface temperature variations such as polar ice caps and equatorial deserts which are present on Earth, nor can they account for dynamical heat transport in the atmosphere except for convection, see e.g. Spiegel et al. (2008), Williams & Kasting (1997).
- Long term geophysical effects such as vulcanism, the carbon-silicate cycle, and biological factors binding or releasing large amounts of greenhouse gases are unsatisfactorily modeled or not considered at all, see for instance Franck et al. (2000), Williams & Kasting (1997).
- Planetary orbits were believed to be circular and remain so. Variations in planetary insolation due to eccentric orbits was not accounted for (Dressing et al. 2010, Spiegel et al. 2010, Williams & Pollard 2002).

- Star-planet interaction may encompass more photochemical and physical long-term effects, such as water loss through increased stellar extreme UV (XUV) or X-ray radiation. High rates of such non-thermal radiation is believed to be common among M-stars, see e.g. Lammer et al. (2011).
- The proposed concept of CHZs was based on the assumption that Earth’s atmosphere was roughly composed of the same constituents throughout its existence. This is not the case. At some point in history CO<sub>2</sub> and CH<sub>4</sub> seem to have been much more abundant (Kaltenegger et al. 2007), which might have compensated for a faint young Sun. Also continuous habitability over 4.5 Ga might not be necessary for life to evolve on a terrestrial planet. In fact, current studies date the first occurrence of life back to roughly 1.5 Ga after the Earth’s formation, see e.g. Gaidos et al. (2005) and references therein.

Especially after Laskar & Robutel (1993) showed that an Earth-like planet without a large moon can be subjected to chaotic changes in its obliquity, questions arose in what way the orientation of the Earth’s rotation axis influences a planet’s climate<sup>1</sup>. Even though the most simple RBMs are able to predict the occurrence of stable snowball and warm states for an Earth-like planet, they can only provide global and temporal averages independent of the planet’s spin rate and obliquity (Spiegel et al. 2008). Consequently, Williams & Kasting (1997) used a more sophisticated zonally averaged (latitudinal) energy balance model (EBM, LEBM) so that the influence of changes in a planet’s spin axis could be studied, see Figure 1.4. They found that the temperature extremes rise rapidly with high planetary obliquities, a result which was confirmed also for cases of eccentric planetary orbits (Dressing et al. 2010, Williams & Pollard 2002). However, Williams & Kasting (1997) admit that very crude approximations were made, in order to account for dynamical weathering and climate effects that would best be modeled with a general circulation model (GCM). GCMs do not require implicit averages such as RBMs and LEBMs. They can take full atmospheric dynamics, photochemistry and anisotropies in land-ocean distribution into account. Some atmospheric phenomena can only be studied via GCMs. The exact patterns of thermal redistribution influenced by Coriolis forces or the climatic behavior over realistic continent-ocean boundaries are only two examples. In fact, GCMs are essential for studying atmospheric circulations in planets close to a tidally locked rotation state<sup>2</sup> (Edson et al. 2011). Yet, these enhanced capabilities come at a cost. High computational resource requirements, many system parameters as well as the demand for a large number of initial and boundary conditions make GCMs powerful but capricious tools.<sup>3</sup>

The increasing complexity of models can also make it difficult to reproduce results convincingly via other approaches. Applying an LEBM Dressing et al. (2010), for instance, tried to find the same dependency of global mean temperatures on orbital longitudes as presented in Williams & Pollard (2002) who were using a GCM in their investigation. Dressing et al. (2010) did find a qualitatively similar behavior of the peaks of global mean temperatures that were produced via LEBMs and GCMs, but there were shifts by as much as 60° in orbital longitude. Also, the relative differences in peak global mean temperatures for lower eccentricities could reach up to 25%. Dressing et al. (2010) stated that the encountered deviations were probably due to the continent of Antarctica, which introduced asymmetries in Williams’ and Pollard’s simulations that could not be accounted for in LEBMs. This introduces another point worth considering. A large number of initial and boundary conditions are required for simulations

<sup>1</sup>The results by Laskar & Robutel (1993) were recently confirmed by Lissauer et al. (2012), although the latter group did not find that the changes in Earth’s obliquity are as drastic as pointed out in Laskar & Robutel (1993).

<sup>2</sup>For a brief discussion of tidal lock states see chapter 4, section 7.

<sup>3</sup>As John von Neumann allegedly put it: ”With four parameters I can fit an elephant, and with five I can make him wiggle his trunk.” (Dyson 2004)

## 1. INTRODUCTION

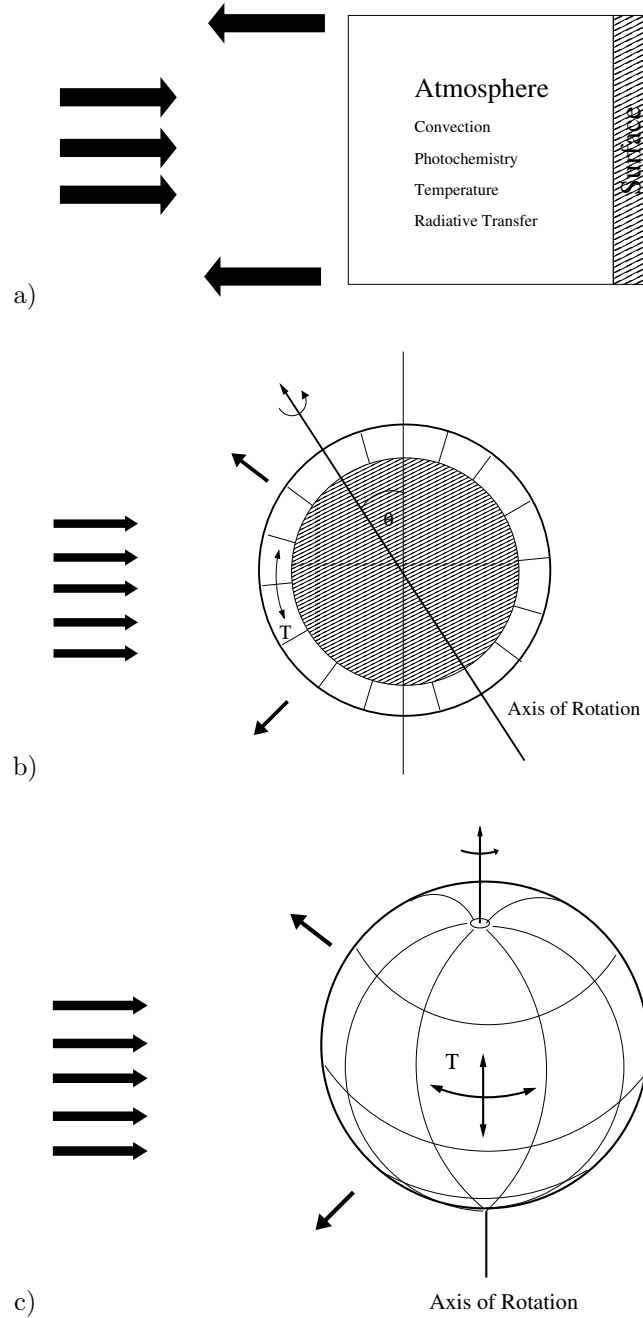


**Figure 1.4:** a) A convective radiation balance model (RBM). Surface temperatures are iteratively modified until the atmosphere is in radiative equilibrium. The energy irradiated by the planet is of thermal nature and generally peaks at longer wavelengths than the incoming Sunlight. Atmospheric photochemistry, radiative transfer and convection are taken into account. No regional differences in surface or atmospheric conditions can be modeled.

b) A latitudinal energy balance model (LEBM). Additionally to the processes accounted for in the RBM models, latitudinal differences in atmosphere and surface properties, such as polar caps or ocean bands, can be described. LEBMs are zonally averaged, i.e. only mean longitudinal values and processes can be modeled.

c) A general circulation model (GCM). Longitudinal as well as latitudinal processes can be modeled. GCMs are the most complex of the three models, but they can account for all major atmospheric effects.

supporting a high level of detail. Currently, those can only be acquired from the one planet that is known to be habitable with certainty - the Earth. Basing our estimates for habitable zones around other stars on models which resemble the Earth in more and more detail might, perhaps, introduce an unnecessary bias of our search towards exact Earth-clones. A third point of critique has roots in meteorology. Lorenz (1963) showed that atmospheric processes can be strongly dependent on initial conditions. In models featuring complex dynamics individual results may be hard to interpret. Hence, probabilistic approaches are required, which will again increase computational demands.

Be that as it may, a careful application of LEBMs and GCMs can offer vital insights into planetary atmospheric dynamics, if detailed parameters are available. Kasting's idea of defining habitable zone borders via atmospheric greenhouse and freeze-out runaway states has, for instance, been generalized using LEBMs and GCMs. In fact, many more possible climatic collapse scenarios were discovered. These include photochemical collapses (Lorenz et al. 1997, Zahnle et al. 2008), atmospheric collapses (Haberle et al. 1994), ice-albedo feedback (Roe & Baker 2010), ocean thermohaline circulation bistability (Epica Community Members et al. 2006, Stommel 1961), as well as enhanced sub-stellar weathering instabilities and sub-stellar dissolution feedback in tidally locked planets (Kite et al. 2011). Thus, runaway greenhouse effects might not be the only instabilities worth considering in order to determine habitable zones. On top of that, LEBMs and GCMs can be used to model and predict observable properties of exoplanets via their thermal phase curves, see e.g. Selsis et al. (2011).

In summary one can say that the introduction of more intricate models has also made the issue of determining habitability more complex. Nowadays, many parameters such as planetary obliquities, rotation rates and the initial percentage of ice, ocean and cloud coverage should be considered, if one wants to investigate planetary habitability in detail. The inclusion of a greater number of atmospheric processes in modern models has also helped to identify numerous scenarios that can cause a planet to become inhospitable. While such detailed approaches allow for more accurate investigations of selected cases, top level guidance on where to look for potentially habitable worlds seems harder and harder to come by. This might be one of the reasons why Kasting's way of determining habitable zones is still so frequently used. Given the recent updates of effective insolation values for main sequence stars (Kopparapu et al. 2013, Selsis et al. 2007, Underwood et al. 2003) the popularity of the method by Kasting et al. (1993) is unlikely to fade any time soon. Consequently, it is all the more important to construct a supporting framework that is capable of taking variations in a planet's orbit into account. Why such a feature is desirable will be discussed in the following section.

### 1.2.5 Habitability of Planets in Binary Star Systems

In contrast to the case of the Earth in the Solar System, where the Sun is the only stellar radiation source and the gravitational perturbations on the Earth's orbit by the other planets are relatively small, terrestrial planets in binary star systems experience a much more variable radiative environment. The combined radiative and gravitational influence of a second star can lead to considerable changes in planetary insolation (see chapter 2), and the additional issue of dynamical stability of the system adds another degree of complexity to this problem. Despite such difficulties it took Su-Shu Huang only one year after introducing the concept of the habitable zone to publish his first results on habitable planets in binary star systems. Huang (1960) gives analytical estimates on the extent of the circumstellar as well as circumbinary habitable zones using results from the analytical treatment of the circular restricted three body

## 1. INTRODUCTION

problem (CR3BP)<sup>1</sup> and observations of the stability limits for satellites in the Solar System. Thus, he was among the first to unite radiative considerations with dynamical ones in order to investigate the existence of dynamically stable habitable planets in binary star systems. Of course, his method is severely limited, because it can neither account for a binary's, nor for a planet's orbital eccentricity. Especially the latter is playing an important role for habitability in double star systems (see chapter 2, section 4). Furthermore, he could not give precise insolation values for the borders of his habitable zone, so that up to Kasting et al. (1993) habitable regions were more or less defined as regions where a planet receives comparable thermal input to the Earth's in the Solar System. Nevertheless, for an Earth-like planet to be habitable in a G2V-G2V binary, Huang (1960) predicts an orbital separation for of at least 4.22 au for the stars, if the planet orbits one star in a distance of 1 au. This is fully compatible with results from the method proposed in chapter 2, see Figure 1.5.

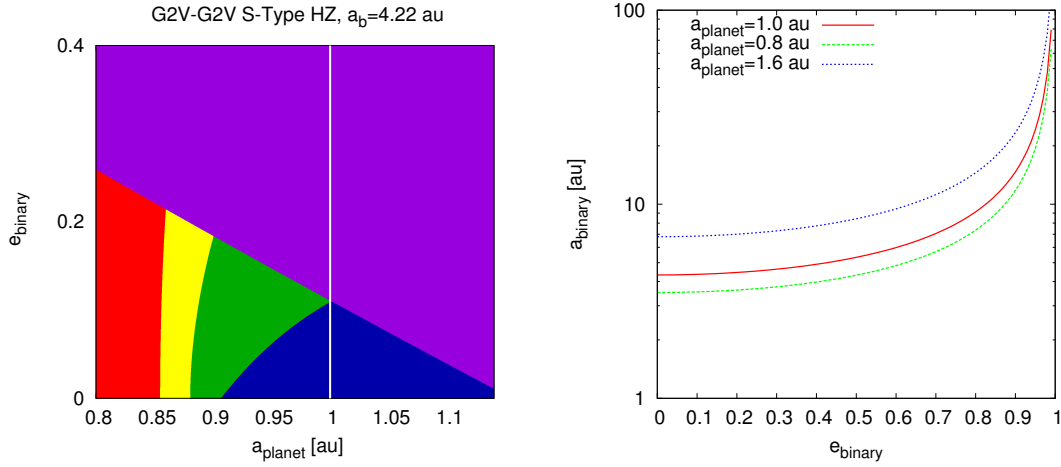


**Figure 1.5:** *Left:* A so-called "habitability map" of an Earth-like planet in a planar G2V-G2V binary star system with a semimajor axis of  $a_2 = 4.22$  au is shown. The planet's semimajor axis with respect to the primary is drawn on the x-axis; on the y-axis the binary's eccentricity is shown. Red colors indicate that the planet either receives too much or too little radiation to be habitable. Blue colored parameter-regions are permanently habitable, if Kasting's maximum and runaway greenhouse radiation boundaries are assumed (Kasting et al. 1993). Yellow and green regions denote Averaged and Extended habitable zones as defined in chapter 2, section 5. Purple areas are dynamically unstable (Holman & Wiegert 1999, Pilat-Lohinger & Dvorak 2002). Huang (1960) predicts that a planet at 1 au - indicated by the white vertical line - can be habitable in such a configuration, if the binary's orbit is circular  $e_{binary} = 0$ . As the white line lies well within the permanently habitable area (blue), both models are in good agreement. *Right:* Critical binary semimajor axis as a function of binary eccentricities according to Harrington (1977). Minimum binary distances for habitable planets on fictitious circular orbits at 0.8, 1 and 1.6 au with respect to their primary are shown. Applying Harrington's model, the minimum binary distance for an Earth-like planet at 1 au to be habitable is  $a_{binary} \geq 4.3$  au. Consequently, all three models produce comparable results where their domains of applicability overlap.

Among the few articles that followed Huang (1960), Harrington (1977) found that the insolation - and with it the mean temperature of Earth - fluctuated due to the dynamical interactions

<sup>1</sup>A massless particle moves in the gravitational field of two celestial bodies represented by point-masses on a circular orbit around their common center of gravity.

of the planet with the binary. Applying a numerically derived stability criterion for planar non-restricted three body problems, he was able to give a semi-analytic estimate for planetary habitability in binary star systems, where he took the binary's eccentricity into account. His estimate reads

$$\frac{(1 - e_2^2) (a_2^2 \sqrt{1 - e_2^2} - L_2)}{L_1} \geq F^2, \quad (1.2)$$

where  $a_2$  and  $e_2$  are the binary's semimajor axis and eccentricity and  $L_1$  and  $L_2$  denote the primary's and secondary's luminosities. The parameter  $F$  represents the numerically derived stability function and reads in our case

$$F = q_2/a_1 = \frac{7}{2} \left( 1 + \frac{7}{10} \log \left[ \frac{2}{3} \left( 1 + \frac{m_2}{m_0 + m_1} \right) \right] \right), \quad (1.3)$$

where  $q_2$  is the secondary's periastron distance,  $a_1$  is the planet's semimajor axis,  $m_0$  and  $m_2$  are the primary's and secondary's masses and  $m_1$  denotes the planet's mass. His prerequisites for habitability demand that a G2V-G2V binary star should have a semimajor axis of at least  $a_2 = 4.2$  au with  $e_2 = 0$  in order to allow for an Earth-like planet to be habitable at a distance of 1 au from its primary. Compared the methodology presented in this work, his estimates are rather conservative. Curiously, Harrington (1977) neglected the planet's eccentricity in his semi-analytical habitability estimates. Thus, he was implicitly assuming that the variations in planetary insolation encountered in his numerical investigations were due to the eccentric orbit of the second star. In chapter 2 we will show that the eccentricity of the planet's - not the secondary's - orbit has the most influence on insolation and, thus, on planetary habitability.

Before the discovery of the first exoplanet in a tight double star system named  $\gamma$  Cephei (Campbell et al. 1988, Hatzes et al. 2003, Neuhäuser et al. 2007) the study of habitable zones in binary stars systems could have been considered an academic exercise. As we now know of roughly 60 cases where planets orbit one star in a double star system, the interest in determining habitable zones within such configurations has risen dramatically. Similarly, the discovery of circumbinary planets via NASA's Kepler spacecraft has boosted interest in finding habitable zones for this type of planetary motion. Numerical insolation studies have been conducted for the systems Kepler-34 and Kepler-35, but with 0.76 and 0.73  $R_J$  those planets are neither Earth-like nor habitable (Welsh et al. 2012).

Not surprisingly, many studies on the topic of habitable planet formation (e.g. Guedes et al. 2008, Haghighipour et al. 2010, Haghighipour & Raymond 2007, Thebault 2011, Thébault et al. 2009, Whitmire et al. 1998) and stability (e.g. Dvorak et al. 2003, Haghighipour 2006, Sándor et al. 2007, Schwarz et al. 2009) followed the discovery of the first planet in a binary star system. Most of them focused on dynamical habitability, simply applying the limits by Kasting et al. (1993) to the primary star and investigating the system for regions of stable planetary motion. In chapter 2 we will see that especially in eccentric double star systems with semimajor axes  $a_2 < 50$  au, such an approach can lead to a considerable overestimation of the extent of the circumprimary habitable zone.

A similar problem was identified by Kane & Hinkel (2012) for planets in circumbinary orbits around double stars. Up until then, habitable zones for planetary systems discovered by the Kepler mission were either calculated numerically or estimated assuming a habitable spherical shell around the brightest star only. Kane & Hinkel (2012) could show that a "single radiation source" approach for such P-Type systems can lead to inaccurate habitable zone boundaries, especially for well separated stars of nearly equal luminosity. However, in their work they assumed the Keplerian motion of the binary stars and the planet to be decoupled. This is problematic, because Welsh et al. (2012) have shown that coupled dynamical effects can cause

## 1. INTRODUCTION

---

insolation variations up to 40% for a potentially habitable planet in the HZ of Kepler 35. Our approach for circumstellar HZs will take the dynamical as well as radiative interaction between both stars and the planet into account. See chapters 2 and 6 for details.

Recently, Forgan (2012) has investigated circumstellar habitability in the  $\alpha$  Centauri system applying LEBMs (see section 1.2.4). He included the radiative influence of the secondary, and considered a range of likely planetary eccentricities. Whereas the time averaged inner borders of  $\alpha$  Cen B's habitable zones are in very good agreement with our simple RBM model (see chapter 3, section 5), his outer borders are much more conservative. This is due to the fact that the studies presented in this thesis used a best case greenhouse scenario for the outer HZ insolation limits (see chapter 2, Table 1), whereas Forgan (2012) assumed an Earth-like atmospheric composition throughout his studies. Similar to the results presented in chapter 2 section 2, Forgan (2012) concluded that the primary's insolation is much more important than the secondary's. Only in systems with a secondary considerably more luminous than the primary one can expect a significant contribution of the second star to planetary insolation.

Doubtlessly, LEBMs can offer a more detailed picture of habitability fractions, i.e. of how much of Earth's surface would be habitable, and on the actual processes caused by the seasonal forcing. However, such investigations have to be conducted numerically, which makes them rather time consuming. Also, Forgan (2012) did not consider a consistent evolution of the terrestrial planet's eccentricity and obliquity. The consequences of such an omission are discussed in detail in section 5.7. One of the goals of this thesis is, therefore, the construction of a self-consistent analytical treatment of the problem of habitability of an Earth-like planet in circumstellar motion within a binary star system.

### 1.2.6 Galactic Habitability

Apart from habitability considerations at the solar/binary system level, there are also other prerequisites for the development and sustenance of planetary habitability. Stellar systems with low metallicity, i.e. systems where heavier elements than hydrogen and helium are rare might not be able to produce planets with atmospheres comparable to that of the Earth (Lineweaver et al. 2004). Sterilization due to near Super Novae might prove to be another issue for planets around stars in dense stellar regions such as in the vicinity of galactic center. In order to account for these effects the concept of the galactic habitable zone (GHZ) has been introduced (Gonzalez et al. 2001, Gowanlock et al. 2011, Lineweaver & Chopra 2012, Lineweaver et al. 2004, Prantzos 2008). Definite estimates on these exterior effects are, however, difficult to pin down and no common consensus on the GHZ borders has been established yet (Prantzos 2008). We will, therefore, assume that the binary star systems in our investigation are in the Solar System's galactic neighborhood, where all necessary conditions are fulfilled.

## 1.3 Orbital Dynamics

In order to be able to make analytic predictions on the habitability of a planet in a binary star system, the underlying dynamical problem must be understood and "tamed" - at least as far as such a thing is possible. Disregarding all physical properties except for the masses of the two stars and the planet, one immediately arrives at the celestial mechanic's constant plight and delight, the gravitational three body problem (3BP). No attempt is being made here as to discuss the gradual progress scientists have made over the last four centuries uncovering layer after layer of this pinnacle of problems in dynamical astronomy.<sup>1</sup> It is similarly futile to try to

---

<sup>1</sup>The problem of three point masses moving in their mutual gravitational fields is considered to be non-integrable. In other words, some solutions do exist for special cases, but no practical global solution to the problem has been



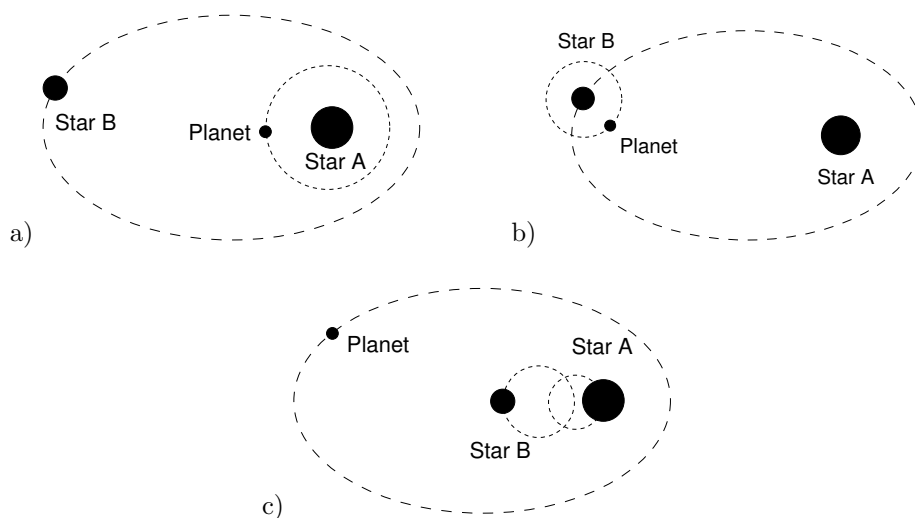


**Figure 1.6:** Observed types of planetary motion in a coplanar binary star system:  
a) S-Type A/I: Here, the planet orbits the more luminous binary star component.  
b) S-Type B/II: The planet orbits the less luminous star.  
c) P-Type: The planet orbits both stars.

list important literature on the topic, as such a list would probably require a volume of its own. We will, however, briefly discuss the fundamental results we will need later on in chapter 2. Following this principle, only one book on the 3BP is to be mentioned here on behalf of all the exquisite literature. The choice has been made according to the fact that we will be using results derived therein - not just because its title reads "The Three Body Problem" (Marchal 1990). In order to construct analytic estimates for planetary habitability in binary stars we require two things from orbital dynamics:

1. We need to find regions where the planet can orbit one or both stars without being ejected from the system or colliding with one of the stars.<sup>1</sup> A system where the planet will not be lost over a given number of binary periods (Dvorak 1986, Holman & Wiegert 1999) is henceforth referred to as being stable.
2. Analytic predictions on the orbital evolution of the planet and the two stars are necessary, since we want to track the combined insolation the planet receives from both stars. Perturbation theory will provide us with fine tools in this respect.

---

found so far. The Finnish mathematician Karl F. Sundman proved in 1912 the existence of a series solution for the 3BP. Unfortunately, the series' convergence is so slow that it is of little practical use. Therefore, approximate analytical and numerical methods are required to investigate this problem.

<sup>1</sup>While the problem of two body collisions in a three body system is quite common in reality - a good example is the case of Sun, Jupiter and the comet Shoemaker-Levi 9, it is not an easy problem in the idealized world of the 3BP. In the case of three point masses moving in their common field of gravity, collisions would lead to singularities, since the forces between the colliding bodies would become infinite. Such cases require regularization measures, see e.g. Stiefel & Scheifele (1975).

## 1. INTRODUCTION

---

### 1.3.1 Stability

Let us first focus on issue of dynamical stability. The three types of planetary motion in binary stars that have been observed in nature so far are (Dvorak 1984, Roell et al. 2012, Welsh et al. 2012, Whitmire et al. 1998):

**S-Type A/I:** The planet orbits the more luminous binary star component.

**S-Type B/II:** The less luminous star is the planet’s host.

**P-Type:** The planet orbits both stars.

Concepts of the three different types of planetary motion are presented in Figure 1.6. Since we excluded 1:1 resonant (Trojan) planetary orbits (Schwarz et al. 2009) the three bodies constitute so-called ”hierarchical triple systems”, meaning that two of the three bodies share a tight orbit, whereas the third body orbits the inner two on a wide ellipse. No close encounters or exchanges between the bodies on the inner and outer orbits are permitted. For very rough estimates on the stability of hierarchical binary-planet systems, the model of the restricted 3BP (R3BP) can be applied. In this approach, one assumes the planet to be a massless particle moving in the gravitational field of the two stars, which orbit their common center of gravity. Since the planet’s mass is very small compared to the stars of a binary, in the case of an Earth-like planet  $m_p/m_\star \approx 10^{-5}$ , such a simplification is permissible as long as we are satisfied with finding only approximate regions of orbital stability. It was briefly mentioned in section 1.2.5 that Huang (1960) has used results from the circular restricted 3BP (CR3BP) in his work on habitability of planets in binary star systems. This means that on top of considering the planet to be massless, the two stars are assumed to orbit their center of gravity on a strictly circular path.

The stability of a system modeled via the CR3BP can be checked by finding periodic orbits and investigate linear stability via Hill’s equation and consequently by means of Floquet theory. Erdi (1974) showed that this method is also applicable to the case of the elliptic restricted 3BP, i.e. for binaries on eccentric orbits. An alternative way is to simply study the system’s zero velocity curves (Szebehely 1967). In the CR3BP zero velocity curves are circumferences to regions which a test particle cannot access - a consequence of the existence of an integral of motion called the Jacobi Integral ( $C_J$ )

$$\dot{x}^2 + \dot{y}^2 + \dot{z}^2 = 2U(x, y, z, m_0, m_2) - C_J, \quad (1.4)$$

where  $\dot{x}$ ,  $\dot{y}$  and  $\dot{z}$  are the components of the test-planet’s velocity  $\mathbf{v}$  in a frame of reference co-rotating with the massive bodies. The problem’s potential,  $U$ , depends on the planet’s position and the masses of the primary ( $m_0$ ) and secondary ( $m_2$ ) respectively. The left hand side of this equation is positively definite, which limits the values for  $U$  and  $C_J$ . Zero velocity curves can now be defined by investigating the limit case where  $\mathbf{v} \rightarrow 0$ . It follows that

$$C_J = 2U(x, y, z, \mu) = x^2 + y^2 + 2\frac{1 - \mu}{\sqrt{(x + \mu)^2 + y^2 + z^2}} + \frac{\mu}{\sqrt{(x + 1 - \mu)^2 + y^2 + z^2}}, \quad (1.5)$$

with  $\mu = m_2/(m_0 + m_2)$ . This integral of motion confines the planetary orbit to a sub-manifold very much like the conservation of energy restricts the whole system’s trajectory in phase space. The size of the permissible region for the test particle depends on the binary star’s mass ratio and the planet’s initial conditions, see Figure 1.7. Unfortunately, such a Jacobi integral does not exist in the more general cases of the 3BP (e.g. Szebehely 1967, and references therein). However, it can be shown that stable hierarchical triple configurations in the 3BP are possible (e.g. Marchal & Saari 1975, and references therein). In a series of papers Szebehely (1977),

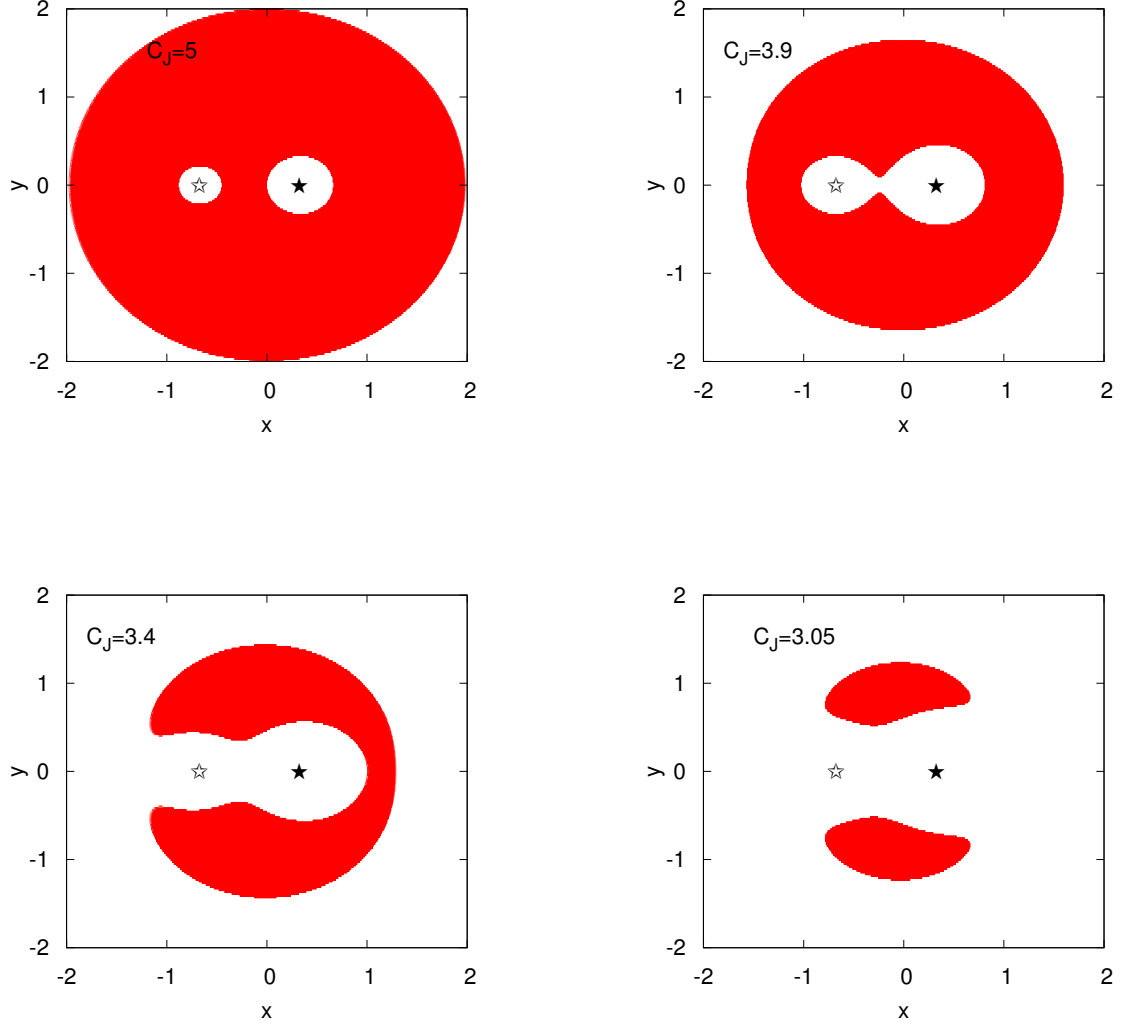


**Figure 1.7:** Forbidden regions (red) in the circular restricted three body problem found via zero velocity curves. A test planet can move within the white areas. The more massive and the less massive component of the binary star are represented by the full and open star symbols, respectively. The stars have a mass ratio of  $\mu = 1/3$ . The graphs show the change in forbidden regions due to various planetary initial conditions mirrored in the different values of the Jacobi Integral  $C_J$ .

Szebehely & Zare (1977) and Szebehely & McKenzie (1977) were able to modify the idea of zero velocity curves to determine the stability of hierarchical systems with three massive bodies by using a function of the system's energy and angular momentum as a stability parameter. Whereas the determination of a planet's dynamical stability in the CR3BP is relatively easy,

## 1. INTRODUCTION

Szebehely's method for the general three body problem is more involved and requires to sort through solutions of a fourth and fifth degree algebraic equation in order to calculate the critical value for the stability parameter (Szebehely & Zare 1977). Consequently, some authors followed a different path. Harrington (1972, 1977), for instance, used numerical methods to solve the full equations of motion of gravitationally bound hierarchical triple systems in order to derive stability criteria for his works on triple stars and habitable zones in binary star systems. Black (1982), Graziani & Black (1981) essentially followed the same approach claiming that their criterion fit better with Szebehely (1977)'s analytic estimates, but was much easier to handle. Since then, many authors used various numerical techniques to derive stability criteria for such systems presenting their results either in the form of plots and tables (e.g. Doolin & Blundell 2011, Georgakarakos 2013, Pilat-Lohinger & Dvorak 2002, Pilat-Lohinger et al. 2003, Sándor et al. 2007), or via polynomial least square fits in the hierarchical triples' masses and orbital parameters (e.g. Dvorak 1986, Holman & Wiegert 1999, Rabl & Dvorak 1988, Whitmire et al. 1998). Dvorak (1986), for instance, investigated coplanar P-Type systems (see Figure 1.6) with equally massed stars and a massless planet. He was able to provide fits for the upper and lower critical planetary semimajor axis, i.e. the semimajor axis where the first (UCO) and finally all (LCO) planetary orbits became unstable. The simple quadratic fits read

$$a_1^{UCO} = a_2(2.37 + 2.76e_2 - 1.04e_2^2), \quad a_1^{LCO} = a_2(2.09 + 2.79e_2 - 2.07e_2^2). \quad (1.6)$$

Here,  $a_1^{UCO}$  and  $a_1^{LCO}$  are the planet's critical semimajor axes with respect to the binary star's center of mass. The parameters  $a_b = a_2$  and  $e_2$  are the binary's semimajor axis and eccentricity, respectively. See Figure 1.8 for an application of the stability estimates presented in equations (1.6). Later on, Rabl & Dvorak (1988) produced similar results for S-Type systems.

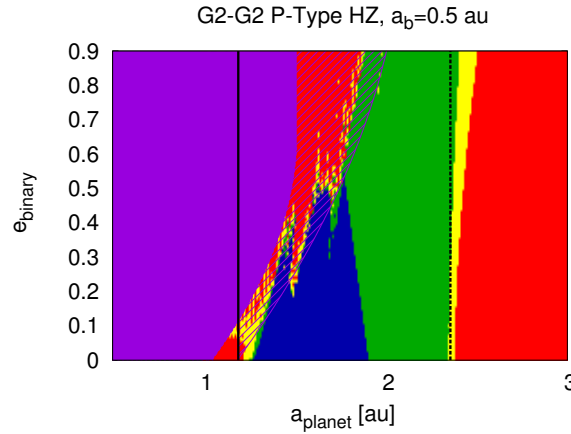


**Figure 1.8:** This figure shows a habitability map for an Earth-like planet in P-Type orbit around a G2-G2 binary star with a semimajor axis of  $a_2 = 0.5$  au. The colors indicate different zones of habitability similar to Figure 1.5. UCO (purple-striped) and LCO (purple-solid) stability estimates by Dvorak (1986) have been applied to determine dynamical stability.

Holman & Wiegert (1999) included binaries with different mass-ratios in their fits. All those criteria were derived for coplanar systems, however. Another approach to identify ejections in hierarchical triple systems was introduced by Mardling & Aarseth (2001). Proposing chaotic energy exchange between the inner binary and the outer body to be fundamental for ejections,

they developed a three dimensional criterion taking the mutual inclination between the inner and outer orbit ( $i_2$ ) into account. Their formula reads Mardling & Aarseth (2001), Naoz et al. (2012b)

$$\frac{a_2}{a_1} > 2.8 \left( 1 + \frac{m_2}{m_0 + m_1} \right)^{2/5} \frac{(1 + e_2)^{2/5}}{(1 - e_2)^{6/5}} \left( 1 - \frac{0.3i_2}{180^\circ} \right), \quad (1.7)$$

where  $i_2$  is given in degrees, and 2.8 as well as the factor including the mutual inclination have been found through numerical studies. While Harrington (1977) did not discover any significant changes of three body stability with mutual inclination, Mardling & Aarseth (2001) claim that inclined systems are actually more stable than coplanar ones. This result was confirmed and extended by Valtonen & Karttunen (2006) but later somewhat mitigated by Valtonen et al. (2008) for inner binaries of equal mass. Another interesting fact is that equation (1.7) does not contain the mass ratio of the inner binary - or in our case the mass ratio of the star and planet. The assumption that the mass ratio of the inner binary can be neglected in a first approximation dates back to numerical experiments by Hills (1984), who investigated close encounters between a star-planet system and a stellar perturber. The approximate independence of orbital stability with respect to the mass ratio of the inner bodies of a hierarchical triple system will be our justification to apply equation (1.7) to our mutually inclined S-type binary-planet systems in chapter 5 despite the fact that the criterion was originally based on ejections of the outer body.

The rapid progress in the numerical study of Hamiltonian systems during the second half of the previous century has spawned more delicate numerical tools to differentiate between ordered and chaotic motion than searching for derailed orbits. These are based on the theory of Lyapunov exponents (Lyapunov 1907). Here, not only the differential equations governing the motion of the system itself but also the so-called "variational equations" are propagated numerically. The variational equations represent the evolution of vectors tangential to the system's trajectory in phase space. If nearby trajectories diverge close to exponentially, this region of phase-space can be classified as being chaotic, or, to be more precise, to react very sensitive to variations in its initial conditions. Many different approaches to utilizing variational equations have evolved, see for instance Benettin et al. (1980), Froeschlé et al. (1997), Oseledec (1968), Sándor et al. (2004), Skokos (2010) or Gerlach et al. (2011). In chapter 2 we will apply the FLI technique by Froeschlé et al. (1997) and Pilat-Lohinger & Dvorak (2002) to assess its correspondence with the results from the ejection criteria used by Holman & Wiegert (1999).

A hybrid approach between numerical and analytical methods has been introduced by Pichardo et al. (2005) and Jaime et al. (2012). They attempt to find the outer or inner-most periodic planetary orbits in a binary star setup numerically in order to adapt coefficients of the Roche lobe approximation by Eggleton (1983). Here, the stability limit is defined as the largest stable periodic circular orbit that can be inscribed in a binary's Roche lobe.

To summarize, one may state that the purely numerically derived fits by Dvorak (1986), Rabl & Dvorak (1988) or Holman & Wiegert (1999) are not necessarily the most precise of all the possible methods to study a system's dynamical stability, but they are the most convenient in terms of usability. Consequently, they have become a widespread tool used for quick estimates on the regions of planetary stability in binary star systems. In order to constrain the parameters of specific systems however, numerical simulations using the actual system parameters give more accurate results (e.g. Goździewski et al. 2012, Welsh et al. 2012).

### 1.3.2 Perturbation Theory

The idea behind perturbation theory is a simple but powerful one. Looking at our Solar System, the gravitationally dominating bodies are the Sun and the gas giants, especially Jupiter. Though, even Jupiter is about a hundred times less massive than the Sun. Now, instead of

## 1. INTRODUCTION

---

searching for complete analytic solutions for a gravitational multi-body problem, one acknowledges that the planets' main movement happens along a Keplerian orbit around the Sun, which is only slightly perturbed by the other massive bodies in the system. This ansatz makes it possible to construct analytic predictions on the evolution of the perturbed planetary orbit. Since its birth in the 18<sup>th</sup> century perturbation theory has been linked to famous names like Newton, Lagrange or Poincaré and it has indeed spawned many useful results throughout the following centuries such as the KAM theorem or Nekhoroshev's stability estimates (e.g. Celletti 2010). Perturbation theory has played and still plays important roles in many scientific fields - from understanding the influence of the giant planets on the asteroid belt (Brouwer 1963), to string theory (Adam 2009, D'Hoker & Phong 1988).

### 1.3.3 Kaula's Approach

Not surprisingly, most of the specific perturbation methodology used in celestial mechanics was originally created for artificial satellites and later expanded to treat problems in the Solar System (Brouwer 1959, Kaula 1961, 1962). Following Murray & Dermott (2000) we will briefly discuss how such an ansatz works. Given a hierarchical 3BP consisting of point masses representing the Sun ( $m_0$ ) and two planets ( $m_1$ ,  $m_2$ ), we can write the equations of motion for the inner planet  $m_1$  in a heliocentric frame of reference

$$\ddot{\mathbf{r}}_1 = -\mathcal{G}(m_0 + m_1)\frac{\mathbf{r}_1}{r_1^3} + \mathcal{G}m_2 \left( \frac{\mathbf{r}_2 - \mathbf{r}_1}{\|\mathbf{r}_2 - \mathbf{r}_1\|^3} - \frac{\mathbf{r}_2}{r_2^3} \right). \quad (1.8)$$

Here  $\mathbf{r}_1$  and  $\mathbf{r}_2$  are the relative positions of the inner and outer planet with respect to the Sun,  $r_1$  and  $r_2$  are the corresponding scalar distances, and  $\mathcal{G}$  denotes the gravitational constant. The right hand side can now be rewritten in terms of the gradient of a scalar potential  $U = \mathcal{K} + \mathcal{R}$  which is the sum of the pure two body potential  $\mathcal{K}$  and the so-called "perturbing function"  $\mathcal{R}$ . Thus,

$$\ddot{\mathbf{r}}_1 = \nabla_{\mathbf{r}_1} U_1 = \nabla_{\mathbf{r}_1} (\mathcal{K}_1 + \mathcal{R}_1), \quad (1.9)$$

where

$$\mathcal{K}_1 = \mathcal{G} \frac{m_0 + m_1}{r_1} \quad \text{and} \quad \mathcal{R}_1 = \frac{\mathcal{G}m_2}{\|\mathbf{r}_2 - \mathbf{r}_1\|} - \mathcal{G}m_2 \frac{\mathbf{r}_1 \cdot \mathbf{r}_2}{r_2^3} \quad (1.10)$$

Here, the perturbing function  $\mathcal{R}_1$  consists of two parts, a "direct" part proportional to  $\|\mathbf{r}_2 - \mathbf{r}_1\|^{-1}$ , which describes the interaction between the two planets, and an "indirect part" proportional to  $\mathbf{r}_1 \cdot \mathbf{r}_2 / r_2^3$  which is due to the choice of the center of our coordinate system. Such equations can also be constructed for the outer planet without much difficulty (Murray & Dermott 2000).

Now, if the outer planet were a test particle, i.e.  $m_2 \rightarrow 0$  and consequently  $\mathcal{R}_1 \rightarrow 0$ , then the inner planet would move on an unperturbed Keplerian orbit around the Sun. As we would like to take the gravitational interaction between massive planets into account, however, we have to deal with the effects caused by a non-vanishing perturbing function  $\mathcal{R}_1 \neq 0$ . Let us, therefore, rewrite the disturbing function in terms of Legendre polynomials ( $P_l$ )

$$\begin{aligned} \mathcal{R}_1 &= \mathcal{G}m_2 \left( \frac{1}{\|\mathbf{r}_2 - \mathbf{r}_1\|} - \frac{\mathbf{r}_1 \cdot \mathbf{r}_2}{r_2^3} \right) \\ &= \mathcal{G}m_2 \left( \frac{1}{r_2} \sum_{l=0}^{\infty} \left( \frac{r_1}{r_2} \right)^l P_l(\cos \psi) - \frac{r_1 r_2 P_1(\cos \psi)}{r_2^3} \right) \\ &= \frac{\mathcal{G}m_2}{r_2} \left( 1 + \sum_{l=2}^{\infty} \left( \frac{r_1}{r_2} \right)^l P_l(\cos \psi) \right), \end{aligned} \quad (1.11)$$

using the fact that  $\mathbf{r}_1 \cdot \mathbf{r}_2 = r_1 r_2 \cos \psi = r_1 r_2 P_1(\cos \psi)$ . The first summand is often omitted as only partial derivatives of  $\mathcal{R}_1$  will ultimately be dealt with, where this term vanishes. Therefore, we have

$$\mathcal{R}_1 \doteq \frac{Gm_2}{r_2} \sum_{l=2}^{\infty} \left( \frac{r_1}{r_2} \right)^l P_l(\cos \psi). \quad (1.12)$$

Since we assume that this disturbing function will cause a deviation of the motion of the inner planet from its Keplerian shape, the rest of the procedure involves the following steps:

- Change the perturbing function's arguments to Keplerian orbital elements. The perturbing function will then read  $\mathcal{R}_1(m_1, r_1, r_2, \psi) \rightarrow \mathcal{R}'_1(\{a, e, i, \omega, \Omega, M\}_{1,2})$ , where one usually has to deal with combinations of integer multiples of the angles within trigonometric functions. Those represent the system's dominating frequencies.<sup>1</sup>
- Write  $\mathcal{R}'_1$  as a power-series in eccentricities and inclinations, and/or ratios of semimajor axes. Decide which combination of frequencies to discard in the problem.
- If one is interested in the long term behavior of a system, it is possible to construct averages over the 'fast angles' like the mean anomalies (or the mean longitudes) of the perturber and the perturbed body, thus, eliminating them from the equations. A simple but controversial approach (Ferraz-Mello 2007) is the so-called "averaging principle" or "scissors method"

$$\langle \mathcal{R}'_1 \rangle(\{a, e, i, \omega, \Omega\}_{1,2}) = \frac{1}{2\pi} \int_0^{2\pi} \int_0^{2\pi} \mathcal{R}'_1(\{a, e, i, \omega, \Omega, M\}_{1,2}) dM_1 dM_2,$$

where the elimination of the short period terms containing trigonometric functions of  $M_1$  and  $M_2$  is performed by a direct integration. A more elegant and self-consistent approach to average  $\mathcal{R}'_1$  is the von Zeipel-Brouwer method discussed in the next section.

- Finally, Lagrange's equations can be used to evaluate variations of orbital elements of the inner planet (Roy 2005)

$$\frac{da_1}{dt} = \frac{2}{n_1 a_1} \frac{\partial \mathcal{R}'_1}{\partial \chi_1}, \quad \frac{de_1}{dt} = \frac{1}{n_1 a_1^2 e_1} \left( (1 - e_1^2) \frac{\partial \mathcal{R}'_1}{\partial \chi_1} - \sqrt{1 - e_1^2} \frac{\partial \mathcal{R}'_1}{\partial \omega_1} \right), \quad \dots$$

with  $\chi = -n \tau$ , where  $n$  is the mean motion and  $\tau$  the time of pericenter passage. Using the averaged  $\langle \mathcal{R}'_1 \rangle$  instead of  $\mathcal{R}'_1$  generally reduces the number of differential equations that need to be solved simultaneously. In some cases, an analytic solution for  $\{a_1(t), e_1(t), \dots\}$  can be found.

As we will not use this exact approach and the rigorous construction of the presented steps is rather tedious in practice, the reader is referred to literature for details (e.g. Kaula 1961, Murray & Dermott 2000).

The interplay between the Sun, the Moon and the Earth, or Jupiter's and Saturn's orbital elements, for instance, can be very convincingly modeled applying perturbation theory. As we have seen, the methods often require series expansions in the bodies' eccentricities and/or inclinations (e.g. Kaula 1961, Murray & Dermott 2000). This is reasonable, when the system's eccentricities and mutual inclinations are small, so that series expansions in those parameters converge rapidly. Binary star-planet systems on the other hand do not necessarily fulfill such

<sup>1</sup>In practice, non singular variants of the angular variables are applied, i.e. the mean longitude  $L = M + \Omega + \omega$  instead of  $M$  and the longitude of the ascending node  $\varpi = \Omega + \omega$  instead of the argument of pericenter  $\omega$ .

## 1. INTRODUCTION

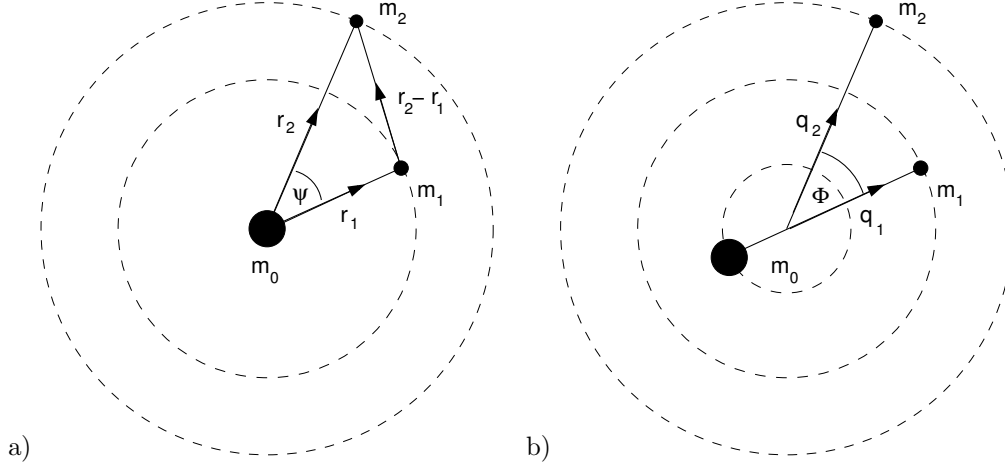


**Figure 1.9:** a) Heliocentric position vectors  $\mathbf{r}_1$  and  $\mathbf{r}_2$  of two planets represented by mass points  $m_1$  and  $m_2$  in orbit around the Sun ( $m_0$ ). The angle  $\psi$  is spanned between vectors  $\mathbf{r}_1$  and  $\mathbf{r}_2$ . b) Jacobian Coordinates of an hierarchical triplet. The relative positions of the close pair is given by the vector  $\mathbf{q}_1$ , the distance of the outer body with respect to the inner binary's center of gravity is given by  $\mathbf{q}_2$ .

conditions. The S-Type systems  $\gamma$  Cephei, HD 41004 and HD 196885 for instance are all known to host planets, even though the secondary stars' orbits have considerable eccentricities,  $e_2 \simeq 0.4$  (Roell et al. 2012). Hence, Kaula's techniques would require lengthy expansions up to high orders in eccentricity to provide adequate results.

### 1.3.4 Brouwer's Approach

A more practical ansatz makes use of the canonical properties of Hamiltonian systems to deal with perturbations. One attempts to split a system's Hamiltonian  $\mathcal{H}$  into an "integrable" part ( $\mathcal{H}_0$ ) and a "perturbation" part ( $\mathcal{H}_1$ ), which is proportional to a small parameter  $\epsilon$ .

$$\mathcal{H}(\mathbf{p}, \mathbf{q}) = \mathcal{H}_0(\mathbf{p}, \mathbf{q}) + \epsilon \mathcal{H}_1(\mathbf{p}, \mathbf{q}) \quad (1.13)$$

The fact that this is a very powerful approach is most obvious, if we change from generalized momenta  $\mathbf{p}$  and coordinates  $\mathbf{q}$  to so-called "action-angle" variables using canonical transformations. Action-angle variables are a set of generalized coordinates which contain (pseudo)<sup>1</sup> invariants of motion  $\mathbf{I}$  (the actions), and their conjugate counterparts  $\boldsymbol{\phi}$  (the angles). The benefit of this transformation lies in the fact that Hamiltonians representing completely integrable systems can be expressed as functions of actions only.

$$(\mathbf{p}, \mathbf{q}) \rightarrow (\mathbf{I}, \boldsymbol{\phi}) \quad (1.14)$$

$$\mathcal{H}(\mathbf{p}, \mathbf{q}) \rightarrow \mathcal{H}^*(\mathbf{I}) \quad (1.15)$$

Hamilton's equation of motion predict that in this case the actions stay constant, whereas the angles become linear functions of time (e.g. Ferraz-Mello 2007)

$$\frac{\partial \mathcal{H}^*(\mathbf{I})}{\partial \phi_i} = -\dot{I}_i = 0, \quad \frac{\partial \mathcal{H}^*(\mathbf{I})}{\partial I_i} = \dot{\phi}_i = w_i(\mathbf{I}), \quad (1.16)$$

<sup>1</sup>Actions are only exact invariants of motion, if the problem is fully integrable.



and consequently

$$I_i(t) = c_i, \quad \phi_i(t) = w_i(\mathbf{I}) t + c_i. \quad (1.17)$$

Here, the subscript  $i$  denotes the  $i^{\text{th}}$  component of the respective vectors,  $\mathbf{c}$  are integration constants and  $\mathbf{w}$  represents the system's angular frequencies:  $w_i = \dot{\phi}_i = 2\pi/T_i$ ,  $\mathbf{T}$  being the system's proper periods. Equation (1.17) shows that, if one can find a Hamiltonian that depends on the actions  $\mathbf{I}$  only, the equations of motion can be solved in a very straight forward manner. Topologically speaking, one attempts to map the system's trajectory in phase space onto an invariant  $n$ -torus<sup>1</sup>, where the actions define the torus' radii and the angles give the system's momentary position on the torus; see Figure 1.10. Finding action angle variables for

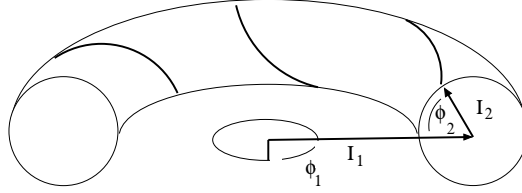


**Figure 1.10:** This graph shows a 2-torus spanned by a set of action angle variables  $(\mathbf{I}, \boldsymbol{\phi})$ .

dynamical systems is not always straight forward (Ferraz-Mello 2007). Fortunately, the action angle variables for Keplerian motion have already been derived by Delaunay (1860)

$$\mathbf{I} = (L, G, H), \quad \boldsymbol{\phi} = (l, g, h) \quad (1.18)$$

where

$$\begin{aligned} L &= \sqrt{\mathcal{G}(m_0 + m_1)a}, & l &= M, \\ G &= L\sqrt{1 - e^2}, & g &= \omega, \\ H &= G \cos i, & h &= \Omega \end{aligned} \quad (1.19)$$

The elegance of formulating perturbation theory in action angle variables becomes evident when we express the Hamiltonian  $\mathcal{H}$  as a function of actions and angles<sup>2</sup>

$$\mathcal{H}(\mathbf{I}, \boldsymbol{\phi}) = \mathcal{H}_0(\mathbf{I}) + \epsilon \mathcal{H}_1(\mathbf{I}, \boldsymbol{\phi}). \quad (1.20)$$

For  $\epsilon \rightarrow 0$  the system becomes integrable as  $\mathcal{H} \rightarrow \mathcal{H}_0$  resulting in constant actions  $\mathbf{I}$  and uniformly progressing angles  $\boldsymbol{\phi}(t)$ . The unperturbed Kepler problem provides a simple example. Here, the Hamiltonian is a function of  $L$  only

$$\mathcal{H} = -\frac{\mathcal{G}(m_0 + m_1)}{2a} = -\frac{\mathcal{G}^2(m_0 + m_1)^2}{2L^2}. \quad (1.21)$$

<sup>1</sup>The integer  $n$  stands for the dimension of the torus. Two independent actions with two corresponding angles can span a 2-torus, see Figure 1.10.

<sup>2</sup>For the sake keeping the notation simple, we will no longer differentiate between Hamiltonians given in action angle variables ( $\mathcal{H}^*$ ) and those given in other variables ( $\mathcal{H}$ ).

## 1. INTRODUCTION

---

From Hamilton's equations we get

$$\begin{aligned}\frac{dl}{dt} &= \frac{\partial \mathcal{H}}{\partial L} \\ &= \frac{\mathcal{G}^2(m_0 + m_1)^2}{L^3} \\ &= \sqrt{\mathcal{G}(m_0 + m_1)a^{-3}} = n,\end{aligned}\tag{1.22}$$

where  $n$  denotes the mean anomaly. Since the partial derivatives with respect to all the other actions and corresponding angles vanish, the solution of the problem is simply

$$\mathbf{I} = \text{const}, \quad g = h = \text{const}, \quad l = n(t - \tau) = M,\tag{1.23}$$

where the angle  $l$  grows linearly with time.

If  $\epsilon$  in equation (1.20) is of finite size, but small, the system becomes no longer globally integrable. KAM theory states that systems can still remain integrable under small perturbations, though, if certain criteria are met<sup>1</sup>. Regarding the topological picture one could say that some  $n$ -tori spanned by the action angle variables survive a slight deformation, whereas others break up. For a detailed account on the application of KAM theory to the spin-orbit problem see, for instance, Celletti (2010).

By applying a method pioneered by Delaunay and developed further by Bohlin and Poincaré one can extend the validity of our analytical estimates beyond the first order in the perturbing parameter  $\epsilon$ . The aim is to consecutively find new sets of action angle variables  $(\mathbf{I}, \phi)_n$  which are linked to the old ones  $(\mathbf{I}, \phi)_0$  via canonical transformations  $S_{0\dots n}$ , so that the transformed Hamiltonian becomes independent of the new angles up to terms of order  $\epsilon^n$ . The integrable part of the analytical solution is, thus, extended to higher orders in the perturbing parameter. If a full elimination of all the angles is not feasible, one can at least attempt to reduce the degrees of freedom of the dynamical system at hand trying to make it integrable in such a way. Using such an approach, Brouwer (1959) was able to describe the secular behavior of the orbit of an artificial satellite assuming a small additional anisotropic correction to the Earth's spherical gravitational potential, which constituted his perturbing function. Applying the averaging method developed by von Zeipel he found successive canonical transformations  $S_{0\dots n}$ , which eliminate short period terms without the need for series expansions in the satellite's eccentricity or inclination. For a detailed discussion of the von Zeipel - Brouwer method including suggestions to circumnavigate problems which arise during this procedure - such as the appearance of small divisors for instance - see e.g. Brouwer (1959) and Ferraz-Mello (2007). A similar approach was later applied to hierarchical triple systems by Harrington (1968, 1969), extended by Soderhjelm (1984) and Marchal (1990) and has since become very popular, as it allows for long term (secular) predictions on the dynamical evolution of a hierarchical triple system without restrictions on eccentricities or inclination (e.g. Beaugé et al. 2012, Eggleton 2006, Farago & Laskar 2010, Ford et al. 2000, Georgakarakos 2002, 2003, Krymowski & Mazeh 1999, Lee & Peale 2003). The Hamiltonian of such a hierarchical three body approach reads (in action angle variables)

$$\mathcal{H}_J = -\frac{\mathcal{G}^2(m_0 m_1)^3}{2L_1^2(m_0 + m_1)} - \frac{\mathcal{G}^2[(m_0 + m_1)m_2]^3}{2L_2^2(m_0 + m_1 + m_2)} - \mathcal{R}_J,\tag{1.24}$$

where  $L_1$  and  $L_2$  are the actions of the inner and outer orbits and  $\mathcal{R}_J$  is the perturbing function. The subscript  $J$  indicates that we will work in a Jacobian frame of reference from now on, see

---

<sup>1</sup>E.g. the system's frequencies must not be resonant (diophantine).

Figure 1.9, right. Consequently, our definition of the system's action variables has to be adapted (Harrington 1968, Krymolowski & Mazeh 1999)

$$\begin{aligned} L_1 &= \frac{m_0 m_1}{m_0 + m_1} \sqrt{\mathcal{G}(m_0 + m_1) a_1}, & G_1 &= L_1 \sqrt{1 - e_1^2}, \\ L_2 &= \frac{m_2(m_0 + m_1)}{m_0 + m_1 + m_2} \sqrt{\mathcal{G}(m_0 + m_1 + m_2) a_2}, & G_2 &= L_2 \sqrt{1 - e_2^2}. \end{aligned} \quad (1.25)$$

Similar to equation (1.12) Legendre expansions of the perturbing function can be used. Before changing to action angle variables  $\mathcal{R}_J$  reads

$$\mathcal{R}_J = \frac{\mathcal{G}}{q_2} \sum_{j=2}^{\infty} M_j \left( \frac{q_1}{q_2} \right)^j P_j(\cos \Phi), \quad (1.26)$$

with  $q_1$  being the scalar distance between  $m_0$  and  $m_1$ . The distance  $q_2$  is then counted from the center of mass of  $m_0$  and  $m_1$  to  $m_2$  (Figure 1.9, right). The relative angle between  $q_1$  and  $q_2$  is denoted by  $\Phi$ , and the mass parameter  $M_j$  is defined as (Harrington 1968)

$$M_j = m_0 m_1 m_2 \frac{m_0^{j-1} - (-m_1)^{j-1}}{(m_0 + m_1)^j}.$$

After expressing the Hamiltonian in action angle variables, where the perturbing function up to Legendre polynomial  $P_2$  is included, a von Zeipel - Brouwer averaging procedure can be applied, see e.g. Marchal (1990).<sup>1</sup> The resulting averaged Hamiltonian for coplanar ( $i_1 = i_2 = 0$ ) hierarchical triple configurations reads

$$\langle \mathcal{H}_J \rangle_{P_2} = -\frac{\mathcal{G}^2}{2} \left[ \frac{\mathcal{M}_1}{L_1^2} + \frac{\mathcal{M}_2}{L_2^2} + \mathcal{M}_3 \frac{L_1^4 (5 - 3G_1^2/L_1^2)}{4L_2^3 G_2^3} \right] \quad (1.27)$$

where

$$\mathcal{M}_1 = \frac{(m_0 m_1)^3}{(m_0 + m_1)}, \quad \mathcal{M}_2 = \frac{[(m_0 + m_1) m_2]^3}{(m_0 + m_1 + m_2)}, \quad \mathcal{M}_3 = \frac{[(m_0 + m_1) m_2]^7}{[m_0 m_1 (m_0 + m_1 + m_2)]^3}. \quad (1.28)$$

Equation (1.27) shows that the averaged Hamiltonian including  $P_2$  terms does neither depend on the mean anomalies  $l_1, l_2$ , nor on the arguments of pericenter  $g_1, g_2$ . Consequently, all actions are preserved meaning that the eccentricities as well as the semimajor axes of both, the inner and the outer orbit, stay constant. The arguments of pericenter and the mean anomalies will grow linearly with time.

It is true that, in reality, the semimajor axes of the inner and outer orbit do stay almost constant. However, this is not the case for the orbital eccentricities in such a system. Numerical integration of the 3BP's full equations of motion allows us to visualize the evolution of orbital elements in hierarchical triple systems, see Figures 1.11 and 1.12.

Since the eccentricity of a planet's orbit in an S-Type binary star configuration is of great importance for its habitability (see chapter 2), more accurate analytical approximations will be required. Hence, we need to include more terms in the Legendre expansion of the perturbing function. Pushing the Legendre expansion to include  $P_3$ , for instance, solves the issue of constants eccentricities already, and produces the following averaged Hamiltonian for coplanar

<sup>1</sup>There is a small misprint of formula (203) in Marchal (1990). The outer semiminor axis should read  $b_T = M L_T G_T / (\mathcal{G} m_3^2 (m_1 + m_2)^2)$ .

## 1. INTRODUCTION

---

hierarchical triple configurations expressed in osculating orbital elements (Georgakarakos 2003, Marchal 1990)

$$\langle \mathcal{H}_J \rangle_{P3} = -\frac{\mathcal{G}m_0m_1}{2a_1} - \frac{\mathcal{G}(m_0+m_1)m_2}{2a_2} + Q_1 + Q_2 + Q_3, \quad (1.29)$$

where

$$\begin{aligned} Q_1 &= -\frac{1}{8} \frac{\mathcal{G}m_0m_1m_2}{(m_0+m_1)a_2(1-e_2^2)^{3/2}} (2+3e_1^2), \\ Q_2 &= \frac{15}{64} \frac{\mathcal{G}m_0m_1m_2(m_0-m_1)a_1^3e_1e_2}{(m_0+m_1)^2a_2^4(1-e_2^2)^{5/2}} \cos(\omega_1-\omega_2)(4+4e_1^2), \\ Q_3 &= -\frac{15}{64} \frac{\mathcal{G}m_0m_1m_2^2a_1^{7/2}e_1^2(1-e_1^2)^{1/2}}{(m_0+m_1)^{3/2}(m_0+m_1+m_2)^{1/2}a_2^{9/2}(1-e_2^2)^3} \\ &\quad \cdot [15+10e_2^2+3e_2^2\cos 2(\omega_1-\omega_2)]. \end{aligned}$$

The  $Q_1$  term originates from the Legendre polynomial  $P_2$ ,  $Q_2$  comes from the Legendre polynomial  $P_3$  and the expression  $Q_3$  arises from the canonical transformations during the von Zeipel - Brouwer procedure. Even though the octupole ( $P_3$ ) expansion allows for changes in the eccentricities of both orbits, its predictions are not very accurate in planar configurations (Figures 1.11 and 1.12). This lack of accuracy is due to the omission of short period terms that were intentionally eliminated during the von Zeipel - Brouwer approach, in order to make the system of differential equations easier to handle. Yet, short period terms can contribute significantly to the overall evolution of the inner orbit's eccentricity.

### 1.3.5 Georgakarakos' Approach

Georgakarakos (2002, 2003, 2005) has found a way to re-introduce short period terms in the analytic solution for the inner eccentricity, making use of the evolution of the 'Laplace-Runge-Lenz' or eccentricity vector ( $\mathbf{e}$ ) of the inner orbit

$$\mathbf{e}_1 = \frac{\mathbf{q}_1}{q_1} + \frac{1}{\mathcal{G}(m_0+m_1)} [\dot{\mathbf{q}}_1 \times (\mathbf{q}_1 \times \dot{\mathbf{q}}_1)]. \quad (1.30)$$

This vector always points in the direction of the pericenter of the corresponding orbit and its length is equal to the orbit's eccentricity. Georgakarakos calculated short period contributions by integrating the  $x$  and  $y$  components of  $\dot{\mathbf{e}}_1$  after expressing them in terms of Legendre polynomials up to  $P_3$ . He then recombined the short period solutions with the secular evolution of the eccentricity gained from the Hamiltonian in equation (1.29). Thus, he was able to produce an improved analytic solution for the inner orbit's eccentricity, containing information on its long term evolution as well as on its short term behavior, see appendix 1.A. Furthermore, Georgakarakos (2005) provides estimates on the average squared eccentricity of the inner orbit, which will be used extensively in chapters 2 and 3. Also, the planet's maximum eccentricity in S-Type configurations could be determined using results from Georgakarakos (2003, 2005), see chapter 2, appendix B. Figures 1.11 and 1.12 have been generated in order to visualize the performance of the analytic estimates based on Georgakarakos' method. The figures present a comparison between

- purely secular predictions on the planet's eccentricity derived from  $\langle \mathcal{H}_J \rangle_{P3}$  via Hamilton's equations of motion, see equations (1.29) and (1.41),
- Georgakarakos' method unifying secular and short period terms for the inner body's eccentricity, see equations (1.31), (1.32) and (1.41),

	$m_0$	$m_1$	$m_2$	$a_2/a_1$	$e_1$	$e_2$	$L_2 - L_1$ [deg]
system a	1	3.04043d-6	1	10	0	0.5	0
system b	1	3.04043d-6	0.5	20	0	0.01	0

**Table 1.1:** Initial conditions for the two different S-Type systems harboring Earth-like planets presented in Figures 1.11 and 1.12. The subscript 1 on the Keplerian orbital elements refers to the inner - in this case the planetary - orbit. The subscript 2 is used for the orbit of the second star around the common center of mass of the host star and the planet. Here,  $a$ ,  $e$  and  $L$  denote initial semimajor axis, eccentricity and mean longitude ( $L = \omega + \Omega + M$ ) respectively. The masses for the primary ( $m_0$ ), the planet ( $m_1$ ) and the secondary ( $m_2$ ) are given in solar masses.

- and a numerical integration of the Newtonian 3BP using a Gauss Radau collocation method (Everhart 1974).

The constancy of the semimajor axes of the inner and outer orbit predicted by perturbation theory is mirrored in the results of the numerical integrations (upper left panels in Figures 1.11 and 1.12). As far as the eccentricities are concerned, there are still discrepancies between the numerical results and Georgakarakos' estimates. However, the improvement compared to the purely secular approach is striking. Especially for perturbers on almost circular orbits as depicted in Figure 1.12 the short period terms dominate the evolution of the planet's eccentricity. The fact that the inner eccentricity's secular period is not as well determined as the eccentricity's amplitude is not going to impact the determination of HZs in binary star systems significantly, see section 5.2.

## 1. INTRODUCTION

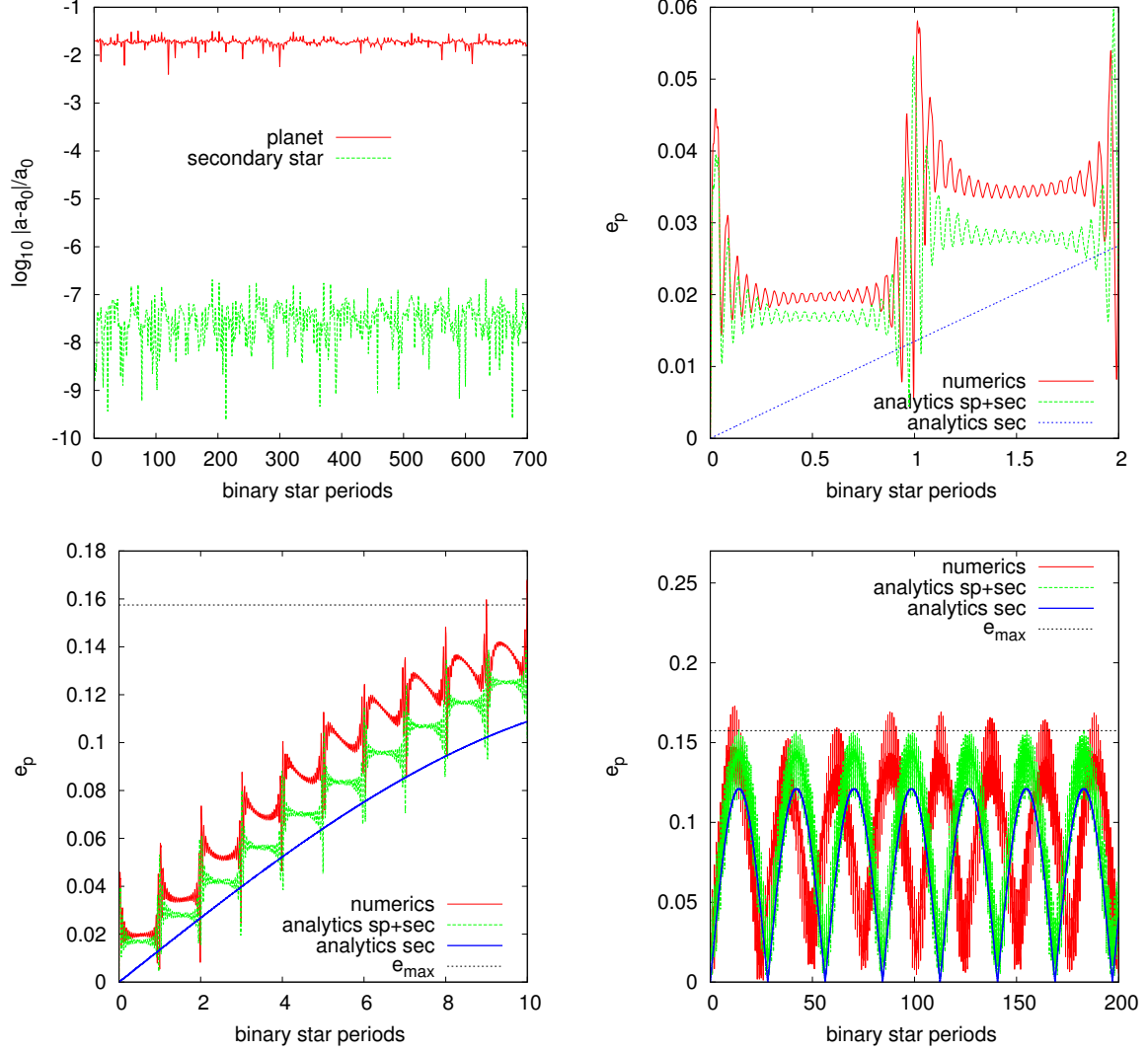


**Figure 1.11:** Evolution of semimajor axes and planetary eccentricities in a coplanar S-Type binary star system hosting an Earth-like planet. The system’s initial conditions are given in Table 1.1, referenced as ‘system a’. The second star is massive and on a close, elliptic orbit. *Top left:* The logarithmic deviation of the secondary star’s and the planet’s semimajor axes from their initial values as found from numerical integrations of the full Newtonian 3BP. Even though the planet’s variations in semimajor axis are larger than the secondary’s, they stay within the range of a few percent. The assumption that both semimajor axes remain constant is, therefore, a reasonable one. Variations in the secondary star’s eccentricity remain below  $10^{-7}$ . *Top right & bottom:* The various figures show a comparison between the predictions on the evolution of the planet’s eccentricity ( $e_p$ ) in ‘system a’ on different timescales. Hereby, numerical integration results are shown in red, a secular analytic approach derived from the averaged Hamiltonian presented in equation (1.29) is shown in blue, and the solutions by Georgakarakos (2003, 2005) reuniting secular and short period terms are colored green. Estimates for the planet’s maximum eccentricity derived in chapter 2 are represented by the dashed horizontal line. While the secular part is dominating the planet’s eccentricity evolution, the addition of the short period terms clearly improves  $e_p$  estimates. However, the analytic predictions for the planetary eccentricity’s secular period are not as precise as the ones for the corresponding amplitudes.

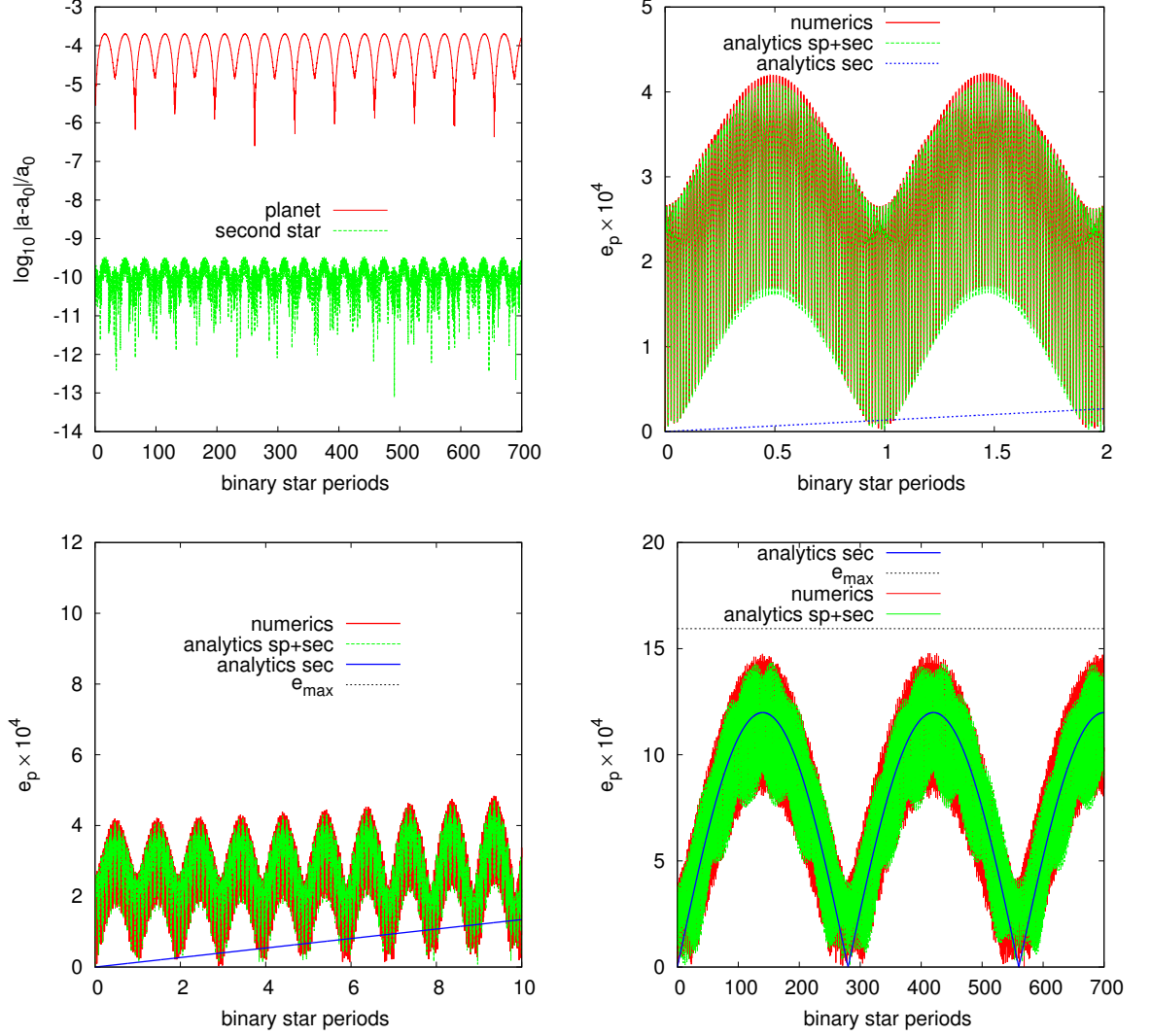


**Figure 1.12:** Same as Figure 1.11 only for 'system b'. The system's initial conditions are given in Table 1.1. As the configuration involves a second star on an almost circular orbit, the short period terms are dominating the planet's eccentricity evolution on short and intermediate timescales. In contrast to 'system a' (Figure 1.11) the secular periods are in good agreement with numerical results when the perturbations remain small (*bottom right*). The estimates for the maximum eccentricity are not as convincing for 'system b' as they were for 'system a'. Since the overall planetary eccentricity is very small, however, the deviations will not cause grave problems in our model for planetary habitability, which is presented in chapter 2. The secondary star's variation in eccentricity remains below  $2 \cdot 10^{-8}$ .

## 1. INTRODUCTION

---

### 1.A Georgakarakos' Solution for the Inner Eccentricity

In a sequence of articles Georgakarakos (2002, 2003, 2005) has improved the analytic estimates for the eccentricity evolution of the inner orbit in coplanar hierarchical triple systems (see Figure 1.9). He achieved this by deriving the secular equations of motion for the eccentricity vector's  $x$  and  $y$  components from the doubly averaged octupole Hamiltonian  $\langle H_J \rangle_{P_3}$  [equation (1.27)] and combining them with the dominating short period terms gained directly from the perturbed eccentricity vector of the inner orbit. Here, a rough outline of the process leading to Georgakarakos' solution for the inner eccentricity is presented. For a detailed derivation of the equations see Georgakarakos (2003, 2005).

Let  $\mathbf{e}_1$  be the time dependent eccentricity vector of the inner orbit as presented in equation (1.30). The eccentricity vector's  $x$  and  $y$  components  $e_{1x}$  and  $e_{1y}$  can be written as a combination of short period ( $sp$ ) and secular ( $sec$ ) terms:

$$\mathbf{e}_1 = \begin{pmatrix} e_{1x} \\ e_{1y} \end{pmatrix} = \mathbf{e}_1^{sp} + \mathbf{e}_1^{sec} - \mathbf{e}_1^c \quad (1.31)$$

where  $\mathbf{e}_1^c = (e_{1x}^c, e_{1y}^c)^T$  are constants of integration. Since we assume coplanarity, the  $z$  component of  $\mathbf{e}_1$  is always zero and will thus not be mentioned. Assuming an initially circular planetary orbit, the dominating short period terms of  $\mathbf{e}_1$  can be expressed as follows (Georgakarakos 2003)

$$\mathbf{e}_1^{sp} = \frac{m_2}{MX^2(1-e_2^2)^3} \left( \mathbf{P}_{21} + \frac{1}{X} \mathbf{P}_{22} + m_* X^{1/3} \mathbf{P}_{31} + \frac{m_*}{X^{2/3}} \mathbf{P}_{32} \right) + \mathbf{e}_1^c. \quad (1.32)$$

The variables  $M$  and  $m_*$  are combinations of the three bodies' masses

$$M = m_0 + m_1 + m_2, \quad m_* = \frac{m_1 - m_0}{(m_0 + m_1)^{2/3} M^{1/3}}. \quad (1.33)$$

The parameter  $X = T_2/T_1 = \sqrt{(m_0 + m_1)/(m_0 + m_1 + m_2)}(a_2/a_1)^{3/2}$  denotes the period ratio between the outer and inner orbit and the terms  $\mathbf{P}_{ij} = (P_{ijx}, P_{ijy})^T$  are originating with the



respective Legendre polynomial  $P_i$ . More specifically:

$$P_{21x} = (1 + e_2 \cos[f_2])^3 \left( -\frac{1}{2} \cos[n_1 t] + \frac{1}{4} \cos[3n_1 t - 2f_2 - 2\varpi_2] + \frac{9}{4} \cos[n_1 t - 2f_2 - 2\varpi_2] \right);$$

$$P_{22x} = \frac{(1 + e_2 \cos[f_2])^4}{(1 - e_2^2)^{3/2}} \left\{ \frac{9}{2} \cos[n_1 t - 2f_2 - 2\varpi_2] + \frac{1}{6} \cos[3n_1 t - 2f_2 - 2\varpi_2] + \right. \\ \left. e_2 \left( -\frac{3}{4} \cos[n_1 t - f_2] + \frac{3}{4} \cos[n_1 t + f_2] + \frac{45}{8} \cos[n_1 t - 3f_2 - 2\varpi_2] + \right. \right. \\ \left. \left. \frac{5}{24} \cos[3n_1 t - 3f_2 - 2\varpi_2] - \frac{9}{8} \cos[n_1 t - f_2 - 2\varpi_2] - \frac{1}{24} \cos[3n_1 t - f_2 - 2\varpi_2] \right) \right\};$$

$$P_{31x} = \sqrt{1 - e_2^2} \left\{ \frac{15}{16} \cos[f_2 + \varpi_2] + \frac{15}{32} e_2 \cos[2f_2 + \varpi_2] + \right. \\ \left. e_2^2 \left( \frac{45}{32} \cos[f_2 + \varpi_2] - \frac{75}{64} \cos[f_2 - \varpi_2] + \frac{5}{64} \cos[3f_2 + \varpi_2] \right) + \right. \\ \left. e_2^3 \left( \frac{45}{128} \cos[2f_2 - \varpi_2] - \frac{45}{128} \cos[2f_2 + \varpi_2] \right) + \right. \\ \left. e_2^4 \left( \frac{5}{32} \cos[3f_2 + \varpi_2] - \frac{5}{32} \cos[3f_2 - \varpi_2] \right) \right\};$$

$$P_{32x} = \frac{(1 + e_2 \cos[f_2])^4}{1 - e_2^2} \left( \frac{3}{32} \cos[2n_1 t - f_2 - \varpi_2] - \frac{45}{32} \cos[2n_1 t - 3f_2 - 3\varpi_2] - \right. \\ \left. \frac{15}{64} \cos[4n_1 t - 3f_2 - 3\varpi_2] \right);$$

$$P_{21y} = (1 + e_2 \cos[f_2])^3 \left( -\frac{1}{2} \sin[n_1 t] + \frac{1}{4} \sin[3n_1 t - 2f_2 - 2\varpi_2] - \frac{9}{4} \sin[n_1 t - 2f_2 - 2\varpi_2] \right);$$

$$P_{22y} = \frac{(1 + e_2 \cos[f_2])^4}{(1 - e_2^2)^{3/2}} \left\{ -\frac{9}{2} \sin[n_1 t - 2f_2 - 2\varpi_2] + \frac{1}{6} \sin[3n_1 t - 2f_2 - 2\varpi_2] + \right. \\ \left. e_2 \left( -\frac{3}{4} \sin[n_1 t - f_2] + \frac{3}{4} \sin[n_1 t + f_2] - \frac{45}{8} \sin[n_1 t - 3f_2 - 2\varpi_2] + \right. \right. \\ \left. \left. \frac{5}{24} \sin[3n_1 t - 3f_2 - 2\varpi_2] + \frac{9}{8} \sin[n_1 t - f_2 - 2\varpi_2] - \frac{1}{24} \sin[3n_1 t - f_2 - 2\varpi_2] \right) \right\};$$

$$P_{31y} = \sqrt{1 - e_2^2} \left\{ \frac{15}{16} \sin[f_2 + \varpi_2] + \frac{15}{32} e_2 \sin[2f_2 + \varpi_2] + \right. \\ \left. e_2^2 \left( \frac{45}{32} \sin[f_2 + \varpi_2] + \frac{75}{64} \sin[f_2 - \varpi_2] + \frac{5}{64} \sin[3f_2 + \varpi_2] \right) + \right. \\ \left. e_2^3 \left( -\frac{45}{128} \sin[2f_2 - \varpi_2] - \frac{45}{128} \sin[2f_2 + \varpi_2] \right) + \right. \\ \left. e_2^4 \left( \frac{5}{32} \sin[3f_2 + \varpi_2] - \frac{5}{32} \sin[3f_2 - \varpi_2] \right) \right\};$$

$$P_{32y} = \frac{(1 + e_2 \cos[f_2])^4}{1 - e_2^2} \left( \frac{3}{32} \sin[2n_1 t - f_2 - \varpi_2] + \frac{45}{32} \sin[2n_1 t - 3f_2 - 3\varpi_2] - \right. \\ \left. \frac{15}{64} \sin[4n_1 t - 3f_2 - 3\varpi_2] \right).$$

## 1. INTRODUCTION

---

Here,  $n_1$  is the inner body's mean motion,  $f_2$  the outer body's true anomaly and  $\varpi_2$  the outer body's longitude of pericenter ( $\varpi = \omega + \Omega$ ). The true anomaly  $f_2$  can be expressed as a function of time via the equation of the center, see chapter 3, appendix A.

In order to find the secular evolution of the inner eccentricity vector, we define its secular  $x$  and  $y$  components as follows

$$k_1 \doteq e_{1x}^{sec} = e_1 \cos \varpi_1 \quad h_1 \doteq e_{1y}^{sec} = e_1 \sin \varpi_1, \quad (1.34)$$

where  $e_1$  denotes the length of  $\mathbf{e}_1^{sec}$ .<sup>1</sup> The time derivative of these quantities can be written as

$$\begin{aligned} \dot{k}_1 &= \dot{e}_1 \cos \varpi_1 - e_1 \sin \varpi_1 \dot{\varpi}_1 = \dot{e}_1 \cos \varpi_1 - h_1 \dot{\varpi}_1 \\ \dot{h}_1 &= \dot{e}_1 \sin \varpi_1 + e_1 \cos \varpi_1 \dot{\varpi}_1 = \dot{e}_1 \sin \varpi_1 + k_1 \dot{\varpi}_1. \end{aligned} \quad (1.35)$$

Let us now use the averaged Hamiltonian from equation (1.29) to find expressions for  $\dot{e}_1$  and  $\dot{\varpi}_1$ . Hamilton's equations of motion for the Delaunay actions  $G_i$  and corresponding angles  $g_i$  read

$$\frac{dG_i}{dt} = -\frac{\partial \langle \mathcal{H}_J \rangle_{P3}}{\partial g_i} \quad \frac{dg_i}{dt} = \frac{\partial \langle \mathcal{H}_J \rangle_{P3}}{\partial G_i}. \quad (1.36)$$

Applying the identity  $e_i = (1 - G_i/L_i)^{1/2}$  to find the time derivative of the eccentricities  $e_i$  we have

$$\frac{de_i}{dt} = \frac{\partial e_i}{\partial L_i} \frac{dL_i}{dt} + \frac{\partial e_i}{\partial G_i} \frac{dG_i}{dt}.$$

Using equations (1.36) and considering that for the averaged Hamiltonian

$$\frac{dL_i}{dt} = -\frac{\partial \langle \mathcal{H}_J \rangle_{P3}}{\partial l_i} = 0,$$

one arrives at

$$\frac{de_1}{dt} = \frac{\sqrt{1 - e_1^2}}{e_1 L_1} \frac{\partial \langle \mathcal{H}_J \rangle_{P3}}{\partial g_1} = \sqrt{\frac{(m_0 + m_1)(1 - e_1^2)}{\mathcal{G}a_1(m_0 m_1 e_1)^2}} \frac{\partial \langle \mathcal{H}_J \rangle_{P3}}{\partial \varpi_1}, \quad (1.37)$$

Here, we have used that  $g_i$  and the longitudes of pericenter  $\varpi_i$  are identical in the coplanar case. We can, therefore, calculate the following time derivative

$$\begin{aligned} \dot{\varpi}_1 &= \frac{dg_1}{dt} = \frac{\partial \langle \mathcal{H}_J \rangle_{P3}}{\partial G_1} = \frac{\partial \langle \mathcal{H}_J \rangle_{P3}}{\partial e_1} \frac{\partial e_1}{\partial G_1} \\ &= -\frac{\sqrt{1 - e_1^2}}{e_1 L_1} \frac{\partial \langle \mathcal{H}_J \rangle_{P3}}{\partial e_1} = -\sqrt{\frac{(m_0 + m_1)(1 - e_1^2)}{\mathcal{G}a_1(m_0 m_1 e_1)^2}} \frac{\partial \langle \mathcal{H}_J \rangle_{P3}}{\partial e_1}. \end{aligned} \quad (1.38)$$

Consequently, the differential equations governing the secular evolution of the eccentricity vector's components can be derived

$$\frac{d}{dt} \begin{pmatrix} k_1 \\ h_1 \end{pmatrix} = \left[ \mathcal{A} \frac{\partial \langle \mathcal{H}_J \rangle_{P3}}{\partial \varpi_1} - \mathcal{B} \frac{\partial \langle \mathcal{H}_J \rangle_{P3}}{\partial e_1} \begin{pmatrix} 0 & 1 \\ 1 & 0 \end{pmatrix} \right] \begin{pmatrix} k_1 \\ h_1 \end{pmatrix}, \quad (1.39)$$

---

<sup>1</sup>Please note that there is a clash in nomenclature regarding  $e_1$ . While generally  $e_1$  refers to the total inner eccentricity, i.e. the combination of short period and secular contributions, it represents only the secular eccentricity in equations (1.34-1.40). This global inconsistency is tolerated, because it helps to keep the derivation of the secular equations as well as sections 1.3.3-1.3.5 intuitively accessible. A similar clash in nomenclature exists for the letter  $L$  which may be referred to as mean longitude, luminosity or a given action.

where

$$\mathcal{A} = \frac{1}{e_1^2 m_0 m_1} \left[ \frac{(1 - e_1^2)(m_0 + m_1)}{9a_1} \right]^{1/2} \quad \text{and} \quad \mathcal{B} = e_1 \mathcal{A}.$$

The partial derivatives of the Hamiltonian will still contain the variables  $\varpi_2$  and  $e_2$ . Hence, their evolution has to be taken into account as well. In order to complete the set of secular differential equations we construct expressions for  $\dot{g}_2 = \dot{\varpi}_2$  and  $\dot{e}_2$ , following Georgakarakos (2003). The full equations for the secular evolution of the eccentricity vector read

$$\begin{aligned} \frac{dk_1}{d\tau} &= \alpha \frac{5}{16} \frac{e_2(1 - e_1^2)^{1/2}}{(1 - e_2^2)^{5/2}} \left[ (4 + 3e_1^2) \sin \varpi_2 + 6(k_1 h_1 \cos \varpi_2 + h_1^2 \sin \varpi_2) \right] \\ &\quad - \left[ \frac{(1 - e_1^2)^{1/2}}{(1 - e_2^2)^{3/2}} + \gamma \frac{25}{8} \frac{3 + 2e_2^2}{(1 - e_2^2)^3} \left( 1 - \frac{3}{2} e_1^2 \right) \right] h_1 \\ &\quad + \gamma \frac{15}{8} \frac{e_2^2}{(1 - e_2^2)^3} \left[ h_1 \cos 2\varpi_2 - k_1 \sin 2\varpi_2 - \frac{h_1}{2} (k_1^2 + 3h_1^2) \cos 2\varpi_2 + k_1 (k_1^2 + 2h_1^2) \sin 2\varpi_2 \right] \\ \frac{dh_1}{d\tau} &= -\alpha \frac{5}{16} \frac{e_2(1 - e_1^2)^{1/2}}{(1 - e_2^2)^{5/2}} \left[ (4 + 3e_1^2) \cos \varpi_2 + 6(k_1 h_1 \sin \varpi_2 + k_1^2 \cos \varpi_2) \right] \\ &\quad + \left[ \frac{(1 - e_1^2)^{1/2}}{(1 - e_2^2)^{3/2}} + \gamma \frac{25}{8} \frac{3 + 2e_2^2}{(1 - e_2^2)^3} \left( 1 - \frac{3}{2} e_1^2 \right) \right] k_1 \\ &\quad + \gamma \frac{15}{8} \frac{e_2^2}{(1 - e_2^2)^3} \left[ k_1 \cos 2\varpi_2 + h_1 \sin 2\varpi_2 - \frac{k_1}{2} (h_1^2 + 3k_1^2) \cos 2\varpi_2 - h_1 (h_1^2 + 2k_1^2) \sin 2\varpi_2 \right] \\ \frac{de_2}{d\tau} &= \alpha \beta \frac{5}{16} \frac{(4 + 3e_1^2)}{(1 - e_2^2)^2} (h_1 \cos \varpi_2 - k_1 \sin \varpi_2) - \beta \gamma \frac{15}{8} \frac{e_2(1 - e_1^2)^{1/2}}{(1 - e_2^2)^{5/2}} [2k_1 h_1 \cos 2\varpi_2 - (k_1^2 - h_1^2) \sin 2\varpi_2] \\ \frac{d\varpi_2}{d\tau} &= \frac{\beta(2 + 3e_1^2)}{2(1 - e_2^2)^2} - \alpha \beta \frac{5}{16} \frac{(1 + 4e_2^2)}{e_2(1 - e_2^2)^3} (4 + 3e_1^2) (k_1 \cos \varpi_2 + h_1 \sin \varpi_2) \\ &\quad + \beta \gamma \frac{5}{8} \frac{(1 - e_1^2)^{1/2}}{(1 - e_2^2)^{7/2}} [5e_1^2(11 + 4e_2^2) + 3(1 + 2e_2^2) ((k_1^2 - h_1^2) \cos 2\varpi_2 + 2k_1 h_1 \sin 2\varpi_2)] . \end{aligned} \tag{1.40}$$

The parameters  $\alpha$ ,  $\beta$ ,  $\gamma$  and  $\tau$  are defined as follows

$$\begin{aligned} \alpha &= \frac{m_0 - m_1}{m_0 + m_1} \frac{a_1}{a_2}, & \beta &= \frac{m_0 m_1 M^{1/2}}{m_2 (m_0 + m_1)^{3/2}} \left( \frac{a_1}{a_2} \right)^{1/2}, \\ \gamma &= \frac{m_2}{M^{1/2} (m_0 + m_1)^{1/2}} \left( \frac{a_1}{a_2} \right)^{3/2}, & d\tau &= \frac{3}{4} \frac{G^{1/2} m_2 a_1^{3/2}}{a_2^3 (m_0 + m_1)^{1/2}} dt, \end{aligned}$$

where  $M$  is given in equation (1.33). In order to find analytical solutions to the set of coupled differential equations (1.40), the following assumptions are made:

- The changes in the eccentricity of the outer body are negligible. Therefore,  $de_2/d\tau \approx 0$ . This is certainly the case for the S-Type binary star systems hosting a terrestrial planet, see for instance Figures 1.11 and 1.12.
- Since the planet-to-binary semimajor axis ratio  $a_1/a_2$  is small, all terms proportional to  $\alpha$  and  $\gamma$  are neglected causing the equation for  $d\varpi_2/d\tau$  to become independent of  $k_1$  and  $h_1$ . However, this simplification modifies the frequencies in the planet's eccentricity evolution, which causes a period error in  $e_1$ , see Figure 1.11, bottom right panel.

## 1. INTRODUCTION

---

- The injected secular planetary eccentricities are small, so that terms proportional to  $e_1^2$  can be neglected. In one of the most extreme cases treated in this work, namely the system HIP 64241 in chapter 4, the maximum eccentricity of the planet's orbit does not rise much above  $e^{max} \approx 0.2$  before dynamical instability sets in. Therefore, this assumption is reasonable for our purposes.

Applying the afore mentioned simplifications, an analytic solution for the secular evolution of the eccentricity vector can be given

$$\mathbf{e}_1^{sec} = \begin{pmatrix} k_1 \\ h_1 \end{pmatrix}^{sec} = \begin{pmatrix} K_1 & K_2 \\ -K_2 & K_1 \end{pmatrix} \begin{pmatrix} \cos[B\tau] \\ \sin[B\tau] \end{pmatrix} + \frac{C}{B-A} \begin{pmatrix} \cos[A\tau + \varpi_{1,0}] \\ \sin[A\tau + \varpi_{1,0}] \end{pmatrix}, \quad (1.41)$$

where  $K_1$  and  $K_2$  are constants of integration

$$K_1 = -e_{1x}^c - \frac{C}{B-A} \cos \varpi_{1,0}, \quad K_2 = e_{1y}^c - \frac{C}{B-A} \sin \varpi_{1,0},$$

and variables  $A$ ,  $B$ , and  $C$  are

$$A = \beta(1 - e_2^2)^{-2}, \quad B = (1 - e_2^2)^{-3/2} + \gamma \frac{25}{8} \frac{3 + 2e_2^2}{(1 - e_2^2)^3}, \quad C = \alpha \frac{5}{4} \frac{e_2}{(1 - e_2^2)^{5/2}}.$$

Finally, short period and secular solutions (1.32) and (1.41) can be combined as pointed out in equation (1.31), to give a full set of time dependent equations for  $\mathbf{e}_1(t)$ . The corresponding equations for  $\varpi_1(t)$  can then be gained via

$$\varpi_1 = \arctan \left( \frac{h_1}{k_1} \right). \quad (1.42)$$

The performance of Georgakarakos' analytic estimates is visualized in Figures 1.11 and 1.12. Furthermore, Georgakarakos (2003, 2005) provided an expression for  $\langle e_1^2 \rangle$  which constitutes an integral part of the analytic method to determine HZs in binary star systems; see sections 2.6

and 5.2 for details. Averaging  $e_1^2$  over time as well as over the initial angles  $f_{2,0}$  and  $\varpi_2$  yields

$$\begin{aligned}
\langle e_1^2 \rangle = & \frac{m_2^2}{M^2} \frac{1}{X^4(1-e_2^2)^{\frac{9}{2}}} \left\{ \frac{43}{8} + \frac{129}{8}e_2^2 + \frac{129}{64}e_2^4 \right. \\
& + \frac{1}{(1-e_2^2)^{\frac{3}{2}}} \left( \frac{43}{8} + \frac{645}{16}e_2^2 + \frac{1935}{64}e_2^4 + \frac{215}{128}e_2^6 \right) \\
& + \frac{1}{X^2(1-e_2^2)^3} \left[ \frac{365}{18} + \frac{44327}{144}e_2^2 + \frac{119435}{192}e_2^4 + \frac{256105}{1152}e_2^6 + \frac{68335}{9216}e_2^8 \right. \\
& + \left. \frac{1}{(1-e_2^2)^{\frac{3}{2}}} \left( \frac{365}{18} + \frac{7683}{16}e_2^2 + \frac{28231}{16}e_2^4 + \frac{295715}{192}e_2^6 + \frac{2415}{8}e_2^8 + \frac{12901}{2048}e_2^{10} \right) \right] \\
& + \frac{1}{X(1-e_2^2)^{\frac{3}{2}}} \left[ \frac{61}{3} + \frac{305}{2}e_2^2 + \frac{915}{8}e_2^4 + \frac{305}{48}e_2^6 + \right. \\
& + \left. \frac{1}{(1-e_2^2)^{\frac{3}{2}}} \left( \frac{61}{3} + \frac{854}{3}e_2^2 + \frac{2135}{4}e_2^4 + \frac{2135}{12}e_2^6 + \frac{2135}{384}e_2^8 \right) \right] \\
& + m_*^2 X^{\frac{2}{3}} (1-e_2^2) \left[ \frac{225}{256} + \frac{3375}{1024}e_2^2 + \frac{7625}{2048}e_2^4 + \frac{29225}{8192}e_2^6 + \frac{48425}{16384}e_2^8 + \frac{825}{2048}e_2^{10} \right. \\
& + \left. \frac{1}{(1-e_2^2)^{\frac{3}{2}}} \left( \frac{225}{256} + \frac{2925}{1024}e_2^2 + \frac{775}{256}e_2^4 + \frac{2225}{8192}e_2^6 + \frac{25}{512}e_2^8 \right) \right] \\
& + \frac{m_*^2}{X^{\frac{4}{3}}(1-e_2^2)^2} \left[ \frac{8361}{4096} + \frac{125415}{8192}e_2^2 + \frac{376245}{32768}e_2^4 + \frac{41805}{65536}e_2^6 \right. \\
& + \left. \frac{1}{(1-e_2^2)^{\frac{3}{2}}} \left( \frac{8361}{4096} + \frac{58527}{2048}e_2^2 + \frac{877905}{16384}e_2^4 + \frac{292635}{16384}e_2^6 + \frac{292635}{524288}e_2^8 \right) \right] \Bigg\} \\
& + 2 \left( \frac{C}{B-A} \right)^2.
\end{aligned} \tag{1.43}$$

## 1. INTRODUCTION

---

## Chapter 2

# An Analytic Method To Determine Habitable Zones For S-Type Planetary Orbits In Binary Star Systems

The following article contains the analytical and conceptual groundwork necessary to investigate possible states of habitability an Earth-like planet can attain on circumstellar orbits in binary star systems. The classical concept of habitability as defined in Kasting et al. (1993) is combined with state of the art analytical estimates for the gravitational interaction between the planet and the binary star (Georgakarakos 2003, 2005).

**authors:** Siegfried Eggl, Elke Pilat-Lohinger, Nikolaos Georgakarakos, Markus Gyergyovits and Barbara Funk<sup>1</sup>

**publication state:** published June 10<sup>th</sup>, 2012

**publication details:** The Astrophysical Journal, 752:74 (11pp), 2012

**contribution of the first author:** The first author was responsible for the idea to combine classical habitability with analytic estimates for the three body dynamics in this problem in order to generate an efficient tool for investigating the different kinds of habitability a planet encounters within an S-Type binary star system. The development, implementation and evaluation of the proposed methodology as well as the composition of the following article were performed by the first author.

**contribution of the co-authors:** The idea to investigate binary star systems as well as the resources necessary for the project's success were mostly supplied by the coauthors. Furthermore, the coauthors' contributions encompassed the analytical estimates of  $e_{max}$  presented in appendix B as well as the idea to find analytic expressions for radiation variances. Finally, the co-authors played a vital role in scientific discussions and in providing proposals for improvements of the article.

---

<sup>1</sup>Author affiliations are presented in the header of the following article.

## AN ANALYTIC METHOD TO DETERMINE HABITABLE ZONES FOR S-TYPE PLANETARY ORBITS IN BINARY STAR SYSTEMS

SIEGFRIED EGGL<sup>1</sup>, ELKE PILAT-LOHINGER<sup>1</sup>, NIKOLAOS GEORGAKARAKOS<sup>2</sup>, MARKUS GYERGYOVITS<sup>1</sup>, AND BARBARA FUNK<sup>1</sup>

<sup>1</sup> Institute for Astronomy, University of Vienna, Türkenschanzstr. 17, A-1180 Vienna, Austria; [siegfried.eggl@univie.ac.at](mailto:siegfried.eggl@univie.ac.at), [elke.pilat-lohinger@univie.ac.at](mailto:elke.pilat-lohinger@univie.ac.at)

<sup>2</sup> 128 V. Olgas str., Thessaloniki 546 45, Greece

Received 2012 January 31; accepted 2012 April 10; published 2012 May 25

### ABSTRACT

With more and more extrasolar planets discovered in and around binary star systems, questions concerning the determination of the classical habitable zone have arisen. Do the radiative and gravitational perturbations of the second star influence the extent of the habitable zone significantly, or is it sufficient to consider the host star only? In this article, we investigate the implications of stellar companions with different spectral types on the insolation a terrestrial planet receives orbiting a Sun-like primary. We present time-independent analytical estimates and compare them to insolation statistics gained via high precision numerical orbit calculations. Results suggest a strong dependence of permanent habitability on the binary's eccentricity, as well as a possible extension of habitable zones toward the secondary in close binary systems.

**Key words:** astrobiology – celestial mechanics – methods: analytical – planet–star interactions

**Online-only material:** color figures

### 1. INTRODUCTION

Fueled by the successes of current transit-observation incentives like *Kepler* (Welsh et al. 2012; Borucki & Koch 2011) and *CoRoT* (Baglin et al. 2009; Tingley et al. 2011) the quest for discovering the first Earth twin has lead to a considerable cross-disciplinary interest in the interplay between stellar and planetary properties necessary to produce habitable worlds. Even though opinions differ on what exactly to look for in a system harboring a terrestrial planet in order to declare it “habitable” (see, e.g., Buccino et al. 2006; Kaltenegger et al. 2007; Selsis et al. 2007; Lammer et al. 2009), the classical assumption investigated by Kasting et al. (1993), i.e., the capacity for water to stay liquid on the planet's surface, may still be considered a prerequisite for the development and sustainability of complex life as we know it (Kaltenegger & Sasselov 2011). This entails restrictions on planetological characteristics, such as mass, atmospheric, and bulk composition, and sets limits to the host star's activity as well as radiation properties (Lammer et al. 2009). Dynamical considerations are of equal importance, since changes in orbital stability or extreme variations in insolation due to large planetary eccentricities ( $e_p > 0.7$ ) may also result in a hostile environment (Williams & Pollard 2002). It is therefore only natural that one would look for a copy of our solar system when searching for habitable worlds. Yet the study of exoplanetary systems so far has clearly shown that a broader perspective is required.

In fact, up to 70% of all stellar systems in our galaxy may not be single-stellar systems but multi-stellar systems (e.g., Kiseleva-Eggleton & Eggleton 2001 and references therein). Together with the approximately 60 planets that have already been discovered in systems harboring two stars (Schneider et al. 2011) this suggests that binary and multiple star systems should not be ignored in the search for habitable worlds.

Investigations of environments that permit planetary formation in binary star systems have progressed rapidly over the last decade (see, e.g., Thebault 2011 and references therein). Even though important questions regarding the early phases of planet formation in binary star systems—especially the transition from planetesimal to planetary embryos—still remain to be answered,

late stage formation scenarios for terrestrial planets in such environments are available (Whitmire et al. 1998; Haghighipour & Raymond 2007; Haghighipour et al. 2010). Since previous studies did consider the extent of the classical habitable zone (KHZ) to be purely a function of the primary star's luminosity and spectral type as introduced by Kasting et al. (1993, hereafter KWR93), we aim to refine this definition to encompass the gravitational and radiative influence of a second star.

This article is structured as follows: after a short recapitulation of the main radiative aspects of habitability as defined in KWR93, Section 2 introduces three exemplary binary–planet configurations, which will serve as test-cases for habitability considerations. Section 3 briefly mentions the dynamical requirements that binary–planet configurations have to fulfill in order to ensure system stability. In Section 4, the maximum radiative influence of the second star on a terrestrial planet in the primary's HZ is estimated and compared to actual insolation simulations. The occurring differences are investigated in the following section. Finally, generalized, analytical estimates are developed and compared to numerical simulations in Sections 6 and 7, and the results concerning the behavior of HZs in binary star systems are presented in Section 8. A discussion of the results concludes this article.

### 2. BINARY–PLANET CONFIGURATIONS

Apart from planetological and dynamical aspects, the insolation a terrestrial planet receives from its host star is naturally the main driver determining the extent of the HZ. When considering planets within a binary star system it is therefore important to track the combined radiation of both stars arriving at the planet. KWR93 showed that not only the sheer amount of insolation but also the spectral distribution is essential to estimate limiting values for atmospheric collapse. In order to model the impact of diverse stellar spectral classes on an Earth-like planet's atmosphere, KWR93 introduced the so-called effective radiation values. These measure the relative impact a comparable amount of radiation (e.g.,  $1360 \text{ [W m}^{-2}\text{]}$ ) with different spectral properties has on a planet's atmosphere. Taking the effects of



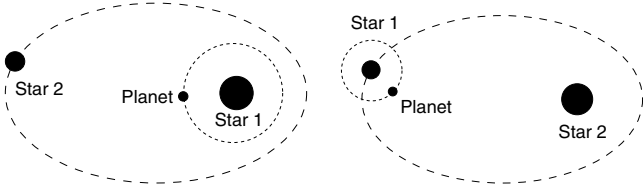


**Figure 1.** Two examples of S-Type motion, i.e., the planet orbits only one binary component (Dvorak 1984); left: S-Type I ( $\mu \leq 0.5$ ), the more massive star is the planet’s host (primary); right: S-Type II ( $\mu > 0.5$ ), the less massive star is the planet’s host.

**Table 1**

Limiting Radiation Values for the Inner (A) and Outer (B) Border of the HZ in Units of Solar Constants ( $1360 \text{ W m}^{-2}$ )

Spectral Type	A	B
F0	1.90	0.46
G2	1.41	0.36
M0	1.05	0.27

**Note.** The values were taken from Kasting et al. (1993) assuming a runaway greenhouse scenario for the inner limit, and a maximum greenhouse effect for the outer limit.

different stellar spectra into account is especially important in binary star systems with different stellar components. Table 1 reproduces the effective radiation values for the inner (runaway greenhouse) and outer (maximum greenhouse) edges of a single star’s HZ as given in KWR93. Notice how the onset of runaway greenhouse effects requires almost twice as much radiation for a spectral distribution akin to F0 class stars compared to M0 spectral types. Even though Kaltenegger & Sasselov (2011) assume similar effective radiation values for M and K spectral classes, actual calculations have only been done for F0, G2, and M0 zero-age main-sequence (ZAMS) stars. For this reason, we first investigate the following three stellar configurations:

1. G2–M0  $\mu \simeq 0.3$ .
2. G2–G2  $\mu \simeq 0.5$ .
3. G2–F0  $\mu \simeq 0.6$ .

All stellar components are considered to be ZAMS stars, and  $\mu = m_2/(m_1 + m_2)$  denotes the binary’s mass ratio. A terrestrial planet is orbiting the Sun-like G2 host-star, hereafter referred to as primary. Such binary–planet configurations are considered to be of satellite type (S-Type), i.e., the planet revolves around one star (Dvorak 1984); see Figure 1. In fact, most of the planets in binary systems have been discovered to be of S-Type (Schneider et al. 2011), e.g., the system Gamma Cephei (Hatzes et al. 2003). In the following, we choose binary systems with semimajor axes between 10 and 50 AU for the comparison of numerical and analytical estimates on the extent of the HZ, as for closer binaries the HZs in G2–G2 and G2–F0 configurations are considerably reduced due to dynamical instability, whereas the qualitative differences for results beyond 50 AU are small. However, the methods presented in Section 6 are viable beyond those limits, as long as the assumptions given in Georgakarakos (2003) remain valid.

The terrestrial planet is assumed to be cloudless (Kaltenegger & Sasselov 2011) and orbits the G2 star only, resulting in configurations (1) and (2) to be classified as S-Type I ( $\mu \leq 0.5$ ) and (3) as S-Type II ( $\mu > 0.5$ ), respectively (see Figure 1).

**Table 2**

Critical, Planetary Semimajor Axis in a Normalized Binary Star System  $a_b = 1$  with Mass-ratio  $\mu$  as Stated in Holman & Wiegert (1999) Compared to the Values Found by Pilat-Lohinger & Dvorak (2002) via Fast Lyapunov Chaos Indicator (FLI)

$e_b$	$\mu = 0.3$		$\mu = 0.5$		$\mu = 0.6$	
	FLI	HW99	FLI	HW99	FLI	HW99
0.0	0.37	0.37	0.27	0.26	0.23	0.23
0.1	0.29	0.30	0.25	0.24	0.21	0.20
0.2	0.25	0.25	0.19	0.20	0.18	0.18
0.3	0.21	0.21	0.16	0.18	0.15	0.16
0.4	0.18	0.18	0.15	0.15	0.12	0.13
0.5	0.13	0.14	0.12	0.12	0.09	0.10
0.6	0.09	0.11	0.08	0.09	0.07	0.08
0.7	0.07	0.07	0.05	0.06	0.05	0.05
0.8	0.04	0.04	0.03	0.04	0.02	0.035
0.9	0.01	...	0.01	...	0.01	...

**Notes.** The higher the binary’s eccentricity  $e_b$ , the smaller the test-planet’s semimajor axis has to be to permit dynamical stability. Even though the results are very similar, the FLI limits tend to be more conservative for higher mass ratios and binary eccentricities.

### 3. DYNAMICAL STABILITY

Binary–planet configurations that lead to highly chaotic orbits and eventual ejection of the planet cannot be considered habitable. Therefore, dynamical stability of the system is a basic requirement for our consideration. In order to assess the dynamical stability of a test planet’s orbit within the given binary star systems, we applied results of numerical stability studies by Rabl & Dvorak (1988; hereafter RD88), Pilat-Lohinger & Dvorak (2002; hereafter PLD02), and Holman & Wiegert (1999; hereafter HW99), determining stable zones in a planar, normalized system (binary semimajor axis  $a_b = 1$ ). In contrast to RD88 and HW99 who classified unstable orbits via ejections of test planets from the system, PLD02 applied the Fast Lyapunov Indicator (FLI) chaos detection method (Froeschlé et al. 1997) implemented in a Bulirsch–Stoer extrapolation code (Bulirsch & Stoer 1964). In Table 2 maximum planetary semimajor axes which still allow for a stable configuration in the normalized setup are shown for different binary orbits and mass ratios. Results gained via FLI by PLD02 are compared to those published in HW99. Even though the critical values are very similar, the onset of dynamical chaos (PLD02) in G2–G2 and G2–F0 configurations appears for smaller planetary semimajor axes than predicted by the ejection criterion in HW99. For the following investigations the more conservative FLI stability estimates by PLD02 are used.

### 4. INFLUENCE OF THE SECONDARY

The main question in dealing with habitability in binary star systems is doubtlessly: “How does the second star affect the HZ around the primary?” Let us focus on the dynamical aspects first, as stability is a prerequisite to habitability. The results from the previous section dictate that not all combinations of a binary’s semimajor axis  $a_b$  and eccentricity  $e_b$  are viable, if orbital stability of planets in the primary’s HZ is required. Figure 2 (top left) shows quadratic fits of the FLI stability data presented in Table 2. The secondary’s allowed eccentricities are higher for planets orbiting the primary near the inner border of the KHZ than for cases where the planet’s semimajor axis is close to the KHZ’s outer rim. Such dynamical restrictions set limits on how close the secondary can approach the planet,

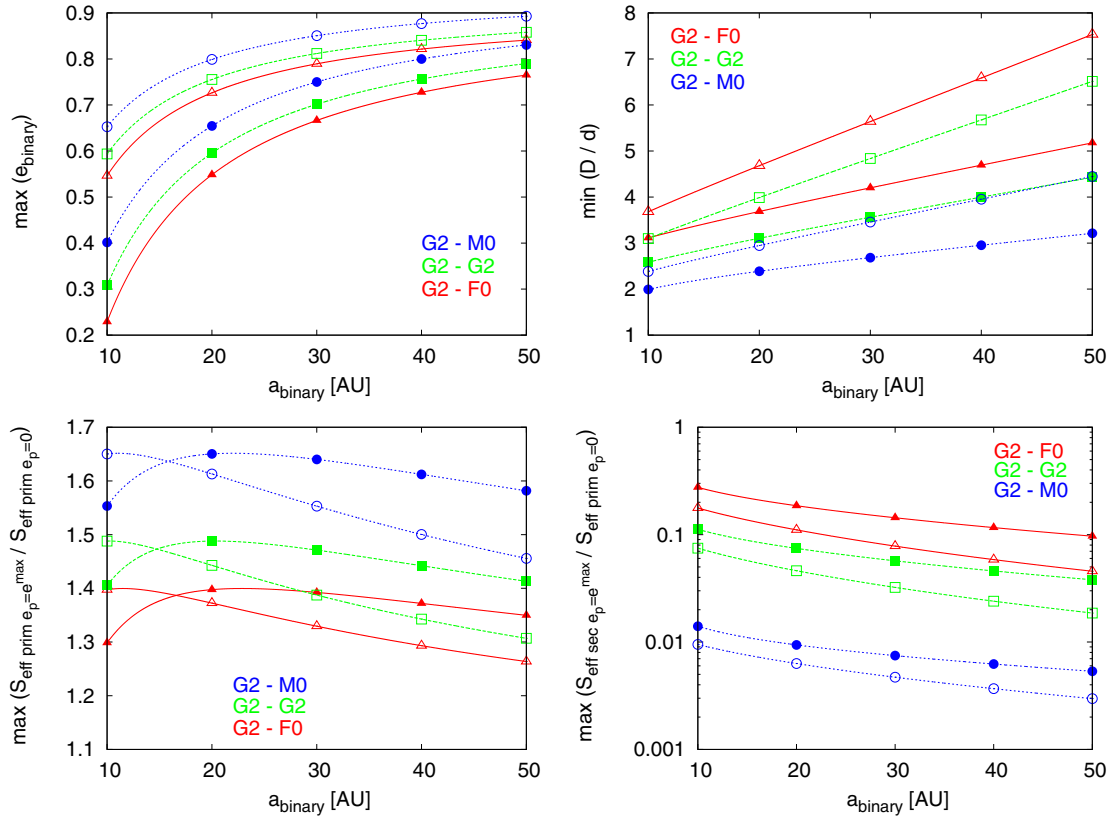


**Figure 2.** Top left: highest possible binary eccentricity as a function of the secondary’s semimajor axis, if a terrestrial planet was to remain dynamically stable on orbits with semimajor axes corresponding to the inner (runaway greenhouse, open symbols) or outer (maximum greenhouse, full symbols) boundaries of the HZ as defined by Kasting et al. (1993). The curves represent quadratic fits of the FLI stability data presented in Table 2. Three different S-Type stellar configurations are shown: G2-F0 ( $\Delta$ ,  $\blacktriangle$ ), G2-G2 ( $\square$ ,  $\blacksquare$ ), and G2-M0 ( $\circ$ ,  $\bullet$ ). Top right: minimum distance between planet and secondary ( $D$ ) permitting planetary orbital stability in units of planetary aphelion distances from the primary ( $d = a_p(1 + e_p^{\text{max}})$ ). The planet’s eccentricity was estimated following Georgakarakos (2005). Bottom left: here, the increase of the primary’s effective insolation onto a terrestrial planet with injected eccentricity is compared to a single-star setup where the planet remains on a circular orbit. The planet is considered to be in periastron position ( $a_p(1 - e_p^{\text{max}})$ ). Bottom right: the secondaries’ maximum radiative contributions to planetary insolation are presented—the planet is in apocenter position with regard to the primary ( $d$ ) and the secondary is at pericenter. Once again, the results are normalized with regard to values which a single-star configuration with a terrestrial planet on a constant circular orbit would exhibit. One can see that the primary’s radiative influence dominates in S-Type I systems, whereas for close S-Type II configurations the secondary’s contribution is almost equally important.

(A color version of this figure is available in the online journal.)

which will in turn limit its insolation on the planet. Applying analytical approximations introduced later in this section Figure 2 (top right) demonstrates that the smallest possible separation between planet and secondary is always larger than the planet’s aphelion distance to its primary. This lessens the second star’s potential radiative contribution considerably for all but close S-Type II configurations. In the latter case, the enhanced luminosity of the secondary compensates larger distances to the planet. Using the minimum distances presented in Figure 2 (top right), one can estimate that in a G2-G2 S-Type I system with  $a_b = 20$  AU, the secondary’s radiative influence on a planet started at the inner edge of the KHZ is in the order of only 10% of the primary’s contribution. As a consequence, the secondary was often considered not to have a significant radiative impact on the extent of the primary’s HZ (Whitmire et al. 1998; Haghighipour & Raymond 2007; Haghighipour et al. 2010).

Such a so-called single-star approach, however, stands in contrast to numerical experiments presented in the left panel of Figure 3. The effective insolation curves shown were generated solving the full Newtonian Three-Body Problem (3BP) numerically via Lie-Series (Hanslmeier & Dvorak 1984; Eggl & Dvorak 2010) and Gauss-Radau (Everhart 1974) integrators, where the actual amount of radiation the planet receives was calculated for each integration step. One can see that a planet started

at the inner edge of the KHZ in a G2-G2 S-Type binary experiences an increase of more than 30% in insolation compared to a planet on a circular orbit with corresponding semimajor axis around a single G2 star. Consequently, an Earth-like planet would spend a considerable time outside the classical, circular HZ in a G2-G2 configuration. Is, therefore, the secondary’s radiative impact more important than assumed? The fact that the variations in insolation perfectly correlate with the dynamical evolution of the planet’s eccentricity (see Figure 3, right panel) permits an alternative explanation: changes in the planetary orbit induced via gravitational perturbation by the second star might be responsible for the increased insolation values. Even though planetary and binary orbits’ semimajor axes are not expected to show any secular variation (e.g., Harrington 1968), it is known that even a distant companion would inject some eccentricity into the orbit of two bodies revolving around their common center of mass (e.g., Mazeh & Shaham 1979; Georgakarakos 2002). Elevated planetary eccentricities would entail smaller periastron distances—allowing for increased insolation by the primary.

In order to draw a clearer picture of whether the perturbation-induced rise in the planet’s eccentricity or the secondary star’s radiative influence are the dominant factors causing the increased insolation onto the planet encountered in Figure 3 (left

panel), we will make three assumptions, which our analytical estimates will be based on:

1. the binary–planet system is coplanar;
2. stellar luminosities  $L$  are constant on timescales of the system’s secular dynamics; and
3. stellar occultation effects are negligible.

Since we assume coplanar orbits, we make extensive use of the analytic expressions in Georgakarakos (2003, 2005) to calculate the time-averaged-squared planetary eccentricity  $\langle e_p^2 \rangle_t$ . In Appendix B, we derive estimates on the planet’s maximum injected eccentricity  $e_p^{\max}$ . Unlike the recent ansatz by Giuppone et al. (2011) and earlier by Thébault et al. (2006), where the eccentricity evolution of a planet in a stellar binary was modeled by empirical formulae, Georgakarakos (2003, 2005) derived an entirely analytical formula for the eccentricity of the inner—in this case the planet’s—orbit of a hierarchical triple system, which is valid for a wide range of mass ratios and initial conditions. Together with the estimates for  $e_p^{\max}$  in Appendix B, the formulae presented in Georgakarakos (2003, 2005) are an analytical extension to the first order with respect to the perturbing mass secular perturbation theory, as given for example in the longstanding work of Heppenheimer (1978).

Assumptions 2 and 3 are reasonable for well-separated binary stars, where both components are on the main sequence. The combination of the dynamical stability results presented in Figure 2 (top left panel) and the analytic expressions for the injected planetary eccentricity allows us to estimate not only the minimum distances between the secondary and the planet as shown in Figure 2 (top right panel), but also the maximum contributions to the planetary insolation from the primary and the secondary star, respectively.

Figure 2 (bottom left panel) shows the primary’s effective insolation onto a terrestrial planet during its closest perihelion passage  $d = a_p(1 - e_p^{\max})$ . Here, the largest dynamically possible perturbation by the secondary is considered. In order to separate the secondary’s radiative and gravitational effects, the second star’s radiation has been excluded in this plot. Given a binary semimajor axis of 10 AU, Earth analogs started at the inner edge of the KHZ permit considerably higher binary eccentricities (Figure 2, top left panel) compared to planets near the outer edge. Therefore, higher insulations for planets near the inner edge of the KHZ are expected, since the injected planetary eccentricities are coupled strongly to the binary’s eccentricity; see Appendix B. This effect abates around  $a_b = 20$  AU, where the primary’s insolation becomes almost equal for planets started near the inner and outer rims of the KHZ. For binary semimajor axes beyond  $a_b = 20$  AU planetary orbits closer to the secondary are more severely perturbed than the ones near the inner edge of KHZ, as the binaries’ maximum allowed eccentricities become similar for inner and outer borders of the KHZ and the perturbation is merely dependent on the binary to planet period ratios.

For planets on eccentric orbits in a G2–G2 configuration with  $a_b = 20$  AU, the primary’s insolation can increase up to almost 50% compared to circular orbits sharing the same semimajor axis. In contrast, even with the planet being as close to the second star as dynamically possible, the secondary’s maximum radiative input only accounts for an additional 10% in the same setup. This can be seen in the bottom right panel of Figure 2. Hence, the primary is the main source of the additional insolation in S-Type I systems, which can only be explained via changes in the planet’s eccentricity. Solely for S-Type II systems

like G2–F0 binaries, the secondary’s radiative contributions to planetary insolation can become comparable to the primary’s (cf. Figure 2, bottom panels).

## 5. CONSEQUENCES FOR THE HABITABLE ZONE

In the previous section, the rise in the planet’s eccentricity was identified as a main driver for the strong variance in simulated insolation curves in S-Type I systems. Eccentric planetary orbits entail strong variations in insolation over an orbital period. Nevertheless, Williams & Pollard (2002) concluded that this might not necessarily be prohibitive for habitability. As long as the average insolation values lie within habitable limits and  $e_p < 0.7$ , the atmosphere should be able to act as a buffer, preventing immediate carbon freeze-out or instantaneous water evaporation. In order to distinguish between cases where the planet remains within the radiative boundaries of the KHZ for all times, configurations where the planet is “on average” within the HZ, and non-habitability, we introduce the following three categories.

*Permanently Habitable Zone (PHZ).* The PHZ is the region where a planet always stays within the insolation limits ( $A$ ,  $B$ ) of the corresponding KHZ, i.e.,

$$A \geq S_{\text{eff}} \geq B, \quad (1)$$

where  $A$  denotes the inner and  $B$  the outer effective radiation limit for a given spectral type; see Table 1.

*Extended Habitable Zone (EHZ).* In contrast to the PHZ—where the planet stays within the KHZ for all times—parts of the planetary orbit lie outside the HZ due to, e.g., the planet’s eccentricity. Yet the binary–planet configuration is still considered to be habitable when most of its orbit remains inside the HZ boundaries:

$$\langle S_{\text{eff}} \rangle_t + \sigma \leq A \wedge \langle S_{\text{eff}} \rangle_t - \sigma \geq B, \quad (2)$$

where  $\langle S_{\text{eff}} \rangle_t$  denotes the time-averaged effective insolation from both stars and  $\sigma^2$  is the effective insolation variance.

*Averaged Habitable Zone (AHZ).* Following the argument of Williams & Pollard (2002), this category encompasses all configurations which allow for the planet’s time-averaged effective insolation to be within the limits of the KHZ:

$$A \geq \langle S_{\text{eff}} \rangle_t \geq B. \quad (3)$$

## 6. ANALYTICAL ESTIMATES

We now propose analytical estimates to achieve a classification of planetary habitability as was suggested in the previous section. The aim is to circumvent time-consuming numerical integrations when global parameter scans are required to check systems for possible habitability. Even though the following analytical estimates are presented utilizing the  $S_{\text{eff}}$  values developed in KWR93, more advanced atmospheric models for exoplanets can easily be introduced by exchanging the effective insolation values  $A$  and  $B$ .

### 6.1. Estimates for the PHZ

Let the second star move on a fixed Keplerian orbit with semimajor axes  $a_b$  and eccentricity  $e_b$ . Accordingly, the planet’s orbit has the semimajor axis  $a_p$  and acquires a maximum eccentricity of  $e_p^{\max}$  due to the secondary’s gravitational perturbations (cf. Figure 3, right panel). This permits us to estimate the maximum

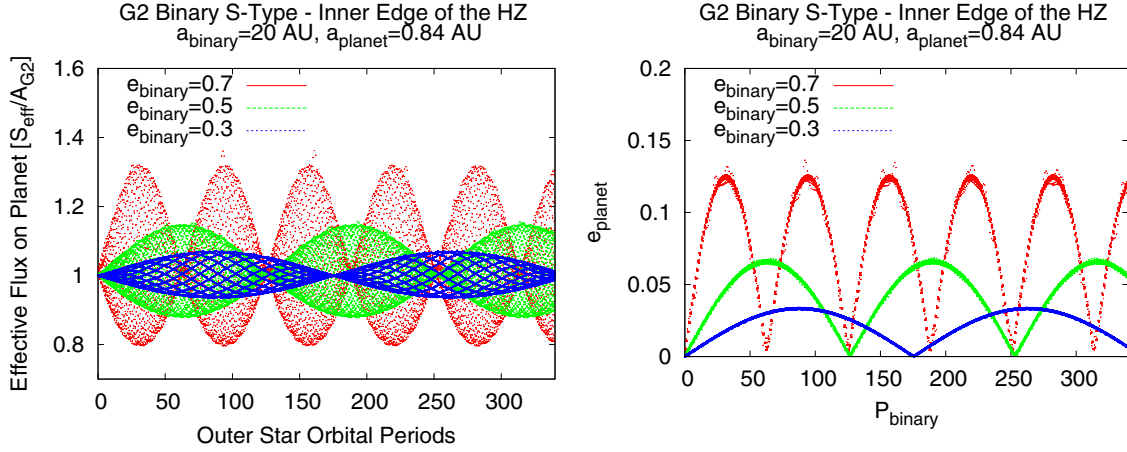


**Figure 3.** Evolution of insolation onto an Earth-like planet in a G2–G2 binary star system. The oscillations (left) are due to the injected changes in the planet’s eccentricity (right) caused by the gravitational perturbations of the secondary. (A color version of this figure is available in the online journal.)

and minimum insolation conditions for the planet to permanently remain within the KHZ.

*Insolation minimum condition.* Both planet and secondary are assumed to be in apocenter position and opposition. The additional normalization of the stellar luminosities per solid angle ( $L = L_{\text{bol}}/(4\pi)$ ) with regard to the respective outer insolation limits for each star ( $B_1, B_2$ ) ensures that different spectral properties are taken into account:

$$1 \leq \frac{L_1}{B_1} (a_p(1 + e_p^{\text{max}}))^{-2} + \frac{L_2}{B_2} (a_b(1 + e_b) + a_p(1 + e_p^{\text{max}}))^{-2}.$$

*Insolation maximum condition.* Again the luminosities are normalized, but this time with regard to the inner insolation limits ( $A_1, A_2$ ). Since we consider S-Type I and II systems, it is possible that the secondary at pericenter may produce a higher insolation on the planet than the primary star. If this is the case, the maximum insolation configuration will have the planet at apocenter with regard to the primary and the secondary at pericenter:

$$1 \geq \max \begin{cases} \frac{L_1}{A_1} (a_p(1 - e_p^{\text{max}}))^{-2} \\ \quad + \frac{L_2}{A_2} (a_b(1 - e_b) - a_p(1 - e_p^{\text{max}}))^{-2}, \\ \frac{L_1}{A_1} (a_p(1 + e_p^{\text{max}}))^{-2} \\ \quad + \frac{L_2}{A_2} (a_b(1 - e_b) - a_p(1 + e_p^{\text{max}}))^{-2}. \end{cases}$$

## 6.2. Estimates for the AHZ

The combined stellar insolation  $S_{\text{tot}}$  on the planet is, of course, a function of time. In order to calculate time-averaged insolation values, we will use that

$$\langle S_{\text{tot}} \rangle_t = \langle S_1 \rangle_t + \langle S_2 \rangle_t, \quad (4)$$

where  $\langle S_1 \rangle_t$  is the time average of the planetary insolation due to its host star and  $\langle S_2 \rangle_t$  is the time-averaged contribution of the second star. Let us focus on the two-body problem planet–host star first. Here,  $\langle S_1 \rangle_t = \langle L_1/\delta^2(t) \rangle_t$  where  $\delta(t)$  denotes the scalar distance between planet and primary. The average insolation a planet on an unperturbed Keplerian orbit experiences can be

calculated using the planet’s angular momentum  $h = \delta^2 \dot{f}$ ,  $f$  being the true anomaly:

$$\begin{aligned} \langle S_1 \rangle_t &= \frac{L_1}{P} \int_0^P \frac{1}{\delta^2(t)} dt \\ &= \frac{L_1 n}{2\pi} \int_0^{2\pi} \frac{1}{h} df \\ &= \frac{L_1 n}{h}. \end{aligned} \quad (5)$$

This expression states that the time-averaged insolation a planet receives over one orbit depends only on the star’s luminosity, the planet’s mean motion  $n$ , and its orbital angular momentum (see, e.g., Seager 2010, p. 18). Now let us construct a circular orbit so that  $h_{\text{circle}} = h_{\text{ellipse}}$ . A planet moving on such an orbit with “equivalence radius”  $r = a_p(1 - \langle e_p^2 \rangle_t)$  will experience the same amount of insolation per unit time as a planet on an elliptic orbit sharing the same angular momentum. The advantage of considering “equivalent circular orbits” is that the insolation remains constant for any orbital position of the planet. Of course, the reduction of elliptic orbits to circular orbits with common angular momentum will decrease the planet’s orbital period, as  $r \leq a$  and  $r = a$  only if  $\langle e_p^2 \rangle_t = 0$ . However, as we have chosen the “equivalent circular orbit” to have the same angular momentum, it will share the same constant rate of change of insolation with the true orbit. Therefore, even an average over the longer period of the elliptic orbit will still yield valid results.

We will now apply the same line of argumentation to construct the equivalence radius  $R$  for the secondary. This allows us to extend the pseudostatic radiation environment to include the average radiative influence of the secondary. Since the distinction between averaged and initial eccentricity is small for the secondary—its secular variance is negligible for the cases investigated—we can safely use the secondary’s initial eccentricity to calculate  $R$ . The suggested configuration is shown in Figure 4. The secondary circles the primary in a fictitious orbit with equivalence radius  $R$ , and the planet orbits the primary in a circle with radius  $r$ .

The insolation on the planet depends on the relative distances of the planet to both stars. In order to estimate the insolation on the planet caused by the secondary ( $S_2$ ), we simply apply law of cosine, and average over all possible geometric configurations



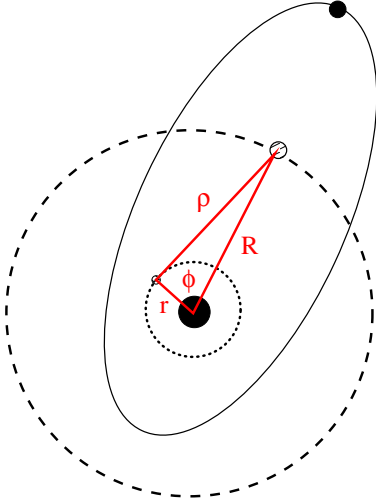


**Figure 4.** “Equivalence orbits” of the planet (dotted) and the secondary (dashed) around the primary.  $R$  denotes the equivalence radius of the secondary’s circular orbit sharing the same angular momentum with its actual elliptic orbit (continuous). The planet’s equivalence radius ( $r$ ), and the distance between the time-averaged secondary’s and planet’s positions ( $\rho$ ) as well as the angle ( $\phi$ ) opposite to  $\rho$  are highlighted. In order to calculate the secondary’s mean insolation on the planet, an averaging over  $1/\rho^2(\phi)$  is required.

(A color version of this figure is available in the online journal.)

(Figure 4):

$$\begin{aligned} \rho^2 &= R^2 + r^2 - 2rR \cos(\phi) \\ \langle S_2 \rangle_t &= \left\langle \frac{L_2}{\rho^2(\phi)} \right\rangle_\phi \\ &= \frac{L_2}{2\pi} \int_0^{2\pi} \frac{1}{R^2 + r^2 - 2rR \cos(\phi)} d\phi \\ &= \frac{L_2}{(R^2 - r^2)} \quad \text{if } R > r, \end{aligned} \quad (6)$$

where  $\rho$  is the planet’s distance to the secondary and  $\phi$  denotes the angle between the distance vectors of planet and secondary to the host star. Since we do not allow for orbit crossings of the planet and the secondary,  $R > r$  will always hold. Consequently, the total, time-averaged insolation onto the planet is given by

$$\langle S_{\text{tot}} \rangle_t = \frac{L_1}{r^2} + \frac{L_2}{(R^2 - r^2)}. \quad (7)$$

Equation (7) does not yet take the different spectral properties of the binary’s components into account. Therefore, we note the following conditions for the planet’s averaged insolation being within habitable limits.

*Average insolation minimum condition:*

$$1 \leq \langle S_{\text{eff},B} \rangle_t = \frac{L_1}{B_1} \frac{1}{r^2} + \frac{L_2}{B_2} \frac{1}{R^2 - r^2}.$$

*Average insolation maximum condition:*

$$1 \geq \langle S_{\text{eff},A} \rangle_t = \frac{L_1}{A_1} \frac{1}{r^2} + \frac{L_2}{A_2} \frac{1}{R^2 - r^2}.$$

Here, the indices 1, 2 indicate the respective star’s KHZ boundary values  $A$  and  $B$ ,  $R = a_b(1 - e_b^2)$ , and  $r = a_p(1 - \langle e_p^2 \rangle_t)$ , where the averaged-squared planetary eccentricity was calculated following Georgakarakos (2005).

### 6.3. Estimates for the EHZ

Having derived the insolation time averages in the previous section, the expected insolation variance ( $\sigma^2$ ) still remains to be determined:

$$\sigma^2 = \langle S_{\text{tot}}^2 \rangle_t - \langle S_{\text{tot}} \rangle_t^2. \quad (8)$$

Using Equation (7), and analytic estimates for  $\langle S_{\text{tot}}^2 \rangle_t$ , the effective insolation variance can be calculated as follows (see Appendix A):

$$\begin{aligned} \sigma_X^2 &= \frac{L_1^2}{X_1^2 r^4} (-1 + 3\langle e_p^2 \rangle - 3\langle e_p^2 \rangle^2 + \langle e_p^2 \rangle^3) \\ &\quad + \frac{L_1^2}{X_1^2 r^4} \sqrt{1 - \langle e_p^2 \rangle} \left( 1 - \frac{\langle e_p^2 \rangle}{2} - \frac{\langle e_p^2 \rangle^2}{2} \right) \\ &\quad - \frac{2L_1 L_2}{X_1 X_2 (r^4 - r^2 R^2)} (1 - \sqrt{1 - \langle e_p^2 \rangle} (1 + \langle e_p^2 \rangle)) \\ &\quad - \frac{2L_2^2 r^2}{X_2^2 (r^2 - R^2)^3}, \end{aligned} \quad (9)$$

where  $X_i \in \{A_i, B_i\}$  and the index  $i$  denotes the respective star. The minimum and maximum conditions for a planet to be within the EHZ are given as follows.

*Extended insolation minimum condition:*

$$1 \leq \langle S_{\text{eff},B} \rangle_t - \sigma_B.$$

*Extended insolation maximum condition:*

$$1 \geq \langle S_{\text{eff},A} \rangle_t + \sigma_A.$$

## 7. RELIABILITY OF ANALYTICAL ESTIMATES

In order to test the reliability of the analytical estimates presented in Section 6, we used high-precision numerical integration methods based on Gauss–Radau quadrature (Everhart 1974) and Lie-Series (Hanslmeier & Dvorak 1984; Eggl & Dvorak 2010) to determine the actual positions of both stars with respect to the Earth-like planet. Assuming that the stellar luminosities will not change significantly on the timescale of the planet’s secular period in eccentricity, good approximations of insolation patterns can be obtained. Figure 6 shows a comparison of analytic habitability classifications versus results gained via numerical orbit integration and direct insolation calculation. The setup consists of a terrestrial planet ( $1 M_\oplus$ ) in S-Type orbit around a G2 host star, with three different spectral types as secondary: F0 (top), G2 (middle), and M0 (bottom). The terrestrial planet was started on circular orbits with semimajor axes between  $0.6 \text{ AU} \leq a_p \leq 2 \text{ AU}$  with the secondaries’ semimajor axes being  $a_b = 50 \text{ AU}$ . The time span of the numerical integrations encompassed at least two secular periods in the planet’s eccentricity. It is evident that for small binary eccentricities, all three types of HZ coincide well with the borders defined in KWR93 indicated by the vertical lines at 0.84 and 1.67 AU. For  $e_b > 0.1$ , however, a splitting into the HZ categories defined in Sections 5 and 6 becomes eminent. The PHZ (black; blue in the online journal) shrinks considerably with growing eccentricity of the binary’s orbit. This is due to the perturbation-induced elevation of the planet’s eccentricity. In contrast, the region defined in KWR93 is best approximated by the AHZ (light gray; yellow in the online journal), which remains virtually unaffected by the secondary’s eccentricity. In this setup all analytically calculated

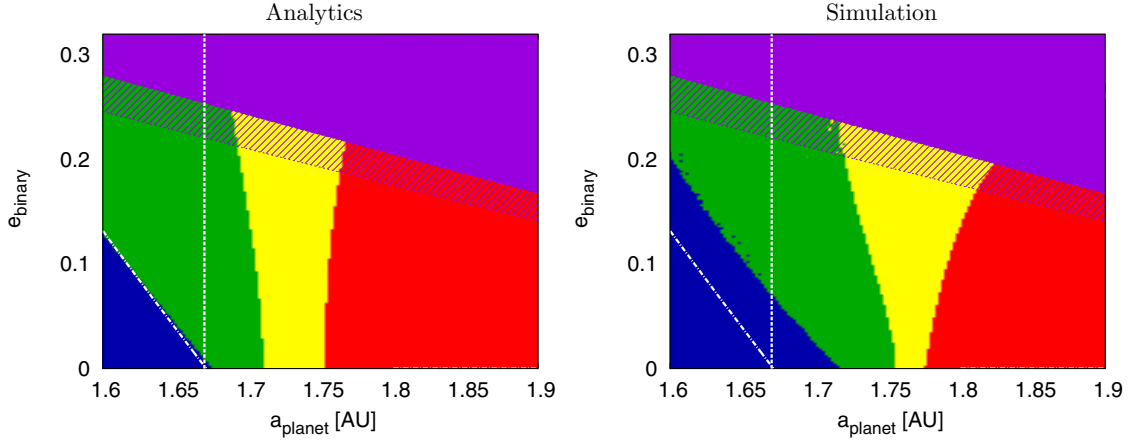


**Figure 5.** Classification of HZs in a G2–F0 binary star system of S-Type II with a semimajor axis  $a_b = 10$  AU. Left: zoom on the outer limit of the classical HZ (dashed line) close to the instability region (purple). The results were gained using analytic estimates presented in Section 6. Black (blue in the online journal) denotes the PHZ, dark gray (green in the online journal) the EHZ, light gray (yellow in the online journal) the AHZ, and white (red in the online journal) indicates that the planet is not habitable. The gray striped area (purple in the online journal) corresponds to the dynamically unstable region (HW99), the striped extension shows the onset of dynamical chaos (PLD02). Right: the numerical simulation results for the same configuration. The HZ limits extend beyond the values defined in Kasting et al. (1993). However, the white dash-dotted line corresponds to the semi-analytic estimates of the PHZ using numerically derived values for  $e_p^{\max}$ . The semi-analytic results agree with the fully analytic estimates. This may indicate shortcomings of the entirely numerical approach to identify PHZ boundaries. The resolution of these calculations is  $\Delta a_p = 0.002$  AU and  $\Delta e_b = 0.002$ .

(A color version of this figure is available in the online journal.)

**Table 3**  
Percentages of Planetary Orbits Classified Identically via a Numerical Simulations and Analytical Estimates as Presented in Section 6

[AU]	G2–M0 (%)				G2–G2 (%)				G2–F0 (%)			
	Total	PHZ	EHZ	AHZ	Total	PHZ	EHZ	AHZ	Total	PHZ	EHZ	AHZ
10	<b>95.9</b>	97.4	99.8	98.3	<b>94.4</b>	97.4	99.2	98.0	<b>93.6</b>	95.8	98.5	98.2
20	<b>98.8</b>	99.3	99.5	99.8	<b>98.5</b>	99.2	99.6	99.6	<b>98.5</b>	99.5	99.4	99.6
30	<b>99.0</b>	99.5	99.7	99.9	<b>99.2</b>	99.7	99.6	99.8	<b>98.9</b>	99.8	99.4	100.0
40	<b>99.2</b>	99.5	99.6	99.9	<b>99.3</b>	99.9	99.6	100.0	<b>99.0</b>	99.8	99.5	99.8
50	<b>99.2</b>	99.6	99.7	99.9	<b>99.4</b>	99.7	99.7	99.9	<b>99.4</b>	99.8	99.7	99.9

**Note.** Three binary component configurations have been investigated; the reference classifications were extracted from numerical orbit integrations and insolation simulations.

HZs are in excellent agreement with the numerical ones. Only close to the stability limit (shaded region; purple in the online journal) the correspondence between simulation and analytical estimates decreases. This can be seen more clearly when the secondary’s influence becomes stronger, e.g., in the cases of  $a_b = 10$  AU; see Figure 7. In general the analytical approach is producing more conservative results compared to the numerical data (cf. Figures 5 and 7). In order to determine whether these deviations in the determination of the PHZ are due to

1. inaccurate analytical estimates for  $e_p^{\max}$ ,
2. insufficient time resolution in numerical simulations with regard to determining  $e_p^{\max}$  values, or
3. insufficient total integration time to reach minimum and maximum insolation conditions,

we constructed semi-analytical PHZs using numerically determined  $e_p^{\max}$  values in the analytic equations to determine the PHZ presented in Section 6.1. The borders of the semi-analytically derived PHZs are depicted as white dash-dotted lines in Figures 5 and 7. As they are nearly identical with the fully analytic estimates, we can exclude (1) and (2), which would have led to significantly different results for semi-analytic and analytic approaches. Therefore, (3) seems most likely to cause the differences between the numerical and analytical PHZs, since

encountering an exact alignment of planetary aphelion and secondary perihelion at the moment where  $e_p = e_p^{\max}$  may take far longer than two secular periods. As the computational efforts required to ensure that a simulation’s time resolution as well as total integration time is sufficient to identify the correct PHZ boundaries are enormous, the necessity to have analytical methods at hand becomes evident.

As far as EHZ and AHZ regions are concerned, clear differences can be seen in high perturbation environments close to the transition to instability (Figures 5 and 7, shaded regions). In these cases, the authors favor the numerical results, as single configurations are not critical for the more statistically oriented measures.

A quantitative overview of the correspondence between numerical and analytical results for all system configurations investigated is given in Table 3. Here, similar maps as presented in Figures 6 and 7 were generated with a resolution of  $\Delta a_p = 0.01$  AU, and  $\Delta e_b = 0.01$  and evaluated statistically. In spite of their shortcomings in determining the PHZ, the numerical classification results have been used as reference values and are compared to the analytical estimates given in Section 6. The total correspondence percentages are calculated as the number of all orbits below the stability limit that were classified identically via numerics and analytics, divided by the total number of orbits

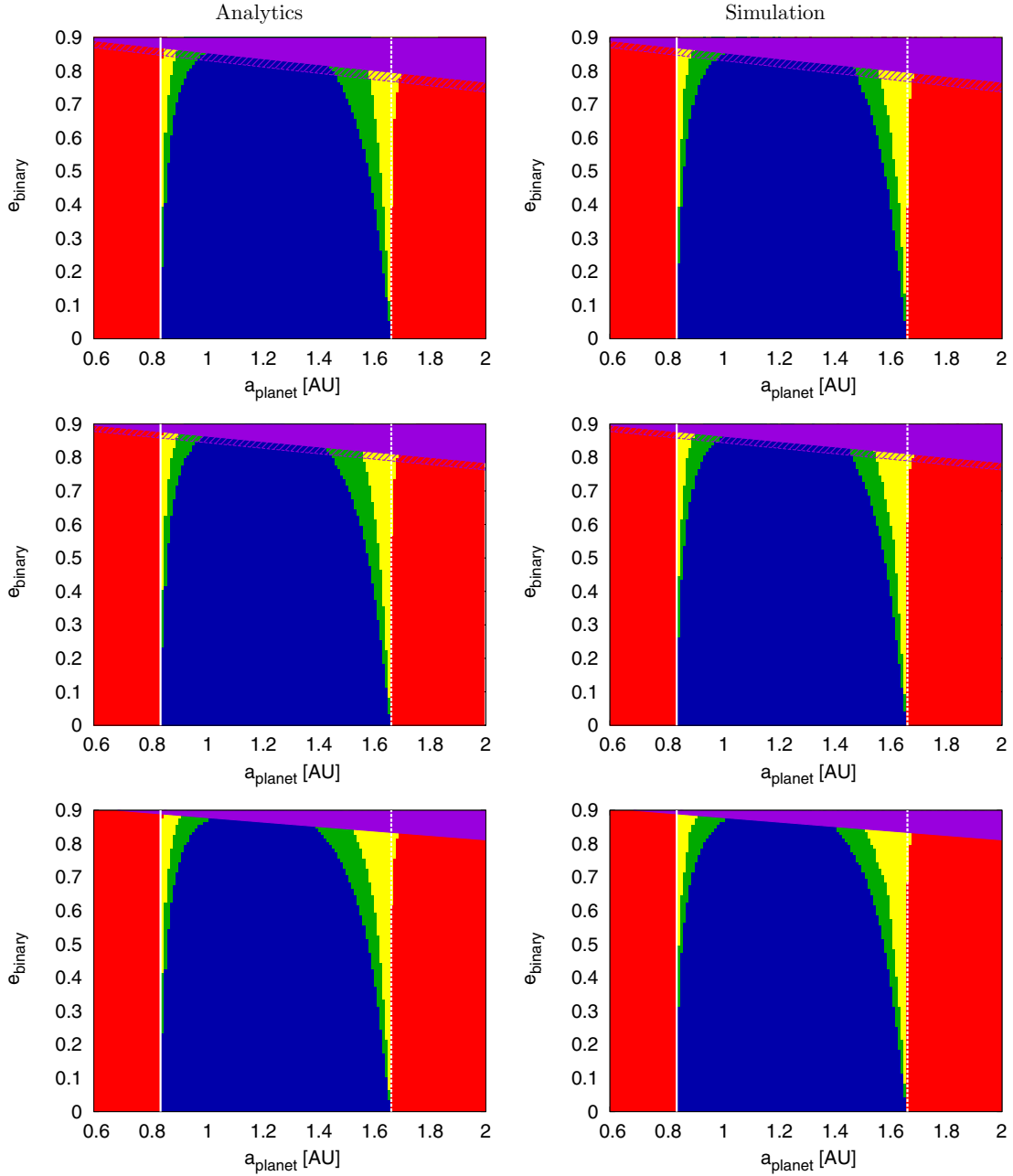


**Figure 6.** Comparison of HZ classifications in three binary star systems with a secondary’s semimajor axis of  $a_b = 50$  AU. Left: analytical estimates as discussed in Section 6; right: reference results gained via numerical integration, with a resolution of  $\Delta a_p = 0.01$  AU and  $\Delta e_b = 0.01$ . The investigated stellar spectral configurations are—top: G2–F0; middle: G2–G2; bottom: G2–M0. The PHZ is represented in black (blue in the online journal), the EHZ is dark gray (green in the online journal), light gray (yellow in the online journal) indicates the AHZ, and white regions (red in the online journal) mean that the planet is outside of any defined HZ. The gray striped area (purple in the online journal) denotes dynamically unstable parameter regions (HW99), whereas the striped extension highlights the onset of dynamical chaos (PLD02); see Section 3. The borders of the classical HZ as defined in KWR93 are represented by the vertical solid and dashed lines.

(A color version of this figure is available in the online journal.)

simulated. The number of orbits classified as PHZs analytically divided by the number of orbits classified as PHZs numerically yields the percentage of PHZs, etc. Table 3 shows that the global correspondence between both methods is quite convincing, which can be considered a strong indicator that the behavior of the respective HZs is modeled correctly.

Also, Figures 5–7 indicate that most of the significant deviations between numerical and analytical results occur near the border of orbital instability, especially for high mass and small period ratios. This might be expected for AHZs and EHZs given

the approximations involved in determining the analytic estimates. In the case of PHZs, however, semi-analytical results suggest caution in using simulation outcomes as reference values.

## 8. RESULTS

Diverse trends in the behavior of the different types of HZs can be seen in Figures 6 and 7. While the AHZ is almost independent of the binary’s eccentricity and coincides well with the KHZ by KWR93 for distant stellar companions, the PHZ and

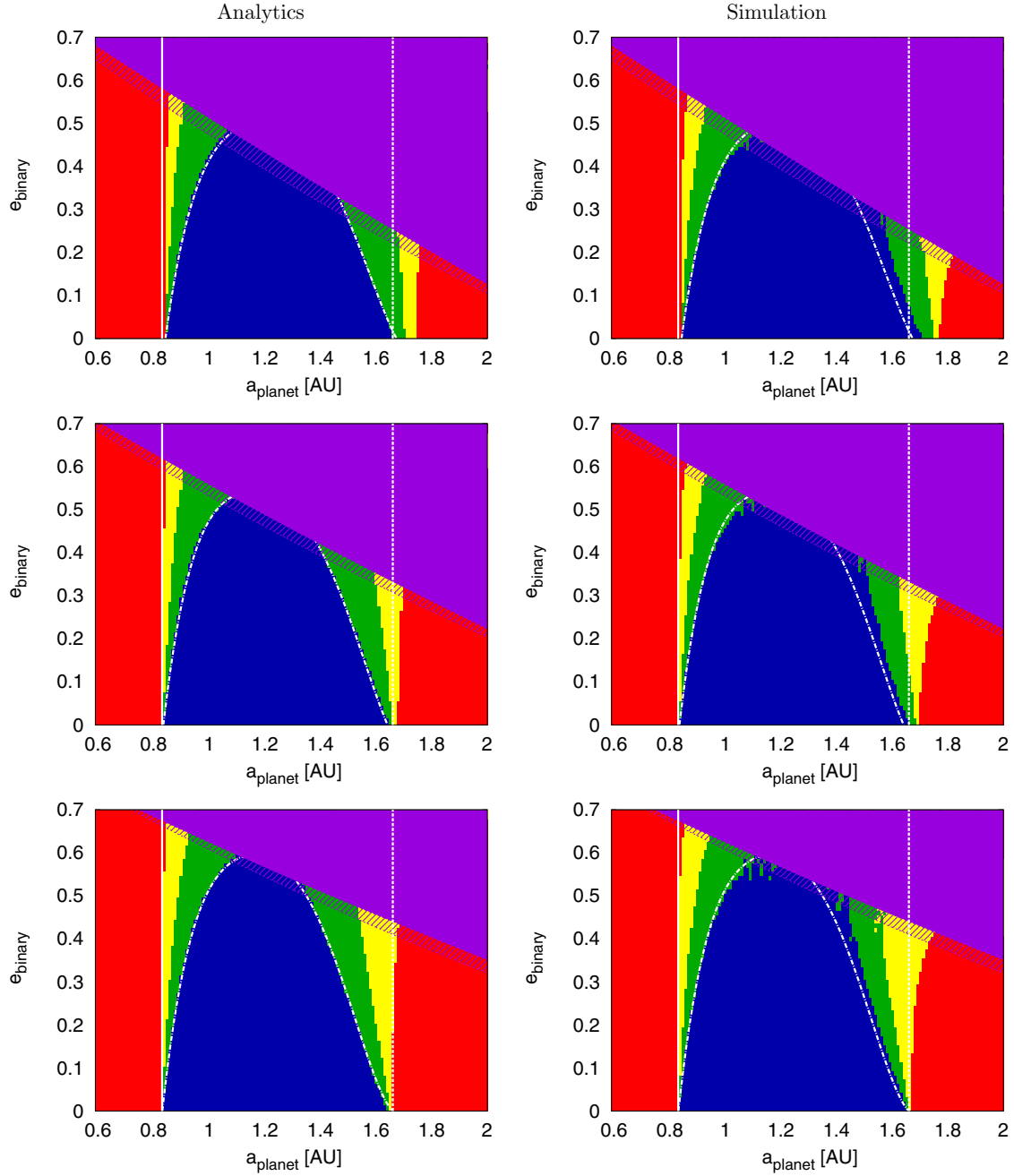


**Figure 7.** Same as Figure 6 but for binary configurations with semimajor axis of  $a_b = 10$  AU. A decrease in the binaries’ semimajor axes leads to more pronounced differences between analytic estimates and numerical simulation results. This can be expected from the approximations used to calculate PHZ, EHZ, and AHZ, see Section 6. Strong perturbations near the area of instability (gray striped; purple in the online journal) are modeled less accurately by the analytical estimates. The white dash-dotted line corresponds to the semi-analytic estimates of the PHZ using numerically derived values for  $e_p^{\max}$ .

(A color version of this figure is available in the online journal.)

EHZ shrink with higher binary eccentricities. The fact that the PHZ and EHZ contract around the center of the KHZ emphasizes the importance of the changes in the planet’s eccentricity, as the secondary’s radiation alone could only account for one-sided features toward the outer edge of the KHZ. The PHZs seem most affected by strong perturbations and shrink to almost half their size before the systems investigated become unstable. Interestingly, in close S-Type II binaries with low eccentricity the extent of the EHZs and AHZs can reach beyond the predicted values by KWR93. This can be seen in Figure 5, where a zoom on the outer border of the KHZ in a G2–F0 configu-

ration is shown. Here, an extension toward the second star of about 0.1 AU seems possible for the system’s AHZ if the binary’s eccentricity remains below the system’s stability limit of  $e_b \simeq 0.2$ .

## 9. CONCLUSIONS

In this work, the impact of the second star on habitable zones in S-Type binary star systems with different stellar constituents has been investigated analytically as well as numerically. The radiative contribution of the secondary on a terrestrial planet is



negligible in all but S-Type II systems, if orbital stability of the planet is required. The gravitational influence of the second star, on the other hand, perturbs in the planet's eccentricity, which in turn can lead to substantial changes in planetary insolation. Therefore, the secondary indeed has to be taken into account when calculating the extent of habitable zones.

Our analytical estimates for planetary eccentricities in binary star systems introduced in Appendix B are an extension to secular perturbation theory as used in, e.g., Heppenheimer (1978). Together with methods presented in Section 6 suggesting an analytic determination of habitable zones, they allow us to paint a global picture of habitability in S-Type binary star systems without having to rely on time consuming numerical orbit integrations. Our approach is quite flexible in the sense that different planetary atmospheric models and average stellar luminosities can be integrated via adaption of the  $S_{\text{eff}}$  values. Thus, the formulae presented in this article grant access to calculating habitable zones for a large set of possible binary–planet configurations.

For the three stellar configurations investigated it could be shown that the permanently habitable zone, i.e., the zone where the planet never exceeds the classical insolation limits for habitability shrinks considerably with the binary's eccentricity. If one considers average insolation values only, the extent of the average habitable zone coincides well with predictions by Kasting et al. (1993) for wide binaries, whereas a significant extension toward the secondary is possible for close, eccentric binary systems. The overall correspondence between numerical and analytical results presented is excellent, as 93%–99% of all investigated orbits were classified identically. The computational efforts required to calculate the true extent of permanently habitable zones numerically, however, can be enormous and might in fact be prohibitive in some cases. In contrast, the analytical method presented offers immediate, reliable estimates.

A more careful approach than the one proposed in this work is advisable when multi-planetary systems, systems close to the stability limit, or resonant configurations are being investigated. In a next step we plan to extend our classification methods to mutually inclined systems.

The authors acknowledge the support of FWF projects AS11608-N16 (E.P.-L., S.E.), P20216-N16 (S.E., M.G., and E.P.-L.), and P22603-N16 (E.P.-L. and B.F.). S.E. acknowledges the support of University of Vienna's Forschungsstipendium 2012.

## APPENDIX A

### INSOLATION VARIANCE

The insolation variance a planet receives on an S-Type orbit in a binary star system was defined in Section 6.3 as

$$\sigma^2 = \langle S_{\text{tot}}^2 \rangle_t - \langle S_{\text{tot}} \rangle_t^2. \quad (\text{A1})$$

Considering the linearity of the expectation value operator, the term  $\langle S_{\text{tot}} \rangle_t^2$  can be decomposed in<sup>3</sup>

$$\langle S_{\text{tot}} \rangle_t^2 = \langle S_1 \rangle_t^2 + 2\langle S_1 \rangle_t \langle S_2 \rangle_t + \langle S_2 \rangle_t^2. \quad (\text{A2})$$

Averages for insolation values from both stars have been derived in Section 6 already and are therefore not repeated here. Instead,

<sup>3</sup> We drop the subscript  $t$  on the averages, as there is no danger of misinterpretation.

we will develop expressions for the first term on the right-hand side of Equation (A1):

$$\langle S_{\text{tot}}^2 \rangle = \langle S_1^2 \rangle + 2\langle S_1 S_2 \rangle + \langle S_2^2 \rangle. \quad (\text{A3})$$

Using equivalence radii  $r$  and  $R$  for the planet and the secondary, respectively, which were introduced in Section 6, we get

$$\langle S_1^2 \rangle = \frac{1}{P} \int_0^P \frac{L_1^2}{\delta^4(t)} dt = \frac{L_1^2}{2\pi r^4} \int_0^{2\pi} dM = \frac{L_1^2}{r^4} = \frac{L_1^2}{a_p^4 (1 - \langle e_p^2 \rangle)^4} \quad (\text{A4})$$

$$\langle S_1 S_2 \rangle = \frac{1}{2\pi} \int_0^{2\pi} \frac{L_1}{r^2} \frac{L_2}{R^2 + r^2 - Rr \cos(\phi)} d\phi = \frac{L_1 L_2}{R^2 r^2 - r^4} \quad (\text{A5})$$

$$\langle S_2^2 \rangle = \frac{1}{2\pi} \int_0^{2\pi} \left( \frac{L_2}{R^2 + r^2 - Rr \cos(\phi)} \right)^2 d\phi = -\frac{L_2^2 (R^2 + r^2)}{(r^2 - R^2)^3}, \quad (\text{A6})$$

where  $\delta(t)$  is again the time-dependent distance of the planet to its host star, and  $a_p$  and  $e_p$  are the planetary semimajor axis and eccentricity, respectively. Given the circular nature of the orbital equivalence approximations we have applied, the results are bound to underestimate the true variances. Since the radiative contribution of the primary dominates the planetary insolation for S-Type I systems and is at least as important as the secondary's insolation for the S-Type II systems investigated, we will use stronger estimates for  $\langle S_1^2 \rangle_t$  than given in relation (A4):

$$\begin{aligned} \langle S_1^2 \rangle &= \frac{1}{P} \int_0^P \frac{L_1^2}{\delta^4(t)} dt = \frac{L_1^2 n}{2\pi h} \int_0^{2\pi} \frac{1}{\delta^2} df \\ &= \frac{L_1^2 n}{2\pi h} \int_0^{2\pi} \left( \frac{1 + \langle e_p \rangle \cos(f)}{a_p (1 - \langle e_p^2 \rangle)} \right)^2 df \\ &= \frac{L_1^2 (1 + \langle e_p^2 \rangle / 2)}{a_p^4 (1 - \langle e_p^2 \rangle)^{5/2}} = \frac{L_1^2}{r^4} (1 - \langle e_p^2 \rangle)^{3/2} \left( 1 + \frac{\langle e_p^2 \rangle}{2} \right). \end{aligned} \quad (\text{A7})$$

As one can see, the difference between relations (A4) and (A7) is negligible for small injected planetary eccentricities, but its contribution becomes important if the injected eccentricities grow. Combining expressions (A7), (A5), and (A6) with the respective terms of  $\langle S_{\text{tot}} \rangle_t^2$  produces the desired variance:

$$\begin{aligned} \sigma^2 &= \frac{L_1^2}{r^4} \left( -1 + 3\langle e_p^2 \rangle - 3\langle e_p^2 \rangle^2 + \langle e_p^2 \rangle^3 + \sqrt{1 - \langle e_p^2 \rangle} \left( 1 - \frac{\langle e_p^2 \rangle}{2} - \frac{\langle e_p^2 \rangle^2}{2} \right) \right) \\ &\quad - \frac{2L_1 L_2}{r^4 - r^2 R^2} \left( 1 - \sqrt{1 - \langle e_p^2 \rangle} (1 + \langle e_p^2 \rangle) \right) - \frac{2L_2^2 r^2}{(r^2 - R^2)^3}. \end{aligned} \quad (\text{A8})$$

## APPENDIX B

### MAXIMUM PLANETARY ECCENTRICITY

The maximum possible eccentricity a terrestrial planet's orbit can acquire in an S-Type setup is composed of

$$e_p^{\text{max}} = e_p^{\text{sp}} + e_p^{\text{sec}}, \quad (\text{B1})$$

where  $e_p^{\text{sp}}$  denotes amplitude of short-period terms and  $e_p^{\text{sec}}$  the planetary eccentricity's secular amplitude. Using expressions

derived in Georgakarakos (2003) via the Laplace–Runge–Lenz vector, we can estimate the maximum short-period contributions for the planet’s eccentricity by taking only terms including the dominant frequencies into account. The amplitude of the secular part of the planet’s eccentricity is given by  $2C/(B - A)$  (Georgakarakos 2003) resulting in the following expressions:

$$e_p^{\text{sp}} = \alpha \left( \frac{15}{64} \frac{\beta}{X^{5/3}} \frac{(4 + 11e_b^2)}{(1 - e_b^2)^{5/2}} + \frac{11}{4} \frac{1}{X^2} \frac{(1 + e_b)^3}{(1 - e_b^2)^3} + \frac{3}{4} \frac{1}{X^3} \frac{(1 + e_b)^4 (6 + 11e_b)}{(1 - e_b^2)^{9/2}} \right) \quad (\text{B2})$$

$$e_p^{\text{sec}} = e_b \beta \left( \frac{5}{4} \frac{\alpha}{X^{1/3}} \frac{3 + 2e_b^2}{(1 - e_b^2)^{1/2}} - \frac{2}{5} \gamma X^{1/3} (1 - e_b^2)^{1/2} + \frac{2}{5} X^{2/3} (1 - e_b^2) \right)^{-1}. \quad (\text{B3})$$

The mass parameters  $\alpha$ ,  $\beta$ , and  $\gamma$  are defined as

$$\alpha = \frac{m_2}{M} \quad \beta = \frac{m_1 - m_p}{(m_1 + m_p)^{2/3} M^{1/3}} \quad \gamma = \frac{m_1 m_p M^{1/3}}{m_2 (m_1 + m_p)^{4/3}},$$

where  $m_p$  is the planetary mass, and  $m_1$  and  $m_2$  are the stellar masses of primary and secondary, respectively.

$M = m_1 + m_2 + m_p$  is the total mass of the system. Finally,  $X$  denotes the secondary-to-planet period ratio:

$$X = \frac{P_b}{P_p} = \left( \frac{m_1 + m_p}{M} \right)^{1/2} \left( \frac{a_b}{a_p} \right)^{3/2}.$$

## REFERENCES

- Baglin, A., Auvergne, M., Barge, P., et al. 2009, in IAU Symp. 253, *Transiting Planets*, ed. F. Pont, D. Sasselov, & M. Holman (Cambridge: Cambridge Univ. Press), 71
- Borucki, W. J., & Koch, D. G. 2011, in IAU Symp. 276, *The Astrophysics of Planetary Systems: Formation, Structure, and Dynamical Evolution*, ed. A. Sozzetti, M. G. Lattanzi, & A. P. Boss (Cambridge: Cambridge Univ. Press), 34
- Buccino, A. P., Lemarchand, G. A., & Mauas, P. J. D. 2006, *Icarus*, 183, 491
- Bulirsch, R., & Stoer, J. 1964, *Numer. Math.*, 6, 413
- Dvorak, R. 1984, *Celest. Mech.*, 34, 369
- Eggl, S., & Dvorak, R. 2010, in *Dynamics of Small Solar System Bodies and Exoplanets*, ed. J. Souchay & R. Dvorak (Lecture Notes in Physics, Vol. 790; Berlin: Springer), 431
- Everhart, E. 1974, *Celest. Mech.*, 10, 35
- Froeschlé, C., Lega, E., & Gonczi, R. 1997, *Celest. Mech. Dyn. Astron.*, 67, 41
- Georgakarakos, N. 2002, *MNRAS*, 337, 559
- Georgakarakos, N. 2003, *MNRAS*, 345, 340
- Georgakarakos, N. 2005, *MNRAS*, 362, 748
- Giuppone, C. A., Leiva, A. M., Correa-Otto, J., & Beaugé, C. 2011, *A&A*, 530, A103
- Haghighipour, N., Dvorak, R., & Pilat-Lohinger, E. 2010, in *Planets in Binary Star Systems*, ed. N. Haghighipour (Astrophysics and Space Science Library, Vol. 366; Dordrecht: Springer), 285
- Haghighipour, N., & Raymond, S. N. 2007, *ApJ*, 666, 436
- Hanslmeier, A., & Dvorak, R. 1984, *A&A*, 132, 203
- Harrington, R. S. 1968, *AJ*, 73, 190
- Hatzes, A. P., Cochran, W. D., Endl, M., et al. 2003, *ApJ*, 599, 1383
- Heppenheimer, T. A. 1978, *A&A*, 65, 421
- Holman, M. J., & Wiegert, P. A. 1999, *AJ*, 117, 621
- Kaltenegger, L., & Sasselov, D. 2011, *ApJ*, 736, L25
- Kaltenegger, L., Traub, W. A., & Jucks, K. W. 2007, *ApJ*, 658, 598
- Kasting, J. F., Whitmire, D. P., & Reynolds, R. T. 1993, *Icarus*, 101, 108
- Kiseleva-Eggleton, L., & Eggleton, P. P. 2001, in *ASP Conf. Ser. 229, Evolution of Binary and Multiple Star Systems*, ed. P. Podsiadlowski, S. Rappaport, A. R. King, F. D’Antona, & L. Burderi (San Francisco, CA: ASP), 91
- Lammer, H., Bredehöft, J. H., Coustenis, A., et al. 2009, *A&AR*, 17, 181
- Mazeh, T., & Shaham, J. 1979, *A&A*, 77, 145
- Pilat-Lohinger, E., & Dvorak, R. 2002, *Celest. Mech. Dyn. Astron.*, 82, 143
- Rabl, G., & Dvorak, R. 1988, *A&A*, 191, 385
- Schneider, J., Dedieu, C., Le Sidaner, P., Savalle, R., & Zolotukhin, I. 2011, *A&A*, 532, A79
- Seager, S. (ed.) 2010, *Exoplanets* (Tucson, AZ: Univ. Arizona)
- Selsis, F., Kasting, J. F., Levrard, B., et al. 2007, *A&A*, 476, 1373
- Thebault, P. 2011, *Celest. Mech. Dyn. Astron.*, 111, 29
- Thebault, P., Marzari, F., & Scholl, H. 2006, *Icarus*, 183, 193
- Tingley, B., Endl, M., Gazzano, J.-C., et al. 2011, *A&A*, 528, A97
- Welsh, W. F., Orosz, J. A., Carter, J. A., et al. 2012, *Nature*, 481, 475
- Whitmire, D. P., Matese, J. J., Criswell, L., & Mikkola, S. 1998, *Icarus*, 132, 196
- Williams, D. M., & Pollard, D. 2002, *Int. J. Astrobiol.*, 1, 61

## Chapter 3

# Detectability of Earth-like Planets in Circumstellar Habitable Zones of Binary Star Systems with Sun-like Components

The analytic estimates developed in the previous article are used to generate expressions mirroring the influence of the binary star on planetary transit probabilities, as well as radial velocity and astrometric signal amplitudes. The resulting methods are then applied to  $\alpha$  Centauri and similar systems. Also, the effects of general relativity as well as the newly discovered planet (Dumusque et al. 2012) on  $\alpha$  Cen B's HZ are investigated.

**authors:** Siegfried Eggl, Nader Haghighipour, Elke Pilat-Lohinger<sup>1</sup>

**publication state:** published February 20<sup>th</sup>, 2013

**publication details:** The Astrophysical Journal, 764:130 (13pp), 2013

**contribution of the first author:** The first author was responsible for the basic idea to use the estimates on the planetary eccentricities applied in chapter 2 to construct formulae quantifying the influence of a binary on radial velocity and astrometric signal amplitudes as well as planetary transit probabilities. The generation of the content of the article including the derivation of the presented analytic estimates are due to the first author.

**contribution of the co-authors:** The application of the analytical signal estimates to the  $\alpha$  Centauri system was proposed by the co-authors. Furthermore, the co-authors corrected and restructured the original manuscript and proposed some simplifications of notation for the presented equations.

---

<sup>1</sup> Author affiliations are presented in the header of the following article.

## DETECTABILITY OF EARTH-LIKE PLANETS IN CIRCUMSTELLAR HABITABLE ZONES OF BINARY STAR SYSTEMS WITH SUN-LIKE COMPONENTS

SIEGFRIED EGGL<sup>1,2</sup>, NADER HAGHIGHIPOUR<sup>3</sup>, AND ELKE PILAT-LOHINGER<sup>1</sup>

<sup>1</sup> University of Vienna, Institute for Astrophysics, Türkenschanzstr. 17, A-1180 Vienna, Austria; [siegfried.eggl@univie.ac.at](mailto:siegfried.eggl@univie.ac.at)

<sup>2</sup> IMCCE, Observatoire de Paris, 77 Avenue Denfert-Rochereau, F-75014 Paris, France

<sup>3</sup> Institute for Astronomy and NASA Astrobiology Institute, 2680 Woodlawn Drive, Honolulu, HI 96822, USA

Received 2012 September 5; accepted 2012 December 19; published 2013 January 31

### ABSTRACT

Given the considerable percentage of stars that are members of binaries or stellar multiples in the solar neighborhood, it is expected that many of these binaries host planets, possibly even habitable ones. The discovery of a terrestrial planet in the  $\alpha$  Centauri system supports this notion. Due to the potentially strong gravitational interaction that an Earth-like planet may experience in such systems, classical approaches to determining habitable zones (HZ), especially in close S-type binary systems, can be rather inaccurate. Recent progress in this field, however, allows us to identify regions around the star permitting permanent habitability. While the discovery of  $\alpha$  Cen Bb has shown that terrestrial planets can be detected in solar-type binary stars using current observational facilities, it remains to be shown whether this is also the case for Earth analogs in HZs. We provide analytical expressions for the maximum and rms values of radial velocity and astrometric signals, as well as transit probabilities of terrestrial planets in such systems, showing that the dynamical interaction of the second star with the planet may indeed facilitate the planets' detection. As an example, we discuss the detectability of additional Earth-like planets in the averaged, extended, and permanent HZs around both stars of the  $\alpha$  Centauri system.

**Key words:** astrobiology – celestial mechanics – methods: analytical – planet–star interactions

### 1. INTRODUCTION

The past decades have seen a great number of discoveries of planets around stars other than our Sun (Schneider et al. 2011). As some of these planets are of terrestrial nature, the hope of identifying Earth analogs has lead to considerable advances toward the detection of possibly habitable worlds (Borucki 2011; Ford et al. 2012). Even though quite frequent in the solar neighborhood (Kiseleva-Eggleton & Eggleton 2001), not many attempts have yet been made to specifically target binary stars in this endeavor. Nonetheless, more than 60 planets have already been found in and around such systems (Haghighipour 2010; Doyle et al. 2011; Welsh et al. 2012; Roell et al. 2012; Orosz et al. 2012a, 2012b; Dumusque et al. 2012). Although several P-type (circumbinary) planets orbiting both stars of a close binary have also been discovered (Doyle et al. 2011; Welsh et al. 2012; Orosz et al. 2012a, 2012b), most planets are in the so-called S-type (Rabl & Dvorak 1988) configuration where the planet orbits only one of the binary's stars. A prominent example of an S-type system is  $\alpha$  Centauri AB which hosts a terrestrial planet around the fainter binary component,  $\alpha$  Cen B (Dumusque et al. 2012).

The reason for the general reluctance to include binary systems in the search for terrestrial, habitable planets lies in the assumption that the additional interactions with a massive companion will make planets harder to find. That is primarily because the gravitational interaction between the second star and a planet may alter the planet's orbit significantly and complicate the task of interpreting the planetary signal. One aim of this work is therefore to show that changes in the planet's orbit can actually enhance its detectability (see Section 5). Of course, the orbit of a binary as well as its stellar parameters have to be well determined in order to be able to identify signals from additional terrestrial planets. Sensing the need for a better understanding of binary star systems, efforts have been intensified to improve physical as well as orbital data for nearby binaries (e.g., Torres et al. 2010)

and to evolve existing data analysis methodologies (Chauvin et al. 2011; Haghighipour 2010; Pourbaix 2002; Pourbaix et al. 2002).

Understanding the complex interactions between a stellar binary and a planet is essential if a system's potential habitability is to be evaluated. For instance, one of the main assumptions of classical habitability, as introduced by Kasting et al. (1993), is that the planet moves around its host star on a circular orbit. This may not be a valid assumption for planets in a binary star system where the gravitational perturbation of the secondary can excite the eccentricity of the planet's orbit (Marchal 1990; Georgakarakos 2002; Eggl et al. 2012). Eggl et al. (2012) found that except for S-type systems where the secondary star is much more luminous than the planet's host star, variations in planetary orbit around the planet-hosting star are the main cause for changes in insolation. Even though Eggl et al. (2012) gave an analytic recipe for calculating the boundaries of the habitable zones (HZs) in S-type binaries, it remains to be seen whether an Earth-like planet in the HZ of a system with two Sun-like stars will in fact be detectable.

In order to answer this question, we consider three techniques, namely, radial velocity (RV), astrometry (AM), and transit photometry (TP), and discuss whether the current observational facilities are capable of detecting habitable planets in such systems. We provide analytical formula for estimating the strength of RV and AM signals for habitable, Earth-like planets, and show that the planet–binary interaction can enhance the chances for the detection of these objects.

The rest of this article will be structured as follows. In Sections 2 and 3 analytic estimates of the maximum and root mean square (rms) of the strength of an RV and an AM signal that an Earth-like planet produces in an S-type binary configuration will be derived. Section 4 will deal with the consequences of such a setup for TP. We will then briefly recall the different types of HZs for S-type binaries established in Eggl et al. (2012), and use their methodology to identify similar habitable

regions in the  $\alpha$  Centauri system (Section 5). This system has been chosen because first, it has inspired many studies on the possibility of the formation and detection of habitable planets around its stellar components (Forgan 2012; Guedes et al. 2008; Thébault et al. 2009) and second, Dumusque et al. (2012) have already discovered an Earth-sized planet in a short-period orbit around its secondary star. Therefore, we will compare our RV estimates to the actual signal of  $\alpha$  Cen Bb, and study its influence on an additional terrestrial planet presumed in  $\alpha$  Cen B's HZ. Finally, in Section 6, the projected RV, AM, and TP trace that terrestrial planets will leave in the HZ of the  $\alpha$  Centauri system are analyzed, and the results are discussed within the context of the sensitivity of the current observational facilities.

## 2. RADIAL VELOCITY

To estimate the RV signal that an Earth-like planet produces in an S-type binary system, we will build upon the formalism presented by Beaugé et al. (2007). We assume that the non-planetary contributions to the host star's RV signal (such as the RV variation caused by the motion of the binary around its center of gravity) are known and have been subtracted, leaving behind only the residual signal due to the planet. The motion of the planet around its host star then constitutes a perturbed two-body problem, where the gravitational influence of the secondary star is still playing a role and is mirrored in the forced variations of the planet's orbit.

In practice, the extraction of the planetary signal is all but a trivial task. Even after subtraction of the binary's barycentric and proper motion, the residual will contain contributions from the binary's orbital uncertainties as well as from non-gravitational sources which could be orders of magnitude larger than the star's reflex signal, such as the Rossiter–McLaughlin effect in transiting systems, for example (Ohta et al. 2005). The discovery of  $\alpha$  Cen Bb showed, however, that a substantial reduction of non-planetary RV interference is possible if the respective binary star has been studied in sufficient detail.

The amplitude of the planet induced RV signal of the host star,  $V_r$ , is given by

$$V_r = K [\cos(f + \omega) + e \cos \omega], \quad (1)$$

where  $K$  is equal to

$$K = \frac{\mu(\kappa n_p)^{1/3} \sin i}{\sqrt{1 - e^2}}. \quad (2)$$

In Equation (2),  $\mu = m_1/(m_0 + m_1)$  is the planet to star mass ratio with  $m_1$  and  $m_0$  being the masses of the planet and host star, respectively. The planet's mean motion,  $n_p = 2\pi/P_p$ , is given by  $n_p = \sqrt{\kappa/a^3}$  with  $\kappa = \mathcal{G}(m_0 + m_1)$ , and  $P_p$  and  $\mathcal{G}$  being the planet's orbital period and gravitational constant. The quantities  $a$ ,  $e$ ,  $i$ ,  $f$ , and  $\omega$  in Equations (1) and (2) denote the planet's semimajor axis, eccentricity, orbital inclination relative to the plane of the sky, true anomaly, and argument of periastron, respectively.

Our goal in this section is to identify the range of the possible peak amplitudes that a terrestrial planet in an S-type binary configuration can produce. We note that the gravitational influence of the second star causes the planet's orbital elements to vary, thus inducing additional time-dependent changes in the RV signal  $V_r$  (Lee & Peale 2003). While we know from secular perturbation theory that  $a$  does not change significantly with

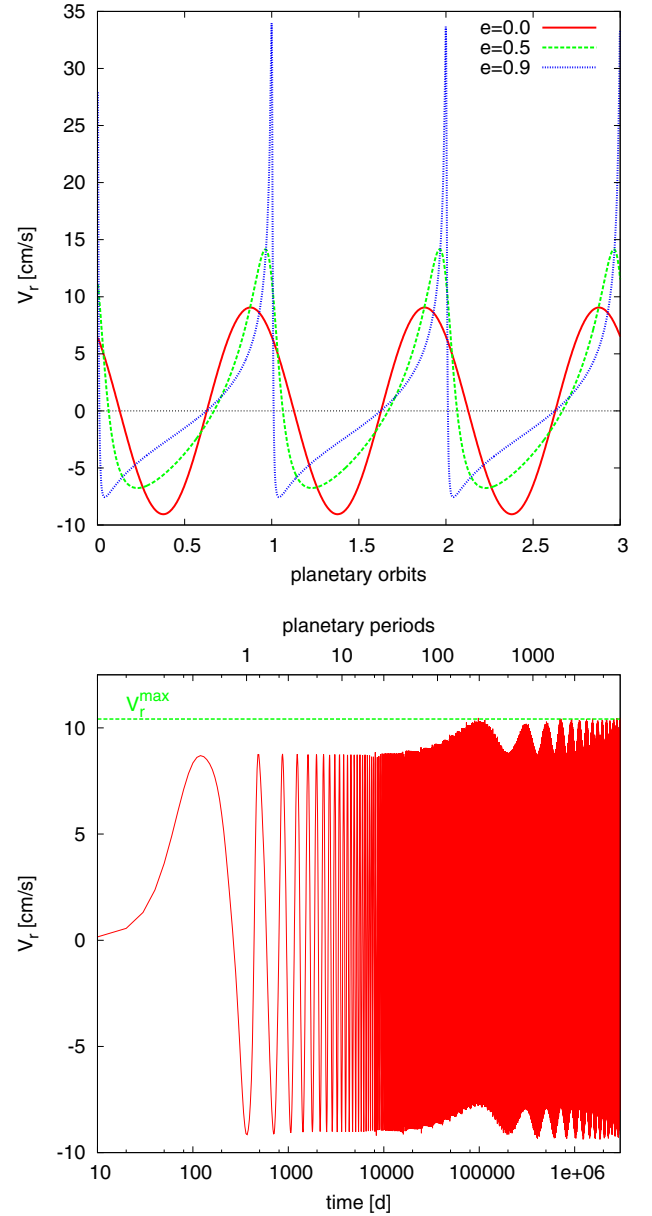


**Figure 1.** Top: the radial velocity signal caused by an Earth-like planet orbiting a Sun-like star with different eccentricities (Beaugé et al. 2007). The planet is at 1 AU with  $\omega = 45^\circ$  when  $e \neq 0$ . Bottom: the amplitude variations of the primary's radial velocity signal due to an Earth-like planet that is subject to the gravitational perturbations of a second star. Both stars are Sun-like with a separation of 20 AU and an orbital eccentricity of 0.5. The planet's initial orbit was circular with a semimajor axis of 1 AU. Our analytically estimated maximum amplitude  $V_r^{\max}$  is also shown.

(A color version of this figure is available in the online journal.)

time for hierarchical systems such as the one under consideration (Marchal 1990; Georgakarakos 2003),  $\omega$  becomes a function of time. We assume coplanar orbits of the planet and the binary star which result in the planet's inclination to the plane of the sky ( $i$ ) to remain constant. In contrast, the planetary eccentricity will vary between zero and a maximum  $e^{\max}$ , where the latter value can be expressed as a function of the system's masses and the binary's orbital parameters (Eggl et al. 2012). This is important, because the reflex RV signal ( $V_r$ ) of a star can be increased significantly by planetary orbital eccentricities (Figure 1). Using Equation (1), we identify the global maximum



of  $V_r$  at  $f = \omega = 0$ , when  $e = e^{\max}$ . This leads to

$$V_r^{\max} = V_r^{\text{circ}} \sqrt{\frac{1 + e^{\max}}{1 - e^{\max}}}, \quad (3)$$

where

$$V_r^{\text{circ}} = \frac{\sqrt{G} m_1 \sin i}{\sqrt{a(m_0 + m_1)}}. \quad (4)$$

Equation (3) presents a fully analytic estimate of the expected maximum RV signal that a terrestrial planet produces in an S-type binary configuration.<sup>4</sup>

As an example for the influence of a double star on a planetary RV signal, the induced variations in the RV of the planet's host star are presented in the bottom panel of Figure 1. The host star is a constituent of a solar-type binary with a semimajor axis of 20 AU and an orbital eccentricity of 0.5. Changes in the amplitude of  $V_r$  are due to variations in the planet's eccentricity.

Since we do not know the state of the planet's orbital eccentricity at the time of observation, we consider a range for the maximum possible amplitudes of its RV

$$V_r^{\text{circ}} \leq V_r|_{f=\omega=0} \leq V_r^{\max}. \quad (5)$$

Although the range of the amplitude of the host star's RV signal, as given by Equation (5), can be used to identify the “best case” detectability limits, the maximum values of the RV signal due to the planet will be “snapshots” that are reached only during brief moments. As a result, their values for assessing the precision needed to trace fingerprints of an Earth-like planet are rather limited. In such cases, expressions for the rms of the astrometric signal are preferable.

Since rms values are by convention time-averaged, we substitute  $f$  by the mean anomaly  $M = n_p t$  in all corresponding functions using the equation of the center expansion up to the sixth order in planetary eccentricities (see Appendix A) and average over  $M$  and  $\omega$ . The vastly different rates of change of these quantities ( $\dot{M} \gg \dot{\omega}$ ) make it possible to consider  $\omega$  to remain constant during one cycle of  $M$ , so that independent averaging can be performed. In order to eliminate short-term variations in the RV signal, we first average over  $M$ . Averaging over  $\omega$  as well might be desirable if for example the initial state of  $\omega$  is unknown, or if observations stretch beyond secular evolution timescales of the planets argument of pericenter. We, therefore, define two different types of rms evaluations for a square-integrable function  $F$ :

$$\langle\langle F \rangle\rangle_M = \langle F^2 \rangle_M^{1/2} = \left[ \frac{1}{2\pi} \int_0^{2\pi} F^2(M) dM \right]^{1/2}, \quad (6)$$

and

$$\langle\langle F \rangle\rangle_{M,\omega} = \frac{1}{2\pi} \left[ \int \int_0^{2\pi} F^2(M, \omega) dM d\omega \right]^{1/2}. \quad (7)$$

Using Equations (6) and (7), the rms values of  $V_r$  are then given by

<sup>4</sup> Larger signals are possible, if the terrestrial planet has a considerable initial eccentricity after its formation and migration phase. Yet, due to the eccentricity dampening in protoplanetary disks, this seems unlikely (Paardekooper & Leinhardt 2010).

$$\langle\langle V_r \rangle\rangle_M = \langle\langle V_r \rangle\rangle_{M,\omega}$$

$$\times \left\{ 1 - \left[ \frac{\langle e^2 \rangle_M}{4} + O(\langle e^2 \rangle_M^2) \right] \cos(2\omega) \right\}^{1/2}, \quad (8)$$

with

$$\langle\langle V_r \rangle\rangle_{M,\omega} = \frac{\sqrt{G} m_1 |\sin i|}{\sqrt{2a(m_0 + m_1)}} = \frac{1}{\sqrt{2}} V_r^{\text{circ}}. \quad (9)$$

Here we have considered  $\langle a \rangle_M = a$  since  $\dot{a} \simeq 0$  (Marchal 1990; Georgakarakos 2003). Also

$$\int_0^{2\pi} \langle e^2 \rangle_M \cos(2\omega) d\omega = 0,$$

as indicated in Appendix B. It is noteworthy that the averaging over  $\omega$  causes the rms value of the RV signal to become independent of  $e$  so that its difference with the peak signal in the circular case ( $V_r^{\text{circ}}$ ) becomes a mere factor of  $1/\sqrt{2}$ . Thanks to their intricate relation to power spectra, rms values can also be valuable for orbit fitting. The choice of singly or doubly averaged rms relations for this purpose will depend on how many planetary orbital periods are available in the data set. In the case of  $\alpha$  Cen Bb, there are order-of-magnitude differences in the rates of change of the mean anomaly ( $\dot{M}$ ) and the argument of pericenter ( $\dot{\omega}$ ). It would therefore make more sense to assume  $\omega$  to be constant and add it as a variable in the fitting process. If stronger perturbations or additional forces act on the planet, the periods can be considerably shorter, so that the fully averaged equations might come in handy.

### 3. ASTROMETRY

In order to derive the maximum and rms values for an astrometric signal, we will use the framework presented in Pourbaix (2002). We again assume that the non-planetary contributions have been subtracted from the combined signal of the host star and planet. The projected motion of the planet on the astrometric plane is then given by

$$\begin{aligned} x_E &= A(\cos E - e) + F\sqrt{1 - e^2} \sin E, \\ y_E &= B(\cos E - e) + G\sqrt{1 - e^2} \sin E, \end{aligned} \quad (10)$$

where  $x_E$  and  $y_E$  are the Cartesian coordinates of the projected orbit,  $e$  is the planet's orbital eccentricity,  $E$  is the eccentric anomaly, and  $A$ ,  $B$ ,  $F$ , and  $G$  are the modified Thiele–Innes constants given by

$$\begin{aligned} A &= \frac{a}{d} (\cos \omega \cos \Omega - \sin \omega \sin \Omega \cos i), \\ B &= \frac{a}{d} (\cos \omega \sin \Omega + \sin \omega \cos \Omega \cos i), \\ F &= -\frac{a}{d} (\sin \omega \cos \Omega + \cos \omega \sin \Omega \cos i), \\ G &= -\frac{a}{d} (\sin \omega \sin \Omega - \cos \omega \cos \Omega \cos i). \end{aligned} \quad (11)$$

In these equations,  $d$  is the distance between the observer and the observed system in units of the planetary semimajor axis  $a$ . We can rewrite Equations (10) in terms of the true anomaly  $f$  as

$$\begin{aligned} x_f &= \frac{A}{a} r \cos f + \frac{F}{a} r \sin f, \\ y_f &= \frac{B}{a} r \cos f + \frac{G}{a} r \sin f. \end{aligned} \quad (12)$$

In these equations,  $r = a(1 - e^2)/(1 + e \cos f)$  represents the planet's radial distance to its host star. Because the motion of the planet itself cannot be traced, we translate these equations into the apparent motion of the host star by the application of Newton's third law. That is

$$\begin{aligned} x_\star &= X - \mu x_f, \\ y_\star &= Y - \mu y_f. \end{aligned} \quad (13)$$

Here,  $X$  and  $Y$  are the projected coordinates of the center of mass of the planet–star system, and  $\mu$  denotes the planet–star mass ratio as defined for Equation (2).

Assuming without the loss of generality that the barycenter of the star–planet system coincides with the origin of the associated coordinate system, the distance of the projected stellar orbit to the coordinate center will be equal to

$$\begin{aligned} \rho^2 &= x_\star^2 + y_\star^2 \\ &= \frac{\mu^2 a^2}{d^2} \frac{(1 - e^2)^2 [1 - \sin^2 i \sin^2(f + \omega)]}{(1 + e \cos f)^2}. \end{aligned} \quad (14)$$

The right-hand side of Equation (14) is independent of  $\Omega$  and has a global maximum at  $f = \pi, \omega = 0$  when  $e = e^{\max}$ . This translates into a maximum astrometric amplitude given by

$$\rho^{\max} = \rho^{\text{circ}} (1 + e^{\max}), \quad (15)$$

where

$$\rho^{\text{circ}} = \frac{\mu a}{d}. \quad (16)$$

The planetary maximum AM signal will again lie between  $\rho^{\text{circ}}$  and  $\rho^{\max}$ . A remarkable feature of  $\rho^{\max}$  and  $\rho^{\text{circ}}$  is their independence of the system's inclination  $i$ . This is visualized in Figure 2. The same figure also shows the time evolution of the AM signal due to an Earth-like planet orbiting  $\alpha$  Cen B at a distance of 1 AU.

The astrometric rms values are given by

$$\begin{aligned} \langle\langle\rho\rangle\rangle_M &= \rho^{\text{circ}} \left[ 1 + \frac{3\langle e^2 \rangle_M}{2} \right. \\ &\quad \left. + \left( -\frac{1}{2} + \frac{\langle e^2 \rangle_M}{4} (5 \cos[2\omega] - 3) \right) \sin^2 i \right]^{1/2}, \end{aligned} \quad (17)$$

and

$$\begin{aligned} \langle\langle\rho\rangle\rangle_{M,\omega} &= \frac{\rho^{\text{circ}}}{2} \left[ 3 + \frac{9}{2} \langle e^2 \rangle_{M,\omega} \right. \\ &\quad \left. + \left( 1 + \frac{3}{2} \langle e^2 \rangle_{M,\omega} \right) \cos(2i) \right]^{1/2}. \end{aligned} \quad (18)$$

Details regarding the derivation of Equations (17) and (18) can be found in Appendix B. In contrast to the doubly averaged equations for the rms of an RV signal, Equation (18) shows a dependence on the binary's eccentricity. In cases where the planetary inclination  $i$  coincides with the inclination of the binary itself, analytic expressions for  $\langle e^2 \rangle_{M,\omega}$  are available (Georgakarakos 2003, 2005).<sup>5</sup>

<sup>5</sup> The analytic expressions given in these articles are also averaged over initial phases, i.e., different relative starting positions of the planet and the binary stars.

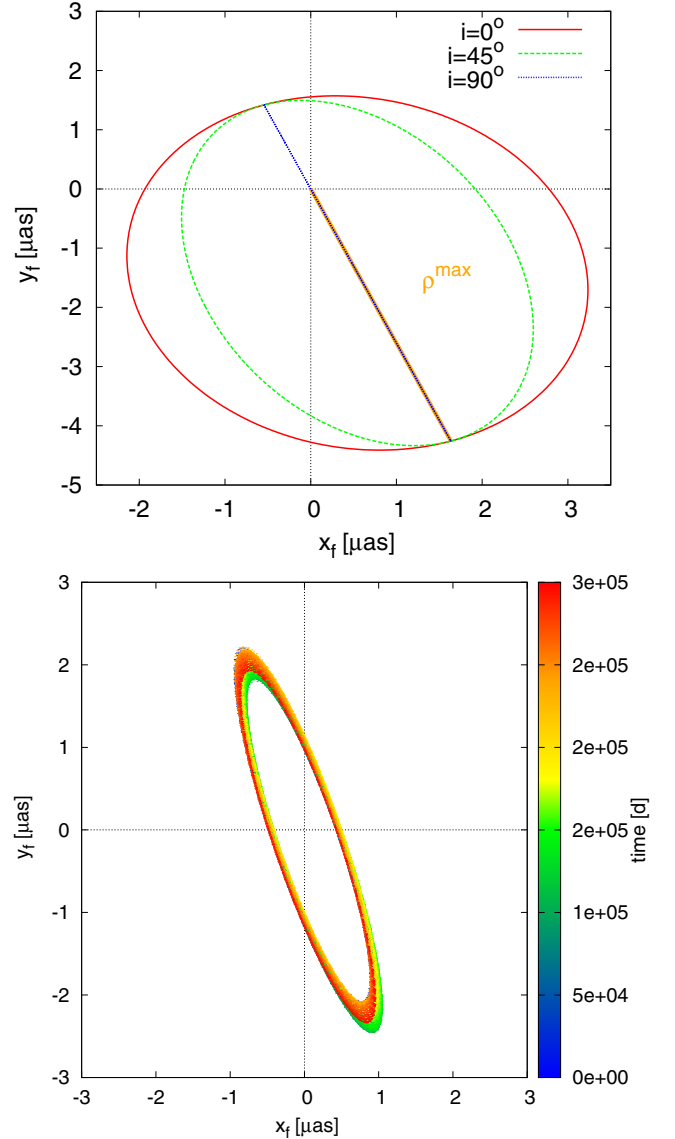


**Figure 2.** Top: the maximum astrometric amplitude,  $\rho^{\max} = \mu (x_f^2 + y_f^2)^{1/2}|_{f=\pi, \omega=0}$ , due to an Earth-like planet orbiting its Sun-like host star. The planet's orbital elements are  $a = 1$  AU,  $e = e^{\max} = 0.5$ ,  $\omega = 0$ ,  $\Omega = 111^\circ$ . As shown here, the maximum distance from the origin of the coordinate system is independent of the system's inclination with respect to the plane of the sky ( $i$ ). Bottom: evolution of the astrometric signal ( $x_f, y_f$ ) caused by an Earth-like planet in a binary star system. The planet is orbiting  $\alpha$  Cen B at a distance of 1 AU. The evolution of the astrometric signal is shown for 3750 periods of  $\alpha$  Centauri AB. Since the system is coplanar, the changes in orientation and shape of the projected ellipse are due to variations in the planet's eccentricity ( $e$ ) and argument of pericenter ( $\omega$ ).

#### 4. TRANSIT PHOTOMETRY

In TP, signal strength is equivalent to the relative depth of the dint the planet produces in the stellar light curve during its transit. Assuming that the star–planet configuration allows for occultations, and excluding grazing transits, the fractional depth of the photometric transit (TD) produced by an Earth-like planet is simply given by the proportion of the luminous area of the disk of the star that is covered by the planet as the planet moves between the observer and the star. Ignoring limb darkening, that means,  $\text{TD} \simeq R_p^2/R_\star^2$  where  $R_p$  is the radius of the planet and  $R_\star$  is the stellar radius. The overall probability to observe a transit

**Table 1**  
Physical and Orbital Parameters of the  $\alpha$  Centauri ABb System  
(Kervella et al. 2003; Guedes et al. 2008; Pourbaix et al. 2002;  
Dumusque et al. 2012)

$\alpha$ Centauri	A	B
Spectral classification	G2V	K1V
Mass ( $M_\odot$ )	$1.105 \pm 0.007$	$0.934 \pm 0.007$
$T_{\text{eff}}$ (K)	5790	5260
Luminosity ( $L_\odot$ )	1.519	0.500
Distance (pc)	$1.339 \pm 0.002$	
Period ( $P_b$ ) (days)	$29187 \pm 4$	
$a_b$ (AU)	$23.4 \pm 0.03$	
$e_b$	$0.5179 \pm 0.00076$	
$i_b$ (deg)	$79.205 \pm 0.0041$	
$\omega_b$ (deg)	$231.65 \pm 0.076$	
$\Omega_b$ (deg)	$204.85 \pm 0.084$	
$\alpha$ Centauri	B b	
$P_p$ (days)	$3.2357 \pm 0.0008$	
$e_p$	0 (fixed)	
Minimum mass ( $m_p^{\text{min}}$ ) ( $M_{\text{Earth}}$ )	$1.13 \pm 0.09$	

is given by (Borucki & Summers 1984)

$$p_T = \frac{R_\star}{r_T}. \quad (19)$$

In Equation (19),  $r_T$  is the radial distance of the planet to the star during the transit. For an eccentric planetary motion, the planet–star distance during transit can be expressed as  $r_T \simeq a(1 - e^2)/(1 + e \cos \bar{\omega})$  (Ford et al. 2008), where  $\bar{\omega}$  denotes the argument of pericenter measured from the line of sight.<sup>6</sup> In analogy to Sections 2 and 3, the maximum and averaged transit probability for a planet perturbed by the secondary star in a planar configuration can be calculated by substituting for  $r_T$  in Equation (19) and averaging over  $\bar{\omega}$ . This will result in

$$p_T^{\text{max}} \simeq \frac{R_\star}{a(1 - e^{\text{max}})}, \quad (20)$$

and

$$\langle p_T \rangle_{\bar{\omega}} \simeq \frac{R_\star}{a(1 - \langle e^2 \rangle_{M,\omega})}. \quad (21)$$

Equations (20) and (21) indicate that the increase in the eccentricity of the planet due to the perturbation of the secondary increases the probability of transit. In deriving these equations, we have ignored the occultation of the planet by the second star. However, depending on the period ratio between the secondary and the planet, such conjunctions are either scarce or short-lived. Consequently, their contribution to the probability of witnessing a planetary transit is negligibly small.

## 5. APPLICATION TO THE $\alpha$ CENTAURI SYSTEM

In this section, we will show that the previously derived analytic expressions produce results that are in good agreement with the current observations of  $\alpha$  Cen Bb. We will also present numerical evidence that the presence—or the absence—of an additional terrestrial planet in the HZ of  $\alpha$  Cen B cannot be derived easily from the orbit evolution of  $\alpha$  Cen Bb. Consequently, we argue that an independent detection of additional

<sup>6</sup> Note that this is different from the conventions used for RV and AM measurements.

**Table 2**  
A Comparison between the Predicted RV Values Using the Analytic Expressions Derived in Section 2 and the Observed Values for the Terrestrial Planet Discovered around  $\alpha$  Cen B (Dumusque et al. 2012).

	Predicted Signal (m s <sup>-1</sup> )	Observed Signal (m s <sup>-1</sup> )
$\langle \langle V_r \rangle \rangle_{M,\omega}$	$0.365 \pm 0.029$	
$V_r^{\text{circ}}$	$0.517 \pm 0.041$	$0.51 \pm 0.04$
$V_r^{\text{max}}$	$0.519 \pm 0.041$	

**Notes.** Coplanarity of the system was assumed. The formal uncertainties have been derived assuming Gaussian error propagation of the uncertainties given in Table 1. The maximum predicted planetary eccentricity for  $\alpha$  Cen Bb is  $e^{\text{max}} = 0.003$ . When taking general relativity into account, however, the orbit of  $\alpha$  Cen Bb will remain practically circular (see Figure 6).

terrestrial companions might be difficult, but more promising. For this purpose, we will determine the HZ of  $\alpha$  Cen B, as well as the RV, AM, and TP signatures of an Earth-like planet orbiting in the HZ of  $\alpha$  Cen B. Since there is no a priori reason why the brighter component of  $\alpha$  Centauri could not be hosting a terrestrial planet as well, we perform a similar analysis for  $\alpha$  Cen A. We will also study the behavior of Equations (1)–(21) for a broad range of binary eccentricities.

### 5.1. $\alpha$ Centauri’s Terrestrial Planet

The planet discovered around  $\alpha$  Cen B offers a perfect opportunity to compare the RV amplitude predictions derived in Section 2 with actual measurements. The planet’s known orbital parameters are given in Table 1. In Table 2, we present the analytic estimates of Section 2 applied to the  $\alpha$  Centauri ABb system. Assuming the system to be coplanar ( $i \simeq 79.2^\circ$ ), the predicted RV amplitude for circular planetary motion ( $V_r^{\text{circ}}$ ) is very close to the observed RV amplitude. This is not surprising, since the planetary parameters were derived from an RV signal using the same methodology in reverse. While still well within measurement uncertainties, the deviation of the maximum RV amplitude ( $V_r^{\text{max}}$ ) from the observed value is larger than that of  $V_r^{\text{circ}}$ . On the one hand, this might indicate that the planet is currently in an orbital evolution phase where its eccentricity is almost zero. On the other hand, the planet may be too close to its host star for our model to predict  $V_r^{\text{max}}$  correctly. In fact, we show in Section 5.3 that the latter explanation is more likely, since the influence of general relativity (GR) cannot be neglected in this case. Estimates based on Newtonian physics exaggerate the actual eccentricity of  $\alpha$  Cen Bb. Its orbit remains practically circular despite the interaction with the binary star (see Section 5.3 for a detailed discussion). This justifies the assumption of a circular planetary orbit made by Dumusque et al. (2012).

Since we are especially interested in additional habitable planets, however, it is worthwhile to ask whether predictions on the orbital evolution of  $\alpha$  Cen Bb can be used to exclude the presence of other gravitationally active bodies in the system. In other words, could an Earth-like planet still orbit in the HZ of  $\alpha$  Cen B or would the accompanying distortions of the orbit of  $\alpha$  Cen Bb be significant enough to detect them immediately? Before we try to answer these questions, we need to briefly recall some important aspects regarding HZs in binary star systems.

### 5.2. Classification of HZs

Combining the classical definition of an HZ (Kasting et al. 1993) with the dynamical properties of a planet-hosting double



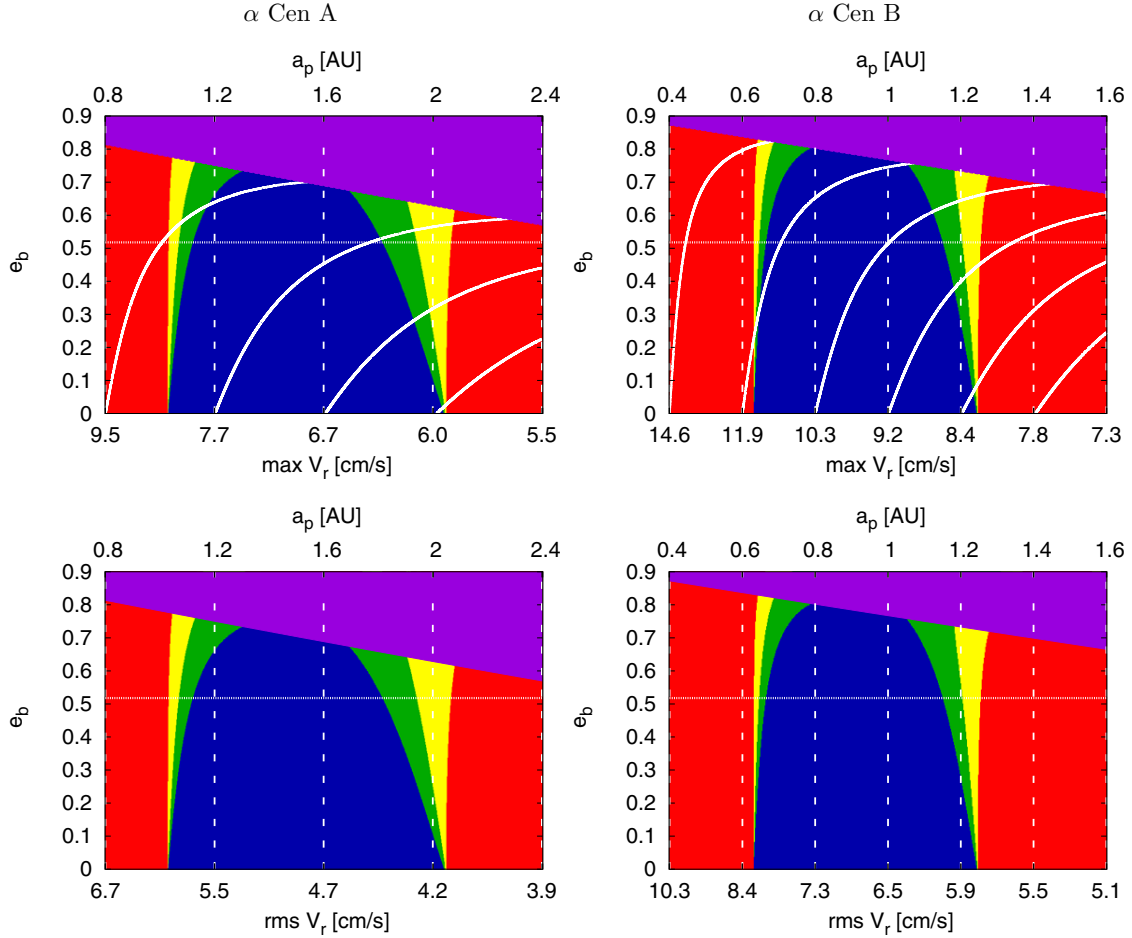


**Figure 3.** Habitability maps showing the maximum amplitudes and rms of the RV signal of the planet-hosting stars for the  $\alpha$  Centauri system. The quantity  $a_p$  is the semimajor axis of the terrestrial planet and  $e_b$  is the binary eccentricity. The color blue shows the PHZ, the EHZ is green, yellow indicates the AHZ, and red means that the planet is outside of any defined HZ. The purple area denotes dynamical instability. The horizontal line in each panel denotes the actual eccentricity of the  $\alpha$  Centauri binary. As shown here,  $V_r^{\max}$  reacts strongly to enhanced binary eccentricities (top row, curved, solid lines) whereas in contrast,  $\langle V_r \rangle_{M,\omega}$  is independent of the binary’s eccentricity (bottom row, straight, vertical lines). The straight, vertical lines in the top row correspond to RV amplitudes for circular orbits ( $V_r^{\text{circ}}$ ). See Section 5.4 for details.

star system, Eggl et al. (2012) have shown that one can distinguish three types of HZ in an S-type binary system.

**The permanently habitable zone (PHZ)** where a planet *always* stays within the insolation limits ( $S_I, S_O$ ) as defined by Kasting et al. (1993) and Underwood et al. (2003). In other words, despite the changes in its orbit, the planet never leaves the classical HZ. The total insolation the planet receives will vary between the inner ( $S_I$ ) and outer ( $S_O$ ) effective radiation limits as  $S_I \geq S_{\text{tot}} \geq S_O$  where, for a given stellar spectral type,  $S_I$  and  $S_O$  are in units of solar constant ( $1360 \text{ W m}^{-2}$ ).

**The extended habitable zone (EHZ)** where, in contrast to the PHZ, parts of the planetary orbit may lie outside the HZ due to the planet’s high eccentricity, for instance. Yet, the binary–planet configuration is still considered to be habitable when most of the planet’s orbit remains inside the boundaries of the HZ. In this case,  $\langle S_{\text{tot}} \rangle_t + \sigma \leq S_I$  and  $\langle S_{\text{tot}} \rangle_t - \sigma \geq S_O$  where  $\langle S_{\text{tot}} \rangle_t$  denotes the time-averaged effective insolation from both stars and  $\sigma^2$  is the effective insolation variance.

**The averaged habitable zone (AHZ).** Following the argument of Williams & Pollard (2002) that planetary eccentricities up to  $e < 0.7$  may not be prohibitive for hab-

itability as long as the atmosphere can act as a buffer, the AHZ is defined as encompassing all configurations which support the planet’s *time-averaged* effective insolation to be within the limits of the classical HZ. Therefore,  $S_I \geq \langle S_{\text{tot}} \rangle_t \geq S_O$ .

Analytic expressions for the maximum insolation, the average insolation ( $\langle S_{\text{tot}} \rangle$ ), and insolation variance that a planet encounters in a binary system have been derived in Eggl et al. (2012). We refer the reader to that article for more details.

Figures 3 and 4 show the application of the proposed habitability classification scheme to the  $\alpha$  Centauri system. In these figures, blue denotes PHZs, green shows EHZs, and yellow corresponds to AHZs. The red areas in Figures 3 and 4 are uninhabitable, and purple stands for dynamically unstable regions. Table 1 shows the physical properties of the system. We used the formulae by Underwood et al. (2003) to calculate  $S_I$  and  $S_O$  for the given effective temperatures of  $\alpha$  Cen A and B. In general, these formulae allow for extending the analytic estimates for HZs, as given by Eggl et al. (2012), to main-sequence stars with different spectral types. Runaway greenhouse and maximum greenhouse insolation limits were used to determine the inner and outer boundaries of HZs, respectively.

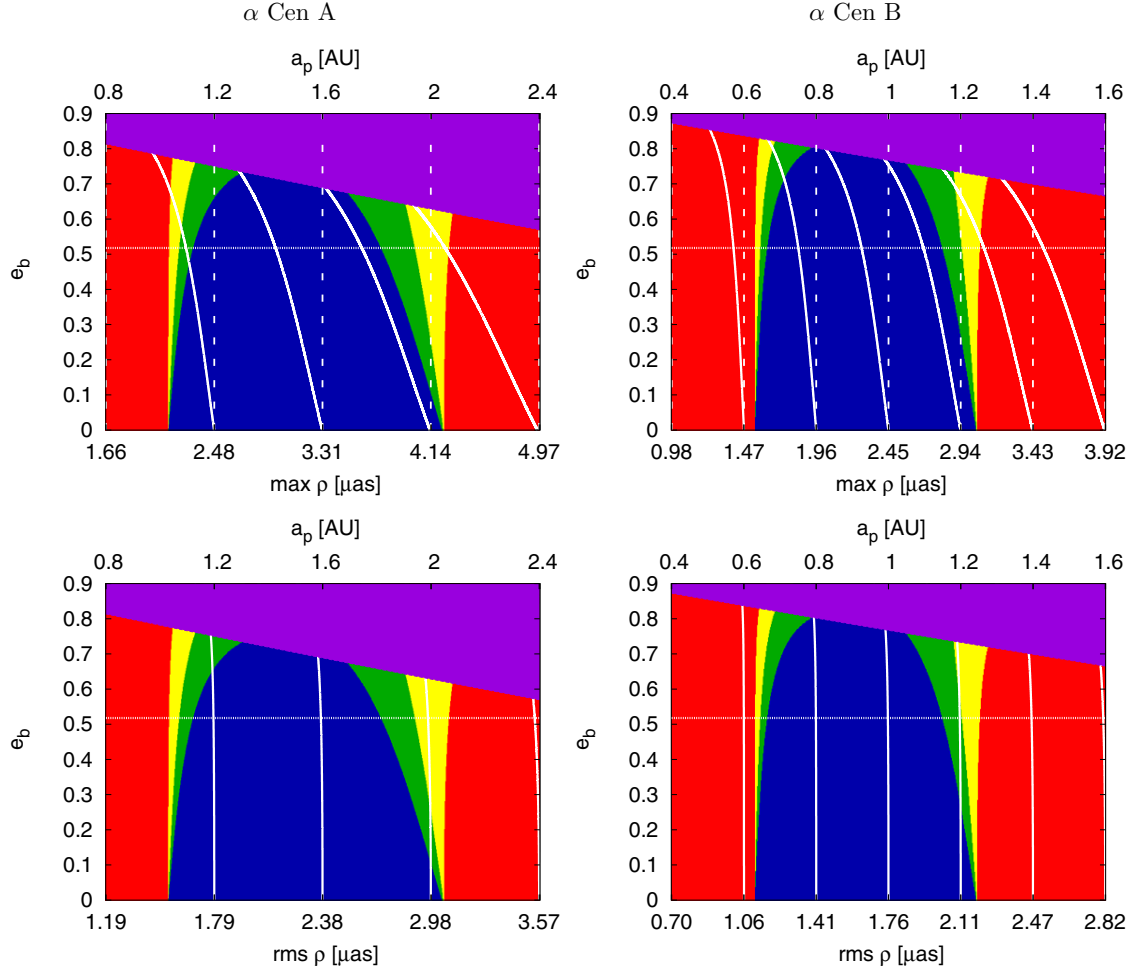


**Figure 4.** Habitability maps showing the maximum amplitudes and rms of the astrometric signals for the  $\alpha$  Centauri system. The color coding is similar to Figure 3. The vertical dashed lines in the top panels represent regions with similar values of  $\rho^{\text{circ}}$ . The curved lines in these panels show regions with similar  $\rho^{\text{max}}$  amplitudes. In the bottom panels, the vertical lines represent areas of equal rms amplitudes,  $\langle\langle\rho\rangle\rangle_{M,\omega}$ . One can see that planetary orbits with dynamically enhanced eccentricities can have smaller semimajor axes and still produce similarly high astrometric amplitudes as circular orbits which are more distant from the host star.

**Table 3**  
Detectability of an Earth-like Planet in the HZs of the  $\alpha$  Centauri System.

$\alpha$ Cen	$a_c$ (AU)	Inner AHZ	Inner EHZ	Inner PHZ	Outer PHZ	Outer EHZ	Outer AHZ		
A	2.76	1.03	1.07	1.12	1.81	1.94	2.06	HZ border	(AU)
		8.97	8.83	8.66	7.14	6.97	6.82	$V_r^{\text{max}}$	(cm s $^{-1}$ )
		5.89	5.78	5.65	4.44	4.30	4.17	$\langle\langle V_r \rangle\rangle_{M,\omega}$	
		2.28	2.37	2.49	4.20	4.52	4.84	$\rho^{\text{max}}$	$(\mu\text{as})$
B	2.51	1.53	1.59	1.66	2.69	2.88	3.06	$\langle\langle \rho \rangle\rangle_{M,\omega}$	
		0.62	0.64	0.65	1.13	1.19	1.23	HZ border	(AU)
		12.21	12.09	11.94	9.37	9.19	9.04	$V_r^{\text{max}}$	(cm s $^{-1}$ )
		8.25	8.16	8.05	6.12	5.98	5.86	$\langle\langle V_r \rangle\rangle_{M,\omega}$	
		1.58	1.62	1.66	2.97	3.12	3.26	$\rho^{\text{max}}$	$(\mu\text{as})$
		1.09	1.11	1.14	1.98	2.08	2.16	$\langle\langle \rho \rangle\rangle_{M,\omega}$	

**Notes.** Each row shows the maximum amplitude of the radial velocity signal as well as the astrometric fingerprints of a terrestrial planet in the  $\alpha$  Centauri HZs. The critical planetary semimajor axis ( $a_c$ ) indicates the onset of dynamical instability (Holman & Wiegert 1999). Computations using chaos indicators are in good agreement with those stability limits (Pilat-Lohinger & Dvorak 2002). Analytic expressions for calculating the boundary values of planetary semimajor axes in the system's HZs are given in Eggl et al. (2012).

As shown in Figures 3 and 4, the locations of the HZs and the detectability of habitable planets in those regions depend strongly on the eccentricity of the binary ( $e_b$ ). The actual eccentricity of the  $\alpha$  Centauri system is denoted by a

horizontal line at  $e_b = 0.5179$ . The values for the borders of the different HZs using  $\alpha$  Centauri's actual eccentricity are listed in Table 3. As shown here, both stars permit dynamical stability for habitable, Earth-like planets. Due to the difference

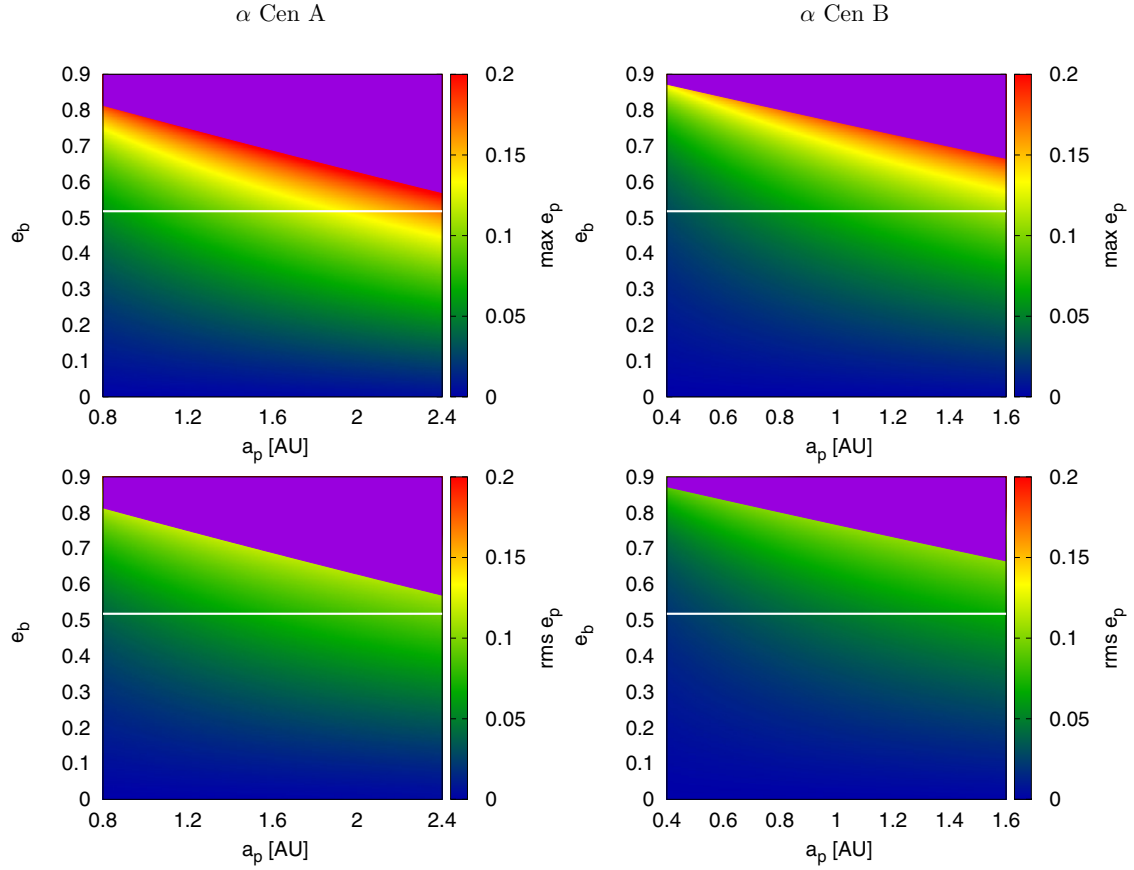


**Figure 5.** Graphs of the maximum ( $e_p^{\max}$ ) and rms ( $(e_p^2 / M, \omega)^{1/2}$ ) values of the planetary eccentricity for different values of the planet semimajor axis ( $a_p$ ) and the binary eccentricity ( $e_b$ ) for  $\alpha$  Cen A (left) and  $\alpha$  Cen B (right). The meshed region (purple online) denotes orbital instability. The horizontal line indicates the actual eccentricity of the  $\alpha$  Centauri binary.

(A color version of this figure is available in the online journal.)

in stellar luminosities, the HZs around  $\alpha$  Cen A are larger and farther away from the host star compared to  $\alpha$  Cen B. Since the binary’s mass ratio is close to 0.45, the gravitational influence of  $\alpha$  Cen B is more pronounced on the PHZ of  $\alpha$  Cen A. This is a consequence of the larger injected planetary eccentricities ( $e_p$ ) as can be seen from the top row of Figure 5. The relatively larger gravitational influence of  $\alpha$  Cen B onto the HZ of  $\alpha$  Cen A is also mirrored in the fact that the region of dynamical instability (meshed, purple online) reaches toward lower binary eccentricities. The change in the range and configuration of HZs with the change in planetary semimajor axis and eccentricity of the binary is pronounced. A clear shrinking trend for PHZ and EHZ can be observed for high values of the binary’s eccentricity. While as shown by Eggl et al. (2012), the AHZ in general expands slightly when the eccentricity is enhanced, Figures 3 and 4 show that in the  $\alpha$  Centauri system, this HZ depends only weakly on  $e_b$ , making it the closest approximation to the classical HZ as defined by Kasting et al. (1993). Comparing these results with the existing studies on the HZs for  $\alpha$  Cen B such as Guedes et al. (2008) and Forgan (2012), one can see that the values of the inner boundaries of the HZs around  $\alpha$  Cen B as given in Figures 3 and 4 coincide well with the previous studies. Forgan (2012) even found a similar shrinking trend with higher planetary eccentricity. Yet, Forgan (2012) did not take the actual coupling between the planet’s eccentricity and the binary’s orbit into account. The limits for the outer boundaries of HZ in our model are different from the ones in Forgan (2012)

since different climatic assumptions were made. In this work, we used insolation limits for atmospheric collapse assuming a maximum greenhouse atmosphere (Kasting et al. 1993) whereas Forgan (2012) focused on emergence from snowball states.

### 5.3. Additional Terrestrial Planets in $\alpha$ Centauri’s HZs

While the classification of HZs presented in the previous section is globally applicable to binary star systems, the analytic estimates to calculate their extent (Eggl et al. 2012) are only strictly valid for three-body systems, e.g., the binary star and a planet. Additional perturbers will influence the shape and size of the HZs. It is thus necessary to investigate which effect the already discovered planet around  $\alpha$  Cen B would have on an additional terrestrial planet in  $\alpha$  Cen B’s HZ.

If the mutual perturbations were large, the HZ boundaries given in Table 3 would have to be adapted, but  $\alpha$  Cen Bb’s orbital evolution could also contain clues on the presence—or the absence—of an additional planet. Should the interaction between the inner planet and an additional terrestrial body in the HZ be small, then the HZ boundaries would hold. However, a detection of the habitable planet via its influence on  $\alpha$  Cen Bb’s orbit would become difficult.

In Figure 6, results of numerical investigations on the coupled orbital evolution of an additional terrestrial planet and  $\alpha$  Cen Bb are presented. The top row of Figure 6 shows the eccentricity evolution of  $\alpha$  Cen Bb altered by an additional Earth-like planet at the inner and outer edge of  $\alpha$  Cen B’s AHZ. The corresponding

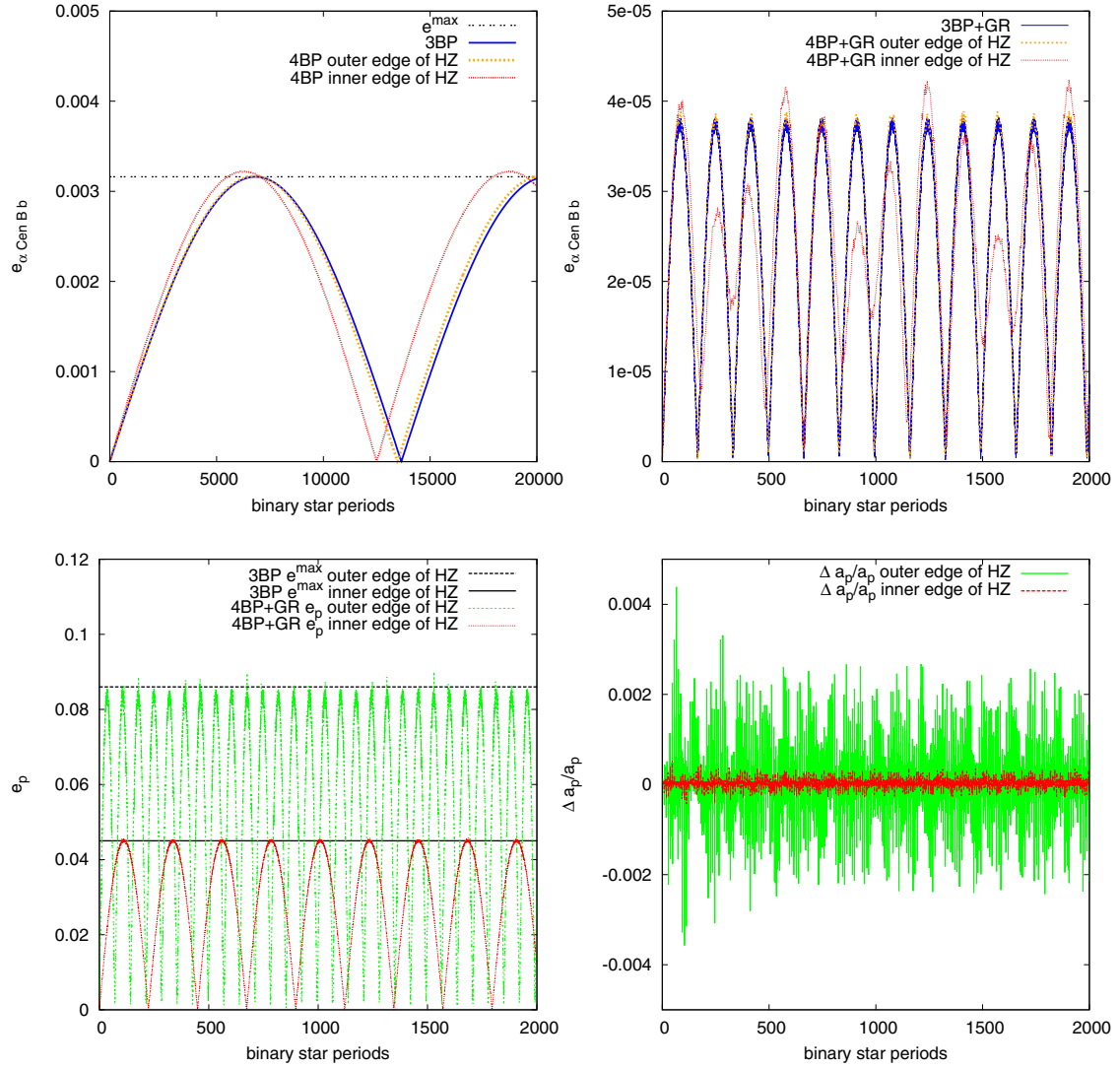


**Figure 6.** Additional terrestrial planet in  $\alpha$  Cen B’s HZ affects the orbit of  $\alpha$  Cen Bb (top row) and vice versa (bottom row). In the top left panel, the numerically computed evolution of the eccentricity of  $\alpha$  Cen Bb in the Newtonian three-body problem (3BP) consisting of the binary  $\alpha$  Cen AB and the planet  $\alpha$  Cen Bb is compared with different four-body problem scenarios (4BP). In one scenario, an additional Earth-sized body orbits  $\alpha$  Cen B at the inner edge of its AHZ (see Table 3). In the other scenario, the terrestrial planet is assumed to be at the outer edge of  $\alpha$  Cen B’s AHZ. The analytic estimate for the maximum eccentricity ( $e^{\text{max}}$ ) in the 3BP is presented as well (horizontal line). The top right panel shows the exact same setup, only with general relativity (GR) taken into account. The orbit of  $\alpha$  Cen Bb becomes practically circular. While the influence of an additional planet at the outer edge of the HZ is barely noticeable in the eccentricity evolution of  $\alpha$  Cen Bb, a planet at the inner edge of the AHZ would cause distinct features. In contrast, neither GR nor  $\alpha$  Cen Bb will influence the eccentricity evolution of planets ( $e_p$ ) in the HZ significantly as is shown in the bottom left panel. Also, the semimajor axes evolution of additional planets in the HZ is negligible (bottom right panel). Here,  $\Delta a_p/a_p$  denotes the normalized difference between the 4BP+GR and the 3BP semimajor axis evolution of planets at the inner and outer edges of  $\alpha$  Cen B’s AHZ, respectively.

(A color version of this figure is available in the online journal.)

reference curve (dashed, blue online) represents  $\alpha$  Cen Bb’s eccentricity influenced only by the binary  $\alpha$  Cen AB. The top left panel of Figure 6 shows the results in Newtonian three (3BP) and four (4BP) body problems. The top right panel depicts similar analysis with GR<sup>7</sup> included. The difference between the two approaches is quite pronounced, as GR clearly prevents the secular rise in Cen Bb’s eccentricity predicted in the classical setup (Blaes et al. 2002; Fabrycky & Tremaine 2007). Thus, the orbit of  $\alpha$  Cen Bb stays circular, even when tidal forces are neglected. The variations in semimajor axis ( $\Delta a$ ) for  $\alpha$  Cen Bb are not shown, because they remain below  $10^{-8}$  AU for all cases.

<sup>7</sup> GR was introduced by numerically solving the Einstein Infeld Hoffman equations (Einstein et al. 1938) for the respective systems.

A possible method to search for additional companions is to measure variations in  $\alpha$  Cen Bb’s orbital period. Yet, the small  $\Delta a$  values make this approach difficult, since  $\Delta P_p \propto P_p^{1/3} \Delta a$ . Disentangling the effects of GR and perturbations due to other habitable planets on  $\alpha$  Cen Bb’s period would require precisions several orders of magnitude greater than currently available. The top right panel in Figure 6 shows that the perturbations an additional planet at the inner edge of  $\alpha$  Cen B’s AHZ causes in  $\alpha$  Cen Bb’s eccentricity are, in principle, distinguishable from the nominal signal. Unfortunately, it is also clear from this graph that neither the required precision nor the observational timescales necessary to identify the presence of an additional Earth-sized companion via observations of  $\alpha$  Cen Bb’s eccentricity seem obtainable in the near future. For habitable planets at the outer edge of  $\alpha$  Cen B’s AHZ the chances for indirect detection

seem even worse, as their influence on  $\alpha$  Cen Bb's orbit is negligible.

In order to confirm that the interaction between  $\alpha$  Cen Bb and Earth-like planets in the HZ is small, as well as to further study the influence of the GR on the dynamics of the system, we examined the orbital evolution of a fictitious habitable planet in that region. The results are shown in the bottom row of Figure 6. The left panel depicts the eccentricity evolution of additional terrestrial planets positioned at the inner and outer edges of  $\alpha$  Cen B's AHZ. The secular variations in the eccentricity (bottom left panel) and semimajor axis (bottom right panel) of the habitable planet were computed numerically, taking the influence of the binary  $\alpha$  Cen AB, the planet  $\alpha$  Cen Bb, as well as GR into account. When comparing the analytic estimates of  $e^{\max}$  with the evolution of the habitable planet's eccentricity in the full system, it is evident that neither GR nor  $\alpha$  Cen Bb alter the results for planets in  $\alpha$  Cen B's HZ significantly. Also, the deviation in the habitable planet's semimajor axis due to GR and  $\alpha$  Cen Bb ( $\Delta a_p$ ) remains below 0.1% and 0.5% for planets at the inner and outer edge of  $\alpha$  Cen B's AHZ, respectively.

We conclude that the interaction between additional terrestrial planets in  $\alpha$  Cen B's HZ and  $\alpha$  Cen Bb is indeed small. Thus, our estimates for the HZs of the  $\alpha$  Centauri system remain valid. The existence of additional terrestrial planets on the other hand cannot be determined easily from observing the orbital evolution of  $\alpha$  Cen Bb.

The presented results are, strictly speaking, only valid for a coplanar configuration, i.e., the binary and both planets are in the same orbital plane. Mutually inclined configurations can exhibit much more involved dynamics such as Kozai resonant behavior (see, e.g., Correia et al. 2011). A detailed study of such effects lies beyond the scope of this work. Nevertheless, the arguments presented in this section suggest that the search for an additional coplanar planet in the HZ around  $\alpha$  Cen B will most likely have to be performed without relying on observations of  $\alpha$  Cen Bb. We will therefore investigate whether habitable planets can actually be detected independently in Sun-like binary star configurations using current observational facilities.

#### 5.4. Detectability through Radial Velocity and Astrometry

We apply our methodology, as derived in Sections 2 and 3, to a fictitious terrestrial planet in the HZ of binary systems similar to  $\alpha$  Centauri AB but with a broadened range of binary eccentricities. In addition to the habitability maps discussed in Section 5.2, Figures 3 and 4 show the results regarding the peak and rms strength of the RV and astrometric signals. Here, the aim is to illustrate how the different types of HZs presented in Section 5.2, as well as the maximum and rms signal strengths defined in Section 2 vary with the binary's eccentricity ( $e_b$ ) and planetary semimajor axis ( $a_p$ ). The left column of Figure 3 shows maximum (top) and rms (bottom) values of the signal strengths for the more massive binary component, in this case similar to  $\alpha$  Cen A. Results for the less massive component akin to  $\alpha$  Cen B are shown in the right column.

The dashed vertical lines in the top rows of Figures 3 and 4 represent the sections of the parameter space with similar  $V_r^{\text{circ}}$  and  $\rho^{\text{circ}}$  values, respectively. Since  $V_r^{\text{circ}}$  and  $\rho^{\text{circ}}$  are independent of the planetary (and consequently the binary's) eccentricity, the different values of these quantities vary linearly with the planet's semimajor axis. In contrast,  $V_r^{\text{max}}$  and  $\rho^{\text{max}}$ , represented by the solid contour lines, depend on the maximum eccentricity of the planet ( $e_p^{\text{max}}$ ) and therefore change with the binary's eccentricity ( $e_b$ ). Since for circular

binary configurations only small eccentricities are induced into the planet's orbit,  $V_r^{\text{max}}$  and  $V_r^{\text{circ}}$  almost coincide. The same holds true for  $\rho^{\text{max}}$  and  $\rho^{\text{circ}}$  in this case. Yet,  $V_r^{\text{max}}$  and  $\rho^{\text{max}}$  grow with the binary's eccentricity. The corresponding contour lines indicate that for high binary eccentricities even small planetary semimajor axes can produce similar AM peak signal strengths. Similarly, planets with larger distances to their host stars can still cause similar RV amplitudes if the binary's eccentricity is sufficiently large. If a fixed detection limit is set, e.g.,  $V_r = 9.5$  m/s, planets with semimajor axes up to 1.5 AU could still be found around stars similar to  $\alpha$  Cen A, assuming a binary eccentricity of  $e_b = 0.7$ . To produce a similarly high RV amplitude, a circular planet has to orbit its host star at roughly 0.8 AU (Figure 3). In other words, high binary eccentricities lead to excited planetary eccentricities which in turn increase the peak signal strengths suggesting that binary–planet interactions can actually improve the chances for detecting terrestrial planets. Naturally, if the planet's eccentricity happens to be close to zero at the time of observation, this advantage is nullified.

The bottom row of Figures 3 and 4 show the same setup with rms signal strengths  $\langle V_r \rangle_{M,\omega}$  and  $\langle \rho \rangle_{M,\omega}$ , respectively. While  $\langle V_r \rangle_{M,\omega}$  is independent of the binary's eccentricity, it is evident from Equation (17) that  $\langle \rho \rangle_{M,\omega}$  depends weakly on  $e_b$  since  $\langle e_p^2 \rangle^{1/2} \simeq 0.1$  for the cases considered and therefore  $\langle e_p^2 \rangle \ll 1$  (see Figure 5, bottom). The slight curvature of the contour lines representing the rms signal in Figure 4 indicates this behavior. A summary of RV and AM signal strengths for an Earth-like planet at the boundaries of  $\alpha$  Centauri's HZ is presented in Table 3.

We illustrated in this section that the dynamical interactions between a terrestrial planet and the secondary star can produce large peak amplitudes which may enhance the detectability of the planet with the RV and AM methods considerably. The rms values of the planet's AM and RV signals, on the other hand, remain almost unaffected by the gravitational influence of the secondary star.

#### 5.5. Transit Photometry

To assess the detectability of a terrestrial planet in the HZ of  $\alpha$  Centauri AB (and similar binaries) through TP, we calculated the relative transit depths that an Earth-like planet would produce during its transit. If such a system hosted a transiting terrestrial planet, TD values would range around 55 ppm for  $\alpha$  Cen A, and 115 ppm for  $\alpha$  Cen B. Such transit depths are detectable by NASA's *Kepler* telescope for instance—stellar and instrumental sources included—as the spacecraft's median noise level amounts to  $\approx 29$  ppm (Gilliland et al. 2011). Therefore, Earth-like planets could in theory be found around  $\alpha$  Centauri stars. However, *Kepler* was not designed to observe stars with apparent magnitudes between 0 and 3 such as those of  $\alpha$  Centauri. The Transiting Exoplanets Survey Satellite mission, for instance, will aim for TP of brighter stars (Ricker et al. 2010). Nevertheless, the example of *Kepler* suggests that the detection of transiting habitable planets in S-type systems would be possible using current technology. In fact, very much similar to the cases discussed in the previous section, the orbit forcing that an Earth-like planet experiences in a binary star system may enhance its possibility of detection via TP (Kane & von Braun 2008; Kane et al. 2012; Borkovits et al. 2003; Schneider 1994; also see Figure 7). Assuming  $\alpha$  Centauri was a transiting system,<sup>8</sup> a comparison of the transit

<sup>8</sup>  $i_b = 90^\circ \pm \theta_{\text{planet}}/2$  (Borucki & Summers 1984).



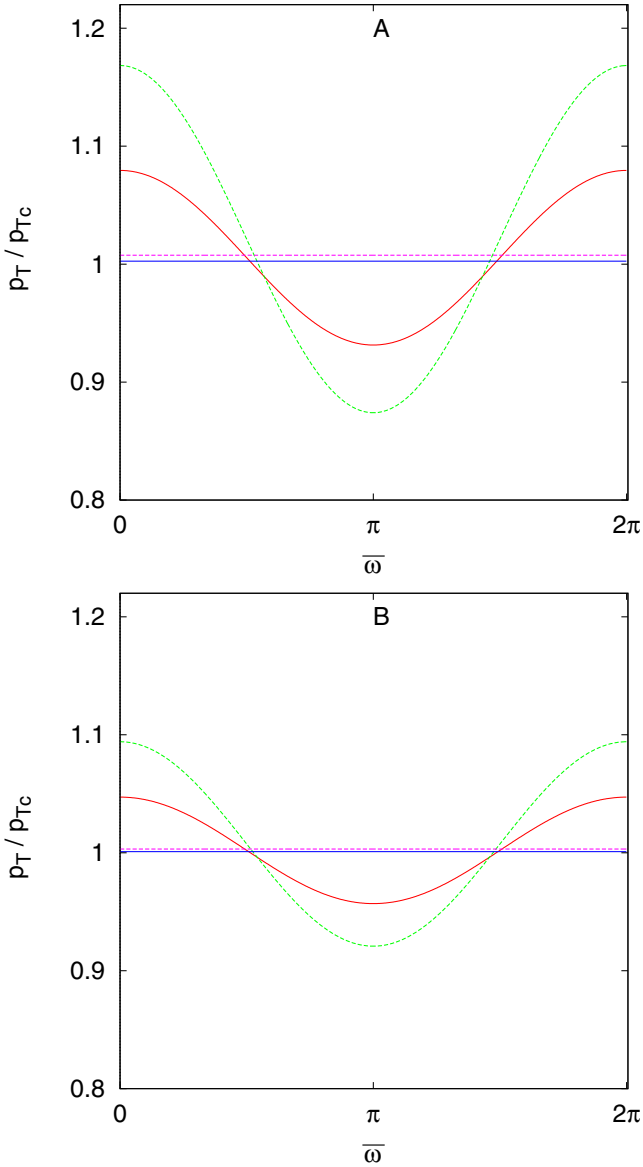


**Figure 7.** Graphs of the ratio of transit probabilities ( $p_T/p_{Tc}$ ) with  $p_T \equiv p_T|_{e=e_{\max}}$  and  $p_{Tc} \equiv p_T|_{e=0}$ , in a binary similar to the  $\alpha$  Centauri system. The graphs show the transit probabilities in terms of the planet's argument of pericenter ( $\bar{\omega}$ ), as measured from the line of sight for component A (top) and component B (bottom). The curved full lines correspond to the planet starting at the inner border of AHZ and dashed-curved line represents planets that started at the outer edge, for each star (see Table 3). The full and dashed straight lines are the corresponding ratios of the averaged transit probabilities ( $\langle p_T \rangle / \langle p_{Tc} \rangle$ ) evaluated using Equation (21). Compared to the transit probability ratios  $p_T/p_{Tc}$ , the ratio of averages  $\langle p_T \rangle / \langle p_{Tc} \rangle$  shows only a weak dependence on the planet's initial position in the HZ.

(A color version of this figure is available in the online journal.)

probabilities of actual planetary orbits to circular orbits shows that an 18% increase in  $p_T$  values seems possible for terrestrial planets at the outer edge of  $\alpha$  Cen A's AHZ (Figure 7). Given the right orbital configuration, it may be more likely to identify a transiting habitable terrestrial planet around a stellar component of a binary than around a single star assuming similar initial planetary eccentricities.

The increase in transit probability for planets in double star systems is less dramatic when the equations are averaged over all possible configurations of the argument of pericenter as in Equation (21). Averaged transit probabilities are represented

by the straight lines in Figure 7. As  $\langle p_T \rangle / \langle p_T|_{e=0} \rangle > 1$ , for terrestrial planets' orbits with  $e > 0$ , the chance for transit is in general higher for Earth-like planets in binary stars than for terrestrial planets in circular orbits around single stars.

## 6. DISCUSSION

Comparing the quantitative estimates of RV, AM, and TP signals, TP seems to be the best choice for finding Earth-like planets in the HZs of a coplanar S-type binary configuration with Sun-like components. Even for a system as near as  $\alpha$  Centauri, AM peak signals only measure  $\mu\text{as}$ . Unfortunately, neither ESO's very long baseline interferometry with PRIMA nor ESA's *Gaia* mission will be able to deliver such precision in the near future (Quirrenbach et al. 2011). *Gaia*'s aim to provide  $\mu\text{as}$  AM will most likely not be achieved until the end of the mission (Hestroffer et al. 2010). Also, from an astrometric point of view, Earth-like planets would be easier to find around  $\alpha$  Cen A than  $\alpha$  Cen B. That is because the HZ around star A is more distant from this star. Naturally, the opposite is true for RV detections. Due to the difference in the stellar masses,  $\alpha$  Cen B offers a better chance of finding a terrestrial planet there using RV techniques. The recent discovery of an Earth-sized planet around this star supports our results. The observed planetary RV signal was reproduced excellently by our analytic estimates for circular planetary orbits.

Our prediction of RV amplitudes for terrestrial planets around  $\alpha$  Cen B are also in good agreement with those presented by Guedes et al. (2008). The four terrestrial planets used in the RV model by these authors produce almost exactly four times the predicted rms amplitude given in Figure 3. Guedes et al. (2008) claim that Earth-like planets in the  $\alpha$  Centauri are detectable even for signal-to-noise ratios of single observations below 0.1. However, obtaining sufficient data to reconstruct the planetary signal requires a great amount of dedicated observing time (approximately five years in their example). Validating this statement, it took Dumusque et al. (2012) about four years of acquired data to detect  $\alpha$  Cen Bb. The data published by Dumusque et al. (2012) also allow a glimpse on the current performance of the HARPS spectrograph revealing a precision around 50–80  $\text{cm s}^{-1}$ . Given the fact that the RV signal of a habitable planet around  $\alpha$  Cen B would be still half an order of magnitude smaller (Figure 3), considerably more observation time would be required to identify habitable companions. HIRES measurements are currently yielding precisions around 1  $\text{m s}^{-1}$ . Identifying RV signals of habitable worlds around  $\alpha$  Cen B therefore seems even more unlikely when using HIRES. The previous examples show that some development of observational capacities is still necessary to achieve the RV resolution required for discovering habitable planets in the  $\alpha$  Centauri system.

The success of NASA's *Kepler* space telescope in identifying countless Earth-sized planetary candidates (e.g., Borucki 2011) that require follow-up observations might provide the necessary momentum to develop instruments capable of resolving RV signals in the range of  $\text{cm s}^{-1}$ . Focusing on less massive binaries would have the advantage of having greatly enhanced RV signals as the HZs will be situated closer to the planet's host stars. How far this might simplify the task of finding habitable worlds will be the topic of further investigations.

In regard to TP, both *Kepler* and *CoRoT* telescopes have proven that it is possible to find terrestrial planets around Sun-like stars (e.g., Léger et al. 2009; Borucki et al. 2012). The

combination of proven technology and the presented argument that the dynamical environment in binary star systems will enhance transit probabilities makes photometry currently the most promising method for finding Earth-like planets in the HZs of S-type binary star systems.

## 7. SUMMARY

In this work, we provided an analytic framework to estimate the detectability of a terrestrial planet using RV, AM, as well as TP in coplanar S-type binary configurations. We have shown that the gravitational interactions between the stars of a binary and a terrestrial planet can improve the chances for the planet's detection. The induced changes in the planet's eccentricity enhance not only RV and AM peak amplitudes, but also the probability to witness a planetary transit. Next to the presented "best case" estimates, we offered rms/averaged expressions which are deemed to be more suited to determine the long-term influence of the second star on planetary fingerprints in S-type systems. In contrast to peak amplitudes, the rms of a planet's AM signal is only modified slightly by the additional gravitational interaction with the second star. A similar behavior can be seen in planetary transit probabilities. The rms values of RV signals are altogether independent of the secondary's gravitational influence, assuming that the system is nearly coplanar.

After defining the permanent, extended, and average habitable zones for both stellar components of the  $\alpha$  Centauri system, we investigated the possible interaction between the newly discovered  $\alpha$  Cen Bb and additional terrestrial companions in  $\alpha$  Cen B's HZ. Our results suggest that  $\alpha$  Cen Bb is on an orbit with very low eccentricity which would not be influenced significantly by habitable, terrestrial companions. Conversely,  $\alpha$  Cen Bb's presence would also not affect Earth-like planets in the HZ of  $\alpha$  Cen B.

We estimated the maximum and rms values of the RV as well as AM signal for a terrestrial planet in the  $\alpha$  Centauri HZs. The peak and rms amplitudes of the RV signal ranged between 4 and 12 cm s<sup>-1</sup>. Astrometric signals were estimated to lie between 1 and 5  $\mu$ as. Given the current observational facilities, enormous amounts of observing time would be required to achieve such precisions. If the  $\alpha$  Centauri was a transiting system, however, a habitable planet could be detectable using current technologies. It seems that the detection of Earth-like planets in circumstellar HZs of binaries with Sun-like components via astrometry and RV is still somewhat beyond our grasp, leaving photometry to be the only current option in this respect.

S.E. and E.P.-L. acknowledge support from FWF through projects AS11608-N16 (EP-L and SE), P20216-N16 (SE and EP-L), and P22603-N16 (EP-L). S.E. acknowledges support from the University of Vienna's Forschungsstipendium 2012. N.H. acknowledges support from the NASA Astrobiology Institute under Cooperative Agreement NNA09DA77A at the Institute for Astronomy, University of Hawaii, and NASA EXOB grant NNX09AN05G. S.E. and E.P.-L. also thank the Institute for Astronomy and NASA Astrobiology Institute at the University of Hawaii-Manoa for their kind hospitality during the course of this project. The authors are thankful to Nikolaos Georgakarakos for his valuable suggestions and to the anonymous referee for constructive comments.

## APPENDIX A

### EQUATION OF THE CENTER

The equation of the center providing a direct relation between the true anomaly  $f$  and the mean anomaly  $M$  is presented up to the sixth order in eccentricity  $e$ :

$$\begin{aligned} f = M &+ \left( 2e - \frac{e^3}{4} + \frac{5e^5}{96} \right) \sin M \\ &+ \left( \frac{5e^2}{4} - \frac{11e^4}{24} + \frac{17e^6}{192} \right) \sin[2M] \\ &+ \left( \frac{13e^3}{12} - \frac{43e^5}{64} \right) \sin[3M] \\ &+ \left( \frac{103e^4}{96} - \frac{451e^6}{480} \right) \sin[4M] \\ &+ \frac{1097}{960} e^5 \sin[5M] + \frac{1223}{960} e^6 \sin[6M] + O(e^7). \quad (\text{A1}) \end{aligned}$$

## APPENDIX B

### AVERAGING OF $\rho^2$

The averaging integrations over  $M$  and  $\omega$  in Equations (17) and (18) were carried out as in the following:

$$\begin{aligned} &\frac{1}{4\pi^2} \int_0^{2\pi} \int_0^{2\pi} \rho^2(M, \omega) dM d\omega \\ &= \frac{1}{2\pi} \int_0^{2\pi} \frac{\mu^2 a^2}{d^2} \left\{ 1 + \frac{3\langle e^2 \rangle_M}{2} \right. \\ &\quad \left. + \left[ -\frac{1}{2} + \frac{\langle e^2 \rangle_M}{4} (5 \cos(2\omega) - 3) \right] \sin^2 i \right\} d\omega. \end{aligned}$$

The integration over  $M$  is trivial. Using the partial integration technique to integrate over  $\omega$ , we obtain

$$\begin{aligned} &\frac{1}{2\pi} \int_0^{2\pi} \frac{5}{4} \langle e^2 \rangle_M \cos(2\omega) d\omega \\ &= \frac{5}{4} \left[ \langle e^2 \rangle_{M,\omega} \cos(2\omega) \Big|_0^{2\pi} + 2 \langle e^2 \rangle_{M,\omega} \int_0^{2\pi} \sin(2\omega) d\omega \right] = 0. \end{aligned}$$

Here we have used the fact that  $\langle e^2 \rangle_{M,\omega} = (1/2\pi) \int_0^{2\pi} \langle e^2 \rangle_M d\omega$  does no longer depend on  $\omega$ . From the definition of averaging given by Equation (6), we have

$$\langle \langle \rho \rangle \rangle_{M,\omega} = \frac{\mu a}{2d} \left[ 3 + \frac{9}{2} \langle e^2 \rangle_{M,\omega} + \left( 1 + \frac{3}{2} \langle e^2 \rangle_{M,\omega} \right) \cos(2i) \right]^{1/2}. \quad (\text{B1})$$

A similar procedure has been applied to derive Equation (8).

## REFERENCES

- Beaugé, C., Ferraz-Mello, S., & Michtchenko, T. A. 2007, in *Planetary Masses and Orbital Parameters from Radial Velocity Measurements*, ed. R. Dvorak (Wiley-VCH), 1
- Blaes, O., Lee, M. H., & Socrates, A. 2002, *ApJ*, **578**, 775
- Borkovits, T., Érdi, B., Forgács-Dajka, E., & Kovács, T. 2003, *A&A*, **398**, 1091
- Borucki, W. J., Koch, D. G., Basri, G., et al. 2011, *ApJ*, **736**, 19
- Borucki, W. J., Koch, D. G., Batalha, N., et al. 2012, *ApJ*, **745**, 120
- Borucki, W. J., & Summers, A. L. 1984, *Icar*, **58**, 121

- Chauvin, G., Beust, H., Lagrange, A.-M., & Eggenberger, A. 2011, *A&A*, **528**, A8
- Correia, A. C. M., Laskar, J., Farago, F., & Boué, G. 2011, *CeMDA*, **111**, 105
- Doyle, L. R., Carter, J. A., Fabrycky, D. C., et al. 2011, *Sci*, **333**, 1602
- Dumusque, X., Pepe, F., Lovis, C., et al. 2012, *Natur*, **491**, 207
- Eggl, S., Pilat-Lohinger, E., Georgakarakos, N., Gyergyovits, M., & Funk, B. 2012, *ApJ*, **752**, 74
- Einstein, A., Infeld, L., & Hoffmann, B. 1938, *AnMat*, **39**, 65
- Fabrycky, D., & Tremaine, S. 2007, *ApJ*, **669**, 1298
- Ford, E. B., Fabrycky, D. C., Steffen, J. H., et al. 2012, *ApJ*, **750**, 113
- Ford, E. B., Quinn, S. N., & Veras, D. 2008, *ApJ*, **678**, 1407
- Forgan, D. 2012, *MNRAS*, **422**, 1241
- Georgakarakos, N. 2002, *MNRAS*, **337**, 559
- Georgakarakos, N. 2003, *MNRAS*, **345**, 340
- Georgakarakos, N. 2005, *MNRAS*, **362**, 748
- Gilliland, R. L., Chaplin, W. J., Dunham, E. W., et al. 2011, *ApJS*, **197**, 6
- Guedes, J. M., Rivera, E. J., Davis, E., et al. 2008, *ApJ*, **679**, 1582
- Haghighipour, N. 2010, *Planets in Binary Star Systems* (New York: Springer)
- Hestroffer, D., Dell’Oro, A., Cellino, A., & Tanga, P. 2010, in *Dynamics of Small Solar System Bodies and Exoplanets*, ed. J. Souchay & R. Dvorak (Lecture Notes in Physics, Vol. 790; Berlin: Springer), 251
- Holman, M. J., & Wiegert, P. A. 1999, *AJ*, **117**, 621
- Kane, S. R., Horner, J., & von Braun, K. 2012, *ApJ*, **757**, 105
- Kane, S. R., & von Braun, K. 2008, *ApJ*, **689**, 492
- Kasting, J. F., Whitmire, D. P., & Reynolds, R. T. 1993, *Icar*, **101**, 108
- Kervella, P., Thévenin, F., Ségransan, D., et al. 2003, *A&A*, **404**, 1087
- Kiseleva-Eggleton, L., & Eggleton, P. P. 2001, in *ASP Conf. Ser. 229, Evolution of Binary and Multiple Star Systems*, ed. P. Podsiadlowski, S. Rappaport, A. R. King, F. D’Antona, & L. Burderi (San Francisco, CA: ASP), 91
- Lee, M. H., & Peale, S. J. 2003, *ApJ*, **592**, 1201
- Léger, A., Rouan, D., Schneider, J., et al. 2009, *A&A*, **506**, 287
- Marchal, C. 1990, *The Three-body Problem* (Amsterdam: Elsevier)
- Ohta, Y., Taruya, A., & Suto, Y. 2005, *ApJ*, **622**, 1118
- Orosz, J. A., Welsh, W. F., Carter, J. A., et al. 2012a, *A&A*, **758**, 87
- Orosz, J. A., Welsh, W. F., Carter, J. A., et al. 2012b, *Sci*, **337**, 1511
- Paardekooper, S.-J., & Leinhardt, Z. M. 2010, *MNRAS*, **403**, L64
- Pilat-Lohinger, E., & Dvorak, R. 2002, *CeMDA*, **82**, 143
- Pourbaix, D. 2002, *A&A*, **385**, 686
- Pourbaix, D., Nidever, D., McCarthy, C., et al. 2002, *A&A*, **386**, 280
- Quirrenbach, A., Geisler, R., Henning, T., et al. 2011, *European Physical Journal Web of Conferences*, **16**, 7005
- Rabl, G., & Dvorak, R. 1988, *A&A*, **191**, 385
- Ricker, G. R., Latham, D. W., Vanderspek, R. K., et al. 2010, *BAAS*, **42**, 459
- Roell, T., Neuhauser, R., Seifahrt, A., & Mugrauer, M. 2012, *A&A*, **542**, A92
- Schneider, J. 1994, *P&SS*, **24**, 539
- Schneider, J., Dedieu, C., Le Sidaner, P., Savalle, R., & Zolotukhin, I. 2011, *A&A*, **532**, A79
- Thébaud, P., Marzari, F., & Scholl, H. 2009, *MNRAS*, **393**, L21
- Torres, G., Andersen, J., & Giménez, A. 2010, *A&ARv*, **18**, 67
- Underwood, D. R., Jones, B. W., & Sleep, P. N. 2003, *IJAsB*, **2**, 289
- Welsh, W. F., Orosz, J. A., Carter, J. A., et al. 2012, *Natur*, **481**, 475
- Williams, D. M., & Pollard, D. 2002, *IJAsB*, **1**, 61



## Chapter 4

# Circumstellar Habitable Zones of Binary Star Systems in the Solar Neighborhood

Binary stars close to the Solar System are being investigated in order to determine their capability to host habitable planets. Hereby, the analytic HZ classifications presented in chapter 2 as well as the analytic estimates from chapter 3 regarding the observability of such planets are applied to real systems selected from the Washington Double Star Catalog.

**authors:** Siegfried Eggl, Elke Pilat-Lohinger, Barbara Funk, Nikolaos Georgakarakos and Nader Haghighipour<sup>1</sup>

**publication state:** published online November 24<sup>th</sup>, 2012

**publication details:** Monthly Notices of the Royal Astronomical Society, Volume 428, Issue 4, p.3104-3113

**contribution of the first author:** The first author was responsible for the final selection of the binary star systems, the calculation of the HZs as well the signal strength estimates. The construction of the article was also performed by the first author.

**contribution of the co-authors:** The co-authors were essential in the initial compilation of the WDC data as well as the in the discussion of the results and the critical reviewing of the article.

---

<sup>1</sup>Author affiliations are presented in the header of the following article.

# Circumstellar habitable zones of binary-star systems in the solar neighbourhood

S. Eggl,<sup>1</sup>\* E. Pilat-Lohinger,<sup>1</sup> B. Funk,<sup>1</sup> N. Georgakarakos<sup>2</sup> and N. Haghighipour<sup>3</sup>

<sup>1</sup>*Institute for Astrophysics (IfA), University of Vienna, Türkenschanzstr. 17, 1180 Vienna, Austria*

<sup>2</sup>*Higher Technological Educational Institute of Serres, Terma Magnesias, Serres 62124, Greece*

<sup>3</sup>*Institute for Astronomy and NASA Astrobiology Institute, 2680 Woodlawn Drive, Honolulu, HI 96822, USA*

Accepted 2012 October 19. Received 2012 October 19; in original form 2012 September 16

## ABSTRACT

Binary and multiple systems constitute more than half of the total stellar population in the solar neighbourhood. Their frequent occurrence as well as the fact that more than 70 planets have already been discovered in such configurations – most notably the telluric companion of  $\alpha$  Cen B – make them interesting targets in the search for habitable worlds. Recent studies have shown that despite the variations in gravitational and radiative environment, there are indeed circumstellar regions where planets can stay within habitable insolation limits on secular dynamical time-scales. In this paper, we provide habitable zones for 19 near S-type binary systems from the *Hipparcos* and Washington Double Star catalogue (WDS) catalogues with semimajor axes between 1 and 100 au. Hereby, we accounted for the combined dynamical and radiative influence of the second star on the Earth-like planet. Out of the 19 systems presented, 17 offer dynamically stable habitable zones around at least one component. The 17 potentially habitable systems contain 5 F, 3 G, 7 K and 16 M class stars. As their proximity to the Solar system ( $d < 31$  pc) makes the selected binary stars exquisite targets for observational campaigns, we offer estimates on radial velocity, astrometric and transit signatures produced by habitable Earth-like planets in eccentric circumstellar orbits.

**Key words:** astrobiology – binaries: general.

## 1 INTRODUCTION

The discovery and confirmation of terrestrial bodies orbiting other stars (e.g. Léger et al. 2009; Borucki 2011; Borucki et al. 2012; Dumusque et al. 2012) have generated enormous public as well as scientific interest. It has shown that after a mere two decades of exoplanetary research finding potentially habitable worlds around other stars seems to be almost within our grasp. Close-by stars and stellar systems are thereby premium targets, as they tend to offer reasonable signal-to-noise ratio (S/N) values for photometry and radial velocity (RV) as well as comparatively large astrometric (AM) amplitudes (Beaugé, Ferraz-Mello & Michtchenko 2007; Guedes et al. 2008; Malbet et al. 2012; Eggl, Haghighipour & Pilat-Lohinger 2012a). As more than half of the stars in the solar neighbourhood are members of binary or multiple systems (Kiseleva-Eggleton & Eggleton 2001), it is not surprising that more than 70 planets in or around binary stars have been discovered (Schneider et al. 2011) despite the current observational focus on single-star systems. Even though NASA's *Kepler* mission has been quite successful in finding circumbinary planets (e.g. Doyle et al. 2011; Orosz et al. 2012;

Welsh et al. 2012), we will focus on binary-star systems with potential *circumstellar* habitable zones (HZs) in this study. In fact, most of the planets discovered in double stars are in these so-called S-type configurations (Rabl & Dvorak 1988; Roell et al. 2012), where the planet orbits one star only. The telluric companion of  $\alpha$  Cen B is such an example (Dumusque et al. 2012).

An interesting question in this regard is doubtlessly: can S-type binary stars harbour habitable worlds? Already Huang (1960) and Harrington (1977) and more recently Forgan (2012) investigated the effects such configurations have on the insolation hypothetical planets would receive. Eggl et al. (2012b) (in the following referred to as EG12) were able to derive analytic expressions to find HZs in binary-star systems unifying dynamical and radiative balance models for S-type binary star–planet systems. While the exact manner in which planets form in tight binary-star systems is still hotly debated in astrophysical literature – see, for instance, Müller & Kley (2012), Batygin, Morbidelli & Tsiganis (2011), Paardekooper & Leinhardt (2010), Thebault (2011) and references therein, the discovery of  $\alpha$  Cen B b has made the existence of terrestrial planets in S-type binary-star systems an observational fact. Opinions still differ on whether it is theoretically possible that planets in  $\alpha$  Centauri's HZs can form on stable orbits. Even though classical N-body simulations with best case accretion scenarios seem to be

\*E-mail: siegfried.eggl@univie.ac.at

able to produce terrestrial planets near the HZs of the  $\alpha$  Centauri system (Guedes et al. 2008; Quintana & Lissauer 2010), Thébault, Marzari & Scholl (2009) and Thébault, Marzari & Scholl (2008) concluded that even when gas drag is included the encounter velocities between kilometre-sized planetesimals would lead to erosive collisions, thus making constant accretion unlikely. However, in their model they did not include a self-consistent evolution of the gas disc, nor did they consider planetesimal self-gravitation or re-accretion of collisional debris. Paardekooper & Leinhardt (2010) used a self-consistent disc model with planetesimals. They were able produced accretion friendly scenarios when the collision frequency was sufficiently high to prevent orbital dephasing. Other possible solutions to the problem of high encounter velocities range from including planetesimal and embryo migration (Payne, Wyatt & Thébault 2009) over mild inclination of planetesimal discs with respect to the binary's orbit (Xie, Zhou & Ge 2010) to more realistic radiative modelling of the system's gaseous disc (Müller & Kley 2012).

Eggl et al. (2012a) show that even if additional Earth-like planets in  $\alpha$  Centauri do exist, it is not an easy task to find them given current observational limitations in RV resolution. The RV signal semi-amplitude of  $\alpha$  Cen B b was near the current edge of feasibility with  $\delta RV \simeq 50 \text{ cm s}^{-1}$ , whereas accuracies lower than  $10 \text{ cm s}^{-1}$  would be necessary to discover telluric planets in  $\alpha$  Cen B's HZs. Astrometry is not much more helpful in this case, as the necessary AM amplitudes to detect habitable worlds in  $\alpha$  Centauri will only be available near the end of the *Gaia* mission's lifetime (Hestroffer et al. 2010).

In this study we tackle the question whether there are S-type systems in the solar neighbourhood that might make for easier targets. For this purpose we select 19 S-type binary systems from 'The Washington Visual Double Star Catalog' (WDC) (Mason et al. 2012) with well-determined stellar parameters that lie within a distance of 31 pc from the Solar system, and calculate HZs for each stellar component using the analytic method presented in EG12. We provide estimates on the RV and AM root mean square (rms) signal strengths expected for an Earth-like planet orbiting at the borders of a system's HZs. Furthermore, we present likely transit depths (TDs) for potentially transiting habitable planets in co-planar S-type double-star systems.

This paper is structured as follows. First, we will discuss the selection criteria for the 19 systems investigated (Section 2). After a brief summary of the main factors that determine habitability for terrestrial planets in binary-star systems (Section 3), the issue of dynamical stability of planets in such configurations is addressed in Section 4. Our results – tables with HZ borders and signal strength estimates – are presented and discussed in Sections 5 and 6. Current problems in modelling tidal-locking of planets in binary systems are mentioned in Section 7. A summary (Section 8) concludes this study.

## 2 SELECTION OF BINARY-STAR SYSTEMS

We preselected all detached binaries with semimajor axes  $1 < a_b < 100 \text{ au}$  using the stellar orbital parameters provided in the WDC, in order to find suitable S-type systems in the solar neighbourhood where Earth-like planets in HZs could be detectable. Hereby, we only considered systems within a distance of  $d < 31 \text{ pc}$  from our Solar system as determined by the *Hipparcos* mission (van Leeuwen 2007). Together with the prerequisite that the binaries' orbital elements had to be available, the aforementioned restrictions reduced the number of admissible double-star systems to 313. Furthermore,

only double-star configurations with known spectral types of both components were used. Peculiar spectra that might have been classified incorrectly by *Hipparcos* such as HIP 17544 and 73695 were also excluded, narrowing the set of candidate systems from 313 to 35. The ultimate selection criterion consisted of calculating the binaries' periods using bolometric luminosity derived masses together with the semimajor axes given in WDS and comparing them to the observed binary periods. The stellar bolometric luminosities and masses required for this purpose were derived as follows: with the distances available through *Hipparcos* data the systems' absolute visual magnitudes could be calculated. In order to assess the bolometric luminosities of the binary sample, we performed bolometric corrections (BCs) of the absolute visual magnitudes using the polynomial fits by Flower (1996). The required effective temperatures were estimated via spectral type and luminosity using the ATLAS9 catalogue of stellar model atmospheres (Castelli & Kurucz 2004). We then calculated the binaries' periods using the masses derived via the mass–luminosity relations given in Salaris & Cassisi (2005). Only those systems whose derived periods did not deviate more than 11 per cent from the observed periods were selected for the final sample. Stellar and orbital parameters for the final set of 19 S-type binary systems are presented in Table 1.

In the next section we will briefly discuss the main points on how to determine HZs for these S-type binary systems.

## 3 HABITABILITY OF EARTH-LIKE PLANETS IN S-TYPE BINARY-STAR SYSTEMS

The most pronounced difference between determining classical HZs and HZs for Earth-like planets in binary-star systems lies in the assumption that planetary orbits are basically circular. In fact, the well-known borders defined by Kasting, Whitmire & Reynolds (1993) are built on the premises that planetary insolation will change only on stellar evolutionary time-scales. Thus, the planet is thought to remain more or less at the same distance from its host star on a circular orbit. This assumption is implicitly made in almost all recent works (e.g. Kaltenegger & Sasselov 2011; Pierrehumbert & Gaidos 2011; Kane & Gelino 2012). However, in three-body systems, such as the planet–binary-star configurations we are investigating, gravitational interactions will alter the planetary orbit.

Perturbation theory of hierarchical triples predicts that the orbit of the inner pair – in our case host star and planet – will experience significant alterations in its eccentricity, whereas its semimajor axis remains almost constant (Marchal 1990; Georgakarakos 2002, 2003). For nearly equiplanar systems, the influence of planetary inclination and ascending node to the overall dynamics can be considered small; they will be neglected in what follows. Even though there may be short-periodic variations, some important changes in a planet's orbit happen also on secular time-scales. Secular periods are usually much larger than the planet's orbital period. However, they are a lot smaller than stellar evolutionary time-scales for detached binary systems with semimajor axes  $a_b < 100 \text{ au}$ . It is thus necessary to include the effects of changing planetary orbits in our estimates regarding HZs within binary-star environments. In their work, EG12 confirmed that variations in the planet's orbit are even more important for changes in its insolation than the additional radiation from the second star! The only exceptions to this rule are systems where the second star is much more luminous than the planet's host-star ( $L_B/L_A > 4$ , where binary component A is the planet's host star in this case). Therefore, a planet's eccentricity is a dominating factor in determining habitability. Yet, how eccentric can a planetary orbit become, in order to still allow for habitability?

**Table 1.** Orbital and stellar parameters of the 19 investigated binary-star systems. The values of parameters printed in bold letters are taken from Mason et al. (2012) and van Leeuwen (2007); the others were derived as described in Section 2. The binary’s eccentricity and semimajor axis are denoted by  $a_b$  and  $e_b$ ;  $I$  is the system’s inclination to the plane of the sky. A binary components’ masses are symbolized by  $M_A$  and  $M_B$ , their respective luminosities by  $L_A$  and  $L_B$  and their effective temperatures are denoted by  $T_{\text{eff}A}$  and  $T_{\text{eff}B}$ . Stellar classifications are given in the columns headed ‘class A’ and ‘class B’.

HIP ID	$a_b$	$e_b$	$I$	$d$	$M_A$	$M_B$	$L_A$	$L_B$	$T_{\text{eff}A}$	$T_{\text{eff}B}$	Class A	Class B
14669	9.0	0.14	96.8	15.8	0.56	0.39	0.096	0.026	3580	3370	M2	M4
30920	4.3	0.37	51.8	4.1	0.22	0.08	0.007	0.001	3370	3145	M4V	M5.5V
31711	42.7	0.34	93.9	21.3	1.03	0.57	1.137	0.109	5860	4060	G2V	K7Ve
44248	10.4	0.15	131.4	16.1	1.44	0.89	4.285	0.638	6740	5250	F3V	K0V
45343	97.2	0.28	21.0	5.8	0.52	0.51	0.073	0.067	3850	3850	M0V	M0V
51986	9.9	0.75	129.1	26.8	1.88	1.29	12.535	2.790	6710	6740	F4IV	F3
58001	11.7	0.30	51.0	25.5	2.94	0.79	65.255	0.397	9520	4780	A0Ve	K2V
64241	11.8	0.50	90.1	17.8	1.30	1.12	2.887	1.553	6440	6360	F5V	F6V
64797	89.2	0.12	93.4	11.1	0.73	0.52	0.277	0.072	5015	3715	K1V	M1V
66492	46.9	0.61	36.3	22.0	0.59	0.48	0.121	0.054	3782	3647	M0.5	M1.5
67422	32.7	0.45	47.4	13.4	0.72	0.65	0.273	0.174	4560	4205	K4V	K6V
84425	7.7	0.49	115.2	30.6	1.23	0.86	2.267	0.556	6280	5860	F7V	G2V
84720	91.6	0.78	35.6	8.8	0.79	0.50	0.393	0.062	5570	3850	G8V	M0V
87895	2.4	0.41	68.0	28.2	1.19	0.90	2.031	0.648	5860	4780	G2V	K2V
93825	32.7	0.32	149.6	17.3	1.27	1.25	2.570	2.432	6200	6200	F8V	F8V
101916	15.7	0.80	107.0	30.1	1.61	0.37	6.794	0.023	5745	4420	G1IV	K2IV
106972	5.3	0.29	69.4	24.5	0.57	0.43	0.105	0.033	3370	3370	M2	M4
114922	6.7	0.44	117.1	30.8	0.49	0.52	0.059	0.073	3715	3580	M1	M2
116132	42.5	0.20	123.5	6.2	0.38	0.20	0.025	0.006	3370	3305	M4	M5
	(au)		(°)	(pc)	( $M_\odot$ )	( $M_\odot$ )	( $L_\odot$ )	( $L_\odot$ )	(K)	(K)		

Williams & Pollard (2002) concluded that an Earth-like atmosphere together with surface oceans can buffer the harsh changes between high insolation at periastron and long cold phases near apoastron up to eccentricities of  $e_p \approx 0.7$ , as long as the average insolation is comparable with the current insolation of the Earth. Although planetary eccentricities of such magnitude are usually not reached in close S-type set-ups (EG12), the region where the planet remains within classical insolation boundaries is still strongly impacted. In order to distinguish orbital zones that are only habitable ‘on average’ and zones where the planet will never exceed classical insolation limits, EG12 introduced three types of HZs for binary-star systems.

*Permanently habitable zone (PHZ).* The PHZ is the region where a planet stays within habitable insolation limits for all times, despite the changes its orbit experiences due to gravitational interactions with the secondary. For this study, we have chosen the classical runaway/maximum greenhouse insolation limits (KHZ) as defined by Kasting et al. (1993) and Underwood, Jones & Sleep (2003).

*Extended habitable zone (EHZ).* The binary–planet configuration is still considered to be habitable when most of its orbit remains within the HZ boundaries. This is true if the average received insolation plus one standard deviation does not put the planet beyond KHZ insolation limits.

*Averaged habitable zone (AHZ).* Even an elevated planetary eccentricity ( $e < 0.7$ ) may not be prohibitive for habitability since the atmosphere acts as a buffer (Williams & Pollard 2002), if the time-averaged insolation stays within habitable limits. The AHZ represents such regions.

For details on the definition and calculation of PHZ, EHZ and AHZ we refer the reader to EG12. We use the interpolation formulae given in Underwood et al. (2003) to calculate effective insolation values for the selected stellar types. After a brief discussion concerning aspects of dynamical stability, the application of the proposed

classification scheme to the 19 selected binary-star systems will be presented in the next section.

#### 4 DYNAMICAL STABILITY OF CIRCUMSTELLAR PLANETS IN BINARY STARS

As was briefly mentioned during the introduction, there are many open questions regarding the formation of planets in double-star environments (Thebault 2011). However, once formed a planet can survive in the dynamically stable region around one of the binary components – a fact proven by observed planets in S-type binary configurations (Dumusque et al. 2012; Giuppone et al. 2012; Roell et al. 2012). If the necessary dynamical prerequisites are fulfilled, even both stars can harbour planets. Generalized dynamical investigations such as Holman & Wiegert (1999), Pilat-Lohinger & Dvorak (2002), semi-analytical (Pichardo, Sparke & Aguilar 2005) or analytical approaches (Szebehely & McKenzie 1977; Eggleton 1983) can be used to determine regions where a test-planet can remain on a stable orbit on secular dynamical time-scales. As the set-up used in this work consists of a planar binary – Earth configuration, the restricted three-body approach used in the articles mentioned above can be considered a reasonable approximation. We will apply the numerical fit by Holman & Wiegert (1999) and results by Pilat-Lohinger & Dvorak (2002) to find critical semimajor axis for circumstellar motion.

#### 5 RESULTS

The different HZs discussed in Section 3 are presented for a fictitious Earth-like planet in each of the selected double-star systems (Fig. 1). The region of instability (striped) is also marked. The left-hand graph of Fig. 1 represents HZs around the primary (S-type A), and the right-hand graph shows HZs around the secondary (S-type B) (Whitmire et al. 1998). Black (red online) denotes regions which are

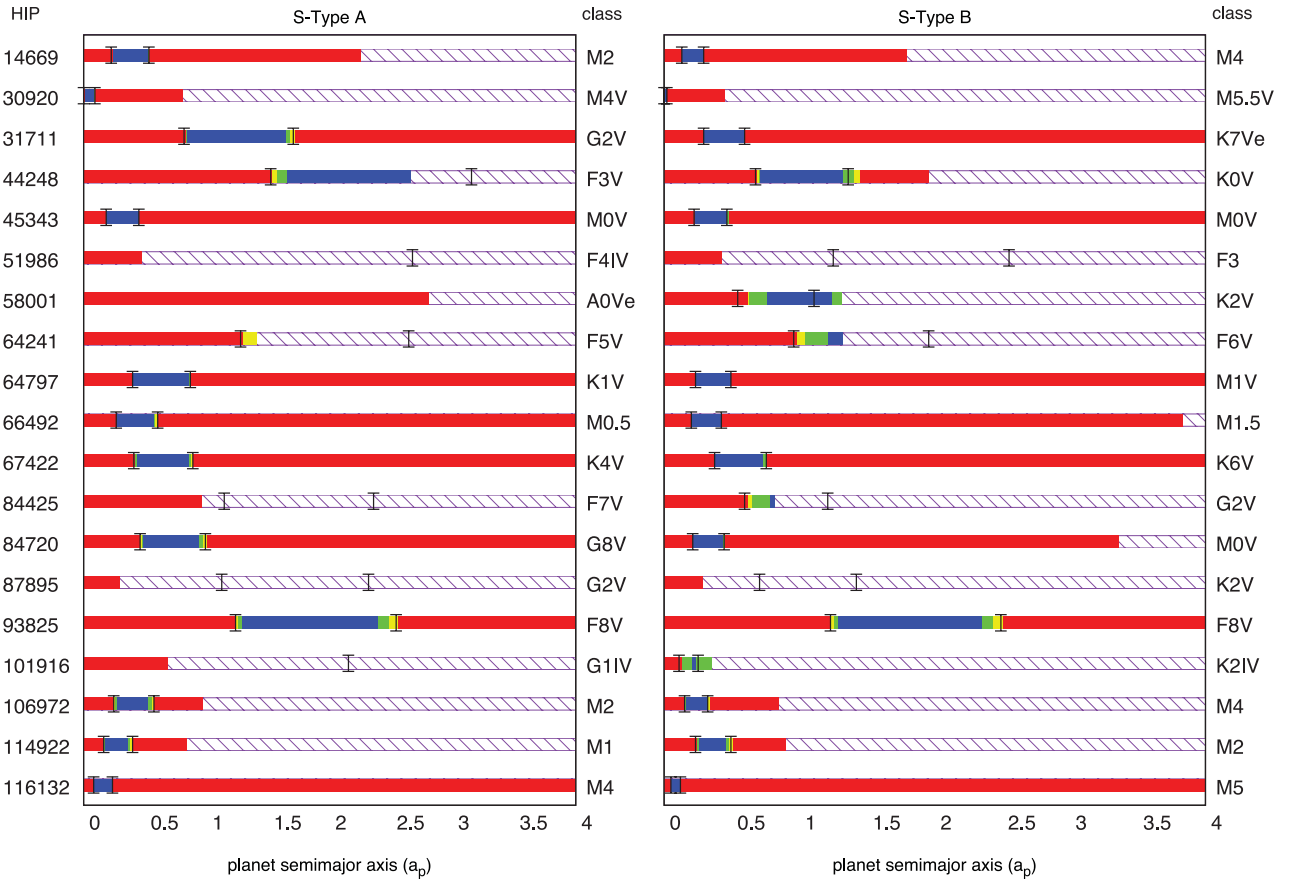


**Figure 1.** Habitable zones of 19 S-type binary-star systems in the solar neighbourhood are shown. The light grey regions (blue online) denote zones of permanent habitability (PHZ), medium grey (green online) extended (EHZ) and dark grey (yellow online) averaged habitable zones (AHZ), see Section 3. Black (red online) are regions where the planet either receives too much or too little radiation to keep atmospheric temperatures stable. The striped areas are zones of dynamical instability (Holman & Wiegert 1999). Left: HZs around the system’s primary star are shown (S-type A); right: habitability of regions around the secondary is investigated (S-type B) (Whitmire et al. 1998). The dashed ‘I’ symbols indicate the inner, and the full symbols indicate the outer border of the classical HZ as defined by Kasting et al. (1993) and Underwood et al. (2003). In most cases, the AHZ and the classical HZ coincide well as was pointed out in Eggl et al. (2012b), except for the systems HIP 58001 and 101916 where the considerable luminosity of the brighter companions shifts the HZs of the S-type B configurations to larger planetary semimajor axes. Evidently, 17 out of the 19 investigated systems allow for dynamically stable terrestrial planets within HZs around at least one of its binary’s components.

non-habitable due to excessive or insufficient insolation, dark grey (yellow online), medium grey (green online) and light grey (blue online) represent the AHZ, EHZ and PHZ, respectively. Dashed and full ‘I’ symbols give the inner and outer borders of the classical HZ as defined by Kasting et al. (1993) and Underwood et al. (2003) (KHZ). EG12 found a good correspondence between the KHZ and the AHZ, which is also mirrored in the results at hand. Exceptions are the systems HIP 58001 and 101916 where the more luminous companion shifts the HZs of the less luminous one considerably. Out of the 19 selected systems, 17 permit Earth-like planets in HZs on dynamically stable orbits around at least one stellar component. In total, the 17 habitable systems feature 16 M, 7 K, 3 G and 5 F class stars. Even if the all F and M class stars were to be excluded from the list of hosts for HZ – either because of their comparatively short lifespans (Kasting et al. 1993) or tidal and radiative effects (see Section 7) – more than 26 per cent of the stars in this sample would be capable of sustaining habitable planets on secular dynamical time-scales. If the stars’ mass loss via stellar winds is negligible, and no cataclysmic events occur (Veras & Tout 2012), habitability might be given even for stellar evolutionary time-scales.

A detailed listing of HZ borders as well as expected RV and AM signal strengths produced by a terrestrial planet in the selected systems is presented in Tables 2–4. Maximum and rms<sup>1</sup> signal strengths have been calculated following Eggl et al. (2012a). The corresponding equations are repeated in Appendix A for the reader’s convenience. Comparing AM and RV signal strengths one can see that – current observational equipment assumed – RV seems to stand a better chance to find Earth-like planets in HZs of nearby double stars. With the discovery of  $\alpha$  Cen B b the currently feasible RV resolution is approximately  $50 \text{ cm s}^{-1}$ . For the detection of habitable planets in the  $\alpha$  Centauri system, however, semi-amplitudes around  $10 \text{ cm s}^{-1}$  would be required (Eggl et al. 2012a). Possible candidate systems such as HIP 14699, 30920, 106972, 114922 or 116132 would offer better conditions for finding habitable Earth analogues via RV than  $\alpha$  Centauri does.

<sup>1</sup> In this case rms values have not only been time averaged, but they were also averaged over the planet’s argument of pericentre.

**Table 2.** Critical semimajor axis [ $a_{\text{crit}}$  (au), column 3] for orbital stability and borders for the HZs [(au), columns 5–9] as measured for the respective host stars A&B are given for 19 binary-star systems in the solar neighbourhood. Additionally, rms radial velocity [RV (cm s<sup>-1</sup>)] and astrometric [AM ( $\mu$ as)] signatures of terrestrial planets have been evaluated at the HZ borders. The conditions required for a planet to be within the averaged (AHZ), extended (EHZ) and permanent (PHZ) habitable zones are discussed in Section 3. Dashed fields (–) represent cases where a given HZ border lies beyond the critical semimajor axis  $a_{\text{crit}}$ . Planets there would be on dynamically unstable orbits.

HIP ID	Comp.	$a_{\text{crit}}$	Inner AHZ	Inner EHZ	Inner PHZ	Outer PHZ	Outer EHZ	Outer AHZ	
14669	A (M2)	2.287	0.306	0.308	0.310	0.590	0.596	0.604	HZ
			22.02	21.95	21.88	16.04	15.96	15.86	Max RV
			15.39	15.34	15.29	11.09	11.03	10.96	rms RV
			0.107	0.108	0.109	0.209	0.211	0.214	Max AM
			0.076	0.076	0.077	0.146	0.147	0.149	rms AM
			0.162	0.162	0.162	0.316	0.318	0.320	HZ
	B (M4)	1.806	36.00	36.00	36.00	25.94	25.86	25.78	Max RV
			25.30	25.30	25.30	18.12	18.06	18.00	rms RV
			0.081	0.081	0.081	0.159	0.160	0.161	Max AM
			0.057	0.057	0.057	0.112	0.112	0.113	rms AM
			0.086	0.086	0.088	0.162	0.166	0.168	HZ
			52.37	52.37	51.80	38.90	38.47	38.26	Max RV
30920	A (M4V)	0.865	36.24	36.24	35.83	26.43	26.11	25.95	rms RV
			0.291	0.291	0.298	0.557	0.571	0.578	Max AM
			0.237	0.237	0.242	0.445	0.456	0.462	rms AM
	B (M5.5V)	0.470	0.027	0.027	0.027	0.051	0.051	0.051	HZ
			157.79	157.79	157.79	115.07	115.07	115.07	Max RV
			110.84	110.84	110.84	80.36	80.36	80.36	rms RV
			0.255	0.255	0.255	0.487	0.487	0.487	Max AM
			0.210	0.210	0.210	0.400	0.400	0.400	rms AM
			0.886	0.894	0.902	1.694	1.724	1.756	HZ
31711	A (G2V)	8.351	9.63	9.59	9.55	7.09	7.03	6.97	Max RV
			6.68	6.65	6.62	4.83	4.79	4.74	rms RV
			0.125	0.126	0.127	0.243	0.247	0.252	Max AM
			0.087	0.088	0.088	0.166	0.169	0.172	rms AM
	B (K7Ve)	5.848	0.316	0.318	0.320	0.614	0.618	0.622	HZ
			21.36	21.29	21.23	15.42	15.37	15.32	Max RV
			15.00	14.95	14.90	10.76	10.72	10.69	rms RV
			0.079	0.080	0.080	0.155	0.156	0.157	Max AM
			0.056	0.056	0.056	0.108	0.109	0.109	rms AM
			1.581	1.619	1.697	2.686	2.686	2.686	HZ
44248	A (F3V)	2.686	4.80	4.75	4.66	–	–	–	Max RV
			3.19	3.15	3.08	–	–	–	rms RV
			0.221	0.226	0.238	–	–	–	Max AM
			0.176	0.181	0.189	–	–	–	rms AM
	B (K0V)	1.967	0.710	0.718	0.734	1.340	1.418	1.456	HZ
			8.76	8.71	8.62	6.59	6.44	6.38	Max RV
			6.03	6.00	5.93	4.39	4.27	4.21	rms RV
			0.154	0.156	0.160	0.300	0.320	0.329	Max AM
			0.127	0.129	0.132	0.241	0.255	0.262	rms AM
			0.263	0.263	0.263	0.515	0.515	0.517	HZ
45343	A (M0V)	17.932	8.79	8.79	8.79	6.30	6.30	6.28	Max RV
			6.20	6.20	6.20	4.43	4.43	4.43	rms RV
			0.265	0.265	0.265	0.520	0.520	0.522	Max AM
			0.256	0.256	0.256	0.501	0.501	0.503	rms AM
	B (M0V)	17.698	0.252	0.252	0.254	0.494	0.496	0.496	HZ
			9.08	9.08	9.04	6.50	6.48	6.48	Max RV
			6.41	6.41	6.38	4.58	4.57	4.57	rms RV
			0.259	0.259	0.261	0.509	0.511	0.511	Max AM
			0.250	0.250	0.252	0.491	0.493	0.493	rms AM
			0.252	0.252	0.254	0.494	0.496	0.496	HZ
51986	A (F4IV)	0.545	–	–	–	–	–	–	HZ
	B (F3)	0.448	–	–	–	–	–	–	HZ
	A (A0Ve)	2.828	–	–	–	–	–	–	HZ
58001	B (K2V)	1.331	0.639	0.653	0.775	1.263	1.331	1.331	HZ
			10.31	10.21	9.46	7.85	–	–	Max RV
			6.98	6.91	6.34	4.97	–	–	rms RV
			0.100	0.102	0.123	0.210	–	–	Max AM
			0.080	0.082	0.097	0.159	–	–	rms AM
			0.080	0.082	0.097	0.159	–	–	rms AM



**Table 3.** Continuation of Table 2. Radial velocity (RV) amplitudes are given in  $\text{cm s}^{-1}$ , and astrometric (AM) amplitudes are given in  $\mu\text{as}$ . The critical planetary semimajor axis  $a_{\text{crit}}$  as well as the HZ borders are given in au.

HIP ID	Comp.	$a_{\text{crit}}$	Inner AHZ	Inner EHZ	Inner PHZ	Outer PHZ	Outer EHZ	Outer AHZ	
64241	A (F5V)	1.465	1.354	1.465	1.465	1.465	1.465	1.465	HZ
			8.19	—	—	—	—	—	Max RV
			4.82	—	—	—	—	—	rms RV
			0.209	—	—	—	—	—	Max AM
			0.126	—	—	—	—	—	rms AM
	B (F6V)	1.339	1.002	1.056	1.226	1.339	1.339	1.339	HZ
			9.76	9.58	9.15	—	—	—	Max RV
			6.05	5.90	5.47	—	—	—	rms RV
			0.173	0.184	0.219	—	—	—	Max AM
			0.109	0.115	0.133	—	—	—	rms AM
64797	A (K1V)	23.212	0.472	0.472	0.474	0.924	0.926	0.926	HZ
			15.48	15.48	15.45	11.08	11.07	11.07	Max RV
			10.93	10.93	10.91	7.81	7.80	7.80	rms RV
			0.179	0.179	0.180	0.351	0.352	0.352	Max AM
			0.126	0.126	0.127	0.248	0.248	0.248	rms AM
	B (M1V)	18.564	0.263	0.263	0.263	0.517	0.517	0.517	HZ
			24.51	24.51	24.51	17.50	17.50	17.50	Max RV
			17.32	17.32	17.32	12.35	12.35	12.35	rms RV
			0.140	0.140	0.140	0.275	0.275	0.275	Max AM
			0.099	0.099	0.099	0.194	0.194	0.194	rms AM
66492	A (M0.5)	4.289	0.339	0.341	0.345	0.645	0.655	0.667	HZ
			12.20	12.17	12.10	8.99	8.92	8.85	Max RV
			8.48	8.46	8.41	6.15	6.10	6.05	rms RV
			0.081	0.081	0.082	0.156	0.158	0.161	Max AM
			0.072	0.072	0.073	0.137	0.139	0.142	rms AM
	B (M1.5)	3.835	0.227	0.229	0.231	0.439	0.443	0.449	HZ
			16.40	16.33	16.26	11.92	11.87	11.80	Max RV
			11.46	11.41	11.36	8.24	8.21	8.15	rms RV
			0.066	0.066	0.067	0.129	0.130	0.132	Max AM
			0.059	0.060	0.060	0.114	0.115	0.117	rms AM
64722	A (K4V)	4.503	0.486	0.490	0.496	0.916	0.934	0.952	HZ
			11.47	11.43	11.36	8.51	8.43	8.36	Max RV
			7.95	7.92	7.87	5.79	5.74	5.68	rms RV
			0.155	0.157	0.159	0.298	0.304	0.310	Max AM
			0.130	0.131	0.133	0.245	0.250	0.255	rms AM
	B (K6V)	4.212	0.398	0.400	0.404	0.754	0.766	0.780	HZ
			13.37	13.34	13.27	9.85	9.78	9.70	Max RV
			9.30	9.27	9.23	6.75	6.70	6.64	rms RV
			0.142	0.143	0.144	0.273	0.277	0.282	Max AM
			0.119	0.120	0.121	0.226	0.229	0.234	rms AM
84425	A (F7V)	1.024	—	—	—	—	—	—	HZ
			0.635	0.667	0.797	0.835	0.835	0.835	HZ
			12.54	12.32	11.67	—	—	—	Max RV
			7.82	7.63	6.98	—	—	—	rms RV
			0.082	0.087	0.107	—	—	—	Max AM
	B (G2V)	0.835	0.056	0.059	0.071	—	—	—	rms AM
			0.535	0.543	0.551	1.003	1.029	1.057	HZ
			8.34	8.29	8.23	6.25	6.17	6.10	Max RV
			5.73	5.69	5.65	4.19	4.13	4.08	rms RV
			0.240	0.244	0.248	0.461	0.474	0.487	Max AM
84720	A (G8V)	4.275	0.213	0.216	0.219	0.399	0.410	0.421	rms AM
			0.242	0.242	0.244	0.462	0.468	0.474	HZ
			15.40	15.40	15.33	11.27	11.20	11.14	Max RV
			10.75	10.75	10.70	7.78	7.73	7.68	rms RV
			0.170	0.170	0.172	0.329	0.333	0.337	Max AM
	B (M0V)	3.364	0.153	0.153	0.154	0.292	0.296	0.300	rms AM
			—	—	—	—	—	—	HZ
			—	—	—	—	—	—	Max RV
			—	—	—	—	—	—	rms RV
			—	—	—	—	—	—	Max AM
87895	A (G2V)	0.371	—	—	—	—	—	HZ	
	B (K2V)	0.312	—	—	—	—	—	HZ	

**Table 4.** Continuation of Table 2. Radial velocity (RV) amplitudes are given in  $\text{cm s}^{-1}$ , and astrometric (AM) amplitudes are given in  $\mu\text{as}$ . The critical planetary semimajor axis  $a_{\text{crit}}$  as well as the HZ borders are given in (au).

HIP ID	Comp.	$a_{\text{crit}}$	Inner AHZ	Inner EHZ	Inner PHZ	Outer PHZ	Outer EHZ	Outer AHZ	
93825	A (F8V)	5.623	1.289	1.311	1.337	2.421	2.505	2.581	HZ
			3.71	3.68	3.65	2.79	2.74	2.71	Max RV
			2.54	2.51	2.49	1.85	1.82	1.79	rms RV
			0.185	0.189	0.193	0.358	0.371	0.383	Max AM
	B (F8V)	5.575	0.168	0.170	0.174	0.315	0.326	0.336	rms AM
			1.254	1.274	1.300	2.358	2.438	2.512	HZ
			3.79	3.76	3.72	2.84	2.80	2.76	Max RV
			2.59	2.57	2.54	1.89	1.86	1.83	rms RV
101916	A (G1IV)	0.754	0.183	0.186	0.190	0.353	0.365	0.377	Max AM
			0.165	0.168	0.171	0.311	0.321	0.331	rms AM
			–	–	–	–	–	–	HZ
			0.155	0.159	0.233	0.261	0.381	0.381	HZ
	B (K2IV)	0.381	38.16	37.73	31.89	30.40	–	–	Max RV
			25.63	25.31	20.91	19.75	–	–	rms RV
			0.045	0.046	0.069	0.078	–	–	Max AM
			0.031	0.032	0.047	0.053	–	–	rms AM
106972	A (M2)	1.034	0.322	0.330	0.338	0.588	0.616	0.640	HZ
			20.73	20.50	20.28	15.94	15.65	15.41	Max RV
			13.99	13.82	13.65	10.35	10.12	9.93	rms RV
			0.074	0.076	0.077	0.139	0.147	0.153	Max AM
	B (M4)	0.865	0.053	0.054	0.055	0.096	0.101	0.105	rms AM
			0.179	0.183	0.185	0.339	0.351	0.359	HZ
			31.41	31.08	30.92	23.35	22.99	22.76	Max RV
			21.63	21.40	21.28	15.73	15.46	15.28	rms RV
114922	A (M1)	0.897	0.053	0.055	0.055	0.103	0.107	0.110	Max AM
			0.039	0.040	0.040	0.074	0.077	0.078	rms AM
			0.239	0.245	0.251	0.435	0.455	0.473	HZ
			24.59	24.31	24.05	18.89	18.53	18.24	Max RV
	B (M2)	0.924	16.60	16.40	16.20	12.30	12.03	11.80	rms RV
			0.050	0.051	0.053	0.094	0.099	0.103	Max AM
			0.037	0.038	0.039	0.068	0.071	0.074	rms AM
			0.266	0.272	0.282	0.480	0.504	0.528	HZ
116132	A (M4)	10.619	22.83	22.60	22.23	17.67	17.32	17.00	Max RV
			15.33	15.16	14.89	11.41	11.14	10.88	rms RV
			0.053	0.055	0.057	0.100	0.105	0.111	Max AM
			0.039	0.040	0.042	0.071	0.075	0.078	rms AM
	B (M5)	7.091	0.158	0.158	0.158	0.310	0.310	0.312	HZ
			30.77	30.77	30.77	22.02	22.02	21.95	Max RV
			21.72	21.72	21.72	15.51	15.51	15.46	rms RV
			0.204	0.204	0.204	0.401	0.401	0.404	Max AM
116132	A (M4)	10.619	0.165	0.165	0.165	0.323	0.323	0.325	rms AM
			0.076	0.076	0.076	0.152	0.152	0.152	HZ
			60.97	60.97	60.97	43.14	43.14	43.14	Max RV
			43.07	43.07	43.07	30.45	30.45	30.45	rms RV
	B (M5)	7.091	0.184	0.184	0.184	0.369	0.369	0.369	Max AM
			0.149	0.149	0.149	0.298	0.298	0.298	rms AM
			0.158	0.158	0.158	0.310	0.310	0.312	HZ
			30.77	30.77	30.77	22.02	22.02	21.95	Max RV

As nine out of the 17 potentially habitable systems feature M stars, it is worth mentioning that determining the effective insolation a terrestrial planet receives might not be enough to claim habitability. In fact, Lammer et al. (2011) are convinced that the potentially elevated level of X-ray and extreme ultraviolet (EUV) radiation in M stars might lead to a different atmospheric evolution of an Earth-like planet in an M-star's HZ, thus preventing the existence of life as we know it. Ultimately, direct observation of the interaction between stellar and planetary atmospheres will be necessary to determine to which degree planets can remain habitable in the vicinity of M-type stars. The proposed transit spectroscopy mission *ECHO* (Tinetti et al. 2012) can be a step in this direction, although currently only super-Earths down to  $1.5 r_{\oplus}$  around K–F

stars are planned to be observed. With RV signal amplitudes of  $\approx 5\text{--}12 \text{ cm s}^{-1}$  for potentially habitable planets in systems containing Sun-like G stars (HIP 31711 and 84425), our estimates are comparable to those for  $\alpha$  Centauri presented in Eggl et al. (2012a) and Guedes et al. (2008). Detecting planets around Sun-like stars would therefore require a considerable amount of dedicated observation time (Guedes et al. 2008; Dumusque et al. 2012).

The AM amplitudes determined for the 19 systems at hand are well below  $1 \mu\text{as}$ . This will put the systems in consideration even beyond the reach of ESA's *Gaia* mission (Hestroffer et al. 2010). However, recently Malbet et al. (2012) proposed the Nearby Earth Astrometric Telescope (NEAT) which would be capable of resolving AM motion down to  $0.05 \mu\text{as}$  at a  $1\sigma$  accuracy level. This



**Table 5.** Transit depths (TDs), visual brightness (V, WDS) and planetary period ( $P_p$ ) ranges are given for potentially transiting planets in the HZs of those selected binary systems with  $I \approx 90^\circ$ .

HIP ID	Comp.	V (mag)	TD (ppm)	$P_p$ (D)
14669	A	10.32	128	270.80–380.35
	B	12.5	369	235.67–331.14
31711	A	6.32	78	338.38–476.35
	B	9.84	187	270.91–380.10
64241	A	4.85	44	372.23
	B	5.53	79	346.09–382.82
64797	A	6.66	171	294.45–412.52
	B	9.5	198	260.18–364.81

instrument would be able to identify habitable planets in most of the presented binary-star systems. Such a mission would indeed be valuable, since AM does not only favour planet detection in binary configurations with Sun-like components – their HZs are further away from their host stars thus producing larger AM amplitudes – it would more importantly grant observational access to all the planet’s orbital parameters. Especially mutual inclinations are of interest in this case, as they could provide answers to many important problems regarding planet-formation as well as migration in binary-star systems (Wu & Murray 2003; Batygin et al. 2011; Thebault 2011).

## 6 POTENTIALLY TRANSITING SYSTEMS

With an inclination of  $I \approx 90^\circ$  with respect to the plane of the sky the systems HIP 14669, 31711, 64241 and 64797 could harbour transiting planets that still would be compatible with our assumptions of a planar-binary-planet configuration. Assuming non-grazing transits, i.e. transits where less than the full planetary disc obscures the stellar surface during transit, and neglecting entry as well as limb-darkening effects, we can estimate the relative TD that the planet will cause in its host star’s photometric signal:

$$\text{TD} \simeq \frac{R_p^2}{R_*^2}. \quad (1)$$

Hereby,  $R_p$  and  $R_*$  denote the planetary and stellar radii, respectively. Table 5 shows the relative TDs for Earth-like planets in systems allowing for transits while still being close to planar. Even though some stellar components are on the verge of being too bright to be observed by *Kepler*, the spacecraft’s current performance (combined noise level  $\approx 29$  ppm; Gilliland et al. 2011) would allow for an Earth-like planet in circumstellar HZs to be found in all of these systems given sufficient observation time.

## 7 TIDAL LOCKING

An orbital state, where the planet rotates around its own axis with the same speed as it orbits its host star – much like the Moon around the Earth – is called 1:1 spin-orbit resonance. A star–planet system might evolve into such a state due to tidal interactions (see e.g. Murray & Dermott (1999)). Therefore, this state is often referred to as tidal lock. Since a tidal locking potentially adds additional instabilities to a planet’s climate (Kite, Gaidos & Manga 2011), regions where 1:1 spin-orbit resonances occur are usually excluded from HZs. Kasting et al. (1993) used an equation dating back to

Peale (1977) to calculate the distance up to which a planet would be tidally locked in a time span equal to age of the Solar system. Inserting such values as chosen in Kasting et al. (1993), the simple estimate reads

$$r_{\text{TL}} \approx 0.46 \left( \frac{\text{au}}{M_\odot^{1/3}} \right) m_*^{1/3}, \quad (2)$$

with  $r_{\text{TL}}$  denoting the tidal-locking radius in au and  $m_*$  the mass of the host star in  $M_\odot$ . Applying this estimate to our selected systems indicates that all HZs in M–M binaries fall at least partly in the tidal-locking zone. However, tidal evolution of a planet in a binary system is much more involved than simple two-body dynamics can account for, as the angular momentum transfer between the host-star–planet system and the secondary needs to be included in the model. Eggleton (2006) provides analytical estimates for the tidal evolution of stellar hierarchical triple systems showing that in fact many possible resonant states other than 1:1 spin-orbit locking exist for the inner pair although with different degrees of stability. Wu & Murray (2003) and Fabrycky & Tremaine (2007) investigated the possibility for tidal migration of planets due to mutually inclined massive perturbers via Kozai cycles (Kozai 1962). Yet, as pointed out by Correia et al. (2011), only quadrupolar secular expansions had been used to evaluate the planet’s eccentricity, which give inaccurate results for low-inclination configurations such as discussed in the study at hand (Lee & Peale 2003). Similar to Eggleton (2006), Correia et al. (2011) show that tidal interactions in inclined hierarchical triple systems can produce many different outcomes, especially when the component’s changes in obliquity are taken into account. Their system’s final states included transformations of retrograde to prograde motion and vice versa, a decay of mutual inclination and rapid circularization of the inner planetary orbit as well as tidally induced migration. As more detailed tidal interaction models require knowledge of the stellar radii (Eggleton 2006; Correia et al. 2011), the model dependence of radii for M dwarfs adds another source of uncertainty, see e.g. Muirhead et al. (2012).

The lack of accurate analytical tools to study the influence of tidal interactions in planar S-type configurations as well as the wealth of possible final states depending on the system’s initial conditions put a detailed analysis of the planet–binary system’s tidal evolution beyond the scope of this work.

## 8 SUMMARY

Applying the analytic methods presented in Eggl et al. (2012a, EG12), we have shown that 17 out of 19 binary-star systems with well-determined stellar and orbital parameters close to the Solar system allow for dynamically stable Earth-like planets in circumstellar HZs. Four of these habitable systems feature F, three feature G, six feature K and nine feature M class stars. Not surprisingly, M–M binary constellations offer the best chances for detecting planets in HZs via RV observations. However, determining habitability in M star doublets may require additional considerations such as tolerable stellar X-ray and EUV fluxes (Lammer et al. 2011) or the system’s potential for tidally locking the planet to its host star (see Section 7). Habitable planets in systems featuring G-type stars have RV amplitudes comparable to the ones found for  $\alpha$  Centauri AB (Guedes et al. 2008; Eggl et al. 2012a). The systems HIP 14699, 30920, 106972, 114922 or 116132 would be promising candidates to search for terrestrial planets in their HZs, as they offer best case RV semi-amplitudes comparable to  $\alpha$  Centauri B b (Dumusque et al. 2012). Four of the 17 systems would allow for transiting planets in

HZs, which could be detected using current technology. Their mid-TDs were estimated to lie between 44 and 369 ppm with planetary periods ranging from 235 to 476 d. AM signal amplitudes for Earth-like planets in all the investigated systems' HZs are, in contrast, well below 1  $\mu$ s. Therefore, dedicated missions such as NEAT (Malbet et al. 2012) will be required in order to detect habitable worlds in binary stars via astrometry. A sample of 19 systems does not offer the possibility to construct a reasonable statistical analysis on the number of potentially habitable binary-star systems in the solar neighbourhood. More precise data on spectral types and orbital elements of nearby double stars are required in this respect. Nevertheless, our findings indicate that including binary-star systems with  $1 < a_b < 100$  in observational campaigns has the potential to enhance our chances of finding habitable worlds.

## ACKNOWLEDGMENTS

The authors would like to acknowledge the support of FWF projects S11608-N16 (EP-L and SE), P20216-N16 (SE, EP-L and BF) and P22603-N16 (EP-L and BF). SE and EP-L would like to thank the Institute for Astronomy and NASA Astrobiology Institute at the University of Hawaii for their hospitality during their visit when some of the ideas for this work were developed. NH acknowledges support from the NASA Astrobiology Institute under Cooperative Agreement NNA09DA77A at the Institute for Astronomy, University of Hawaii, and NASA EXOB grant NNX09AN05G. SE acknowledges the support of University of Vienna's Forschungsstipendium 2012. This research has made use of the Washington Double Star Catalog maintained at the U.S. Naval Observatory.

## REFERENCES

- Batygin K., Morbidelli A., Tsiganis K., 2011, *A&A*, 533, A7
- Beaugé C., Ferraz-Mello S., Michtchenko T. A., 2007, in Dvorak R., ed., *Planetary Masses and Orbital Parameters from Radial Velocity Measurements*, Wiley-VCH, p. 1
- Borucki W. J. et al., 2011, *ApJ*, 736, 19
- Borucki W. J. et al., 2012, *ApJ*, 745, 120
- Castelli F., Kurucz R. L., 2004, e-print (arXiv: astro-ph/0405087)
- Correia A. C. M., Laskar J., Farago F., Boué G., 2011, *Celest. Mech. Dynamical Astron.*, 111, 105
- Doyle L. R. et al., 2011, *Sci*, 333, 1602
- Dumusque X. et al., 2012, *Nat*, doi:10.1038/nature11572
- Eggl S., Haghighipour N., Pilat-Lohinger, 2012a, *ApJ*, submitted
- Eggl S., Pilat-Lohinger E., Georgakarakos N., Gyergovits M., Funk B., 2012b, *ApJ*, 752, 74 (EG12)
- Eggleton P. P., 1983, *ApJ*, 268, 368
- Eggleton P., 2006, *Evolutionary Processes in Binary and Multiple Stars*. Cambridge Univ. Press, Cambridge
- Fabrycky D., Tremaine S., 2007, *ApJ*, 669, 1298
- Flower P. J., 1996, *ApJ*, 469, 355
- Forgan D., 2012, *MNRAS*, 422, 1241
- Georgakarakos N., 2002, *MNRAS*, 337, 559
- Georgakarakos N., 2003, *MNRAS*, 345, 340
- Georgakarakos N., 2005, *MNRAS*, 362, 748
- Gilliland R. L. et al., 2011, *ApJS*, 197, 6
- Giuppone C. A., Morais M. H. M., Boué G., Correia A. C. M., 2012, *A&A*, 541, A151
- Guedes J. M., Rivera E. J., Davis E., Laughlin G., Quintana E. V., Fischer D. A., 2008, *ApJ*, 679, 1582
- Harrington R. S., 1977, *AJ*, 82, 753
- Hestroffer D., Dell'Oro A., Cellino A., Tanga P., 2010, in Souchay J., Dvorak R., eds, *Lecture Notes in Physics*, Vol. 790, *Dynamics of Small Solar System Bodies and Exoplanets*. Springer-Verlag, Berlin, p. 251
- Holman M. J., Wiegert P. A., 1999, *AJ*, 117, 621
- Huang S.-S., 1960, *PASP*, 72, 106
- Kaltenegger L., Sasselov D., 2011, *ApJ*, 736, L25
- Kane S. R., Gelino D. M., 2012, *PASP*, 124, 323
- Kasting J. F., Whitmire D. P., Reynolds R. T., 1993, *Icarus*, 101, 108
- Kiseleva-Eggleton L., Eggleton P. P., 2001, in Podsiadlowski P., Rappaport S., King A. R., D'Antona F., Burderi L., eds, *ASP Conf. Ser. Vol. 229, Evolution of Binary and Multiple Star Systems*. Astron. Soc. Pac., San Francisco, p. 91
- Kite E. S., Gaidos E., Manga M., 2011, *ApJ*, 743, 41
- Kozai Y., 1962, *AJ*, 67, 591
- Lammer H., Lichtenegger H. I. M., Khodachenko M. L., Kulikov Y. N., Griessmeier J., 2011, in Beaulieu J. P., Dieters S., Tinetti G., eds, *ASP Conf. Ser. Vol. 450, Molecules in the Atmospheres of Extrasolar Planets*. Astron. Soc. Pac., San Francisco, p. 139
- Lee M. H., Peale S. J., 2003, *ApJ*, 592, 1201
- Léger A. et al., 2009, *A&A*, 506, 287
- Malbet F. et al., 2012, *Exp. Astron.*, 34, 385
- Marchal C., 1990, *Studies in Astronautics*. Elsevier, Amsterdam
- Mason B. D., Wycoff G. L., Hartkopf W. I., Douglass G. G., Worley C. E., 2012, *VizieR Online Data Catalog*, 1, 2026
- Muirhead P. S., Hamren K., Schlawin E., Rojas-Ayala B., Covey K. R., Lloyd J. P., 2012, *ApJ*, 750, L37
- Müller T. W. A., Kley W., 2012, *A&A*, 539, A18
- Murray C. D., Dermott S. F., 1999, *Solar System Dynamics*. Cambridge Univ. Press, Cambridge
- Orosz J. A. et al., 2012, *ApJ*, 758, 87
- Paardekooper S.-J., Leinhardt Z. M., 2010, *MNRAS*, 403, L64
- Payne M. J., Wyatt M. C., Thébault P., 2009, *MNRAS*, 400, 1936
- Peale S. J., 1977, in Burns J. A., ed., *IAU Colloq. 28, Planetary Satellites*. Univ. Arizona Press, Tucson, p. 87
- Pichardo B., Sparke L. S., Aguilar L. A., 2005, *MNRAS*, 359, 521
- Pierrehumbert R., Gaidos E., 2011, *ApJ*, 734, L13
- Pilat-Lohinger E., Dvorak R., 2002, *Celest. Mech. Dynamical Astron.*, 82, 143
- Pourbaix D., 2002, *A&A*, 385, 686
- Quintana E. V., Lissauer J. J., 2010, in Haghighipour N., ed., *Astrophysics and Space Science Library*, Vol. 366, *Planets in Binary Star Systems*. Springer, Berlin, p. 265
- Rabl G., Dvorak R., 1988, *A&A*, 191, 385
- Roell T., Neuhauser R., Seifahrt A., Mugrauer M., 2012, *A&A*, 542, A92
- Salaris M., Cassisi S., 2005, *Evolution of Stars and Stellar Populations*. Wiley-VCH, Berlin
- Schneider J., Dedieu C., Le Sidaner P., Savalle R., Zolotukhin I., 2011, *A&A*, 532, A79
- Szebehely V., McKenzie R., 1977, *AJ*, 82, 79
- Thebault P., 2011, *Celest. Mech. Dynamical Astron.*, 111, 29
- Thebault P., Marzari F., Scholl H., 2008, *MNRAS*, 388, 1528
- Thebault P., Marzari F., Scholl H., 2009, *MNRAS*, 393, L21
- Tinetti G. et al., 2012, *Exp. Astron.*, 34, 311
- Underwood D. R., Jones B. W., Sleep P. N., 2003, *Int. J. Astrobiol.*, 2, 289
- van Leeuwen F., 2007, *A&A*, 474, 653
- Veras D., Tout C. A., 2012, *MNRAS*, 422, 1648
- Welsh W. F. et al., 2012, *Nat*, 481, 475
- Whitmire D. P., Matese J. J., Criswell L., Mikkola S., 1998, *Icarus*, 132, 196
- Williams D. M., Pollard D., 2002, *Int. J. Astrobiol.*, 1, 61
- Wu Y., Murray N., 2003, *ApJ*, 589, 605
- Xie J.-W., Zhou J.-L., Ge J., 2010, *ApJ*, 708, 1566

## APPENDIX A: MAXIMUM AND RMS SIGNAL AMPLITUDES

Following Beaugé et al. (2007) and Eggl et al. (2012a), the RV amplitude a planet causes on its host star is given by

$$RV = \frac{\sqrt{Gm_1} \sin I}{\sqrt{m_0 + m_1}} \frac{e \cos \omega + \cos(f + \omega)}{\sqrt{a(1 - e^2)}}, \quad (\text{A1})$$

where  $G$  denotes the gravitational constant, and  $m_0$  and  $m_1$  are the host star's and planet's masses. The quantities  $a$ ,  $e$ ,  $I$  and  $\omega$  denote the planet's semimajor axis, eccentricity, the system's inclination to the plane of the sky and the planet's argument of pericentre, respectively. The planet's true anomaly is represented by  $f$ . We can write the maximum possible RV amplitude caused by a terrestrial planet in a circumstellar orbit around one binary component as follows:

$$\max \text{RV} = \frac{\sqrt{G} m_1 \sin I}{\sqrt{m_0 + m_1}} \frac{(1 + e^{\max})}{\sqrt{a[1 - (e^{\max})^2]}}. \quad (\text{A2})$$

The maximum possible eccentricity the planet can acquire due to gravitational interaction with the double star is denoted by  $e^{\max}$  (Eggl et al. 2012b). Expressions for the rms values of the RV signal are given as follows (Eggl et al. 2012a):

$$\text{rms RV} = \frac{1}{2\pi} \left[ \int_0^{2\pi} \text{RV}^2 dM d\omega \right]^{1/2} = \frac{\sqrt{G} m_1 |\sin I|}{\sqrt{2a(m_0 + m_1)}}. \quad (\text{A3})$$

In a similar manner we can use the formalism applied in Pourbaix (2002) to determine maximum AM signal strengths:

$$\max \text{AM} = \frac{\mu a(1 + e^{\max})}{d}, \quad (\text{A4})$$

where  $d$  is the observer's distance to the observed system, and  $\mu = m_1/(m_0 + m_1)$  is the planet-host-star system's mass ratio. The AM rms amplitudes are given by

$$\text{rms AM} = \frac{\mu a}{2d} \left[ 3 + \frac{9}{2} \langle e^2 \rangle + \left( 1 + \frac{3}{2} \langle e^2 \rangle \right) \cos(2I) \right]^{1/2}. \quad (\text{A5})$$

Here,  $\langle e^2 \rangle$  is the averaged squared planetary eccentricity. An analytic expression for  $\langle e^2 \rangle$  can be found in Georgakarakos (2003, 2005). For a detailed derivation of all rms and maximum signal amplitudes, see Eggl et al. (2012a).

This paper has been typeset from a  $\text{\LaTeX}$  file prepared by the author.

#### 4. CIRCUMSTELLAR HABITABLE ZONES OF BINARY STAR SYSTEMS IN THE SOLAR NEIGHBORHOOD

---

## Chapter 5

# Discussion

In chapter 2 an analytic framework to efficiently characterize circumstellar HZs in binary stars has been developed. Analytic estimates for radial velocity, astrometric as well as transit photometric fingerprints of Earth-like planets in such environments were given in chapters 3 & 4. In this chapter, the significance and influence of approximations and prerequisites regarding the presented methodologies are reviewed in a more detailed fashion.

### 5.1 Analytic Insolation Estimates

A correct modeling of planetary insolation is crucial for the analytic determination of HZs in binary star systems as presented in chapter 2. Throughout this work, analytical descriptions of the evolution of planetary orbits in hierarchical triple systems have been applied to construct insolation estimates. Hereby, the planet's maximum and average square eccentricities were of particular interest. In order to establish these quantities, analytical approximations based on Georgakarakos' method were heavily relied on. While the implementation of the formulae for  $e_p^{max}$  (chapter 2, appendix B) and  $\langle e_p^2 \rangle$  (chapter 1, appendix 1.A) is straight forward, the sheer number of terms involved might provoke the question, whether it is truly necessary to use such advanced estimates? Perhaps, simpler models would suffice as well? This issue was discussed partly in section 1.3.5, where it was shown that the planet's eccentricity evolution in close binary star systems is not well represented by secular approaches alone. Nevertheless, it remains to be shown that the use of less accurate techniques to determine planetary eccentricities does indeed have a noticeable influence on the predicted planetary insolation patterns. Therefore, we will compare time dependent planetary insolation curves established using the relatively simple secular perturbation equations by Heppenheimer (1978) with results based on Georgakarakos' method. Numerical simulation results will also be considered.

Neglecting variations in stellar luminosities ( $dL_{1,2}/dt = 0$ ) the momentary insolation is determined by the total radiation arriving at the planet's upper atmosphere

$$S_{tot}(t) = \frac{L_1}{\delta(t)^2} + \frac{L_2}{\Delta(t)^2}, \quad (5.1)$$

where  $\delta = r_1 = \|\mathbf{r}_1\|$  and  $\Delta = \|\mathbf{r}_2 - \mathbf{r}_1\|$  are the time dependent distances of the planet to its host and secondary star respectively, see also Figure 1.9. In order to simplify the construction of analytical insolation models, we will restrict ourselves to coplanar systems. We then can

## 5. DISCUSSION

---

express equation (5.1) in terms of Keplerian orbital elements as follows

$$S_{tot} = \frac{L_1}{\delta^2} + \frac{L_2}{\Delta^2} = L_1 r_1^{-2} + L_2 (r_1^2 + r_2^2 - 2r_1 r_2 \cos \Psi)^{-1}, \quad (5.2)$$

where we insert

$$r_1 = \frac{a_p(1 - e_p^2)}{1 + e_p \cos f_p}, \quad r_2 = \frac{a_b(1 - e_b^2)}{1 + e_b \cos f_b}, \quad \Psi = \varpi_p + f_p - f_b. \quad (5.3)$$

Here,  $a_p$  and  $a_b$  are the planet's and the binary's semimajor axes,  $e_p$  and  $e_b$  are the corresponding eccentricities and  $f_p$  and  $f_b$  denote the planetary and binary true anomalies, respectively. The planetary longitude of pericenter is represented by  $\varpi_p$ , and we have assumed, without loss of generality, that the binary's longitude of pericenter  $\varpi_b$  is initially zero. As we are interested in systems hosting Earth-like planets, we will neglect the planet's perturbative effect on the orbit of the binary. From perturbation theory we also know that the planetary semimajor axis stays constant with time, while the planet's eccentricity does not; see, for instance, section 1.3.4. In short we assume

$$\frac{da_p}{dt} = \frac{da_b}{dt} = \frac{de_b}{dt} = \frac{d\varpi_b}{dt} = 0.$$

In contrast,  $e_p$ ,  $\varpi_p$  as well as the true anomalies  $f_p$  and  $f_b$  remain functions of time. Fortunately, explicit expressions exist for all these quantities. The true anomalies can be transformed into functions of time via the equation of the center, see e.g. chapter 3, appendix A. Simple secular evolution equations for the orbit of a massless particle in an S-Type binary star system can be found for instance in Heppenheimer (1978). Using an expansion of the disturbing function in the R3BP based on Kaula's approach Heppenheimer derived the following time evolution equations

$$e_p(t) = \frac{5}{2} \frac{a_p}{a_b} \frac{e_b}{1 - e_b^2} \left| \sin \left[ \frac{u}{2} (t - t_0) \right] \right| \quad \tan \varpi_p(t) = \frac{-\sin [u (t - t_0)]}{1 - \cos [u (t - t_0)]} \quad (5.4)$$

with

$$u = \frac{3}{4} \mathcal{G}^{1/2} \frac{m_2}{m_0^{1/2}} \frac{a_p^{3/2}}{a_b^3} (1 - e_b^2)^{-3/2}.$$

Here,  $\mathcal{G}$  is the gravitational constant,  $m_0$  and  $m_2$  are the respective masses of primary and secondary, and the planet's mass is neglected ( $m_1 = 0$ ). Furthermore, the planetary eccentricity's secular frequency is represented by the symbol  $u$ , and it is assumed that  $e_p(0) = \varpi_p(0) = 0$ . Analytical estimates for  $e_p^{max}$  and  $\langle e_p^2 \rangle$  are readily derived from equations (5.4)

$$e_p^{max} = \frac{5}{2} \frac{a_p}{a_b} \frac{e_b}{1 - e_b^2} \quad \langle e_p^2 \rangle = \frac{u}{2\pi} \int_0^{2\pi/u} e_p(t) dt = \frac{25}{8} \left[ \frac{a_p}{a_b} \frac{e_b}{1 - e_b^2} \right]^2 \quad (5.5)$$

Inserting the planet's orbit evolution equations (5.4) into the total insolation estimates (5.2-5.3) and using the equation of the center up to the fourth order in eccentricities (chapter 3, appendix A) to exchange true for mean anomalies we arrive at a time-dependent analytic description of the planetary insolation based on Heppenheimer's estimates.

Insolation evolution estimates resulting from Georgakarakos' method are derived in a similar manner, where we replace Heppenheimer's expressions with Georgakarakos' functions  $e_p(t) = \|e_1\|(t)$  and  $\varpi_p(t)$  as given in appendix 1.A. Using Everhart's Gauss Radau integrator

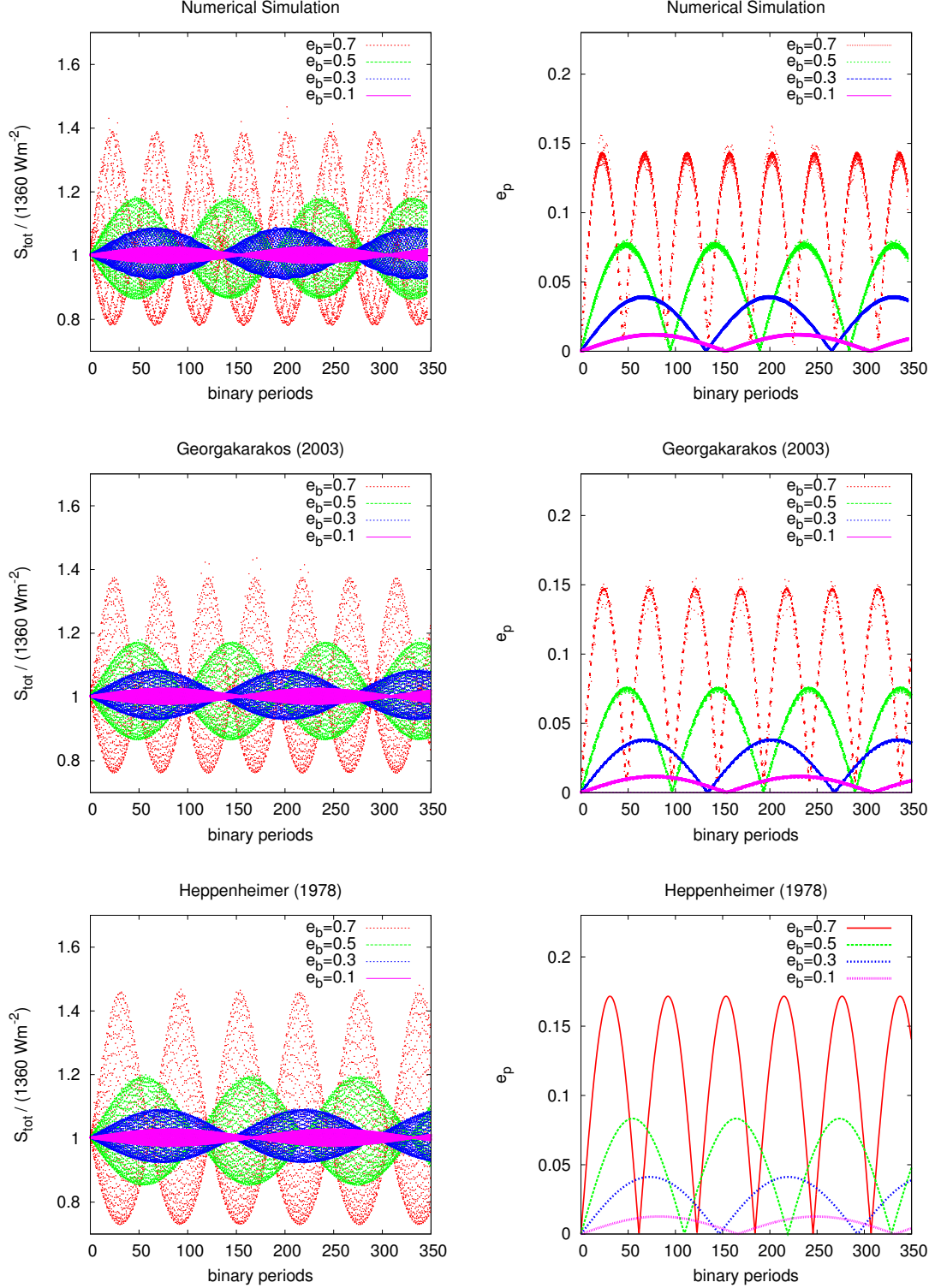


**Figure 5.1:** Total planetary insolation ( $S_{tot}$ ) and eccentricity ( $e_p$ ) evolution in four G2V-G2V binary star systems with semimajor axes of  $a_b = 20$  au and different binary eccentricities ( $e_b$ ). The planet was started on a circular orbit with a semimajor axis of  $a_p = 1$  au. Numerical simulation results (*top*) are compared to analytical estimates using time evolution equations for the planetary eccentricity and longitude of pericenter by Georgakarakos (2003) (*mid*) and Heppenheimer (1978) (*bottom*). See also Table 5.1.

## 5. DISCUSSION

$P_{sec}(S_{tot}) [P_b]$	$e_b = 0.1$	$e_b = 0.3$	$e_b = 0.5$	$e_b = 0.7$
Simulation	152.9	132.6	94.6	44.9
Georgakarakos	154.4	134.2	96.6	48.4
Heppenheimer	166.1	146.4	109.5	61.4

**Table 5.1:** Secular periods ( $P_{sec}$ ) of the total planetary insolation  $S_{tot}$  for different binary eccentricities  $e_b$  in G2V-G2V S-Type systems with  $a_b = 20$  au. The planet has a semimajor axis of 1 au. Results from numerical insolation simulations are compared to analytic period estimates by Georgakarakos (2003) and Heppenheimer (1978), see Figure 5.1. All secular periods are given in units of binary periods  $P_b \approx 23100.9$  D  $\approx 63.25$  yrs. The secular periods for the numerically simulated insolation curves were derived using a simplex based non-linear least squares fit  $[O(t) = a|\sin(bt)|]$  of the corresponding planetary eccentricity signal (Nelder & Mead 1965).

(Everhart 1974) as well as a Lie Series based extrapolation method (Eggl & Dvorak 2010, Hanslmeier & Dvorak 1984) to solve the equations of motion for the binary star and the planet numerically, it is also possible to directly calculate the evolution of the total radiation according to equation (5.1). The resulting insolation curves for a planet with a semimajor axis of 1 au in G2V-G2V S-Type binary star systems are presented in Figure 5.1. Similarly, Figure 3 in chapter 2 shows the insolation on a planet started at the inner edge of the KHZ. Both figures illustrate the correlation between planetary eccentricity and insolation. Figure 5.1 also contains analytically derived insolation curves based on Georgakarakos’ as well as Heppenheimer’s orbit evolution equations. Comparing the results produced by the three different techniques, one can clearly see that the estimates utilizing Georgakarakos’ method are vastly superior to Heppenheimer’s simple secular approach. When the planet’s orbit is subjected to large perturbations caused by a binary star on a highly eccentric orbit, insolation amplitudes resulting from Heppenheimer’s model overestimate numerical simulation values considerably. In contrast, Georgakarakos’ evolution equations produce insolation amplitudes that remain very close to the numerical ones. However, both analytical approaches show significant deviations in the secular period of  $e_p$ , see Table 5.1. At least Georgakarakos’ estimates prove to be relatively reliable up to binary eccentricities of  $e_b = 0.5$ , whereas results based on Heppenheimer’s method overestimate the period even for  $e_b = 0.1$ . Noticing the weak performance of Heppenheimer’s method in this respect, attempts have been made to correct the secular frequency using semi-analytical approaches (Thébault et al. 2006). Giuppone et al. (2011a) even proposed amplitude adjustments based on introducing numerically derived correction terms. While these attempts have been successful in reducing prediction errors for the very model systems they were derived from, the overall performance of the corrected equations is poor compared to Georgakarakos’ estimates, especially regarding planetary eccentricity amplitudes. Figure 5.2 displays such a comparison between different approaches to calculating maximum amplitudes of planetary eccentricities ( $e_p^{max}$ ). Here, the relative deviation of  $e_p^{max}$  with respect to numerical simulations is shown as a function of planetary semimajor axis and binary eccentricity. S-Type systems with different stellar constituents having mass ratios ( $\mu = m_2/(m_0 + m_2)$ ) that range between  $\mu \simeq 0.3$  to  $\mu \simeq 0.6$  (see chapter 2, section 2) and binary semimajor axes between 10 and 30 au are investigated. Interestingly, the corrected  $e_p^{max}$  estimates by Giuppone et al. (2011a) work slightly better than the analytical  $e_p^{max}$  equations presented in chapter 2 in a parameter region that resembles  $\gamma$  Cephei ( $a_b \simeq 20$  au,  $e_b \simeq 0.4$ ) in spite of the different mass ratio of the investigated G2V-F0V system, see Figure 5.2, top panel, second graph. However, the  $e_p^{max}$  estimates established in chapter 2 based on Georgakarakos’ method, show a convincing correspondence to numerical simulation results over the entire parameter space. The only major discrepancies



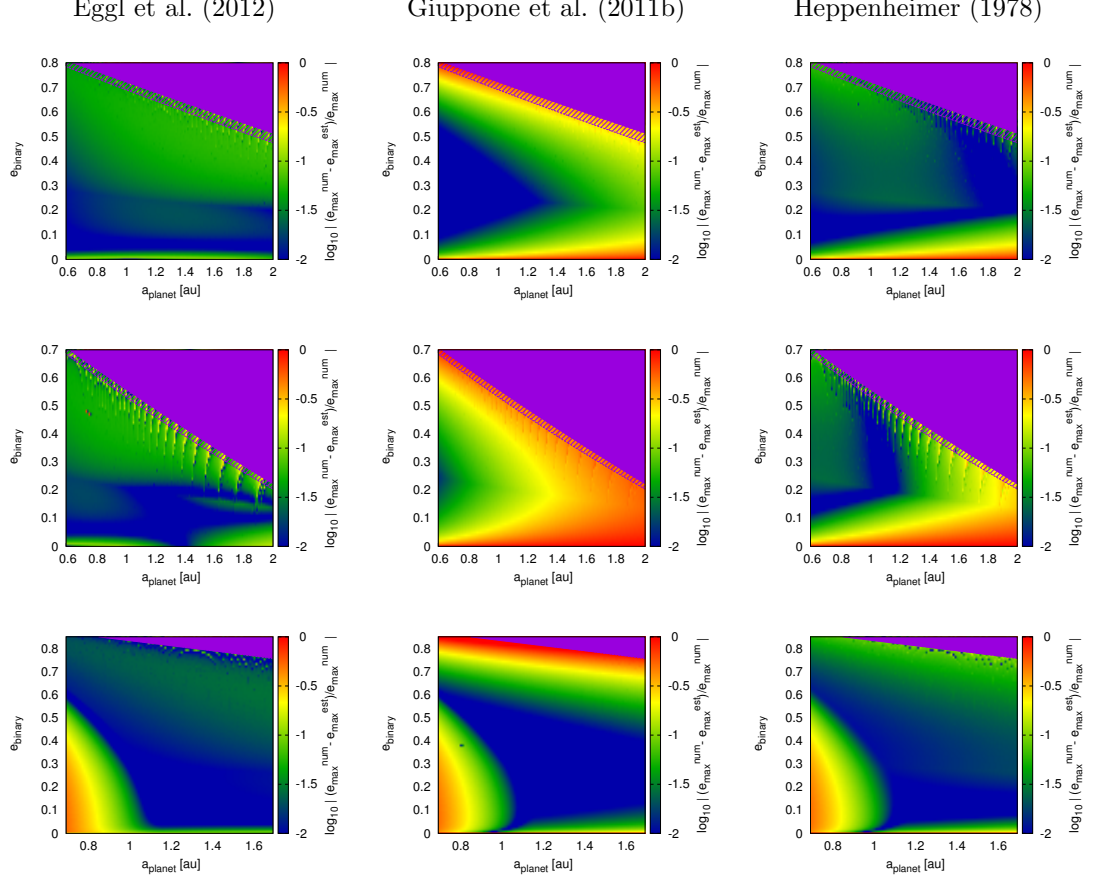


**Figure 5.2:** Analytical estimates for the maximum planetary eccentricity in different binary star-planet configurations are compared to numerical simulation values. Deviations of the analytical estimates ( $e_{max}^{est}$ ) from numerical results ( $e_{max}^{num}$ ) are color-coded ( $\log_{10} |e_{max}^{est} - e_{max}^{num}| / e_{max}^{num}$ ). Each panel shows the discrepancy between analytical and numerical maximum eccentricity estimates as a function of planetary semimajor axis and binary eccentricity. Blue regions denote good correspondence between numerical and analytical results, whereas red zones show deviations up to 100% compared to the numerical value. The purple zones denote regions of orbital instability (Holman & Wiegert 1999, Pilat-Lohinger & Dvorak 2002). The performance of the analytic expression for  $e_p^{max}$  presented in chapter 2, appendix B (*left column*) is compared to semianalytic results following Giuppone et al. (2011a) (*mid column*), as well as to the secular solution by Heppenheimer (1978) (*right column*). The *top panel* represents planetary eccentricity deviations in a G2V-F0V binary star system with  $a_b = 20$  au, the *mid* and *bottom panels* show results for G2V-G2V systems with  $a_b = 10$  au and G2V-M0V systems with  $a_b = 30$  au, respectively. The planet orbits the Sun-like star in all cases.

seem to appear near orbital instability limits where resonances become more potent, as well as in G2V-M0V systems with small planetary semimajor axes as depicted in the bottom panel of Figure 5.2. Both of these issues are expected. First, the influence of resonances was not taken into account in any of the analytical or semi-analytical  $e_p^{max}$  estimates. Second, when injected planetary eccentricities become very small, as is the case for G2V-M0V systems with  $a_p < 0.8$  au, numerical round-off error starts to play a more significant role in this kind of comparison. Therefore, all methods appear to perform similarly poorly in such areas.

## 5. DISCUSSION

Finally, we shall see whether the varying quality of planetary eccentricity estimates affects HZ classifications. Following the method presented in chapter 2, PHZ, EHZ and AHZ in G2V-G2V binary star systems are constructed using eccentricity estimates based on Georgakarakos' and Heppenheimer's formulae for  $e_p^{max}$  and  $\langle e_p^2 \rangle$ . The results are presented in Figure 5.3. The global classification pattern remains the same for both methods, but visible differences occur near the outer edges of the PHZ, EHZ and AHZ. Heppenheimer's PHZ extends further than Georgakarakos', whereas the opposite is true for the AHZs. Hence, differences in HZ classification do arise when the more precise estimates by Georgakarakos are exchanged with Heppenheimer's.

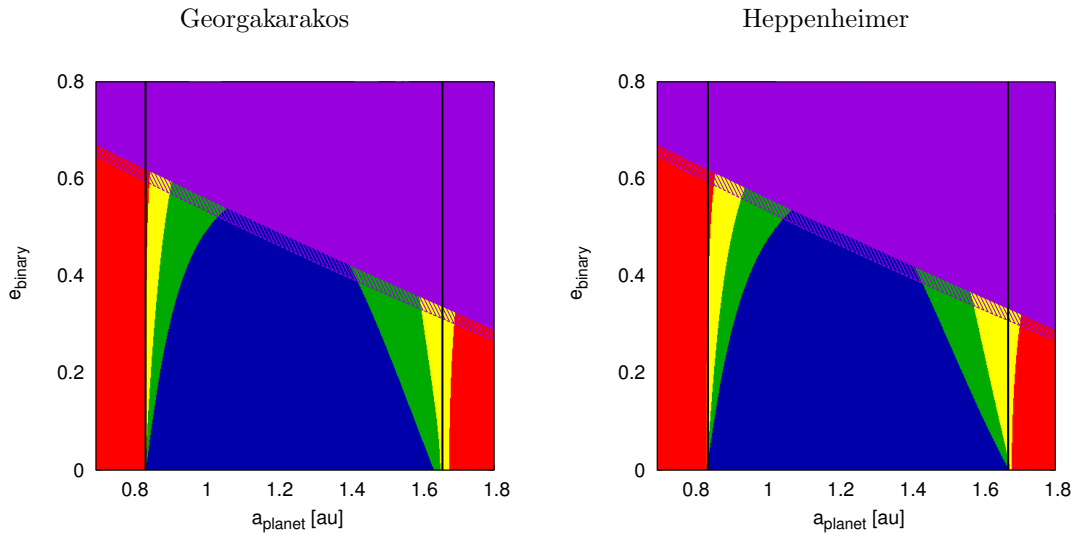


**Figure 5.3:** Two habitability maps of G2V-G2V S-Type systems with semimajor axes of  $a_b = 10$  au are shown. The maps were constructed using analytic estimates for  $e_p^{max}$  and  $\langle e_p^2 \rangle$  based on chapter 2, appendix B and Georgakarakos (2005) (*left*) as well as Heppenheimer (1978) (*right*). Red zones are uninhabitable due to excessive or insufficient insolation. Yellow regions denote AHZs, EHZs are colored green and blue zones represent configurations supporting permanent habitability (PHZs). Purple zones denote regions of orbital instability (Holman & Wiegert 1999, Pilat-Lohinger & Dvorak 2002), see also Figure 5 in chapter 2. Around  $a_{planet} \simeq 1.65$  au visible differences occur especially regarding the PHZ and AHZ borders. The black vertical lines denote KHZ borders.

Concerning the initial question of whether the choice of the analytical method describing the planet's orbit evolution matters for insolation estimates, we can summarize that there are noticeable differences between simpler and more advanced methodologies. Modified equations based on Heppenheimer's secular approach might work for a limited parameter region, but in order to cover all of the binary-planet systems discussed in this work with reasonable accuracy, Georgakarakos' estimates are required.

## 5.2 Insolation Averaging

As pointed out in chapter 2, the calculation of both, EHZs and AHZs requires averaging procedures with respect to planetary insolation. Time averaging is generally a non trivial task in orbital dynamics. Yet, Keplerian orbits are well studied in this regard, so that analytic averages

are readily available. Equation (5) in chapter 2 shows that in a 2BP with closed orbits the time average of the host star's insolation on the planet,  $\langle S_1 \rangle_t$ , is given by

$$\langle S_1 \rangle_t = \frac{L_1 n_p}{h_p}. \quad (5.6)$$

where  $L_1$  is the host star's luminosity,  $n_p$  and  $h_p$  are the planet's mean motion and angular momentum, respectively. Equation (5.6) is perfectly valid for a fixed orbit of a planet around a host star with constant luminosity, but difficulties arise when the planet's motion is perturbed by an additional massive body. Fortunately, secular perturbation theory can be invoked to tell us that the planetary semimajor axis will stay practically constant in an S-Type binary configuration. This was pointed out in chapters 1 and 2. In contrast, the planet's eccentricity varies with time and  $h_p$  will no longer be fixed. Expressing the planet's eccentricity as a function of time and subsequently performing an average via direct integration is always difficult and sometimes even impossible. It is, therefore, necessary to find more subtle ways to include information on orbital variability into averages. Applying the methodology proposed in chapter 2, appendix A, equation (7), one could make the following attempt to account for a planet's varying eccentricity in insolation estimates

$$\langle S_1 \rangle_t = \left\langle \frac{L_1 n_p}{h_p} \right\rangle_t \approx \frac{L_1}{a_p^2 (1 - \langle e_p^2 \rangle)^{1/2}}. \quad (5.7)$$

where the quantities  $a_p$  and  $e_p$  are the planetary semimajor axis and eccentricity. Equation (5.7) suggests implicitly that there is no difference between the average insolation a planet receives on its perturbed orbit and the insolation another planet encounters when moving on a virtual orbit with an average (squared) eccentricity  $\langle e_p^2 \rangle$ .

In chapter 2, equation (7), however, another approach has been used to calculate the planet's average insolation. Here, the planetary equivalence radius ( $r$ ), as introduced in chapter 2.6, has been used

$$\langle S_1 \rangle_t \approx \frac{L_1}{r^2} = \frac{L_1}{a_p^2 (1 - \langle e_p^2 \rangle)^2}, \quad (5.8)$$

with  $r = a_p(1 - \langle e_p^2 \rangle)$ . In equation (5.8) it is assumed that

$$\left\langle \frac{1}{\delta^2} \right\rangle \approx \frac{1}{\langle \delta \rangle^2} \approx \frac{1}{r^2}, \quad (5.9)$$

where  $\delta$  denotes the instantaneous distance of the planet to its host star and  $\delta$  and  $r$  are always greater than zero. Obviously, equation (5.9) requires the variance of  $\delta$  to be small, since it was assumed that  $\langle \delta \rangle^2 \approx \langle \delta^2 \rangle$  which is only true when  $\sigma^2 = \langle \delta^2 \rangle - \langle \delta \rangle^2 \approx 0$ . Furthermore, we have  $\langle \delta \rangle^2 \approx r^2$ . This makes sense, since the equivalence radius  $r$  is comparable to the two-body mean distance averaged over the mean anomaly

$$\langle \delta \rangle_M = a_p(1 - e_p^2/2) \simeq r \quad \text{for} \quad e_p \ll 1 \text{ and } \sigma^2 \approx 0. \quad (5.10)$$

Given all the approximations involved, both estimates for  $\langle S_1 \rangle_t$  presented in equations (5.7) and (5.8) can be considered to be rather crude. More importantly, a difference in the exponent of  $(1 - \langle e_p^2 \rangle)$  becomes apparent when equations (5.7) and (5.8) are compared. Consequently, one might ask, why one approximation was chosen over the other in equations (7) and (A7) of chapter 2? And why was the equivalence radius distilled from equation (5.8) with  $r \doteq a_p(1 - \langle e_p^2 \rangle)$

## 5. DISCUSSION

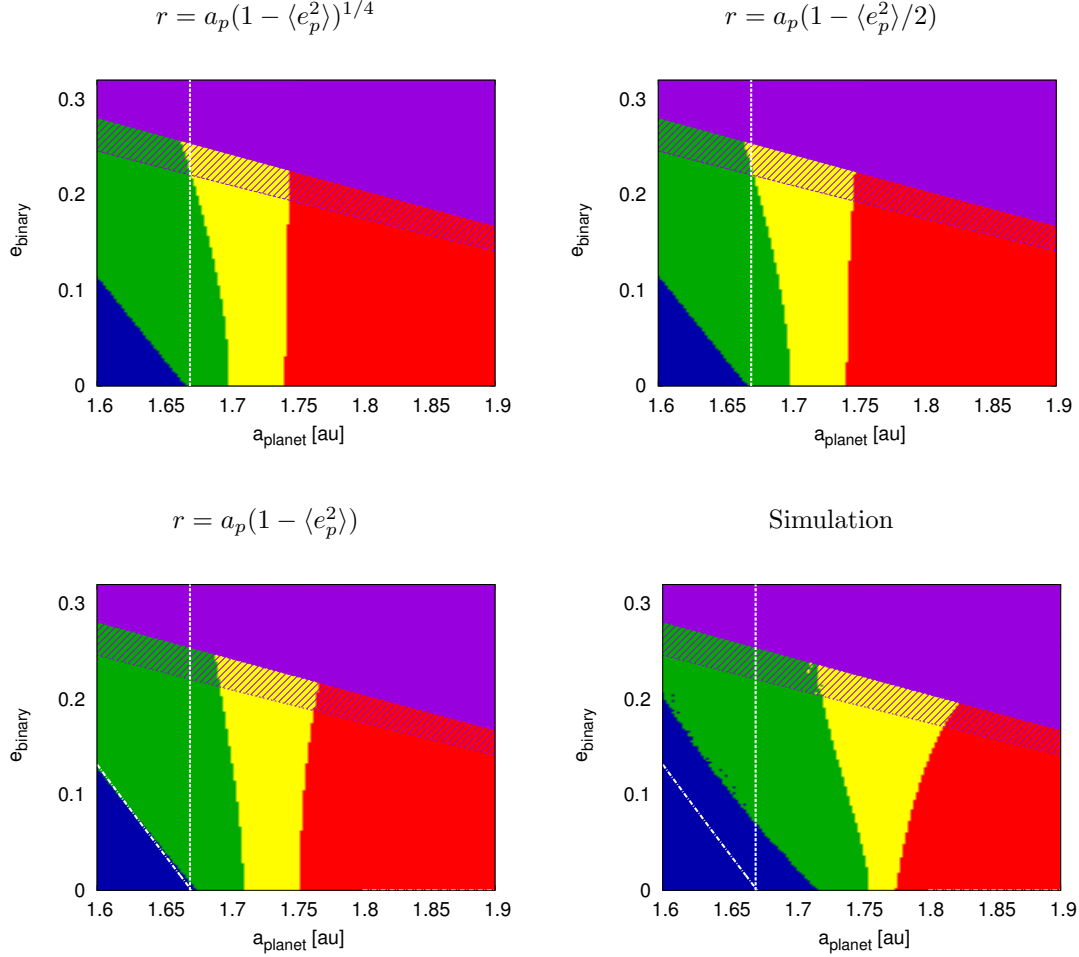


**Figure 5.4:** Habitability map zooms on the outer HZ border of G2V-F0V S-Type binary star systems with a mass ratios  $\mu \simeq 0.57$  and binary semimajor axes of  $a_b = 10$  au are shown. Results gained by applying different analytical expressions for planetary equivalence radii ( $r$ ) (*top*) are compared to the published analytical method as defined in chapter 2 (*bottom, left*), as well as to numerical calculations (*bottom, right*). The analytic form of the equivalence radii for the second star ( $R$ ) is consistent with the planet's. The color coding corresponds to Figure 5.3.

instead of  $r \doteq a_p(1 - \langle e_p^2 \rangle)^{1/4}$  - which would have been a consequence of equation (5.8)? Could  $r \doteq \langle \delta \rangle_M \approx a_p(1 - \langle e_p^2 \rangle/2)$  not could be another option?

In short, the equivalence radii for the planet ( $r$ ) and the second star ( $R$ ) were chosen to best represent numerical simulation data. In order to illustrate this, four habitability maps of G2V-F0V binary star systems with various eccentricities are shown in Figure 5.4, all having a semimajor axis of 10 au.<sup>1</sup> The planet was started near the outer edge of the G star's KHZ in all cases. The top panels were generated applying alternative definitions of the equivalence radii  $r$  and  $R$ . Results from the nominal analytic method as proposed in chapter 2 using  $r = a_p(1 - \langle e_p^2 \rangle)$  are compared to numerical simulation outcomes in the bottom panels of Figure

<sup>1</sup>For a description of the color coding, see Figure 5.3.

5.4. Evidently, the analytical approach taken in equation (5.8) using the nominal equivalence radius  $r = a_p(1 - \langle e_p^2 \rangle)$  tends to represent the numerical outcomes most faithfully. Especially the curvature of the AHZ towards the second star is quite pronounced in the numerical results. A similar trend could be identified in all the cases investigated in chapter 2. Since this feature is best expressed in the lower left panel of Figure 5.4, the equivalence radius  $r = a_p(1 - \langle e_p^2 \rangle)$  was the preferred choice.

Of course, taking numerical results as a reference for choosing analytical models requires the identification and circumnavigation of potential pitfalls. One such trap has already been identified in chapter 2, section 7. Using semi-analytical estimates, it could be shown that the numerically computed PHZ overestimated the true borders for permanent habitability. This over-extension of the PHZ in numerical simulations is most probably due to a combination of low time resolution in the discrete integration output intervals and the finite integration time span that would not permit a lot of opportunities to reach extreme configurations. It is, therefore, likely that the actual extremum configurations were never exactly hit during the simulations. Test calculations featuring a higher time resolution indicated the correctness of this hypothesis.

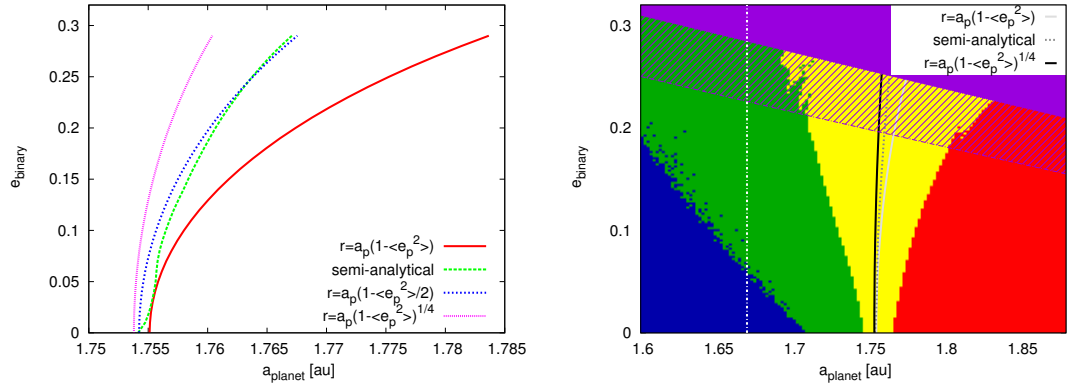


**Figure 5.5:** Results of different analytic and semi-analytic approaches to calculate the outer AHZ border in a G2V-F0V S-Type binary star system (*left*). Similar curves are drawn on top of a numerically computed habitability map (*right*). The numerically determined AHZ is presented in yellow color. The remaining colors are explained in Figure 5.3.

In order to see, whether the differences in numerically and analytically determined AHZs occurring in Figure 5.4 are caused by similar shortcomings in the numerical simulations or by deficits in the analytical modeling, we will now attempt to construct a semi-analytical approach to this problem. Following the path established in the previous section, we use equations (5.1-5.4), where we replace Heppenheimer’s eccentricity and longitude of pericenter evolution equations with Georgakarakos’ estimates (appendix 1.A), in order to construct the time dependent analytical insolation curve  $S_{tot}(t)$ . The planet’s and binary stars’ orbital elements at  $t = t_0$  serve as initial conditions, so do the system’s masses. The actual expression for  $S_{tot}(t)$  consists of many hundred terms, and will not be given explicitly here. However, for a planet started at 1 au in a G2V-G2V binary with  $a_b = 20$  au, the resulting insolation patterns are presented in Figure 5.1 (*left column, mid graph*). The averaging process then consists of an

## 5. DISCUSSION

integration over the longest occurring period in the system ( $L$ )

$$\langle S_{tot} \rangle_t = \frac{1}{L} \int_0^L S_{tot}(t) dt, \quad (5.11)$$

We will assume that  $L$  corresponds to the planetary eccentricity's secular period  $L = 2\pi dt(Bd\tau)^{-1}$ , see appendix 1.A. Given the complexity of the expression for  $S_{tot}(t)$ , a direct integration is out of the question. After all, if such an integration was feasible, there would have been no need to introduce approximations (5.6-5.10) in the first place. Abandoning the goal to rely solely on analytics, we can approximate the integration in equation (5.11) by a summation of discretely sampled insolation data points so that

$$\langle S_{tot} \rangle_t = \frac{1}{L} \int_0^L S_{tot}(t) dt \approx \frac{1}{N} \sum_{j=0}^N S_{tot}(t_j). \quad (5.12)$$

Here,  $N$  denotes the number of sample points and  $t_j = t_0 + jL/N$ . We can achieve semi-analytical estimates for the planetary average insolation by sampling the function  $S_{tot}$  and evaluating the sum in equation (5.12). In order to calculate the AHZ boundaries for a given system, the Newton-Raphson method is applied to numerically solve the equation

$$\langle S_{eff,tot} \rangle_t - 1 = 0$$

for  $a_p$  while keeping all the remaining parameters  $\{e_b, a_b, L_1, L_2, m_0, m_1, m_2, X_1, X_2\}$  constant. Note, that the only difference between  $\langle S_{tot} \rangle_t$  and  $\langle S_{eff,tot} \rangle_t$  is the normalization of the individual stellar contributions with respect to Kasting's effective radiation limits ( $X_1$  and  $X_2$ ), see chapter 2, sections 6.2 and 6.3. Outer AHZ borders for G2V-F0V S-Type systems with  $a_b = 10$  au are presented in Figure 5.5. Here, results from the analytical, semi-analytical and numerical approaches discussed so far are compared. The semi-analytical solution follows a path between two analytically derived curves, namely the ones that were generated using the nominal equivalence radius as defined in chapter 2,  $r \doteq a_p(1 - \langle e_p^2 \rangle)$ , and the time averaged distance  $r \doteq a_p(1 - \langle e_p^2 \rangle/2)$ . For higher binary eccentricities, the semianalytic solution converges towards the estimates containing the time averaged distance. Since most of the relevant dynamics has been incorporated in the semi-analytic approach, the consistency of the semianalytic and analytic results suggests that equivalence orbits are a suitable tool for calculating averaged insolation values.

Yet, there still is a relatively large discrepancy between those results and the numerical solutions for systems exhibiting strong perturbations (Figure 5.5, *right*). The simplifications performed to find analytical AHZ estimates, e.g. putting both the planet and the secondary on circular orbits with modified angular momenta, are not to be blamed for the large deviations, as the correspondence between semi-analytical and analytical results is quite satisfactory. Consequently, other explanations have to be explored. The following reasons for the discrepancy between semi-analytical and numerical results seem possible:

- AHZ estimates are sensitive to the averaging time span,
- AHZ estimates are influenced by the simulation's time resolution just like PHZs,
- the dynamical model incorporated in the semi-analytical approach is not comprehensive enough to deal with strong perturbations.

Let us discuss these propositions point by point. Since the planetary eccentricity is very important for insolation, it is not unreasonable to assume that imprecise estimates of the associated

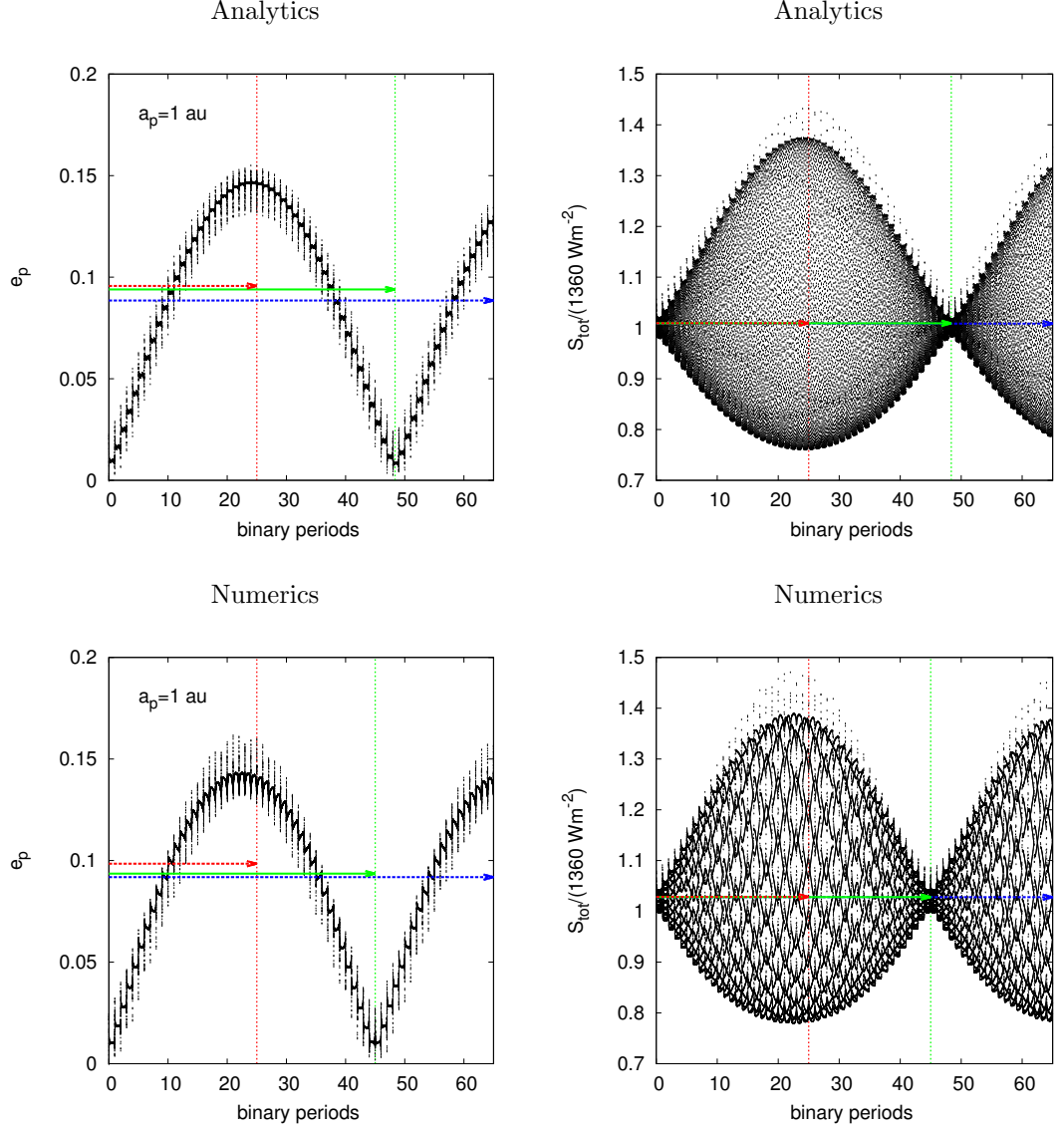


**Figure 5.6:** Averages of analytical (*top*) and numerical (*bottom*) planetary eccentricity ( $e_p$ ) and total insolation ( $S_{tot}$ ) estimates over different time spans in a G2V-G2V binary with  $a_b = 20$  au and  $e_b = 0.7$ . The colored arrows indicate values for averages over time intervals delimited by the corresponding vertical lines. Eccentricity and insolation data has been sampled identically for all graphs. Misjudging the secular period can have a visible impact on planet’s average eccentricity (*left*). Insolation averages are, in contrast, practically unaffected by this problem (*right*). Even Georgakarakos’ evolution equations do not contain all dynamical effects, e.g. nonlinear variations in the planet’s mean anomaly. Therefore, differences in insolation averages as well as in the secular periods occur between analytical and numerical results.

## 5. DISCUSSION

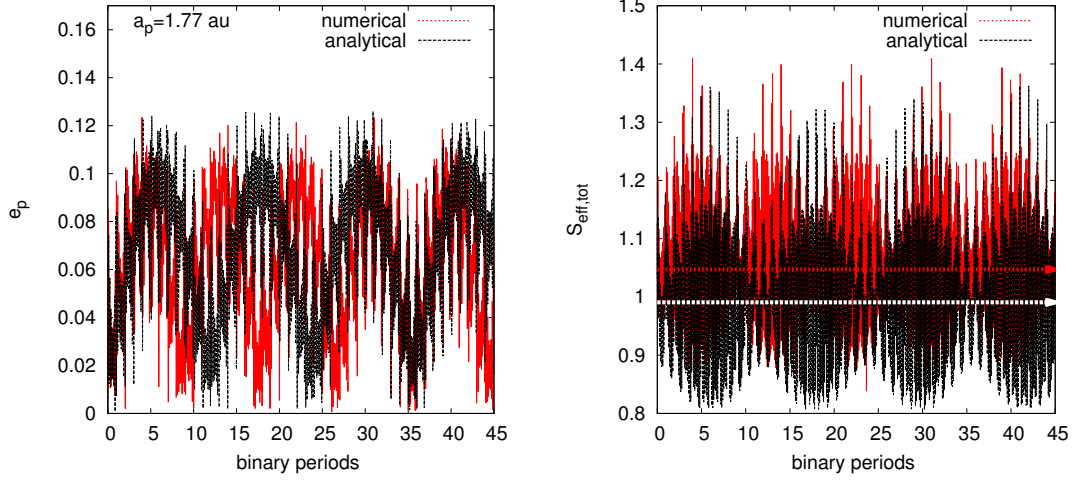


**Figure 5.7:** Time evolution of planetary eccentricity ( $e_p$ , left) and effective insolation ( $S_{eff,tot}$ , right). The planet orbits the G2V component of a close G2V-F0V system with  $\mu \simeq 0.57$ ,  $a_b = 10$  au and  $e_b = 0.2$  near the outer edge of the AHZ. The system is similar to the ones discussed in Figures 5.4 and 5.5. Analytical predictions for eccentricity and insolation variations deviate significantly from their numerical reference values. This has a substantial effect on insolation averages, which are represented by the horizontal, dashed lines in the right panel. For a planetary semimajor axis of  $a_p = 1.77$  au, analytical estimates would classify the orbit as non-habitable, whereas numerical predictions would place it within the AHZ.

secular period might lead to averaging problems. As we have seen in sections 1.3.5 and 5.1, there are certain issues in this respect. The left column in Figure 5.6 contains colored arrows that represent averages of the underlying eccentricity curve over different time spans. One can clearly see that the choice of the averaging period has a noticeable influence on  $\langle e \rangle_t$ . As shown in the right panels of Figure 5.6, however, this effect is negligible for  $\langle S_{tot} \rangle_t$ . Even if the secular period is gravely misjudged, insolation averages do not differ much.

Numerical insolation averages are not very sensitive to time resolution issues, either. The average insolation values of Figure 5.6 were recovered with a precision of  $10^{-5}$  even for resolutions two orders of magnitude below the ones used in the nominal calculations.

This leaves us with the third option, namely that the dynamical model used in Georgarakos' eccentricity evolution equations might not be elaborate enough to reconstruct insolation patterns faithfully in the case of strongly perturbed planetary orbits. A first hint that this might indeed be the case can be gathered from a comparison of numerical and analytical insolation curves in Figure 5.6. The additional patterns occurring in the numerical data are partly due to nonlinear variations in the planet's mean anomaly. Since our analytical insolation model contains the assumption that  $da_p/dt = 0$  (see section 5.1), the corresponding planetary mean motion stays constant. The corresponding mean anomaly can, thus, only change linearly with time. As a consequence, the analytical and numerical average insolation values cannot perfectly coincide. The (semi-)analytically<sup>1</sup> derived average insolation for a planet at 1 au in a G2V-G2V S-Type binary with  $a_b = 20$  au amounts to  $1372 \text{ Wm}^{-2}$ , whereas the numerical

<sup>1</sup>Recall at this point that the insolation estimates are fully analytic, but the calculation of the insolation averages requires numerical intervention, 7 see equation (5.12).



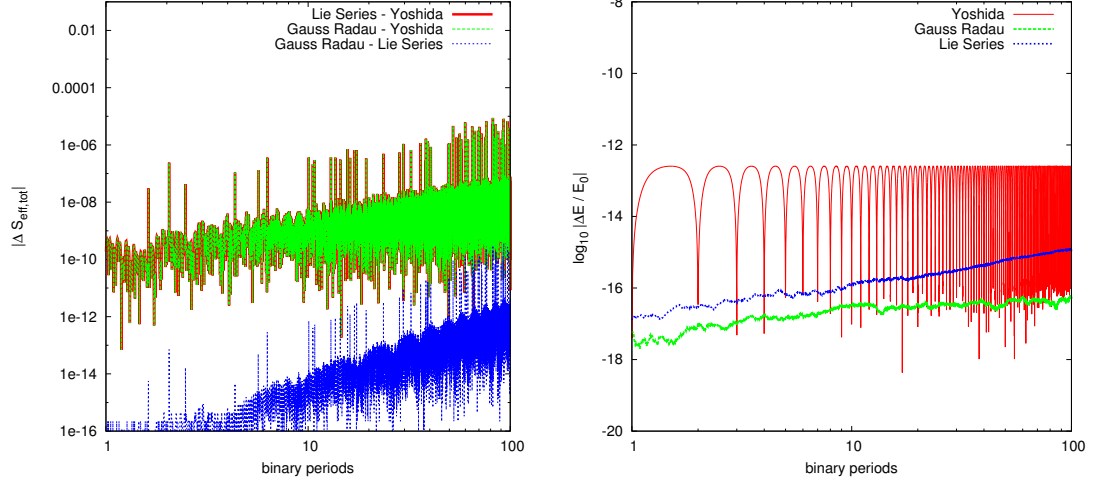


**Figure 5.8:** *Left:* Differences in simulated planetary insolation due to the choice of numerical integrators for the same G2V-F0V system that is presented in Figure 5.7. The curves denote insolation differences between Gauss Radau and Lie Series (blue), Gauss Radau and Yoshida’s 8<sup>th</sup> order symplectic scheme (green) and Lie Series and Yoshida’s scheme (red). The step size for the symplectic algorithm is  $\tau = 1D$ ; Gauss Radau and Lie Series algorithms support an adaptive step size. For our purpose, the methods are giving practically identical results. At closer inspection, however, the non-symplectic, adaptive schemes (Gauss Radau and Lie Series) show a high degree of correspondence, whereas the deviations from symplectic results are more pronounced. *Right:* The integrators’ different behavior regarding the conservation of the system’s total energy ( $E$ ) is responsible for the discrepancies in insolation predictions. See section 5.2 for details.

result is  $1398 \text{ Wm}^{-2}$ . This discrepancy grows in unison with the second star’s luminosity as well as with its potential to influence the planet’s orbit. Such considerations certainly play a role for the G2V-F0V systems presented in Figure 5.5, but can the associated deviations become large enough to cause AHZ classification differences?

Figure 5.7 shows the insolation and eccentricity evolution of a planet in a G2V-F0V binary - planet system which has been classified as non habitable by analytic and semianalytic predictions. Numerical simulation results suggest, however, that the planet is still within the AHZ. The discrepancies between analytically and numerically generated insolation curves are, in fact, large enough to cause a substantial difference in the average values. With  $\langle S_{eff,tot} \rangle_t^{ana} = 0.99$  and  $\langle S_{eff,tot} \rangle_t^{num} = 1.05$  the same system would indeed be classified differently by our (semi-)analytical and numerical approaches, see chapter 2, section 6.2. Discovering discrepancies is one thing, but identifying whether the analytical or the numerical solution lies closer to the truth requires a little extra work.

So far we have assumed that the numerical insolation curves are the correct ones, whereas the analytical curves are considered to be only approximations. In order to confirm that this is indeed the case, we have to be able to reproduce the numerical insolation results gained via Everhart’s Gauss Radau method (Everhart 1974) using other numerical approaches. We, therefore, chose another variable step-size integrator based on Lie Series (Eggl & Dvorak 2010), as well as an 8<sup>th</sup> order symplectic method by Yoshida (1990) based on potential and kinetic energy splitting to validate our numerical results.

## 5. DISCUSSION

---

Figure 5.8 shows that the numerical insolation results can be reproduced with a high degree of accuracy suggesting that the previous numerical results are indeed close to the true solution. The main discrepancies between the three integrator results are due to the different energy conservation behavior of the three numerical integration methods. In spite of the fact that the 8<sup>th</sup> order symplectic integrator shows no secular increase in the local energy error, it jumps quickly to its predestined local deviation of  $|E/E_0| \approx 10^{-12}$ . This is a consequence of the fact that a nearby Hamiltonian is solved instead of the actual one (e.g. Yoshida 1993). The Lie Series algorithm, in contrast, exhibits a secular increase in energy error, but due to its capacity to choose the integration step size adaptively, the overall error remains below the symplectic method on short timescales. Unfortunately, energy preservation is not an apriori feature of Everhart’s algorithm, either. It can, however, be achieved fairly easily by requiring the convergence of the polynomial fitting to machine precision during each individual integration step. The near flawless energy conservation up to accumulated round-off errors exhibited by the Gauss Radau method in the right panel of Figure 5.8 supports this claim.

In order to summarize the main points of this section, let us briefly recall previous results regarding the over-extend of numerically generated PHZs. Using a combination of numerically evaluated  $e_p^{max}$  values and analytically derived extremum conditions, it could be shown that the purely numerical predictions were overestimating the actual borders of the PHZs. In contrast, here the numerical AHZ estimates seem to be more trustworthy than the analytical and semi-analytical predictions. This underlines the importance of a multifaceted approach to the problem of HZ determination in binary star systems featuring both analytical and numerical aspects.

### 5.3 Mutual Inclination

The analytical method used to estimate the extent of circumstellar HZs developed in chapter 2 assumes a coplanar system. In other words, the planet is thought to move in the same orbital plane as the binary star. However, it was claimed in chapter 4 that the coplanar solution can also be used as an approximation for systems with low mutual inclination. In order to confirm the validity of this statement, let us briefly study the changes of the HZs with planetary inclination. For this purpose we assume an Earth-like planet which orbits one component of a G2V-G2V binary with  $a_b = 10$  au. We then alter the inclination of planet’s orbital plane with respect to the binary’s. Since the analytic determination of HZs in mutually inclined systems goes beyond the scope of this work, our investigation will be conducted numerically using the Gauss Radau method presented in the previous section. Preliminary results are shown in Figure 5.9.

The changes in the HZs up to the onset of the Kozai-Lidov dynamical regime where  $i \approx 39^\circ$  (Kozai 1962, Lidov 1962) are very small. Thus, the analytic method to determine HZs introduced in chapter 2 can be expected to work reasonably well for low mutual inclination, as long as  $i \ll 38^\circ$ . However, different dynamical as well as geometrical aspects become relevant in such configurations.

One can see, for instance, that the asymmetry in the PHZ borders with regard to small and large planetary semimajor axes decreases with mutual inclination. This is expected, since that asymmetry is due to the direct radiative contribution of the second star. The maximum distance between the planet and the secondary tends to increase with growing mutual inclination and, thus, its direct radiative influence on the planet is reduced. In contrast, the minimum and maximum planetary distances to the host star remain independent of the planet’s orbital inclination. As a consequence, the inner PHZ borders remain practically unchanged up to  $i \approx 38^\circ$ . Beyond  $i \approx 50^\circ$ , the PHZ and EHZ tend to vanish leaving only AHZs. This seems reasonable given the well known coupling between inclination and eccentricity in the Kozai-

### 5.3 Mutual Inclination

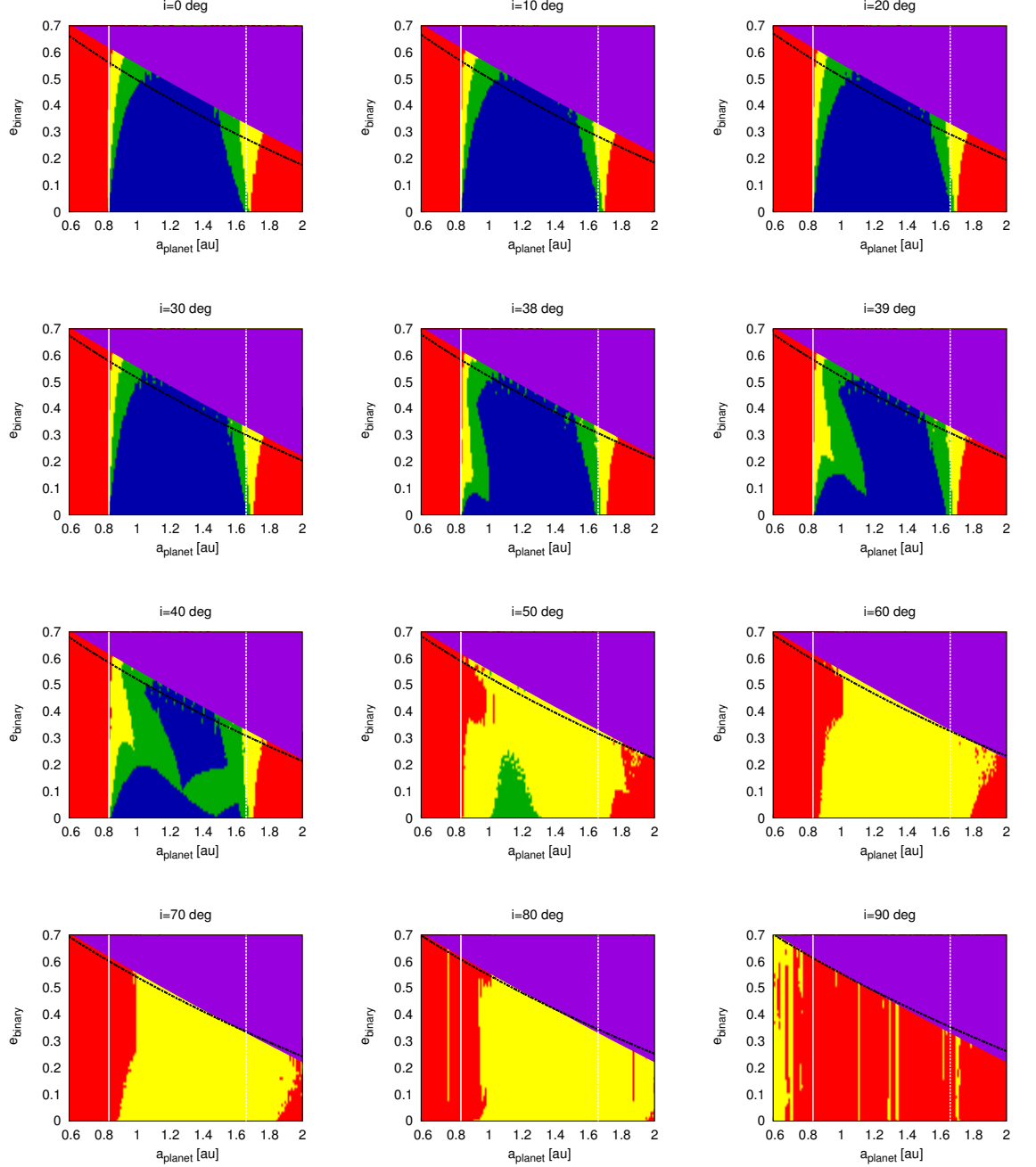


**Figure 5.9:** Habitability maps for planets on inclined orbits in G2V-G2V binary star systems with  $a_b = 10$  au. The color coding is similar to Figure 5.3. The black curved line represents orbital stability limits by Mardling & Aarseth (2001). Compared to coplanar classifications, only little change is noticeable up to the Kozai-Lidov dynamical regime where  $i \approx 39^\circ$  (Kozai 1962, Lidov 1962). For higher mutual inclination ( $i$ ) PHZs and EHZs vanish. See section 5.3 for details.

## 5. DISCUSSION

---

Lidov regime. Nevertheless, those results should be considered preliminary until they can be validated with analytical models.

Orbital stability is another interesting aspect that has to be considered carefully in mutually inclined systems. Strictly speaking, the purple regions of orbital instability shown in the graphs of Figure 5.9 are only valid for the coplanar case, since they were calculated using the fit function by Holman & Wiegert (1999). While it seems counter-intuitive to apply estimates for coplanar configurations to mutually inclined systems, we can justify this with results by Harrington (1972). He found the stability limits of S-Type systems to be basically independent of mutual inclination, except for a small region of instability around  $i = 90^\circ$ . In contrast, the stability criterion by Mardling & Aarseth (2001) based on chaotic orbital energy exchange (equation (1.7)) predicts a weak increase of stability with mutual inclination. The estimates by Mardling & Aarseth (2001) are represented by the black curves in Figure 5.9. One can see that those stability limits are more conservative than the ones by Holman & Wiegert (1999) for coplanar configurations, but both stability criteria tend to produce similar results for high mutual inclinations. In fact, the small region of orbital instability around  $i = 90^\circ$  predicted by Harrington (1972), but not taken into account by Mardling & Aarseth (2001), might be visible in Figure 5.9 (*bottom right*). Close to a mutual inclination of  $i = 90^\circ$  not even zones of average habitability remain in this system, which could indicate complete orbital instability. Maximum planetary eccentricity values around 1 for most of the corresponding orbits support this notion. The remaining yellow AHZ bands are merely numerical residuals. Of course, this sort of orbital instability is thought to be a property of hierarchical triple systems specifically. A similar configuration that could - in theory - possess habitable worlds is the well known Sitnikov problem (Sitnikov 1960). The intriguing interplay between regular and chaotic motion in Sitnikov configurations (Kovács & Érdi 2009, Soulis et al. 2007, and references therein) might merit a - perhaps somewhat academic - investigation into possible habitable worlds in such configurations. Such research, however, lies beyond the scope of this work.

The previous example suggests that a small mutual inclination between planetary and binary orbits does not influence planetary habitability considerably. This is in agreement with well known results concerning classical hierarchical triple systems, where radical changes in the dynamical behavior are only expected close to resonances and near the boundary to the Kozai regime (e.g. Krymowski & Mazeh 1999, Libert & Delsate 2012).

Yet, mutually inclined systems are not only interesting with respect to habitability. Also, the detectability of terrestrial exoplanets in binary star systems can be influenced by the well known eccentricity - inclination coupling

$$\frac{H_p}{L_p} = \sqrt{1 - e_p^2} \cos i_p = \text{const}, \quad (5.13)$$

where  $H_p$  and  $L_p$  are the planet's Delaunay elements as defined in section 1.3.4, and  $e_p$  and  $i_p$  the planetary eccentricity and inclination respectively. Relation (5.13) is a direct consequence of total angular momentum conservation when we assume that the planet's influence on the binary's angular momentum is negligible ( $\dot{H}_b \simeq 0$ ). It is easily seen that, given the right initial conditions, high planetary eccentricities are possible in mutually inclined configurations. Those can boost the chances of a planet's detection as was pointed out in chapter 3. Furthermore, in a series of articles Schneider (1994), Schneider & Chevreton (1990) and Schneider & Doyle (1995) concluded that the transit probability for planets on P-Type orbits increases drastically with mutual inclination due to the additional precession of the planet's ascending node. In S-Type systems, however, the timescale for nodal-precession ranges between tens and several hundreds of binary periods, where most of the periods for the systems investigated in this work span decades. Thus, a continuous observation over hundreds of years would be required in order

to benefit from elevated transit probabilities due to the precession of nodes. For this reason, the advantageous effects of mutual inclination were not considered in our transit probability estimates established in chapter 3.

## 5.4 Retrograde Planetary Motion

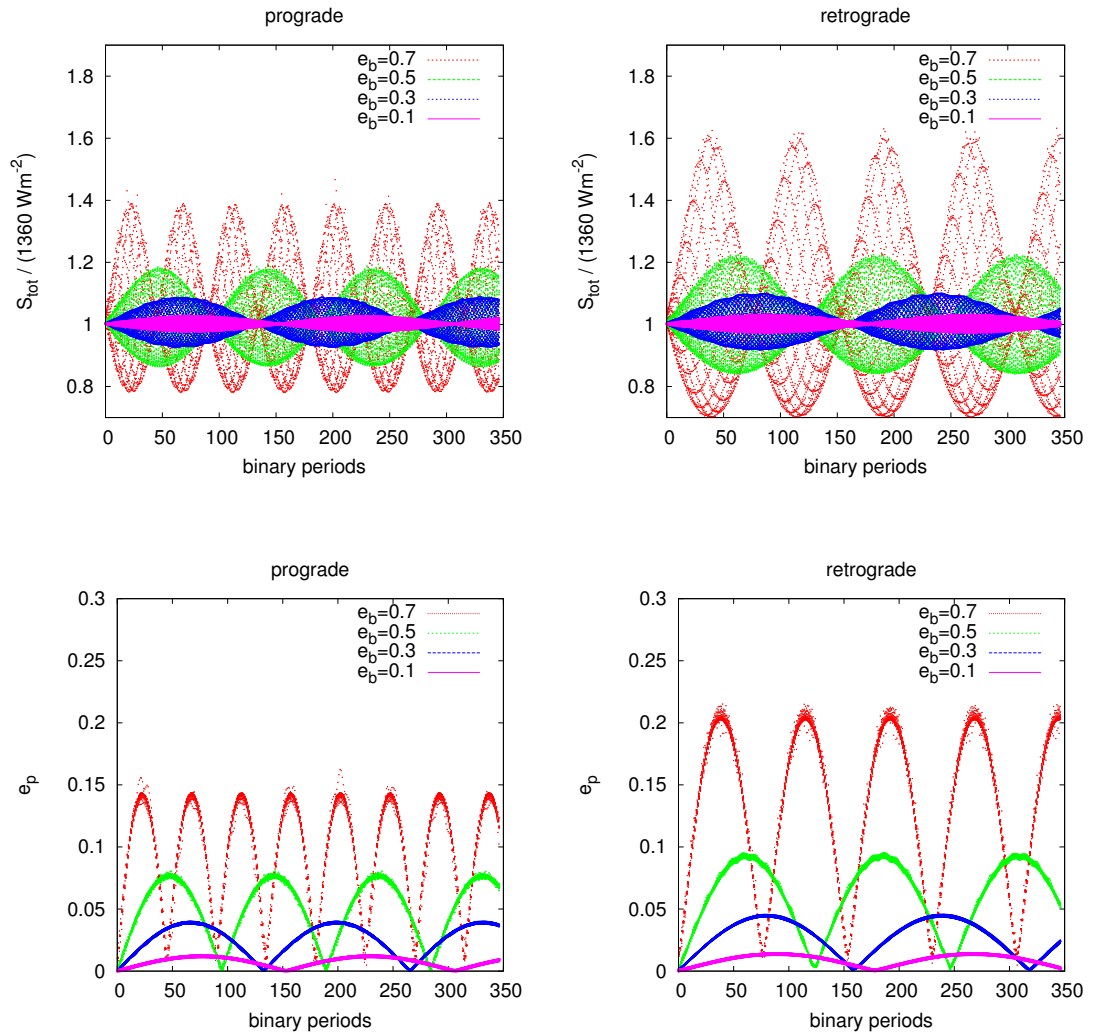


**Figure 5.10:** Numerical simulation results regarding planetary insolation (*top*) and eccentricity (*bottom*) evolution in G2V-G2V S-Type binary star systems ( $a_b = 20$  au) with different eccentricities ( $e_b = 0.1, 0.3, 0.5, 0.7$ ) for prograde and retrograde planetary motion. The Earth-sized planet was started on a circular orbit with a semimajor axis of  $a_p = 1$  au. Retrograde amplitudes as well as the corresponding secular periods (*right*) are considerably larger than their prograde counterparts (*left*).

## 5. DISCUSSION

---

Roughly a quarter of the so-called "hot Jupiter" population<sup>1</sup> orbit their host stars in a retrograde fashion, i.e. opposite to the stars' own direction of rotation (Triaud et al. 2010). Recent studies consider a dynamically induced spin-flip of planetary orbits in mutually inclined hierarchical systems to be a possible cause for creating such configurations (Correia et al. 2011, Naoz et al. 2012a). Whether such mechanisms could indeed produce anti-aligned orbits of terrestrial planets in HZs has to be studied more carefully. Nevertheless, it is interesting to briefly tackle the possible consequences of retrograde (coplanar) motion for a terrestrial planet's insolation and eccentricity evolution. Figure 5.10 contains results of such an investigation. Retrograde and prograde planetary orbits in G2V-G2V S-Type binary star systems with various eccentricities are compared with respect to planetary insolation and eccentricity evolution. The differences in amplitudes and secular periods are considerable, which suggests that modifications in the analytical method to determine HZs would be required to account for retrograde planetary motion. Despite the fact that retrograde orbits are generally considered to be more favorable in terms of orbital stability, see e.g. Dvorak (1997), Valtonen & Karttunen (2006) and references therein, it is most likely that the increased eccentricity and insolation amplitudes would shrink the HZs in binary stars systems considerably. Further investigations are necessary to determine the exact consequences of retrograde planetary motion for habitability in S-Type binary star systems.

### 5.5 Initial Planetary Eccentricity

At this point it has become very clear that the planet's eccentricity evolution plays a crucial role in the determination of a system's potential habitability. Up to now, it was assumed that the planet was on an initially circular orbit after its formation. While this assumption seems reasonable from an astrophysical point of view, it is also a necessary prerequisite for estimates based on Georgakarakos' method to produce correct results. Conversely, should a discovered planet's orbit exhibit a substantial initial eccentricity, then it is likely that the HZ estimates presented in chapter 2 will produce inaccurate results. In order to quantify the term "substantial initial eccentricity", test calculations featuring a telluric planet with different initial eccentricities in a G2V-G2V binary with  $a_b = 10$  au and  $e_b = 0.5$  were performed. Once more, Everhart's Gauss Radau integrator (Everhart 1974) was used to solve the corresponding equations of motion numerically. The left panel in Figure 5.11 shows simulation results where the planet was started in phase with the second star, i.e. their mean longitudes  $L_p$  and  $L_b$  coincided, whereas the right panel presents calculations that were performed with the planet being started in opposition to the second star ( $L_p = 0^\circ, L_b = 180^\circ$ ). All of the eccentricity curves exhibit secular and short-periodic modulation. While the amplitudes of these oscillations tend to increase with initial eccentricity, a remarkable break in this trend can be found for initial eccentricities around 0.1. Here, the amplitude of modulation decreases significantly even compared to the trajectories started with zero initial eccentricity. This behavior is expected and can be explained using the concept of "free" and "forced" eccentricity components, see e.g. Murray & Dermott (2000). Planets started with  $e_p = 0.1$  are closer to the forced eccentricity components and have, therefore, smaller "free" oscillations. The further the gap between initial and "forced" eccentricity, the larger the "free" component becomes. Thus, our analytic HZ estimates developed in chapter 2 are strictly valid only for planets on initially circular orbits. For small initial eccentricities, however, the analytic AHZ borders can still serve as conservative estimates.

---

<sup>1</sup>Hot Jupiters are Jovian extrasolar planets orbiting very close to their host star.

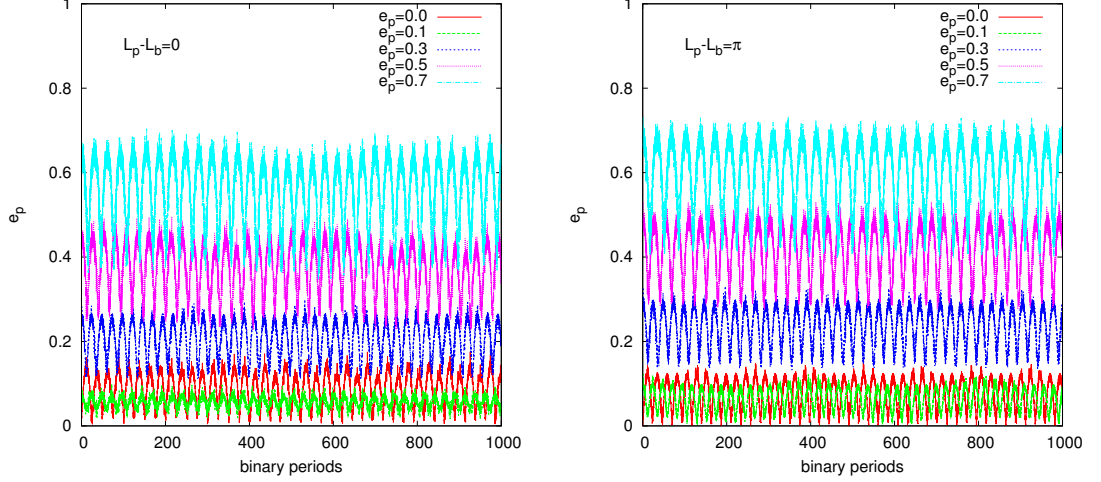


**Figure 5.11:** Planetary eccentricity evolution in a G2V-G2V binary with  $a_b = 10$  au and  $e_b = 0.5$ . The colored curves represent solutions for different initial eccentricities of the planet. The planet and binary are started at equal phase (left), and at opposite phase (right). The remaining initial conditions are presented in Table 1.1 (system a).

## 5.6 General Relativity and R3BP Approximations

The omission of general relativity (GR) in our method might constitute another potential issue. It is well known that the additional pericenter drift introduced by GR generally leads to smaller eccentricities in hierarchical triples (e.g. Blaes et al. 2002, Fabrycky & Tremaine 2007, Naoz et al. 2012b, Soffel 1989). Also, the semimajor axes of the individual orbits are affected. Yet, GR was not included in our dynamical models used to determine HZs in binary star systems, because relativistic effects in S-Type configurations are generally considered to be negligible. It remains to be shown, however, that this is indeed the case for the systems investigated in chapter 4.

Planets around HIP 30920 B have to be very close to their host star in order to be habitable, whereas the PHZ in HIP 84425 reaches right up to the system's stability limit, see Figure 1 in chapter 4. In order to test the influence of GR on these two systems, the corresponding Einstein-Infeld-Hoffman (EIH) equations are solved numerically, and the planetary eccentricity and pericenter evolution are compared to the corresponding Newtonian reference curves. Figure 5.12 shows the evolution of planetary orbital elements for the systems HIP 30920 and HIP 84425 at different levels of approximation. Results from R3BP approaches ( $m_p = 0$ ) are presented together with full 3BP ( $m_p \neq 0$ ) solutions, both with and without taking GR into account. The reference model is the one applied in our analytical HZ estimates, namely the Newtonian 3BP, and the planets were started at  $a_p = 0.027$  au and  $a_p = 0.834$  au for HIP 30920 and HIP 84425, respectively. The top panel of Figure 5.12 shows the deviation of planetary semimajor axes relative to their initial values ( $\Delta a_p = a_p - a_{p0}$ ). The mid and bottom panels of the left column compare orbital element evolution curves for planetary eccentricities ( $e_p$ ) and longitudes of pericenter ( $\varpi_p$ ) in the HIP 30920 system directly. In the right column the line corresponding to the reference model is given together with deviation curves for HIP 84425. Deviation curves were generated by subtracting the reference signal from the other results, e.g.  $\Delta e_p = e_p^{EIH} - e_p^{ref}$ . The numerical predictions for  $e_p^{max}$  in HIP 84425 are represented by the colored horizontal lines

## 5. DISCUSSION

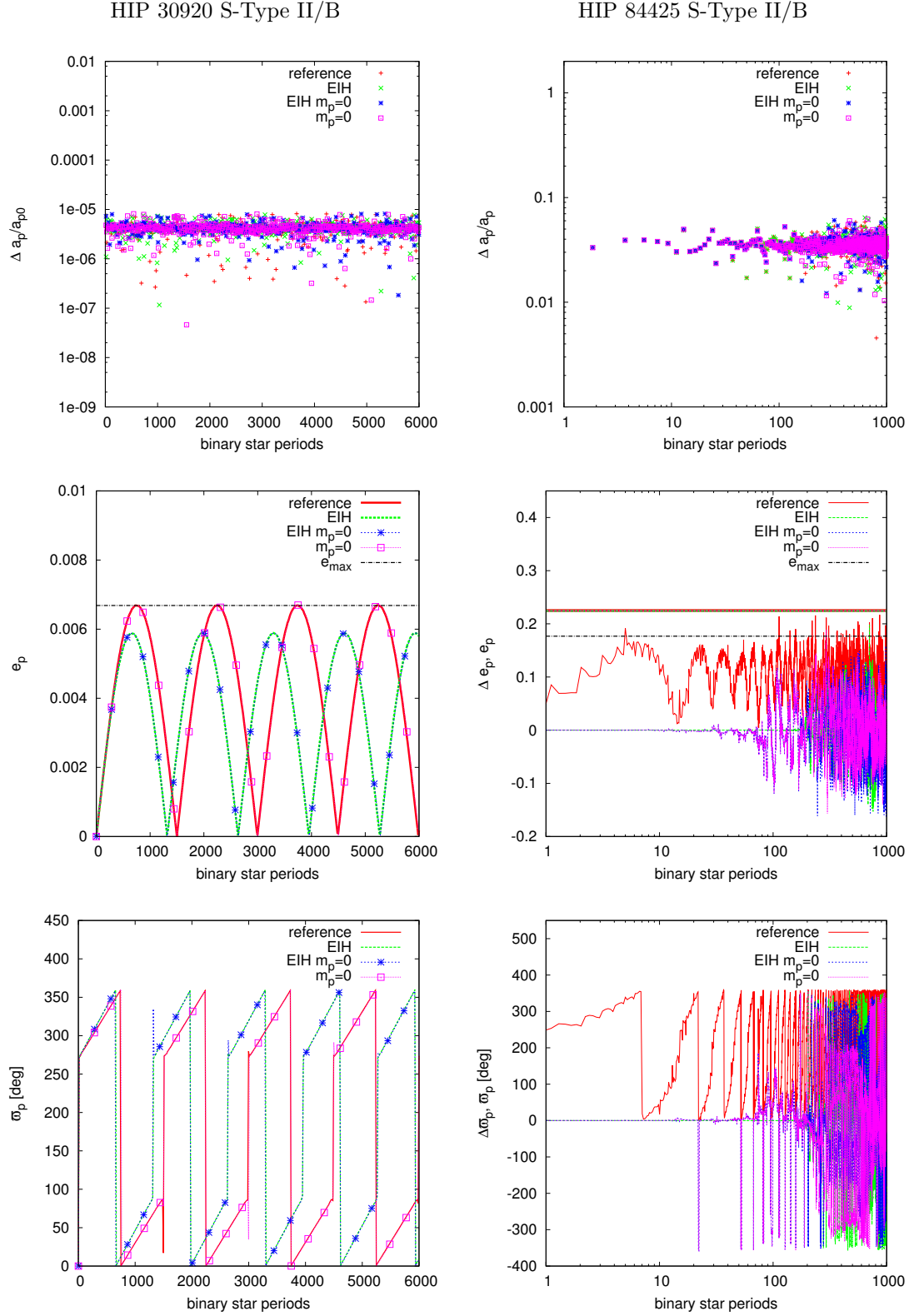


**Figure 5.12:** Evolution of planetary orbital elements for two systems discussed in chapter 4 which are likely to be affected by general relativity. Results of four different dynamical models are compared. See section 5.6 for details.



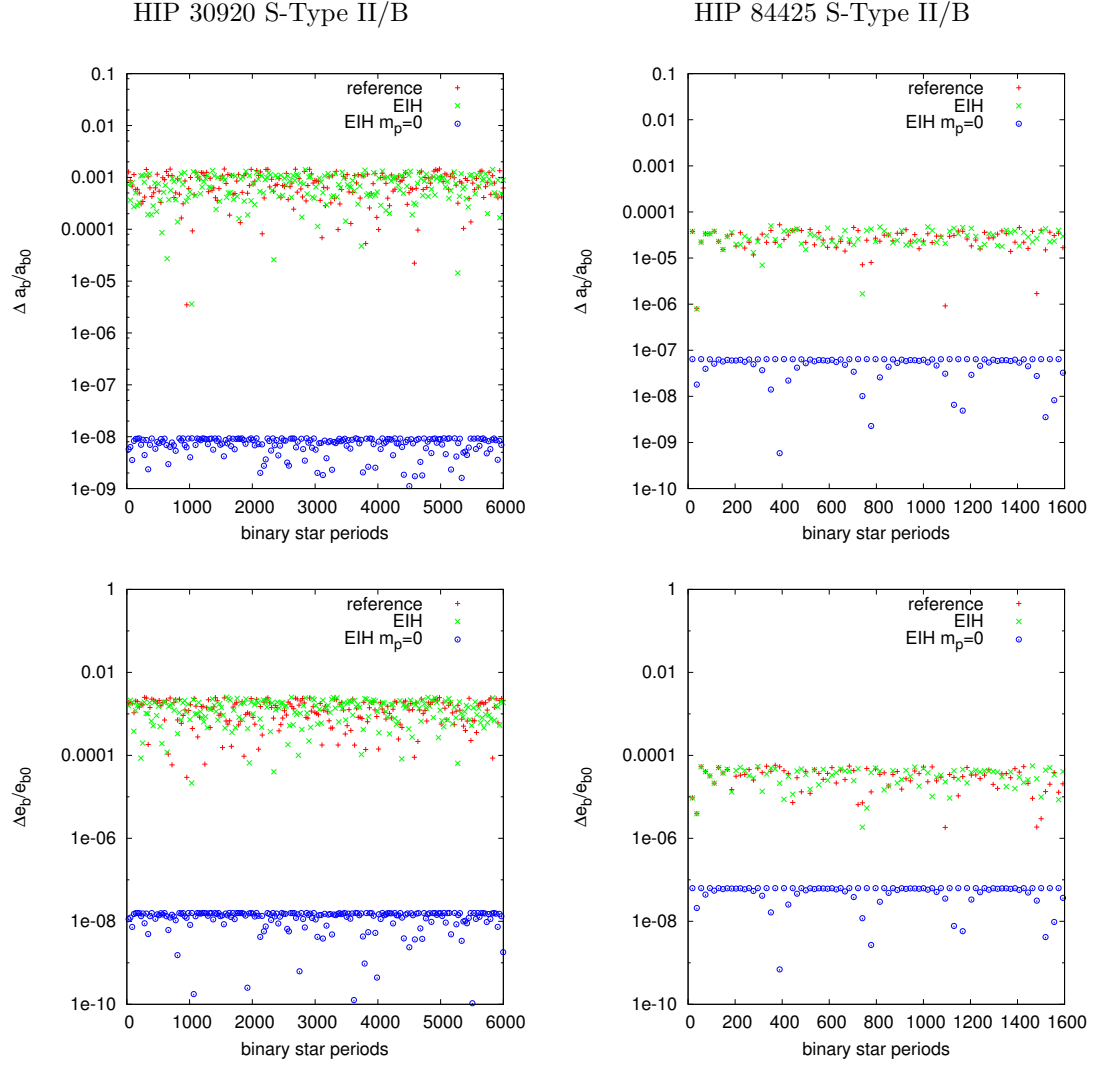


**Figure 5.13:** Same as Figure 5.12 but for the binaries' semimajor axes ( $a_b$ ) and eccentricities ( $e_b$ ) instead of the planet's. The deviations in  $a_b$  and  $e_b$  are normalized with regard to the respective initial values ( $a_{b0}, e_{b0}$ ). Relativistic effects are negligible compared to three body perturbations. See text for details.

close to  $e_p = 0.22$  in the center right graph of Figure 5.12.

For habitable planets experiencing weak external perturbations - as would be the case in the HIP 30920 system - the semimajor axis ( $a_p$ ) remains practically constant. This is important, since  $da/dt = 0$  is an essential requirement for our HZ estimates to be applicable. As expected for Earth-sized planets, the massless and massive solutions basically coincide for HIP 30920. Visible differences between GR and Newtonian models occur in HIP 30920, but the fact that our analytically derived  $e_p^{max}$  (chapter 2, appendix B) overestimates the actual EIH eccentricities slightly only causes our HZ boundaries to be more conservative than necessary. This close to the host star, also tidal effects should be included in the planet's orbit evolution equations. The effects of tides on the orbit, however, cannot be decoupled from the evolution of the planet's

## 5. DISCUSSION

---

rotation and obliquity (see e.g. chapter 4, section 7) which would in turn influence the planetary atmosphere. Thus, a study on combined atmospheric and dynamic effects would be required to produce reasonable results. Such a study goes beyond the scope of this thesis. We will, therefore, not commit halfhearted attempts to include tidal effects in our current investigations.

The strong stellar perturbations encountered by a planet in HIP 84425 lead to deviations up to 6% in  $a_p$  with respect to the initial value  $a_{p0}$ . The middle graph in the right column of Figure 5.12 shows that the analytic  $e_p^{max}$  estimates can no longer account for the brief spikes in planetary eccentricity. Hence, our values for the PHZ so close to the border of orbital instability might be too optimistic. This is a consequence of Newtonian physics, though, as the perturbations due to the secondary are dominating the planetary dynamics. All numerical predictions for  $e_p^{max}$  are practically identical ( $e_p^{max} = 0.2245 \pm 0.0005$ ) but roughly 20% higher than our analytical value ( $e_p^{max} = 0.1768$ ), cf. the horizontal lines in the right center panel of Figure 5.12. A clear sign of the dynamical unrest in this configuration is mirrored in the fact that the different solutions start to diverge rapidly with time. This can be seen in the mixing of the deviation curves in the  $e_p$  and  $\varpi_p$  graphs for HIP 84425 towards the end of the simulation. Interestingly, for  $e_p$  and  $\varpi_p$  the EIH solution seem to agree longer with the reference curves than the restricted models. This suggests that it is more important to include the planet's mass than GR, if the gravitational interaction between the planet and the second star grows strong.

Of course, GR will also affect the orbits of the binaries HIP 30920AB and HIP 84425AB themselves. Results regarding those changes are presented in Figure 5.13. In the relativistic R3BP ( $EIHm_p = 0$ ), there are small deviations from the initial orbits in both binaries that are solely attributable to GR. Yet, the dominating changes in orbits of the binaries HIP 30920 and HIP 84425 are due to the gravitational interactions with the habitable Earth-mass planet.

In summary, we find that the analytic  $e_p^{max}$  estimates for both systems HIP 30920 and HIP 84425 seem to be off by about 15-20%. GR is mainly responsible for model discrepancies in HIP 30920, whereas the second star's gravitational interplay with the planet outweighs the additional influence of GR in HIP 84425. The consequences for the PHZ in HIP 30920 remain small, since  $e_p$  is very low and  $a_p$  does not change significantly with time. In contrast, the strong gravitational interactions in HIP 84425 will reduce the PHZ by roughly 10%. These results suggest, that the quality of HZ estimates would benefit more from improved estimates regarding strongly perturbed Newtonian systems than from an incorporation of GR.

### 5.7 Planetary Atmospheric Models

Many recent studies on planetary habitability make use of LEBMs and GCMs in order to be able to study the time dependent climate forcing such as encountered by planets on eccentric orbits (e.g. Dressing et al. 2010, Forgan 2012, Kite et al. 2011, Williams & Pollard 2002, and references therein). Since the coupled time variation of the planet's insolation and eccentricity have been identified as key-parameters for habitability in this work, the question arises why an RBM was chosen over LEBMs or GCMs in order to study habitable zones in binary star systems? Would it not have been wiser to select a spatially-resolved and time-dependent atmospheric model, as was done by Forgan (2012), instead of using a globally averaged one? In this section we will discuss why RBMs are better suited for our purpose.

As pointed out in section 1.2.3, estimating the impact of stellar radiation onto a planet's atmosphere is not a trivial task. One reason for KHZs to have become so popular is the ability of Kasting et al. (1993) to condense the complex effects of atmospheric processes on Earth's climate into a single parameter, namely  $S_{eff}$ . Such  $S_{eff}$  values are precomputed, so that a simple relation for the extent of KHZs can be derived, see equation (1.1).

The second reason for the widespread use of Kasting’s method is the constancy of KHZs up to stellar evolutionary timescales. This, however, is based on a common misconception, namely that KHZs are independent of planetary motion (e.g. Kane & Gelino 2012). While allowing for a straight forward construction of HZs around other stars by simply drawing a constant spherical shell around potential targets, this assumption is basically wrong. The extent of HZs generally depends on planetary motion as was shown in chapter 2. Only for planets on circular orbits around single stars can the KHZ be considered to remain constant on dynamical timescales.

Consequently, we aimed to construct a framework for HZs that retains all the popular qualities of Kasting’s approach while still accounting for the dynamical changes in a planet’s orbit

- In order for the new framework to be readily applicable, it should either be fully analytical or rely on precomputed values. The use of resource demanding numerical simulations in order to calculate individual HZs should be avoided.
- Since planetary orbit variations are non-negligible in binary star systems, the method should incorporate information on the variability of planetary insolation. On the other hand, for HZs to remain constant up to stellar evolution timescales time dependencies such as pulsating borders have to be avoided.

Precomputed  $S_{eff}$  values are readily available for RBMs (Kasting et al. 1993, Kopparapu et al. 2013, Underwood et al. 2003). The fact that those values were derived using a globally averaged insolation allows us to treat the planet in a point-mass approximation without having to account for the evolution of additional properties of the system like planetary spin, obliquity and insolation direction. Thus, the problem of determining HZs for binary stars reduces to finding ways to incorporate the three-body dynamics into our HZ model. This has been accomplished by introducing PHZs, EHZs and AHZs, which fulfill the requirement of remaining constant on dynamical timescales while accounting for a planetary orbit’s variability. Details on this process can be found in chapter 2. The beauty of being able to treat the dynamical and atmospheric parts individually lies in the fact that it makes an analytic treatment of the problem possible. Hence, when updated  $S_{eff}$  values become available, they can be incorporated instantly without rerunning a large set of numerical simulations. Kopparapu et al. (2013), for instance, provided new sets of  $S_{eff}$  values for HZ borders around main sequence stars. Applying the analytical methods presented in chapters 2 and 3, updated HZs for all the systems presented in chapter 4 could be obtained in a matter of seconds. The impact of the new  $S_{eff}$  values on previous HZ border estimates is discussed in Table 5.2. A visualization of the systems’ newly derived HZs is provided in Figure 5.14 and a table containing all updated borders and observables is given in appendix 5.A. Updates for the  $\alpha$  Centauri system are included in those tables [HIP 71681(83), (Perryman et al. 1997)]. The changes in most HZ borders stay below 20-25%. Yet, a significant shift of 75% occurs for the system HIP 58001 that contains an A-class star. This discrepancy is due to the fact that the equations determining  $S_{eff}$  in Kopparapu et al. (2013) are of fourth order in stellar effective temperature ( $T_{eff}$ ), whereas the estimates by Underwood et al. (2003) applied previously depend only quadratically on  $T_{eff}$ . As neither author included A-class stars explicitly in their calculations, extrapolations of different order in  $T_{eff}$  are bound to produce diverging results. The lack of consistent  $S_{eff}$  values for spectral types younger than F is one of the reasons for excluding binary stars containing hot components in our HZ studies. A similar effect can be observed for the system HIP 101916 which contains G and K sub-giants. Obviously such systems have to be studied more carefully in the future. While two more systems lose their PHZs to orbital instability, the global picture presented in chapter 4 remains largely unaffected by the new  $S_{eff}$  values.

## 5. DISCUSSION

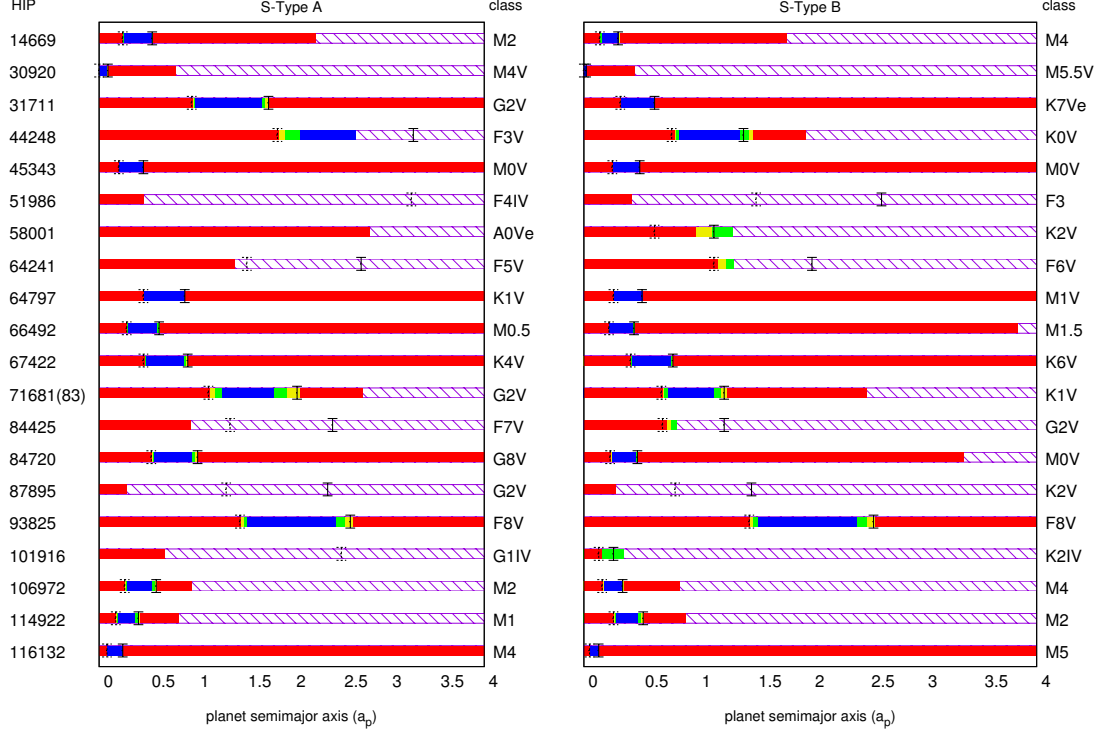


**Figure 5.14:** Updated HZs for selected binary star systems in the solar neighborhood. The systems are ordered by their respective Hipparchos catalog number (HIP). Since the binary stars’ eccentricities are well known, the corresponding habitability maps become pure functions of the semimajor axis of a potential terrestrial planet ( $a_p$ ) orbiting the more massive star (S-Type A) or the less massive companion (S-Type B). If a planet is discovered in red regions it will be uninhabitable due to excessive or insufficient insolation. Critical insolation limits (maximum and runaway greenhouse) were chosen after Kopparapu et al. (2013). In contrast, blue regions denote zones of permanent habitability (PHZs), green zones represent EHZs, and AHZs are drawn in yellow color. Purple stripes denote planetary semimajor axes that would lead to dynamical instability (Holman & Wiegert 1999). The black bars represent KHZ limits. See also Figure 1 in chapter 4. The  $\alpha$  Centauri system [HIP 71681(83)] has been added to this list. The exact values for the new HZ borders can be found in appendix 5.A. For details see section 5.7.

So far, only the benefits of using RBMs have been pointed out. There are, of course, disadvantages of RBMs compared to temporally and spatially resolved atmospheric models. Resonance effects between climate and orbital forcing cannot be accounted for (Dressing et al. 2010). An averaging over global temperatures will also destroy information on potentially habitable temperate zones at high latitudes. Thus, estimates on fractional habitability (e.g. Forgan 2012, Spiegel et al. 2008) become inaccessible. Furthermore, RBMs contain many implicit assumptions on a planet’s rotation rate and the energy distribution within the atmosphere which make them poor tools to study tidal lock states (Kite et al. 2011). So, why not use LEBMs and GCMs?

Unfortunately, there are also difficulties associated with spatially and temporally resolved models. First, while not impossible, it is hard to generate meaningful  $S_{eff}$  values, as many

more parameters will influence the results. Effective insolation values would then have to become functions of obliquities, ocean and landmass distribution, atmospheric energy diffusion constants, etc. Given the dynamic nature of atmospheric behavior it would be difficult to justify smooth interpolation functions since they would annihilate the desired information on resonant or chaotic effects for given initial conditions. A much more severe issue, however, is the need for self-consistent modeling. For LEBMs and GCMs this means that the planet's spin rate, its obliquity as well as its orbital evolution in a binary star system have to be modeled together with the planet's atmospheric dynamics and energy transport. Such a large and intertwined system of equations will not easily permit analytic solutions. Even numerical modeling of such systems is difficult, since the changes of the dynamical parameters happen on different timescales. Consequently, computational feasibility becomes a limiting factor.

Forgan (2012) has attempted to use an LEBM to study habitability in the  $\alpha$  Centauri system. He modified the orbital-longitude and solar declination in his model to account for the light of both stars coming from different directions. He also considered mutual stellar occultations. However, different insolation directions can enhance or reduce temperature gradients between a planet's day and night side. This information is partly<sup>1</sup> lost in LEBMs due to the longitudinal averaging. Most importantly, however, Forgan (2012) could not evolve the planetary orbit and spin self consistently. Instead, he used orbits with fixed eccentricities and obliquities. Arguably, the timescales for atmospheric settling can be much shorter than the timescales of eccentricity and obliquity variation. In the case of  $\alpha$  Centauri however, the settling time of 1000 yrs corresponds to 15 binary orbits. During this time the planet's eccentricity grows from 0 to  $\sim 0.05$  causing an insolation boost of at least 10% during settling time. Whether such changes in insolation would alter Forgan's results drastically can only be speculated upon. In any case, this example shows that self-consistent evolution of a planet's orbit and spin should be considered in time resolved investigations.

Even if all computational obstacles could be overcome, the question remains as what to do with a relatively small number of simulation results? Scanning the parameter space of all likely initial and boundary values via numerical simulations is currently unthinkable. Therefore, the potential merits of using LEBMs and GCMs for a quick determination of HZs in binary star systems seem limited. The study of specific systems could, of course, benefit from advanced models which can reproduce more than averaged quantities. Selsis et al. (2011), for instance, use spatially resolved models to investigate the behavior of likely observables for exoplanet characterization. Yet, considering all options, RBMs seem to be best suited for the purpose of this work.

---

<sup>1</sup>The actual loss of information on stellar insolation direction depends on the planet's obliquity.

## 5. DISCUSSION

HIP ID	$a_b$	$e_b$	S-Type	$a_{crit}$	$\Delta iA$	$\Delta iE$	$\Delta iP$	$\Delta oP$	$\Delta oE$	$\Delta oA$	class
14669	8.96	0.14	A	2.29	5	5	5	10	6	6	M2
			B	1.81	6	3	3	12	6	6	M4
30920	4.29	0.37	A	0.87	6	-	6	-	-	-	M4V
			B	0.47	-	-	-	-	-	-	M5.5V
31711	42.72	0.34	A	8.35	3	3	3	18	18	17	G2V
			B	5.85	5	5	5	9	9	9	K7Ve
44248	10.38	0.15	A	2.69	-	-	-	25	22	21	F3V
			B	1.97	3	4	4	18	15	15	K0V
45343	97.16	0.28	A	17.93	4	4	4	12	12	12	M0V
			B	17.70	4	4	6	12	12	12	M0V
51986	9.88	0.75	A	0.54	-	-	-	-	-	-	F4IV
			B	0.45	-	-	-	-	-	-	F3
58001	11.73	0.30	A	2.83	-	-	-	-	-	-	A0Ve
			B	1.33	-	-	6	71	77	58	K2V
64241	11.78	0.50	A	1.46	-	-	-	-	-	8	F5V
			B	1.34	-	-	-	9	20	20	F6V
64797	89.20	0.12	A	23.21	3	3	4	15	15	15	K1V
			B	18.56	4	4	4	12	12	12	M1V
66492	46.95	0.61	A	4.29	4	6	5	12	9	9	M0.5
			B	3.83	4	7	5	9	9	9	M1.5
67422	32.67	0.45	A	4.50	4	4	3	12	12	12	K4V
			B	4.21	4	4	5	12	10	10	K6V
71681(83)	23.40	0.52	A	2.76	3	3	3	19	18	17	G2V
			B	2.51	4	3	4	17	14	16	K1V
84425	7.73	0.49	A	1.02	-	-	-	-	-	-	F7V
			B	0.84	-	-	-	5	18	17	G2V
84720	91.62	0.78	A	4.28	3	3	3	16	17	17	G8V
			B	3.36	6	4	4	13	13	8	M0V
87895	2.37	0.41	A	0.37	-	-	-	-	-	-	G2V
			B	0.31	-	-	-	-	-	-	K2V
93825	32.73	0.32	A	5.62	3	3	3	19	19	19	F8V
			B	5.57	3	3	3	19	19	18	F8V
101916	15.66	0.80	A	0.75	-	-	-	-	-	-	G1IV
			B	0.38	-	-	46	65	12	12	K2IV
106972	5.30	0.29	A	1.03	5	5	5	9	9	9	M2
			B	0.87	6	6	6	5	11	6	M4
114922	6.74	0.44	A	0.90	6	7	5	12	13	8	M1
			B	0.92	4	6	4	11	11	7	M2
116132	42.48	0.20	A	10.62	6	6	6	6	6	6	M4
			B	7.09	7	7	7	-	-	-	M5
	[au]			[au]	[%]	[%]	[%]	[%]	[%]	[%]	

**Table 5.2:** Differences in HZ borders caused by the switch from  $S_{eff}$  estimates by Underwood et al. (2003) to values published in Kopparapu et al. (2013) are presented. The systems are ordered by their Hipparchos catalog numbers (HIP ID) (Perryman et al. 1997). Binary star semimajor axes ( $a_b$ ) and eccentricities ( $e_b$ ) are given together with the critical semimajor axis ( $a_{crit}$ ) for orbital stability (Holman & Wiegert 1999) and the spectral class of the respective star (last column). The  $\Delta i\{A,E,P\}$  values denote the deviation of inner AHZ, EHZ and PHZ borders, and  $\Delta o\{A,E,P\}$  are the corresponding values for the outer borders' shift. Most of the HZ shifts caused by the exchange of  $S_{eff}$  values remain below 25%. The hotter stars are generally more affected. However, for HIP 85001 containing an A-class star, a much larger discrepancy was found. This is also the case for the sub-giant system HIP 101916. See section 5.7 for details.

## 5.A Updated HZ Borders for Nearby Binary Stars

An updated listing of HZ borders and detectability thresholds for terrestrial planets in binary star systems closer than 30 pc is presented. The original data can be found in chapter 4, Table 2. Column three represents the critical semimajor axes ( $a_{crit}$  [au]) for orbital stability (Holman & Wiegert 1999). Updated borders for the HZs ([au]) using the  $S_{eff}$  values by Kopparapu et al. (2013) are presented in columns 4 to 9. Additionally, rms radial velocity (RV [cm/s]) and astrometric (AM [ $\mu$ as]) signatures of terrestrial planets have been re-evaluated at the HZ borders. The conditions required for a planet to be within the Averaged (AHZ), Extended (EHZ) and Permanently (PHZ) Habitable Zone are discussed in chapter 2. Fields containing dashes (-) represent cases where a given HZ border lies beyond the critical semimajor axis  $a_{crit}$ . Such systems would not be dynamically stable. Question marks occur in some boundaries, for instance in those of the HIP 30920 and 84425 systems, because it was shown in section 5.6 that the analytic dynamical modeling becomes unreliable, if the planet orbits near the stability limit or very close to its host-star (we neglected tidal forces).

HIP ID	star	$a_{crit}$	inner AHZ	inner EHZ	inner PHZ	outer PHZ	outer EHZ	outer AHZ	
14669	A (M2)	2.287	0.332	0.334	0.338	0.618	0.626	0.634	HZ
			21.18	21.12	21.00	15.69	15.60	15.50	max RV
			14.78	14.74	14.65	10.84	10.77	10.70	rms RV
			0.116	0.117	0.119	0.219	0.222	0.225	max AM
			0.082	0.082	0.083	0.152	0.154	0.156	rms AM
	B (M4)	1.806	0.175	0.175	0.177	0.331	0.335	0.337	HZ
			34.69	34.69	34.49	25.37	25.22	25.15	max RV
			24.36	24.36	24.22	17.71	17.61	17.55	rms RV
			0.087	0.087	0.088	0.166	0.168	0.169	max AM
			0.062	0.062	0.062	0.117	0.118	0.119	rms AM
30920	A (M4V)	0.865	0.092	0.094	0.094	0.170	0.174	0.178	HZ
			50.84	50.32	50.32	38.10	37.69	37.30	max RV
			35.14	34.76	34.76	25.84	25.54	25.25	rms RV
			0.310	0.317	0.317	0.584	0.598	0.612	max AM
			0.252	0.257	0.257	0.466	0.477	0.488	rms AM
	B (M5.5V)	0.470	0.028?	0.028?	0.028?	0.054	0.054	0.054	HZ
			154.95	154.95	154.95	111.89	111.89	111.89	max RV
			108.82	108.82	108.82	78.08	78.08	78.08	rms RV
			0.264	0.264	0.264	0.516	0.516	0.516	max AM
			0.218	0.218	0.218	0.424	0.424	0.424	rms AM
31711	A (G2V)	8.351	1.035	1.047	1.059	1.741	1.773	1.809	HZ
			8.94	8.89	8.84	7.00	6.94	6.87	max RV
			6.18	6.14	6.11	4.76	4.72	4.67	rms RV
			0.146	0.148	0.150	0.250	0.254	0.260	max AM
			0.101	0.103	0.104	0.171	0.174	0.177	rms AM
	B (K7Ve)	5.848	0.350	0.350	0.352	0.642	0.646	0.650	HZ
			20.29	20.29	20.24	15.08	15.04	14.99	max RV
			14.24	14.24	14.20	10.52	10.48	10.45	rms RV
			0.088	0.088	0.088	0.162	0.163	0.164	max AM
			0.062	0.062	0.062	0.113	0.114	0.114	rms AM
44248	A (F3V)	2.686	1.913	1.971	2.117	2.686?	2.686?	2.686?	HZ
			4.44	4.39	4.28	-	-	-	max RV
			2.90	2.85	2.75	-	-	-	rms RV
			0.272	0.281	0.305	-	-	0.000	max AM
			0.213	0.220	0.236	-	-	-	rms AM
	B (K0V)	1.967	0.820	0.830	0.856	1.386	1.472	1.512	HZ
			8.19	8.14	8.03	6.50	6.35	6.29	max RV
			5.61	5.58	5.50	4.32	4.19	4.13	rms RV
			0.179	0.181	0.187	0.312	0.333	0.343	max AM
			0.147	0.149	0.154	0.249	0.264	0.272	rms AM
45343	A (M0V)	17.932	0.288	0.290	0.290	0.540	0.540	0.542	HZ
			8.41	8.38	8.38	6.15	6.15	6.14	max RV
			5.93	5.91	5.91	4.33	4.33	4.32	rms RV
			0.290	0.292	0.292	0.545	0.545	0.547	max AM
			0.280	0.282	0.282	0.525	0.525	0.527	rms AM
	B (M0V)	17.698	0.276	0.278	0.278	0.518	0.518	0.520	HZ
			8.67	8.64	8.64	6.34	6.34	6.33	max RV
			6.12	6.10	6.10	4.47	4.47	4.46	rms RV
			0.284	0.286	0.286	0.534	0.534	0.536	max AM
			0.274	0.276	0.276	0.515	0.515	0.517	rms AM
51986	A (F4IV)	0.545	-	-	-	-	-	-	HZ
	B (F3)	0.448	-	-	-	-	-	-	HZ
58001	A (A0Ve)	2.828	-	-	-	-	-	-	HZ
	B (K2V)	1.331	1.013	1.147	1.331?	1.331?	1.331?	1.331?	HZ
			8.47	8.09	-	-	-	-	max RV
			5.55	5.21	-	-	-	-	rms RV
			0.164	0.188	-	-	-	-	max AM
			0.127	0.144	-	-	-	-	rms AM
64241	A (F5V)	1.465	-	-	-	-	-	-	HZ
	B (F6V)	1.339	1.200	1.274	1.339?	1.339?	1.339?	1.339?	HZ
			9.20	9.05	-	-	-	-	max RV
			5.53	5.37	-	-	-	-	rms RV
			0.213	0.229	-	-	-	-	max AM
			0.130	0.139	-	-	-	-	rms AM

## 5. DISCUSSION

HIP ID	star	$a_{crit}$	inner AHZ	inner EHZ	inner PHZ	outer PHZ	outer EHZ	outer AHZ	
64797	A (K1V)	23.212	0.538	0.538	0.538	0.958	0.958	0.960	HZ
			14.49	14.49	14.49	10.88	10.88	10.86	max RV
			10.23	10.23	10.23	7.67	7.67	7.66	rms RV
			0.204	0.204	0.204	0.364	0.364	0.365	max AM
			0.144	0.144	0.144	0.257	0.257	0.258	rms AM
	B (M1V)	18.564	0.287	0.287	0.287	0.541	0.541	0.543	HZ
			23.46	23.46	23.46	17.10	17.10	17.07	max RV
			16.57	16.57	16.57	12.07	12.07	12.05	rms RV
			0.152	0.152	0.152	0.287	0.287	0.288	max AM
			0.108	0.108	0.108	0.203	0.203	0.204	rms AM
66492	A (M0.5)	4.289	0.371	0.375	0.379	0.675	0.687	0.699	HZ
			11.68	11.62	11.57	8.80	8.72	8.65	max RV
			8.11	8.06	8.02	6.01	5.96	5.91	rms RV
			0.088	0.089	0.090	0.163	0.166	0.169	max AM
			0.079	0.080	0.081	0.143	0.146	0.149	rms AM
	B (M1.5)	3.835	0.248	0.250	0.252	0.460	0.466	0.470	HZ
			15.73	15.67	15.60	11.67	11.60	11.55	max RV
			10.98	10.94	10.89	8.06	8.01	7.97	rms RV
			0.072	0.072	0.073	0.135	0.137	0.138	max AM
			0.064	0.065	0.065	0.120	0.121	0.122	rms AM
67422	A (K4V)	4.503	0.546	0.552	0.558	0.954	0.972	0.992	HZ
			10.86	10.80	10.74	8.35	8.28	8.20	max RV
			7.50	7.46	7.42	5.68	5.62	5.57	rms RV
			0.175	0.177	0.179	0.311	0.317	0.323	max AM
			0.146	0.148	0.149	0.255	0.260	0.265	rms AM
	B (K6V)	4.212	0.440	0.444	0.450	0.788	0.802	0.814	HZ
			12.74	12.68	12.60	9.65	9.58	9.51	max RV
			8.84	8.80	8.74	6.61	6.55	6.50	rms RV
			0.157	0.158	0.161	0.285	0.290	0.295	max AM
			0.132	0.133	0.135	0.236	0.240	0.244	rms AM
71681(83)	A (G2V)	2.763	1.207	1.257	1.329	1.861	1.993	2.123	HZ
			8.39	8.25	8.06	7.07	6.90	6.75	max RV
			5.45	5.34	5.19	4.39	4.24	4.11	rms RV
			2.691	2.811	2.986	4.319	4.665	5.011	max AM
			1.788	1.863	1.970	2.764	2.961	3.156	rms AM
	B (K1V)	2.508	0.716	0.734	0.758	1.170	1.226	1.276	HZ
			11.46	11.33	11.17	9.24	9.06	8.91	max RV
			7.69	7.60	7.48	6.02	5.88	5.76	rms RV
			1.830	1.878	1.943	3.077	3.236	3.378	max AM
			1.253	1.285	1.327	2.050	2.149	2.237	rms AM
84425	A (F7V)	1.024	-	-	-	-	-	-	HZ
			0.752	0.794	0.835?	0.835?	0.835?	0.835?	HZ
			11.86	11.68	-	-	-	-	max RV
			7.19	7.00	-	-	-	-	rms RV
			0.100	0.106	-	-	-	-	max AM
84720	A (G8V)	4.275	0.620	0.632	0.642	1.034	1.060	1.092	HZ
			7.79	7.72	7.66	6.16	6.09	6.01	max RV
			5.33	5.28	5.24	4.13	4.07	4.01	rms RV
			0.279	0.285	0.290	0.476	0.488	0.504	max AM
			0.247	0.251	0.255	0.412	0.422	0.435	rms AM
	B (M0V)	3.364	0.264	0.266	0.268	0.484	0.490	0.498	HZ
			14.77	14.71	14.66	11.03	10.97	10.88	max RV
			10.29	10.26	10.22	7.60	7.56	7.49	rms RV
			0.186	0.187	0.189	0.344	0.349	0.355	max AM
			0.167	0.168	0.169	0.306	0.310	0.315	rms AM
87895	A (G2V)	0.371	-	-	-	-	-	-	HZ
	B (K2V)	0.312	-	-	-	-	-	-	HZ
93825	A (F8V)	5.623	1.527	1.555	1.593	2.487	2.575	2.657	HZ
			3.43	3.40	3.36	2.75	2.71	2.67	max RV
			2.33	2.31	2.28	1.83	1.79	1.77	rms RV
			0.221	0.225	0.231	0.368	0.382	0.395	max AM
			0.198	0.202	0.207	0.323	0.335	0.346	rms AM
	B (F8V)	5.575	1.484	1.512	1.548	2.422	2.508	2.584	HZ
			3.50	3.47	3.43	2.80	2.76	2.73	max RV
			2.38	2.36	2.33	1.86	1.83	1.80	rms RV
			0.217	0.222	0.227	0.363	0.377	0.389	max AM
			0.196	0.199	0.204	0.319	0.331	0.341	rms AM
101916	A (G1IV)	0.754	-	-	-	-	-	-	HZ
			0.179	0.183	0.381?	0.381?	0.381?	0.381?	HZ
			35.75	35.40	-	-	-	-	max RV
			23.83	23.57	-	-	-	-	rms RV
			0.052	0.053	-	-	-	-	max AM
106972	A (M2)	1.034	0.036	0.037	-	-	-	-	rms AM
			0.350	0.358	0.368	0.616	0.646	0.674	HZ
			19.98	19.78	19.53	15.65	15.36	15.11	max RV
			13.43	13.28	13.10	10.12	9.88	9.68	rms RV
			0.080	0.082	0.085	0.146	0.154	0.162	max AM
	B (M4)	0.865	0.057	0.059	0.060	0.101	0.106	0.111	rms AM
			0.195	0.199	0.201	0.357	0.369	0.377	HZ
			30.20	29.91	29.77	22.83	22.49	22.28	max RV
			20.76	20.55	20.44	15.34	15.09	14.92	rms RV
			0.058	0.059	0.060	0.109	0.113	0.115	max AM
114922	A (M1)	0.897	0.042	0.043	0.044	0.078	0.080	0.082	rms AM
			0.262	0.268	0.276	0.454	0.476	0.496	HZ
			23.58	23.34	23.04	18.55	18.19	17.89	max RV
			15.85	15.67	15.45	12.04	11.76	11.52	rms RV
			0.055	0.056	0.058	0.099	0.104	0.109	max AM
B (M2)	0.924	0.041	0.042	0.043	0.071	0.074	0.077	rms AM	
		0.290	0.298	0.308	0.502	0.530	0.554	HZ	
		21.97	21.70	21.39	17.35	16.98	16.68	max RV	
		14.69	14.49	14.25	11.16	10.87	10.63	rms RV	
		0.058	0.060	0.062	0.105	0.111	0.116	max AM	
116132	A (M4)	10.619	0.043	0.044	0.046	0.074	0.079	0.082	rms AM
			0.171	0.171	0.171	0.327	0.327	0.327	HZ
			29.63	29.63	29.63	21.46	21.46	21.46	max RV
			20.91	20.91	20.91	15.12	15.12	15.12	rms RV
			0.221	0.221	0.221	0.423	0.423	0.423	max AM
	B (M5)	7.091	0.178	0.178	0.178	0.340	0.340	0.340	rms AM
			0.083	0.083	0.083	0.159	0.159	0.159	HZ
			58.31	58.31	58.31	42.16	42.16	42.16	max RV
			41.19	41.19	41.19	29.76	29.76	29.76	rms RV
			0.202	0.202	0.202	0.387	0.387	0.387	max AM
0.163	0.163	0.163	0.312	0.312	0.312	rms AM			



## Chapter 6

# The Road Ahead

The previous sections have shown that there is still room for improvement of the analytical HZ determination method presented in chapter 2. A comprehensive investigation of HZs in mutually inclined systems (see section 5.3) will be one of our next steps. Analytic eccentricity estimates for mutually inclined hierarchical triple systems are available in literature (e.g. Krymowski & Mazeh 1999, Naoz et al. 2012a). Those include, however, only secular approximations that do not account for short periodic terms. Whether the inclusion of short periods in analytic eccentricity and inclination estimates for mutually inclined systems is absolutely necessary will have to be checked very carefully given the considerable analytic effort such an endeavor would require. The extension of our model to three dimensions will also make the analytic determination of minimum and maximum insolation conditions more challenging. All these points considered, it will not be a trivial task to generate HZ estimates for mutually inclined systems that are of equal quality as the ones presented for the coplanar case. We consider it to be a worthwhile goal, though.

Given the discovery of more and more circumbinary planets in the wake of the Kepler mission (e.g. Welsh et al. 2012), the application of the PHZ, EHZ and AHZ classification system to P-Type configurations may become another potentially important contribution to HZ research. Preliminary studies show that changes in the planet's eccentricity play a crucial role for planetary insolation in P-Type as well as in S-Type systems. Numerical evidence supporting this claim is presented in Figure 6.1. Short period terms also seem important for circumbinary planetary eccentricities (right panel of Figure 6.1), especially since relatively small changes in a planet's eccentricity are sufficient to change a circumbinary planet's insolation drastically, cf. Figure 3 in chapter 2 and Figure 6.1. Yet, planetary eccentricity variations are completely ignored in current studies (e.g. Kane & Hinkel 2012).

If a given P-Type system can be modeled as a hierarchical triple configuration with initially circular binary and planetary orbits, Georgakarakos (2009) provides expressions for the evolution of the outer - in this case the planetary - eccentricity vector. His estimates are again based on a combination of secular solutions and short period terms acquired from a Legendre-expansion of the outer Laplace-Runge-Lenz vector. A similar approach was discussed in appendix 1.A for the eccentricity vector of the inner orbit.

The expressions in Georgakarakos (2009) allow us to construct analytical PHZ estimates for P-Type systems on initially circular orbits following the methodology presented in chapter 2. In order to derive the planet's maximum eccentricity ( $e_p^{max}$ ) we consider the case where all the short periodic and secular oscillations of the outer eccentricity vector interfere constructively. Assuming furthermore that constructive interference may happen at moments when the

## 6. THE ROAD AHEAD

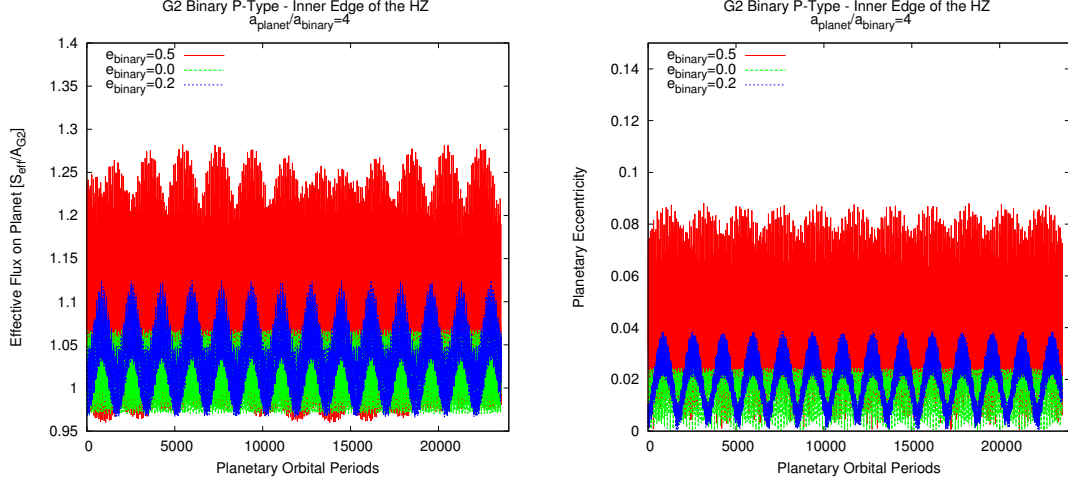


**Figure 6.1:** Effective insolation (*left*) and eccentricity (*right*) evolution of an Earth-like planet in P-Type orbit around three G2V-G2V binaries with different eccentricities ( $e_b$ ) and a semimajor axis of  $a_b = 0.3$  au. The coupling between planetary eccentricity and effective insolation can clearly be identified.

eccentricity vector has no "y"-component, we can use equation (4) in Georgakarakos (2009) to calculate

$$e_p^{max} = \frac{m_0 m_1}{(m_0 + m_1)^{4/3} M^{2/3} X^{4/3}} \left[ \frac{3}{4} + \frac{1}{X} \left( \frac{3}{16} + \frac{21}{16} \right) \right] + e_p^{sec}, \quad (6.1)$$

where  $m_0$  and  $m_1$  are the masses of the primary and secondary,  $M$  is the total mass of the system and  $X$  is the system's period ratio, see appendix 1.A. The secular eccentricity amplitude ( $e_p^{sec}$ ) can be estimated from the fact that the initial planetary eccentricity at  $t = 0$  vanishes, whereas the short period contribution ( $e_p^{sp}$ ) does not. Therefore, we have

$$e_p^{sec} \simeq -e_p^{sp} \quad \text{for} \quad t = 0. \quad (6.2)$$

Using the short period contributions of equations (4) and (5) in Georgakarakos (2009) at  $t = 0$  we find

$$|e_p^{sec}| \simeq |e_p^{sp}|_{t=0} = \frac{3}{16} \frac{m_0 m_1 (113 - 64X + 16X^2)^{1/2}}{(m_0 + m_1)^{4/3} M^{2/3} X^{7/3}}. \quad (6.3)$$

Combining the short period and secular eccentricity amplitudes finally results in

$$e_p^{max} = \frac{3}{16} \frac{m_0 m_1 [8 + 4X + (113 - 64X + 16X^2)^{1/2}]}{(m_0 + m_1)^{4/3} M^{2/3} X^{7/3}}. \quad (6.4)$$

Please note that this estimate is only valid in P-Type systems where the binary's and the planet's orbit are initially circular. Preliminary results on the performance of the analytic  $e_p^{max}$  estimate of equation (6.4) are presented in Figure 6.2 (top left panel).

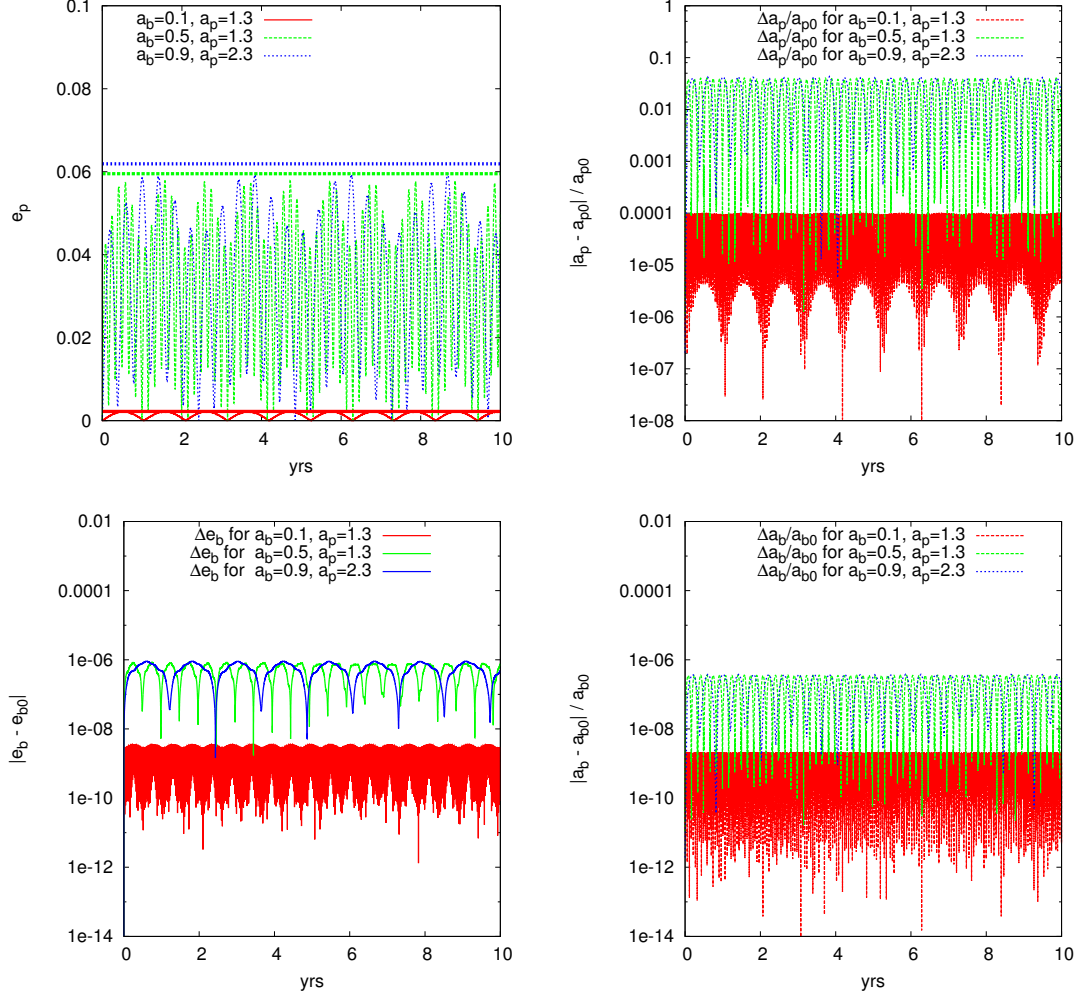


**Figure 6.2:** Eccentricity and semimajor axis evolution in P-Type systems consisting of three G2V-G2V binaries orbited by an Earth-like planet. The systems’ orbital evolution is investigated in a Newtonian model. All bodies were started on coplanar circular orbits. *Top left:* Planetary eccentricity ( $e_p$ ) evolution for three different P-Type configurations. The horizontal lines represent analytical maximum eccentricity estimates ( $e_p^{max}$ ), see equation (6.4). The coloring indicates the corresponding ( $e_p$ ,  $e_p^{max}$ ) pairs. *Top right:* Deviation of the planetary semimajor axes ( $a_p$ ) from their initial values ( $a_{p0}$ ), where  $\Delta a_p = |a_p - a_{p0}|$ . Changes in  $a_p$  remain below 5% in all cases. *Bottom:* In all three systems, the binary stars’ orbits do not vary significantly.

Having analytical estimates for the planet’s eccentricity at our disposal, formulae for P-Type PHZs can be constructed. We, therefore, have to identify those binary-planet configurations that produce extreme planetary insolation conditions. Let us consider Figure 6.3. Even though the shortest distance between one star and the planet ( $\delta$ ) is clearly attributable to configuration II (Figure 6.3, right), one might wonder, whether the contribution of second star in configuration I (Figure 6.3, left) could make up for the increased distance between the planet and first star? In other words, is there any planetary pericenter distance  $q = a_p(1 - e_p^{max})$

## 6. THE ROAD AHEAD

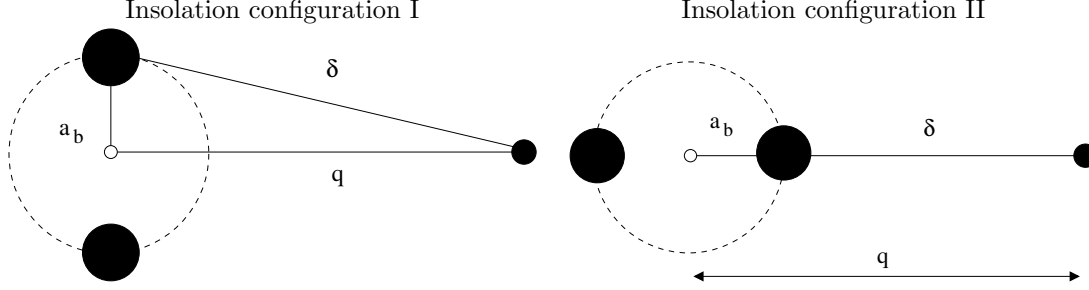


**Figure 6.3:** Two possible insolation configurations in P-Type binary-planet systems. The binary is represented by the big filled circles, whereas the planet is shown as a smaller black disc. The planet’s pericenter distance in Jacobian coordinates is named  $q$ ,  $\delta$  is the planet’s distance to one binary component, and  $a_b$  represents the binary’s semimajor axis. If the orbit of the binary is circular and  $q > a_b$ , then configuration II always yields the maximum planetary insolation, see equations (6.5-6.7).

where configuration I offers higher insolation values than configuration II?

As our  $e_p^{max}$  are only valid for binaries on circular orbits, we will restrict ourselves to such cases.

Should the binary consist of stars with different luminosities, maximum planetary insolation values will be achieved when the distance to the more luminous<sup>1</sup> star is shortest. Hence, configuration II will yield the highest and lowest possible insolation values depending on whether the planet is closest to or farthest from the more luminous star. In reality this is not exactly true, of course, since stellar occultation would split and shift the insolation maximum slightly to configurations where the second star is (partly) visible from a planetary perspective. However, for stellar separations much larger than the stars’ radii ( $a_b \gg R_\star$ ), such shifts are negligible. Accepting this condition as a prerequisite, we neglect occultation effects in our following considerations.

Should both stars have the same luminosity ( $L_1 = L_2 = L$ ), one could try to find a relation between  $q$  and  $a_b$  for the limit case  $S_{tot}^I = S_{tot}^{II}$ , i.e. the total planetary insolation in configuration I equals the total insolation in configuration II. If such a pair ( $q, a_b$ ) exists, a unique maximum insolation configuration cannot be identified. Let us, therefore, investigate, whether there are values for  $q$  and  $a_b$  which would allow for  $S_{tot}^I = S_{tot}^{II}$ . Simple geometric considerations lead to

$$S_{tot}^I = \frac{2L}{a_b^2 + q^2} = S_{tot}^{II} = \frac{L}{(q - a_b)^2} + \frac{L}{(q + a_b)^2} \quad (6.5)$$

Solving equation (6.5) for  $q$  one finds

$$q = \frac{1}{3}(1 + 2a_b) - \frac{1 - 8a_b + a_b^2}{3A(a_b)} - \frac{A(a_b)}{3} \quad (6.6)$$

where  $A(a_b) = (-1 + 12a_b + 15a_b^2 + 28a_b^3 + 3^{3/2}\sqrt{-3a_b^2 + 32a_b^3 + 26a_b^4 + 32a_b^5 + 29a_b^6})^{1/3}$ . Since we also require orbital stability for our P-Type systems, we must have  $q \geq 2.37a_b$ . This conservative limit corresponds to a planet on an UCO assuming that  $e_b = 0$ , see equation (1.6). However, trying to solve

$$2.37a_b = \frac{1}{3}(1 + 2a_b) - \frac{1 - 8a_b + a_b^2}{3A(a_b)} - \frac{A(a_b)}{3} \quad (6.7)$$

<sup>1</sup>Please note that it is, in fact, the effective luminosity that is referred to here, i.e. the star’s luminosity normalized with respect to the corresponding effective insolation values.

only results in values  $a_b \leq 0$ . In other words, there is no positive binary semimajor axes in a P-Type system where configuration I would cause a higher insolation on a planet than configuration II. Hence, we can conclude that configuration II (Figure 6.3, right) always produces the maximum planetary insolation. In analogy to S-Type systems (chapter 2), we can, therefore, formulate maximum and minimum insolation conditions for PHZs in P-Type systems with initially circular orbits.

The *maximum insolation condition* for the PHZ reads

$$1 \geq \max \left( \frac{L_1}{A_1} (q \mp a_b)^{-2} + \frac{L_2}{A_2} (q \pm a_b)^{-2} \right), \quad (6.8)$$

and the *minimum insolation condition* is

$$1 \leq \min \left( \frac{L_1}{B_1} (Q^2 + a_b^2)^{-1} + \frac{L_2}{B_2} (Q^2 + a_b^2)^{-1}, \frac{L_1}{B_1} (Q \mp a_b)^{-2} + \frac{L_2}{B_2} (Q \pm a_b)^{-2} \right). \quad (6.9)$$

where  $q = a_p(1 - e_p^{max})$ ,  $Q = a_p(1 + e_p^{max})$  and  $A_{1,2}$  and  $B_{1,2}$  are the effective insolation limits for the inner and outer borders of the KHZ, see chapter 2. More recent effective insolation limits can be found in Kopparapu et al. (2013). In the derivation of equations (6.4), (6.8) and (6.9) we have assumed that the planet's influence on the binary's orbit is negligible, and that the planet's semimajor axis remains constant. Figure 6.2 shows that this is the case, at least for the three G2V-G2V systems investigated therein. While it seems straight forward to follow the recipe presented in chapter 2 from this point on, i.e. to derive analytic expressions for AHZ and EHZ boundaries, one should keep in mind that non Newtonian dynamical aspects have to be taken more seriously, when binary stars with  $a_b < 1$  au are studied. Neglecting tidal and GR interactions may be permissible for hierarchical triples exhibiting reasonable separations, but in the case of two stars packed within 1 au, such effects become important (Eggleton 2006). It is, therefore, very likely that tidal effects and GR have to be included in any analytical HZ classification framework.

A preliminary PHZ, EHZ and AHZ classification of planetary P-Type orbits around F0V-F0V and G2V-G2V binary stars without accounting for tidal effects or GR will not provide reliable HZ border estimates, but interesting first insights can be gained. As mentioned earlier, the planet does not have a significant influence on the double star's orbit (Figure 6.2, bottom). Also, the injected planetary eccentricities appear to remain low if all orbits are initially circular (Figure 6.2, top left panel). Nevertheless, a considerable shrinkage of the PHZ with growing binary semimajor axes can be observed (Figure 6.4). The semi-analytical PHZ results (blue) are in good correspondence with the analytically derived PHZs. The latter are delimited by the white dashed and dotted lines in Figure 6.4. Similar to S-Type systems, the AHZ and EHZ correspond better to the commonly applied KHZ estimates. The AHZ also extends a bit further than single-source KHZ limits would predict. While no analytical estimates are available for P-Type systems on eccentric orbits, numerical investigations suggest a negative correlation between the PHZs' extent and binary's eccentricity as well, see e.g. Figure 1.8.

It is clear, however, that extensive analytical as well as numerical studies will be necessary to confirm these preliminary results. Whether the incorporation of GR and stellar tides into HZ models will change our preliminary findings drastically remains to be seen.

Apart from binary star systems, there are other scenarios where the analytical estimates derived in this work could come in handy. Our analytic HZ estimates are applicable to extrasolar Sun-Jupiter-Earth systems, for instance. In fact, our HZ classification framework can be easily modified to such cases. One simply neglects the luminosity of the "secondary" ( $L_2 = 0$ ) while retaining its gravitational influence on the planet. Since Georgakarakos' eccentricity estimates

## 6. THE ROAD AHEAD

were tested to be valid for a large range of mass ratios, no alterations in the analytical estimates should be necessary.

Ultimately, it can be imagined to expand our analytical description of planetary insolation to include more than three bodies. Providing a self-consistent evolution of a planet's orbit, its spin and its obliquity could be another worthy goal. The latter has already been studied semi-analytically by Correia et al. (2011). Similar analytic results could then serve as input for LEBMs or GCMs and allow for a self-consistent treatment of planetary atmospheres in binary star systems.

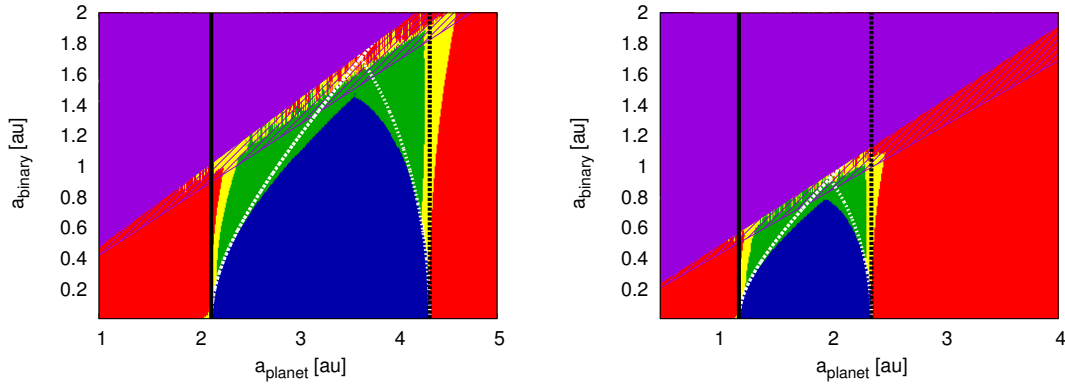


**Figure 6.4:** Habitability maps of two coplanar P-Type systems, where an Earth-like circumbinary planet orbits two F0V stars (*left*) and two G2V stars (*right*), respectively. Instead of investigating the influence of the binary's eccentricity on habitability, a correlation between initial binary and planetary semimajor axes is presented. The orbital elements are given in a Jacobian reference frame. All bodies have been started on circular orbits, but the planetary and binary orbits were free to evolve thereafter. The color coding is similar to Figure 5.3, except for the borders of orbital stability (purple) which have been calculated following Dvorak (1986). The purple striped area represents UCOs, the solid purple region LCOs, see section 1.3.1. The black vertical lines indicate KHZ limits for a single radiation source at the binary's barycenter. PHZs (blue) have been calculated semi-analytically, where numerically evaluated planetary eccentricities were inserted in equations (6.8) and (6.9). EHZ (green) and AHZ (yellow) have been calculated numerically. The white dotted lines represent analytically derived PHZ borders, where equation (6.4) was used. There is a pronounced dependency of P-Type HZs on the binary's initial semimajor axis.

## Chapter 7

# Summary & Conclusions

Given the large number of nearby stars that are members of binary and multiple star systems (Duquennoy & Mayor 1991, Raghavan et al. 2010) it is not unreasonable to think that some of them host Earth-like planets. This notion is supported by the recent discovery of a terrestrial planet in one of our galactic neighborhood's binary stars,  $\alpha$  Centauri AB (Dumusque et al. 2012). Whether such telluric planets can form in regions that would permit liquid water on their surface is a hotly debated question in astrophysics (e.g. Thebault 2011) which, ultimately, can be answered by observational evidence alone. Yet, in order to find habitable worlds in double star systems, one must first know where to look for them.

We tackled this issue by investigating the processes that govern planetary habitability in binary star systems. Reproducing results by Harrington (1977) we found that planets in binary star systems face large variations in insolation. In chapter 2 we were able to show, however, that most of the planetary insolation changes commonly attributed to the second star (e.g. Harrington 1977) are, in fact, due to a gravity-induced deformation of the planet's orbit. The forced changes in planetary eccentricity cause noticeable differences in the distance between the planet and its host star, which, in turn, affect planetary insolation. The additional radiative contribution of the second star will only become equally important, if the planet orbits a host star considerably less luminous than the other binary component (chapter 2, Figure 2). Abandoning the anthropocentric view that habitable worlds should have a nearly constant stellar energy input comparable to the Earth's, we constructed analytical estimates for the maximum and average planetary insolation (sections 2.6, 5.1 and 5.2). Hereby, we used results from state-of-the-art perturbation theory (section 1.3.5).

Apart from stellar radiation atmospheric processes can have a decisive influence on a planet's habitability (section 1.2.3). In order to account for the effects of a planet's atmosphere, we used the precomputed RBM results by Kopparapu et al. (2013), Underwood et al. (2003) and Kasting et al. (1993). Combining our analytical insolation estimates with the RBM based effective insolation limits allowed us to introduce three kinds of habitable regions: the PHZ, the EHZ and the AHZ (section 2.5). The PHZ permits permanent habitability, whereas planets in EHZ and AHZ may venture beyond habitable insolation limits to a certain extent. Each planet within the EHZ and AHZ receives an average amount of radiation that could sustain liquid water on its surface. The EHZ requires additionally that most of the planet's orbit remains within areas that permit habitable insolation conditions. This extended classification is capable of taking the dynamical variations in planetary orbits into account while retaining important traits of Kasting's original HZ, such as the time invariance up to stellar evolution timescales (section 5.7). While it is possible to derive analytic expressions for calculating PHZs, EHZs

## 7. SUMMARY & CONCLUSIONS

---

and AHZs on a mathematical basis alone, we found that a combined approach using analytical and numerical tools yields the most reliable models (section 5.2).

After studying the consequences of relaxing certain assumptions that were made during the construction of our analytical HZ determination model (sections 5.3-5.6) we applied our classification scheme to fictitious binary star systems.

Consequent results showed that the circumstellar PHZ tends to shrink considerably with growing binary eccentricity, whereas the AHZ expands slightly towards the second star (chapter 2, Figures 6 and 7). On the one hand this means that the region where a planet receives the "right amount" of radiation throughout its existence is fairly small given an eccentric orbit of the binary star. On the other hand, if Williams & Pollard (2002) are correct and the planet's atmosphere can act as a temperature buffer over months, even average insolation levels might suffice to keep a planet habitable. Then, double stars would offer a greater potential for hosting habitable worlds than single stars. Once again, observational data is required to test these hypotheses.

We, therefore, proceeded to investigate, whether habitable planets in binary star systems can be detected using current observational facilities (chapter 3). To be more precise, we used our previous results to derive analytical estimates for a habitable planet's RV and AM signatures as well as TPs and TDs. Considering  $\alpha$  Centauri a likely candidate for future observations, we investigated similar binary stars featuring Sun-like components and found that the gravitative interaction between a double star and a planet can actually boost the chances for a planet's discovery. Yet, transit photometry seems to be the only method that is currently capable of detecting Earth-like planets in HZs around Sun-like stars (chapter 3). Unfortunately, a discovery of additional habitable planets around  $\alpha$  Centauri B by tracking changes in the orbit of the already known planet  $\alpha$  Cen Bb will be difficult (chapter 3, section 5.3). Hence, we broadened our search for potential observational targets to include binary star systems of other spectral types within a distance of 30 pc from our Solar System (chapter 4). Using the WDC data, we selected systems with well known orbital parameters, calculated the extent of their HZs and determined RV and AM signatures, as well as TPs and TDs of possible habitable planets. Most of the systems were found to be capable of harboring habitable worlds, even after updating the effective insolation estimates following Kopparapu et al. (2013) (section 5.7 and appendix 5.A). Except for M-class binaries where habitable planets could be on the brink of detectability via RV measurements, transit photometry again seems to be the most promising method to detect Earth-sized planetary candidates at the moment. Given the emphasis put on transit photometry missions such as CoRoT, Kepler, TESS and CHEOPS<sup>1</sup> by ESA as well as NASA, the two space agencies may have drawn a similar conclusion.

Finally, we discussed preliminary findings for P-Type configurations and summarized potential future applications of the HZ classification method to mutually inclined S-Type and Sun-Jupiter-Earth systems in chapter 6.

---

<sup>1</sup><http://cheops.unibe.ch/>, retrieved 11.02.2013



# References

- Adam, I. 2009, *General Relativity and Gravitation*, 41, 691, 10.1007/s10714-008-0745-y 20
- Batalha, N. M. et al. 2013, *ApJS*, 204, 24, 1202.5852 1
- Bate, M. R. 2012, *MNRAS*, 419, 3115, 1110.1092 4
- Beaugé, C., Ferraz-Mello, S., & Michtchenko, T. A. 2012, *Research in Astronomy and Astrophysics*, 12, 1044 24
- Benettin, G., Galgani, L., Giorgilli, A., & Strelcyn, J.-M. 1980, *Meccanica*, 15, 9 19
- Benner, S. A. 2010, *Astrobiology*, 10, 1021 1
- Black, D. C. 1982, *AJ*, 87, 1333 18
- Blaes, O., Lee, M. H., & Socrates, A. 2002, *ApJ*, 578, 775, arXiv:astro-ph/0203370 93
- Borucki, W. J., & Koch, D. G. 2011, in *IAU Symposium*, Vol. 276, IAU Symposium, ed. A. Sozzetti, M. G. Lattanzi, & A. P. Boss, 34–43 1
- Brouwer, D. 1959, *AJ*, 64, 378 20, 24
- . 1963, *AJ*, 68, 152 20
- Buccino, A. P., Lemarchand, G. A., & Mauas, P. J. D. 2006, *Icarus*, 183, 491, arXiv:astro-ph/0512291 1, 5
- Campbell, B., Walker, G. A. H., & Yang, S. 1988, *ApJ*, 331, 902 1, 13
- Celletti, A. 2010, *Stability and Chaos in Celestial Mechanics* (Springer Science+Business Media) 20, 24
- Correia, A. C. M., Laskar, J., Farago, F., & Boué, G. 2011, *Celestial Mechanics and Dynamical Astronomy*, 111, 105, 1107.0736 92, 108
- Delaunay, C. 1860, *Théorie du mouvement de la lune, Théorie du mouvement de la lune* No. vol. 1 (Mallet-Bachelier) 23
- Des Marais, D. J. et al. 2002, *Astrobiology*, 2, 153 6
- D’Hoker, E., & Phong, D. H. 1988, *Rev. Mod. Phys.*, 60, 917 20
- Dole, S. H. 1964, *Habitable planets for man* 5
- Doolin, S., & Blundell, K. M. 2011, *MNRAS*, 418, 2656, 1108.4144 18
- Dressing, C. D., Spiegel, D. S., Scharf, C. A., Menou, K., & Raymond, S. N. 2010, *ApJ*, 721, 1295, 1002.4875 8, 9, 96, 98
- Driver, G. R. 1956, *The Journal of Theological Studies*, VII, 1 2
- Dumusque, X. et al. 2012, *Nature* 1, 49, 109, 119, 121
- Duquennoy, A., & Mayor, M. 1991, *Astronomy and Astrophysics*, 248, 485 1, 2, 4, 5, 109
- Dvorak, R. 1984, *Celestial Mechanics*, 34, 369 2, 16
- . 1986, *A&A*, 167, 379 15, 18, 19, 108
- . 1997, *Celestial Mechanics and Dynamical Astronomy*, 68, 63 92
- Dvorak, R., Pilat-Lohinger, E., Funk, B., & Freistetter, F. 2003, *A&A*, 398, L1, arXiv:astro-ph/0211289 13
- Dyson, F. 2004, *Nature*, 427, 297 9
- Edson, A., Lee, S., Bannon, P., Kasting, J. F., & Pollard, D. 2011, *Icarus*, 212, 1 9
- Eggl, S., & Dvorak, R. 2010, in *Lecture Notes in Physics*, Berlin Springer Verlag, Vol. 790, *Lecture Notes in Physics*, Berlin Springer Verlag, ed. J. Souchay & R. Dvorak, 431–480 78, 87
- Eggl, S., Pilat-Lohinger, E., Georgakarakos, N., Gyergyovits, M., & Funk, B. 2012, *ApJ*, 752, 74, 1204.2496 79
- Eggleton, P. 2006, *Evolutionary Processes in Binary and Multiple Stars* 2, 4, 5, 24, 107
- Eggleton, P. P. 1983, *ApJ*, 268, 368 19
- Epica Community Members et al. 2006, *Nature*, 444, 195 11

## REFERENCES

---

- Erdi, B. 1974, *AJ*, 79, 653–16
- Everhart, E. 1974, *Celestial Mechanics*, 10, 35–27, 78, 87, 92
- Fabrycky, D., & Tremaine, S. 2007, *ApJ*, 669, 1298, 0705.4285–93
- Farago, F., & Laskar, J. 2010, *MNRAS*, 401, 1189, 0909.2287–24
- Ferraz-Mello, S., ed. 2007, *Astrophysics and Space Science Library*, Vol. 345, *Canonical Perturbation Theories - Degenerate Systems and Resonance* 21, 22, 23, 24
- Ford, E. B., Kozinsky, B., & Rasio, F. A. 2000, *ApJ*, 535, 385–24
- Forgan, D. 2012, *MNRAS*, 422, 1241, 1202.1265–14, 96, 98, 99
- Franck, S., Block, A., von Bloh, W., Bounama, C., Schellnhuber, H.-J., & Svirezhev, Y. 2000, *Planet. Space Sci.*, 48, 1099–8
- Froeschlé, C., Lega, E., & Gonczi, R. 1997, *Celestial Mechanics and Dynamical Astronomy*, 67, 41–19
- Gaidos, E., Deschenes, B., Dundon, L., Fagan, K., Menviel-Hessler, L., Moskovitz, N., & Workman, M. 2005, *Astrobiology*, 5, 100–9
- Georgakarakos, N. 2002, *MNRAS*, 337, 559–24, 26, 30
- . 2003, *MNRAS*, 345, 340–24, 26, 28, 30, 33, 34, 37, 77, 78
- . 2005, *MNRAS*, 362, 748–26, 28, 30, 34, 37, 80
- . 2009, *MNRAS*, 392, 1253, 0811.1146–103, 104
- . 2013, *ArXiv e-prints*, 1302.5599–18
- Gerlach, E., Eggl, S., & Skokos, C. 2011, *ArXiv e-prints*, 1104.3127–19
- Gingold, R. A., & Monaghan, J. J. 1977, *MNRAS*, 181, 375–4
- Giuppone, C. A., Leiva, A. M., Correa-Otto, J., & Beaugé, C. 2011a, *A&A*, 530, A103, 1105.0243–78, 79
- Giuppone, C. A., Leiva, A. M., Correa-Otto, J., & Beaugé, C. 2011b, *Astronomy and Astrophysics*, 530, A103+, 1105.0243–79
- Gonzalez, G., Brownlee, D., & Ward, P. 2001, *Icarus*, 152, 185, arXiv:astro-ph/0103165–14
- Gowanlock, M. G., Patton, D. R., & McConnell, S. M. 2011, *Astrobiology*, 11, 855, 1107.1286–14
- Goździewski, K. et al. 2012, *MNRAS*, 425, 930, 1205.4164–19
- Graziani, F., & Black, D. C. 1981, *ApJ*, 251, 337–18
- Guedes, J. M., Rivera, E. J., Davis, E., Laughlin, G., Quintana, E. V., & Fischer, D. A. 2008, *ApJ*, 679, 1582, 0802.3482–13, 117
- Haberle, R. M., Tyler, D., McKay, C. P., & Davis, W. L. 1994, *Icarus*, 109, 102–11
- Haghighipour, N. 2006, *ApJ*, 644, 543, arXiv:astro-ph/0509659–13
- Haghighipour, N., Dvorak, R., & Pilat-Lohinger, E. 2010, in *Astrophysics and Space Science Library*, Vol. 366, *Astrophysics and Space Science Library*, ed. N. Haghighipour, 285–+, 0911.0819–13
- Haghighipour, N., & Raymond, S. N. 2007, *ApJ*, 666, 436, arXiv:astro-ph/0702706–13
- Hanslmeier, A., & Dvorak, R. 1984, *Astronomy and Astrophysics*, 132, 203–78
- Harrington, R. S. 1968, *AJ*, 73, 190–24, 25
- . 1969, *Celestial Mechanics*, 1, 200–24
- . 1972, *Celestial Mechanics*, 6, 322–18, 90
- . 1977, *AJ*, 82, 753–12, 13, 18, 19, 109
- Hart, M. H. 1978, *Icarus*, 33, 23–5
- . 1979, *Icarus*, 37, 351–5, 8
- Hatzes, A. P., Cochran, W. D., Endl, M., McArthur, B., Paulson, D. B., Walker, G. A. H., Campbell, B., & Yang, S. 2003, *Astrophysical Journal*, 599, 1383, arXiv:astro-ph/0305110–13
- Heintz, W. D. 1969, *JRASC*, 63, 275–5
- Heppenheimer, T. A. 1978, *A&A*, 65, 421–75, 76, 77, 78, 79, 80
- Herschel, W. 1803, *Royal Society of London Philosophical Transactions Series I*, 93, 339–3
- Hills, J. G. 1984, *AJ*, 89, 1559–19
- Holman, M. J., & Wiegert, P. A. 1999, *AJ*, 117, 621, arXiv:astro-ph/9809315–4, 12, 15, 18, 19, 79, 80, 90, 98, 100, 101
- Huang, S.-S. 1959, *PASP*, 47, 397–5
- . 1960, *PASP*, 72, 106–11, 12, 16
- Hut, P. 1985, in *IAU Symposium*, Vol. 113, *Dynamics of Star Clusters*, ed. J. Goodman & P. Hut, 231–247–4
- Jaime, L. G., Pichardo, B., & Aguilar, L. 2012, *ArXiv e-prints*, 1208.2051–19
- Kaltenegger, L., Traub, W. A., & Jucks, K. W. 2007, *ApJ*, 658, 598, arXiv:astro-ph/0609398–6, 9

## REFERENCES

- Kane, S. R., & Gelino, D. M. 2012, *PASP*, 124, 323, 1202.2377 97
- Kane, S. R., & Hinkel, N. R. 2012, *ArXiv e-prints*, 1211.2812 13, 103
- Kasting, J. F. 1988, *Icarus*, 74, 472 5, 6
- Kasting, J. F., Whitmire, D. P., & Reynolds, R. T. 1993, *Icarus*, 101, 108 4, 5, 6, 7, 8, 11, 12, 13, 37, 96, 97, 109, 119, 121
- Kaula, W. M. 1961, *Geophysical Journal International*, 5, 104 20, 21
- . 1962, *AJ*, 67, 300 20
- Kite, E. S., Gaidos, E., & Manga, M. 2011, *ApJ*, 743, 41, 1109.2668 11, 96, 98
- Kopparapu, R. k. et al. 2013, *ArXiv e-prints*, 1301.6674 4, 6, 8, 11, 97, 98, 100, 101, 107, 109, 110, 119, 121
- Kovács, T., & Érdi, B. 2009, *Celestial Mechanics and Dynamical Astronomy*, 105, 289 90
- Kozai, Y. 1962, *AJ*, 67, 591 88, 89
- Krymolowski, Y., & Mazeh, T. 1999, *MNRAS*, 304, 720 24, 25, 90, 103
- Lammer, H. et al. 2009, *A&A Rev.*, 17, 181 6
- Lammer, H., Lichtenegger, H. I. M., Khodachenko, M. L., Kulikov, Y. N., & Griessmeier, J. 2011, in *Astronomical Society of the Pacific Conference Series*, Vol. 450, *Astronomical Society of the Pacific Conference Series*, ed. J. P. Beaulieu, S. Dieters, & G. Tinetti, 139 1, 9
- Laoupi, A. 2006, *Mediterranean Archaeology and Archaeometry*, 6, 33 2
- Laskar, J., & Robutel, P. 1993, *Nature*, 361, 608 9
- Lee, M. H., & Peale, S. J. 2003, *ApJ*, 592, 1201, *arXiv:astro-ph/0304454* 24
- Libert, A.-S., & Delsate, N. 2012, *MNRAS*, 422, 2725, 1203.2849 90
- Lidov, M. L. 1962, *Planet. Space Sci.*, 9, 719 88, 89
- Lineweaver, C. H., & Chopra, A. 2012, *Annual Review of Earth and Planetary Sciences*, 40, 597 14
- Lineweaver, C. H., Fenner, Y., & Gibson, B. K. 2004, *Science*, 303, 59, *arXiv:astro-ph/0401024* 14
- Lissauer, J. J., Barnes, J. W., & Chambers, J. E. 2012, *Icarus*, 217, 77 9
- Lorenz, E. N. 1963, *Journal of Atmospheric Sciences*, 20, 130 11
- Lorenz, R. D., McKay, C. P., & Lunine, J. I. 1997, *Science*, 275, 642 11
- Lyapunov, A. M. 1907, *Annales de la faculté des sciences de Toulouse*, 9, 203 19
- Marchal, C. 1990, *The three-body problem* 15, 24, 25, 26
- Marchal, C., & Saari, D. G. 1975, *Celestial Mechanics*, 12, 115 16
- Mardling, R. A., & Aarseth, S. J. 2001, *MNRAS*, 321, 398 18, 19, 89, 90
- Marks, M., & Kroupa, P. 2011, *MNRAS*, 417, 1702, 1109.2896 4
- Mayor, M., & Queloz, D. 1995, *Nature*, 378, 355 1
- Mullaney, J. 2005, *Double and Multiple Stars, and How to Observe Them* 3
- Murray, C. D., & Dermott, S. F. 2000, *Solar System Dynamics*, ed. Murray, C. D. & Dermott, S. F. 20, 21, 92
- Müller, H. 2004, *Der geschmiedete Himmel. Die Welt im Herzen Europas vor 3600 Jahren* (Theiss) 2
- Naoz, S., Farr, W. M., & Rasio, F. A. 2012a, *ApJ*, 754, L36, 1206.3529 92, 103
- Naoz, S., Kocsis, B., Loeb, A., & Yunes, N. 2012b, *ArXiv e-prints*, 1206.4316 19, 93
- Nelder, J. A., & Mead, R. 1965, *The Computer Journal*, 7, 308, <http://comjnl.oxfordjournals.org/content/7/4/308.full.pdf+html> 78
- Neuhäuser, R., Mugrauer, M., Fukagawa, M., Torres, G., & Schmidt, T. 2007, *Astronomy and Astrophysics*, 462, 777, *arXiv:astro-ph/0611427* 13
- Oseledec, V. I. 1968, *Trans. Moscow Math. Soc.*, 19, 197 19
- Pernicka, E., & Wunderlich, C.-H. 2002, *Archäologie in Sachsen-Anhalt*, 1, 24 2
- Perryman, M. A. C. et al. 1997, *A&A*, 323, L49 97, 100
- Pichardo, B., Sparke, L. S., & Aguilar, L. A. 2005, *MNRAS*, 359, 521, *arXiv:astro-ph/0501244* 19
- Pilat-Lohinger, E., & Dvorak, R. 2002, *Celestial Mechanics and Dynamical Astronomy*, 82, 143 4, 12, 18, 19, 79, 80
- Pilat-Lohinger, E., Funk, B., & Dvorak, R. 2003, *A&A*, 400, 1085 18
- Prantzos, N. 2008, *Space Sci. Rev.*, 135, 313, *arXiv:astro-ph/0612316* 14
- Rabl, G., & Dvorak, R. 1988, *A&A*, 191, 385 4, 18, 19

## REFERENCES

---

- Raghavan, D. et al. 2010, *ApJS*, 190, 1, 1007.0414 1, 4, 109
- Rasool, S. I., & de Bergh, C. 1970, *Nature*, 226, 1037 5
- Roe, G. H., & Baker, M. B. 2010, *Journal of Climate*, 23, 4694 11
- Roell, T., Neuhäuser, R., Seifahrt, A., & Mugrauer, M. 2012, *A&A*, 542, A92, 1204.4833 1, 16, 22
- Roy, A. E. 2005, *Orbital motion* 21
- Sándor, Z., Érdi, B., Széll, A., & Funk, B. 2004, *Celestial Mechanics and Dynamical Astronomy*, 90, 127 19
- Sándor, Z., Süli, Á., Érdi, B., Pilat-Lohinger, E., & Dvorak, R. 2007, *MNRAS*, 375, 1495 13, 18
- Schneider, J. 1994, *Planetary and Space Science*, 42, 539 90
- Schneider, J., & Chevreton, M. 1990, *A&A*, 232, 251 90
- Schneider, J., Dedieu, C., Le Sidaner, P., Savalle, R., & Zolotukhin, I. 2011, *A&A*, 532, A79, 1106.0586 1
- Schneider, J., & Doyle, L. R. 1995, *Earth Moon and Planets*, 71, 153 90
- Schulze-Makuch, D., & Irwin, L. N., eds. 2004, *Life in the universe. Expectations and constraints* 6
- Schwarz, R., Süli, Á., & Dvorak, R. 2009, *MNRAS*, 398, 2085 13, 16
- Selsis, F., Kasting, J. F., Levrard, B., Paillet, J., Ribas, I., & Delfosse, X. 2007, *A&A*, 476, 1373, 0710.5294 6, 11, 119, 121
- Selsis, F., Wordsworth, R. D., & Forget, F. 2011, *A&A*, 532, A1, 1104.4763 11, 99
- Sitnikov, K. 1960, *Dokl. Akad. Nauk. USSR*, 133, 303 90
- Skokos, C. 2010, in *Lecture Notes in Physics*, Berlin Springer Verlag, Vol. 790, *Lecture Notes in Physics*, Berlin Springer Verlag, ed. J. Souchay & R. Dvorak, 63–135, 0811.0882 19
- Soderhjelm, S. 1984, *A&A*, 141, 232 24
- Soffel, M. H. 1989, *Relativity in Astrometry, Celestial Mechanics and Geodesy* 93
- Soulis, P., Bountis, T., & Dvorak, R. 2007, *Celestial Mechanics and Dynamical Astronomy*, 99, 129 90
- Spiegel, D. S., Menou, K., & Scharf, C. A. 2008, *ApJ*, 681, 1609, 0711.4856 6, 8, 9, 98
- Spiegel, D. S., Raymond, S., Dressing, C. D., Scharf, C. A., Mitchell, J. L., & Menou, K. 2010, in *Astronomical Society of the Pacific Conference Series*, Vol. 430, *Pathways Towards Habitable Planets*, ed. V. Coudé Du Foresto, D. M. Gelino, & I. Ribas, 109 8
- Stiefel, E. L., & Scheifele, G. 1975, *Linear and regular celestial mechanics. Perturbed two-body motion. Numerical methods. Canonical theory.* 15
- Stommel, H. 1961, *Tellus*, 13, 224 11
- Szebehely, V. 1967, *Theory of orbits. The restricted problem of three bodies* 16
- . 1977, *Celestial Mechanics*, 15, 107 16, 18
- Szebehely, V., & McKenzie, R. 1977, *AJ*, 82, 79 17
- Szebehely, V., & Zare, K. 1977, *A&A*, 58, 145 17, 18
- Thebault, P. 2011, *Celestial Mechanics and Dynamical Astronomy*, 111, 29, 1103.3900 13, 109
- Thébault, P., Marzari, F., & Scholl, H. 2006, *Icarus*, 183, 193, arXiv:astro-ph/0602046 78
- . 2009, *MNRAS*, 393, L21, 0811.0673 13
- Torres, G., Andersen, J., & Giménez, A. 2010, *A&A Rev.*, 18, 67, 0908.2624 4
- Triaud, A. H. M. J. et al. 2010, *A&A*, 524, A25, 1008.2353 92
- Underwood, D. R., Jones, B. W., & Sleep, P. N. 2003, *International Journal of Astrobiology*, 2, 289, arXiv:astro-ph/0312522 4, 6, 11, 97, 100, 109, 119, 121
- Valtonen, M., & Karttunen, H. 2006, *The Three-Body Problem* 19, 92
- Valtonen, M., Mylläri, A., Orlov, V., & Rubinov, A. 2008, in *IAU Symposium*, Vol. 246, *IAU Symposium*, ed. E. Vesperini, M. Giersz, & A. Sills, 209–217 19
- van Winckel, H. 2003, *ARA&A*, 41, 391 4
- Wallis, J. 1693, in *In several Letters of May the 2d, June 29. and July 20. 1693. from Dr. John Wallis to William Molineux Esq;*, Vol. 17, *Philosophical Transaction giving some account of the present undertakings, studies and labours of the ingenious, in many considerable parts of the world*, ed. T. N. for John Martyn and James Allestry, printers to the Royal-Society, London, 84 ix
- Welsh, W. F. et al. 2012, *Nature*, 481, 475, 1204.3955 1, 13, 16, 19, 103
- Wertheimer, J. G., & Laughlin, G. 2006, *AJ*, 132, 1995, arXiv:astro-ph/0607401 1
- Whitmire, D. P., Matese, J. J., Criswell, L., & Mikkola, S. 1998, *Icarus*, 132, 196 13, 16, 18

## REFERENCES

---

- Williams, D. M., & Kasting, J. F. 1997, *Icarus*, 129, 254 8, 9
- Williams, D. M., & Pollard, D. 2002, *International Journal of Astrobiology*, 1, 61 8, 9, 96, 110
- Wolszczan, A., & Frail, D. A. 1992, *Nature*, 355, 145 1
- Yoshida, H. 1990, *Physics Letters A*, 150, 262 87
- . 1993, *Celestial Mechanics and Dynamical Astronomy*, 56, 27 88
- Zahn, J.-P. 1989, *A&A*, 220, 112 4
- Zahnle, K., Haberle, R. M., Catling, D. C., & Kasting, J. F. 2008, *Journal of Geophysical Research (Planets)*, 113, 11004 11



## Errata

**Chapter 4, Table 2:** The first sentence in the caption should read: "Critical semi-major axis [ $a_{crit}$  (au), column 3] for orbital stability and borders for the HZs [(au), columns 4–9] as measured for the respective host stars A & B are given for 19 binary-star systems in the solar neighbourhood."

**Chapter 4, p. 3110:** The second sentence in the right column should read: "With RV signal amplitudes of  $\approx 5 - 12 \text{ cm s}^{-1}$  for potentially habitable planets in systems containing Sun-like G stars (HIP 31711 & 84425), our estimates are comparable to those for  $\alpha$  Centauri presented in Eggl et al. (2012a) and Guedes et al. (2008)."





## Abstract

This thesis contains an analytic framework to determine circumstellar habitable zones in binary star systems. The influence of a second star on a terrestrial planet's capacity to host liquid water on its surface is studied in detail. Assuming that the telluric planet orbits one component of a stellar binary (S-Type system) where all three bodies share the same orbital plane, it can be shown that long term habitability in such environments is possible in spite of the strong gravitational forcing and the additional stellar radiation. Thereby, the gravitationally induced changes of the planet's eccentricity constitute the dominating effect that determines the orbital limits for permanent habitability. For planets on non-circular orbits, the well known habitable zone boundaries by Kasting et al. (1993), Underwood et al. (2003), Selsis et al. (2007) and recently Kopparapu et al. (2013) used in most current studies are only valid in an average sense. In order to take the considerable variability of a planet's orbit in a binary star system into account, a new methodology to classify planetary habitability had to be developed. Therefore, the concepts of a permanently habitable zones (PHZ), extended habitable zones (EHZ) and average habitable zones (AHZ) were introduced. The PHZ denotes circumstellar regions where planets will remain within habitable insolation limits regardless of the dynamical evolution of their orbits. The EHZ corresponds to areas in which the planet will leave the habitable zone from time to time, yet, insolation conditions permit habitability along most of the planet's track. Planets that orbit their stars within AHZs may spend a substantial amount of time outside habitable regions as long as the average insolation still permits liquid water on the planet's surface. This classification is not only universally applicable to planets on eccentric orbits, it also retains information on the variability of planetary insolation conditions while providing estimates that are valid up to geological and even stellar evolutionary timescales, if the planet's atmospheric conditions are known. It was found that the analytic methods developed in this thesis are applicable to binary star systems without restrictions to planetary masses or climate models as long as corresponding effective insolation values ( $S_{eff}$ ) are available. Strong perturbations near resonances, regions of orbital instability, other gravitationally active bodies, or drastic changes in the planet's atmospheric behavior, such as capture into tidal lock states can, however, reduce the quality of the presented estimates.

Applying the new classification scheme to binary stars in the solar neighborhood we could show that a large percentage of the investigated systems are capable of hosting habitable worlds. Further results do not only suggest that terrestrial planets can be habitable in nearby binary star systems, they might even be easier to spot than Earth-twins orbiting single stars. Gravitational interactions with the double star tend to increase planetary radial velocity signatures, astrometric signal amplitudes and transit probabilities, thus improving the chances for a planet's detection.

The discovery of an Earth-sized planet around  $\alpha$  Centauri B (Dumusque et al. 2012) has shown that a confirmation of the existence of habitable worlds in binary stars

is on the brink of technical feasibility. Given the large number of stellar multiple systems, an efficient identification of potentially interesting systems is required to optimize target selection. The methodology proposed in this thesis can serve as a quick and reliable tool to determine binary star systems capable of sustaining habitable planets.

## Zusammenfassung

Die vorliegende Dissertation hatte die Entwicklung eines analytischen Verfahrens zum Ziel, das es ermöglicht die Bewohnbarkeit erdähnlicher Planeten auf zirkumstellaren Bahnen in Binärsternsystemen effizient zu untersuchen und zu kategorisieren. In diesem Rahmen konnte gezeigt werden, dass die Existenz habitabler Planeten in derartigen Konfigurationen trotz starker, gravitativer Wechselwirkungen sowie der zusätzlichen Einstrahlung durch den zweiten Stern möglich ist. Die in gängiger Literatur meist verwendeten Grenzen für Habitable Zonen nach Kasting et al. (1993), Kopparapu et al. (2013), Selsis et al. (2007) und Underwood et al. (2003) bleiben besten Falls im Mittel gültig. Tatsächlich bedurfte es einer Neukategorisierung habitabler Zonen bei der darauf zu achten war, dass der Planet trotz gravitationsbedingter Bahnänderungen, immer, oder zumindest zu einem großen Prozentsatz, innerhalb zumutbarer Einstrahlungsniveaus verbleibt. Die entsprechenden Parameterbereiche wurden in Zonen permanenter Habitabilität (PHZ) und erweiterter Habitabilität (EHZ) unterteilt. Geht man von zeitgemittelten Einstrahlungslimits aus (AHZ) so werden die klassischen Grenzen nach Kasting reproduziert.

Eine Anwendung dieses Klassifikationsschemas auf nahe Doppelsternsysteme ergab, dass ein hoher Prozentsatz habitable Planeten um zumindest eine Doppelsternkomponente zulässt. Weiters war es möglich durch analytisch-dynamische Abschätzungen zu zeigen, dass erdähnliche, bewohnbare Planeten in Doppelsternen leichter auffindbar sein können als deren Pendants um Einzelsterne. Diese Effekte folgen aus der gravitativen Einwirkung des zweiten Sterns auf die vom Planeten induzierte Radialgeschwindigkeit, die astrometrische Signalstärke, sowie die planetare Transitwahrscheinlichkeit. Das hier präsentierte analytische Verfahren ist - unabhängig von der Masse des Planeten - auf Binärstern-Planetensysteme mit geringer gegenseitiger Bahnneigung anwendbar, solange verlässliche Effektivstrahlungswerte ( $S_{eff}$ ) für die jeweiligen planetaren Atmosphären verfügbar sind. Befinden sich weitere Planeten im Doppelsternsystem, so muss eine gesonderte Überprüfung die Gültigkeit der präsentierten Methodik belegen.

Die Entdeckung eines erdähnlichen Planeten in unserem Nachbar-Doppelstern  $\alpha$  Centauri AB (Dumusque et al. 2012) zeigt, dass die Erforschung habitabler Planeten in Binärsternsystemen ein zukunftsreiches Gebiet darstellt. Bedenkt man die enorme Anzahl an Doppelsternsystemen in der galaktischen Umgebung, so ist es nicht unwahrscheinlich, dass erdähnliche, bewohnbare Planeten in solchen Konfigurationen gefunden werden. Die in dieser Arbeit entwickelten Methoden zur Auffindung viel versprechender Systeme könnten wesentlich zu derartigen Entdeckungen beitragen.



# CURRICULUM VITAE

**NAME** Siegfried Eggl

**CITIZENSHIP** Austrian

## MILITARY SERVICE

Austrian Federal Military, Fliegerhorst Fiala-Fernbrugg	A-8943 Aigen im Ennstal, Austria	02.10.2000 - 01.06.2001
---	----------------------------------	-------------------------

## WORK EXPERIENCE

IMCCE-Observatoire de Paris Project Scientist	F-75014 Paris, France	01.10.2012-30.09.2013
University of Vienna Project Scientist/Lecturer	A-1180 Vienna, Austria	01.02.2008-30.09.2012
Natural History Museum Vienna Scientific Visualization Project	A-1110 Vienna, Austria	01.09.2006-01.12.2006
P.S.K Accountant clerk	A-8940 Liezen, Austria	04.07. - 03.09.2000

## TEACHING EXPERIENCE

Lecturer at the Institute for Astronomy, University of Vienna	2009-2012
“Exercises in numerical methods for Astronomy”	2009-2012
“Mathematical and physical foundations of Astronomy”	2011-2012
“Practical in numerical Astronomy”	2010

## IN ACADEMIA

PhD studies in Natural Science at University of Vienna. Thesis title: “Circumstellar Habitable Zones in Binary Star Systems”	since 2008 to be completed: 2013
graduated Master of Natural Science (Physics) at University of Vienna with distinction	19.11.2009
graduated Master of Natural Science (Astronomy) at University of Vienna with distinction	18.02.2008
graduated Bachelor of Natural Science at University of Vienna with distinction	06.04.2005

## **BASIC EDUCATION**

Matura passed with distinction	05.06.2000
private school Stiftsgymnasium Admont	1992 - 2000
elementary school	1988 - 1992

## **AWARDS & SCHOLARSHIPS**

University of Vienna's research grant 2012	01.01.2012
International Space University's (ISU) Morla Milne Award for Academic Excellence	09.09.2011
FFG Austrian Research Promotion Agency and TU Graz: full scholarship for ISU participation	09.07.-11.09 2011
ESA & FFG Austrian Research Promotion Agency, full scholarship for ESA summer-school Alpbach 2009	21.07.-30.07.2009
University of Vienna's Performance Scholarships	2001-2004

## **LANGUAGE SKILLS**

German	mother tongue
English	fluent
French	basic
Latin	basic

## **CODE DEVELOPMENT AND APPLICATIONS SKILLS**

FORTTRAN 77/95	MS Office
C, C++	Wolfram Mathematica
JAVA	POVray raytracer
HTML	Windows, UNIX

## **OTHER SKILLS**

driving license	diving license
-----------------	----------------

## REFEREED PUBLICATIONS

Gyergyovits, M., **Eggl, S.**, Pilat – Lohinger, E., Theis C.: On the influence of self-gravitating protoplanetary bodies on circumprimary discs in binary star systems, *Astronomy & Astrophysics* (submitted)

**Eggl, S.**, Pilat-Lohinger, E., Funk, B., Georgakarakos, N., Haghighipour, N.: Circumstellar habitable zones of binary-star systems in the solar neighbourhood, *Monthly Notices of the Royal Astronomical Society*, Volume 428, Issue 4 (2013)

**Eggl, S.**, Haghighipour, N., Pilat-Lohinger, E.: Detectability of Earth-like Planets in Circumstellar Habitable Zones of Binary Star Systems with Sun-like Components, *The Astrophysical Journal*, Volume 764:130 (2013)

**Eggl, S.**, Pilat-Lohinger, E., Georgakarakos, N., Gyergyovits, M. Funk, B.: An Analytic Method to Determine Habitable Zones for S-Type Planetary Orbits in Binary Star Systems, *Astrophysical Journal*, Volume 752, Issue 1, article id. 74 (2012)

Gerlach, E, **Eggl, S.**, Skokos, Ch.: Efficient integration of the variational equations of multi-dimensional Hamiltonian systems: Application to the Fermi-Pasta-Ulam lattice, *International Journal of Bifurcation and Chaos*, Volume 22, Issue 9 (2012)

Schwarz, R., Haghighipour, N., **Eggl, S.**, Pilat-Lohinger, E., Funk, B.: Prospects of the Detection of Circumbinary Planets With Kepler and CoRoT Using the Variations of Eclipse Timing, *Monthly Notices of the Royal Astronomical Society*, Volume 414, Issue 3, pp. 2763-2770 (2011)

**Eggl, S.**, Dvorak, R.: An Introduction to common Numerical Integration Codes used in Dynamical Astronomy, *Lecture Notes in Physics* Vol 790 (2010)

**Eggl, S.**: Refinement of Near Earth Asteroids' orbital elements via simultaneous observations by two Satellites, *Celestial Mechanics and Dynamical Astronomy*, Volume 109, Issue 3, pp. 211-228 (2010)

Funk, B., Wuchterl, G., Schwarz, R., Pilat-Lohinger, E., **Eggl, S.**: The stability of ultra-compact planetary systems, *Astronomy and Astrophysics*, Volume 516, id.A82 (2010)

Funk, B., Süli, Á., Pilat-Lohinger, E., Schwarz, R., **Eggl, S.**: Dynamical Stability in the Habitable Zones of Nearby Extrasolar Planetary Systems, *Pathways Towards Habitable Planets*, proceedings of a workshop held 14 to 18 September 2009 in Barcelona, Spain. Astronomical Society of the Pacific, p.430 (2010)

Mohler M., Bühl, J. Doherty, S., **Eggl, S.**, Eybl, V. T., Farago, F., Jaćimović, A., Hunger, L., Lauritsen, N. L. B., Ludena, D., Meisnar, M., Reissner, A., Sarda, N., Toullec, B., Tió, M. V.: Opening a new window to other worlds with spectropolarimetry, *Experimental Astronomy*, Volume 28, Issue 2-3, pp. 101-135 (2010)

## SCIENTIFIC STAYS, CONFERENCES AND PROGRAMS

<b>Astrobiological and cosmochemical implications of Marco Polo-R sampling of a primitive asteroid</b> , Barcelona, Spain (poster)	16.01.-17.01.2013
<b>Scientific stay at the Institute for Astronomy and NASA Astrobiology Institute Hawaii Manoa</b> Invited guest at IfA Hawaii, Honolulu, USA (talk)	30.06.-1.08.2012
<b>Workshop on Astrobiology</b> , Vienna, Austria (talk)	21.05.-22.05.2012
<b>International Space University Space Studies Program</b> Graz, Austria (talk)	09.07.-11.09.2011
<b>EGU 2011</b> , Austria Center Vienna, Austria (poster)	03.04.-08.04 2011
<b>8<sup>th</sup> Alexander von Humboldt Colloquium for Celestial Mechanics</b> Bad Hofgastein, Austria (LOC, talk)	20.03.-26.03.2011
<b>Nonlinear Dynamics and Complexity: Theory Methods and Applications</b> , Thessaloniki, Greece (poster)	12.07.-16.07.2010
<b>ESF Exploratory Workshop on Observation, characterization and evolution of habitable exoplanets and their host stars</b> , Bairisch Koellendorf, Styria, Austria (talk)	29.11.-01.12.2009
Selected for <b>Post-Alpbach workshop</b> , Graz, Styria, Austria (talk)	24.11.-27.11.2009
<b>ESA-Summer-school Alpbach 2009</b> on Characterization of Exoplanets Alpbach, Tyrol, Austria (talk)	21.07.-30.07.2009
<b>N-Body 2008</b> , Turku, Finland	10.08.-14.08.2008
<b>21<sup>st</sup> Conference/Summer-school on Nonlinear Science and Complexity</b> , Athens, Greece	21.07.-02.08.2008
<b>7<sup>th</sup> Alexander von Humboldt Colloquium for Celestial Mechanics</b> Bad Hofgastein, Austria (talk)	30.03.-05.04.2008
<b>4<sup>th</sup> Austrian Hungarian Workshop on Trojans and related Topics</b> Budapest, Hungary	23.06.-25.06.2005